Deciphering the function of GCNF in human neural stem cells during neuronal differentiation

Dissertation
zur Erlangung des Doktorgrades (Dr. rer. nat.)
der Mathematisch-Naturwissenschaftlichen Fakultät
der Rheinisch Friedrich-Wilhelms-Universität Bonn

vorgelegt von
Frederike Klaus
aus Minden

Bonn, 2023

Angefertigt mit der Genehmigung der Mathematisch-Naturwissenschaftlichen Fakultät
der Rheinischen Friedrich-Wilhelms-Universität Bonn

1. Gutachter: Prof. Dr. med. Oliver Brüstle
2. Gutachter: Prof. Dr. rer. nat. Waldemar Kolanus

Tag der Promotion: 26 May 2023
Erscheinungsjahr: 2023

Man bewältigt ein Gebirge
und man stolpert über einen Stein.

One masters a mountain range
and one stumbles over a stone.

Gertrud von Le Fort

Abstract

The human brain is one of the most complex structures described in the biological world and the development of such an intricate organ is tightly regulated by neural stem cell (NSC) proliferation and differentiation. However, the molecular mechanisms regulating these processes are still under investigation.

Different animal studies have suggested a critical role of the orphan nuclear factor and transcriptional repressor GCNF in neural lineage development. In model organisms, GCNF has been associated with the development of definitive NSCs, neural tube closure and correct regionalization. However, not much is known about GCNF's role in human brain development.

This work aimed at deciphering the function of GCNF during human neuronal development using small molecule neural precursor cells (smNPCs) as *in vitro* model of human NSCs.

The spatial and temporal expression pattern of GCNF hinted to an important role of GCNF during neuronal development, since GCNF was expressed in NSCs and the expression was decreasing during neuronal differentiation. The modulation of GCNF expression in smNPCs had a profound effect on smNPC proliferation and differentiation. Overexpression of GCNF increased the proliferation capacity and maintenance of smNPCs at the expense of neuronal differentiation. The knockdown of GCNF had opposite effects, leading to increased numbers of neuronal cells and less proliferative NSCs after 7 days of differentiation. Interestingly, reversing the function of GCNF by fusing the transactivator domain of VP16 to GCNF led to a prominent increase in neuronal cells and an exhaustion of smNPCs. Furthermore, the modulation of GCNF expression also affected smNPC clustering. GCNF overexpression increased the area of the formed cell clusters, while the expression of GCNF-VP16 decreased cluster formation and the area of the formed clusters.

Transcriptome microarray analyses were used to understand the molecular mechanisms of the effects of GCNF on smNPC proliferation and neuronal differentiation. Integration of these data with bioinformatic prediction methods was used to identify potential of GCNF. Indeed, BCL11A, a transcriptional repressor involved in murine CNS development, could be confirmed as a direct target gene of GCNF by chromatin immunoprecipitation (ChIP) followed by qRT-PCR.

On the translational side, GCNF-VP16 could be employed as tool for accelerated neuronal differentiation of hNSCs with significantly reduced cell cluster formation. Upon GCNF-VP16 expression, smNPCs differentiated into mature neurons displaying similar features as neurons generated by NGN2 overexpression, the gold standard of neuronal forward programming today.

Taken together, GCNF was demonstrated to play an important role during human neurogenesis by promoting NSC proliferation, maintenance and cell clustering, while inhibiting neuronal differentiation. These effects might be mediated by BCL11A, a novel target gene of GCNF identified in this study. Exploitation of GCNF-VP16 for rapid and cluster-free neuronal differentiation might provide a versatile tool for setting up high-throughput assays and automated image analyses.

Table of contents

1 Introduction

1.1 The development of the central nervous system

The fertilization of the human oocyte by the sperm cell leads to the formation of a diploid cell, which generates the blastocyst within five days by undergoing multiple and rapid cell divisions (Clift and Schuh, 2013; Shahbazi, 2020). The blastocyst consists of the outer cell layer, the trophoblast, the inner cell mass, the embryoblast, which are pluripotent stem cells able to differentiate into all cells of the human body, and the inner cavity, the blastocoel (Zhai *et al.*, 2022). In a step called gastrulation, the cells of the inner cell mass undergo critical movement and local reorganization steps to finally form the three germ layers, which give rise to the specific cells of different organs. The three germ layers are the endoderm, the mesoderm and the ectoderm (Keller, 2005). Most of the internal organs differentiate from endodermal cells (Nowotschin *et al.*, 2019), while the mesoderm, contains cells that differentiate into diverse cell types, including bone, cartilage and muscle cells, as well as heart and blood cells (Ferretti and Hadjantonakis, 2019). The outer cell layer is the ectoderm, that develops into epithelial and neural tissues (Murry and Keller, 2008) (Figure 1.1).

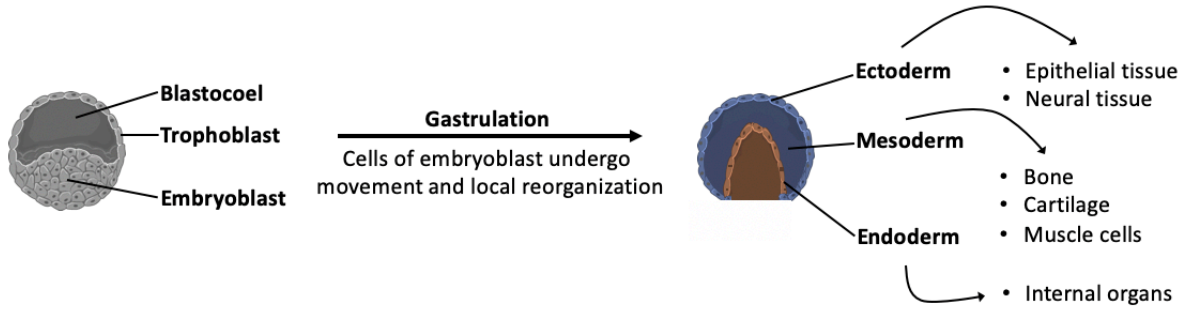

Figure 1.1: Schematic of the blastocyst and the three germ layers, which are established after gastrulation. The blastocyst consists of the trophoblast, embryoblast and blastocoel. The cells of the embryoblast undergo critical rearrangements and form the germ layers – ectoderm, mesoderm and endoderm, which give rise to the different cell types of the human body. Components of the figure were adapted from SMART Servier Medical Art.

The formation of neural structures from the ectoderm is promoted by certain molecules, by so-called neural inducers (Sasai and De Robertis, 1997), such as Noggin (Smith and Harland, 1992), Chordin (Sasai, 1994) and Follistatin (Hemmati-Brivanlou *et al.*, 1994), which are described to act by inhibiting the transforming growth factor β/bone morphogenetic protein (TGFβ/BMP) signaling function (which in turn is described as neural inhibitor (Sasai and De Robertis, 1997)). Upon neural induction, the formed multipotent neural stem cells (NSCs), which are able to differentiate into neurons and glial cells of the brain (Breunig *et al.*, 2011), undergo well controlled steps of proliferation and differentiation as basis of the formation of a functioning human brain (Belmonte-Mateos and Pujades, 2022).

1.1.1 Importance of cell proliferation and differentiation

The function of the highly complex human brain relies on the interplay of various cell types that are located within different regions in distinct proportions (Herculano-Houzel, 2009). The number of generated neurons in the brain is regulated among others by the proliferative potential of NSCs, meaning the number of symmetric and asymmetric cell divisions, which they undergo (Mira and Morante, 2020). Thus, tight control of cell proliferation and differentiation of NSCs is essential for proper brain

development (Belmonte-Mateos and Pujades, 2022). Furthermore, several neurodevelopmental diseases are described which are caused by altered timing of cell differentiation (Lancaster *et al.*, 2013; Iefremova *et al.*, 2017; Gomes *et al.*, 2020).

Overall on tissue level, early during brain development, the NSCs undergo various cell divisions to increase the NSC pool, while later during development NSC differentiation dominates (Belmonte-Mateos and Pujades, 2022). There are different modes of cell division, symmetric and asymmetric cell division (Figure 1.2). Symmetric cell division describes the process, in which the mother cell divides into two identical daughter cells. Here, a NSC gives rise to two new NSCs (proliferative division) or two differentiated cells (terminal self-consuming division) (Figure 1.2 A). Asymmetric cell division means that a NSC is dividing into a new NSC and a differentiating cell (Casas Gimeno and Paridaen, 2022) (Figure 1.2 B). Initially, the expansion of the stem cell pool organized in a stem cell niche occurs via symmetric proliferative divisions. Symmetric proliferative division is replaced by asymmetric cell divisions, which facilitate the maintenance of the progenitor pool and the generation of differentiated cells, and is finally followed by terminal self-consuming symmetric division into differentiated cells or direct differentiation of NSCs (Zechner *et al.*, 2020). The stem cell niche is further defined during brain development and is inhabited by quiescent adult NSCs in the mature brain (Gage, 2000; Ma *et al.*, 2009). Nevertheless, Llorca and colleagues demonstrated that individual NSCs might display a heterogenous neuronal progeny (Llorca *et al.*, 2019), which might be regulated by spatiotemporal changes and different molecular influences on NSCs during development (Ma *et al.*, 2020).

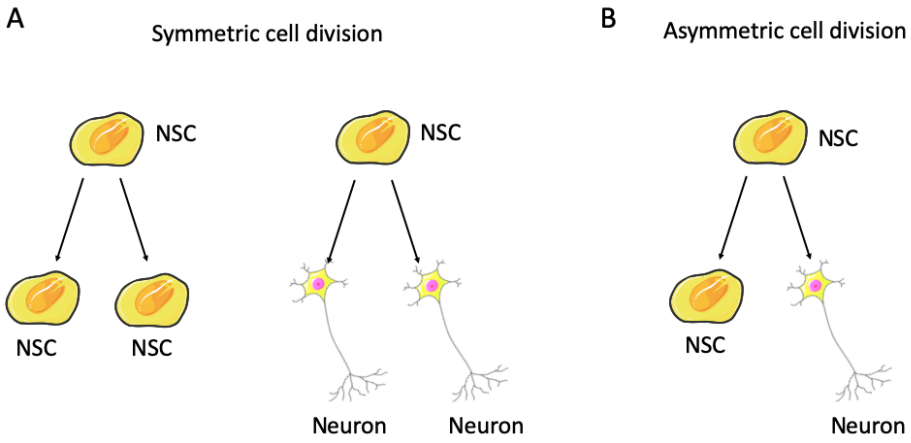

Figure 1.2: Schematic of symmetric and asymmetric cell division. (A) Symmetric cell division means that a stem cells gives rise to two cells of the same cell type. **(B)** The term asymmetric cell division describes the process in which one stem cell divides into cells of different types. Elements of the figure were adapted from SMART Servier Medical Art.

The spatiotemporal control of NSC division mode, their quiescent state and the timing of differentiation is based on different molecular mechanisms, specifically on transcriptional clues (Periyasamy and Mowry, 2022).

In the past, different genes were identified, which induce NSC differentiation or are responsible for their maintenance.

1.1.2 Transcriptional regulation of brain development

The tight and strictly regulated control of gene expression is necessary for proper stem cell maintenance and differentiation. Gene expression could be for instance coordinated by controlling processes up- or downstream of gene transcription by micro RNAs (miRNAs) and transcription factors (Lang and Shi, 2012; Martynoga *et al.*, 2012) (Figure 1.3).

The NOTCH pathway is well-known to regulate stem cell maintenance and to inhibit premature neuronal differentiation (Lasky and Wu, 2005). The engagement of NOTCH by its ligand triggers the expression of basic helix-loop-helix (bHLH) transcription factors, such as hairy and enhancer of split (HES) and hairy/enhancer-of-split related with YRPW motif protein (HEY) (Andersson *et al.*, 2011), which are transcriptional repressors of pro-neural genes. Thus, HES and HEY inhibit neuronal differentiation, while they maintain stem cell proliferation (Sakamoto *et al.*, 2003; Kageyama *et al.*, 2007). The expression pattern of HES oscillates inversely to the oscillating expression of the bHLH transcription factor neurogenin 2 (NGN2) (Shimojo *et al.*, 2011). The switch from oscillated expression towards sustained expression of NGN2 is critical for neuronal differentiation (Barton and Fendrik, 2013) (Figure 1.3 A). Sustained NGN2 expression has distinct pro-neuronal effects, since NGN2 expression drives the formation of neurons from stem cells and is nowadays often used for direct forward programming approaches to turn pluripotent or neural stem cells into neurons (Ho *et al.*, 2016) (for additional information see Chapter 1.5).

However, other transcription factors are essential for NSC maintenance and avoid pre-mature differentiation, such as sex determining region Y-box 2 (SOX2) and paired box 6 (PAX6).

The transcription factor SOX2 is demonstrated to be important for NSC maintenance and inhibition of neuronal differentiation (Bani-Yaghoub *et al.*, 2006), with decreasing protein levels during neuronal development (Cui *et al.*, 2018). Dynamic ubiquitylation and subsequent degradation of SOX2 is essential for proper regulation of NSC maintenance and differentiation, as knockdown of the SOX2 ubiquitinating machinery leads to increased SOX2 levels and inhibited neuronal cell differentiation (Cui *et al.*, 2018). Conversely, the repression of SOX2 induces cell cycle exit of NSCs and the expression of early neuronal differentiation genes (Graham *et al.*, 2003). On the molecular level, SOX2 seems to act upstream of the NOTCH signaling pathway, as its overexpression increases the expression level of *Notch1* and *Hes5*. Thus, SOX2 might regulate NSC maintenance indirectly via the NOTCH signaling pathway (Bani-Yaghoub *et al.*, 2006) (Figure 1.3 B).

Another transcription factor representing a NSC marker like SOX2 is PAX6 (Gómez-López *et al.*, 2011). During development, *Pax6* is expressed in the proliferative neuroepithelium (Duan *et al.*, 2013). In cortical progenitor cells, PAX6 controls their maintenance and inhibits neuronal differentiation, since the knockout of *Pax6* shortens the cell cycle of cortical NSCs, increases the proportion of asymmetric cell division and enhances the expression of neural-specific markers early in corticogenesis (Estivill-Torrus *et al.*, 2002). Furthermore, Sansom and colleagues drew a more defined picture of the role of PAX6 during NSC maintenance and differentiation control. The expression level of *Pax6* in the neocortex determines if NSCs proliferate or differentiate (Figure 1.3 C).

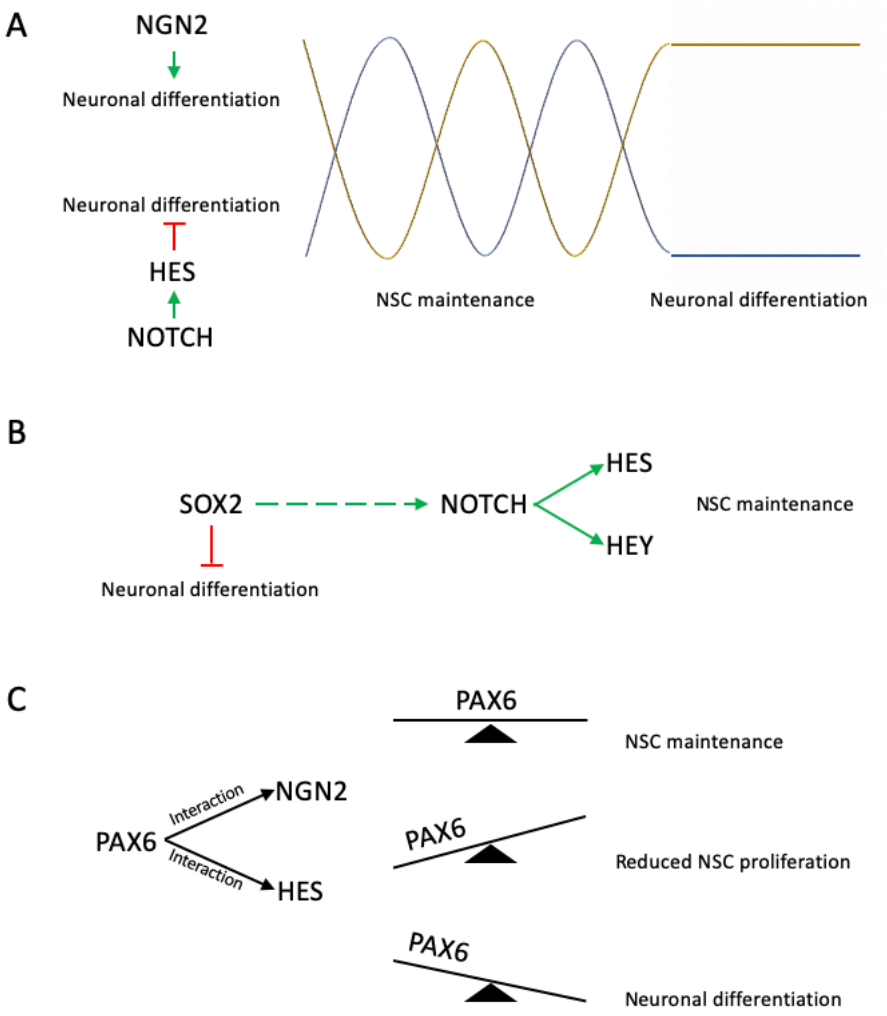

Figure 1.3: Schematics of the function of different important transcriptional regulation pathways involved in neuronal differentiation. (A) NGN2 is a transcription factor strongly expressed during neuronal differentiation. The expression of the transcription factor HES is regulated by NOTCH signaling and is downregulated during neuronal differentiation. NGN2 and HES expression display inverse oscillation during NSC maintenance. The schematic is adapted from Shimojo *et al.,* 2011. **(B)** SOX2 is a transcription factor important for NSC maintenance, which counteracts neuronal differentiation. SOX2 expression and NOTCH expression are positively correlated and SOX2 expression influences NOTCH expression, as well as the expression of its target genes HES and HEY. **(C)** The transcription factor PAX6 interacts with the transcription factors NGN2 and HES. PAX6 expression is important for NSC maintenance. Downregulation of PAX6 is associated with reduced NSC proliferation, while upregulation of PAX6 leads initially to neuronal differentiation.

Thus, elevated PAX6 levels promote neuronal differentiation at the expense of progenitor cell self-renewal by promoting the expression of downstream target genes. However, decreased PAX6 levels negatively affect cortical NSC self-renewal by reducing the expression of cell cycle regulators. Furthermore, PAX6 interacts with the bHLH transcription factors NGN2, achaete-scute homolog 1 (ASCL1) and HES1 to regulate NSC self-renewal and neurogenesis in an antagonistic network (Sansom *et al.*, 2009).

However, transcriptional regulation is not only restricted to the interaction of transcription factors and also includes the interplay of miRNAs and transcription factors. Previous studies in the Institute of Reconstructive Neurobiology have unraveled the importance of two miRNAs for the control of NSC proliferation and neuronal differentiation, miR9/9* and miRNA181 a/a* (Figure 1.4).

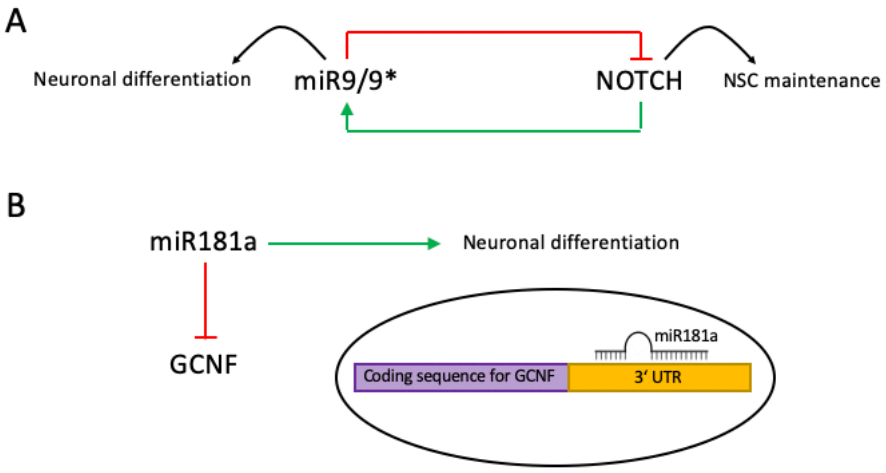

Figure 1.4: Schematics of the function of miR9/9* and miR1181a during neuronal differentiation. (A) The pro-neural miR9/9* inhibits NOTCH, an important regulator of human NSC maintenance. NOTCH on the other hand positively regulates miR9/9* expression. Schematic is adapted from Roese-Koerner *et al.*, 2016. **(B)** MiR181a induces neuronal differentiation by inhibiting GCNF translation via direct binding to its 3'UTR.

MicroRNA9/9* was demonstrated to interact and fine-tune the NOTCH pathway and to induce neuronal differentiation of NSCs. Roese-Koerner and colleagues showed, that miR9/9* regulates *NOTCH2* expression by binding to the 3'Untranslated region (UTR) of the *NOTCH2* gene, ultimately leading to downregulated expression. In turn, the level of NOTCH protein influences the expression level of miR9/9*, since the binding of the NOTCH receptor with its ligand mediates an intracellular signaling that induces miR9/9* expression, thus generating a negative feedback loop (Roese-Koerner *et al.*, 2016) (Figure 1.4 A). Another miRNA described with pro-neuronal effects is miR181a. The expression profile of 330 miRNAs in human embryonic stem cells (hESC), in NSCs derived from those hESCs and in their neuronal progeny demonstrated that miR181a/a* is expressed in human NSCs (hNSCs) with increasing levels during neuronal differentiation. In a paradigm of neuronal differentiation of hNSCs, Stappert *et al.,* confirmed that miR181a promotes the shift from hNSC self-renewal to neuronal differentiation (Stappert *et al.*, 2013). The analysis of putative target genes of miR181a revealed the germ cell nuclear factor (GCNF) as possible target gene, and indeed, binding assays could confirm binding of miR181a to the 3'UTR of GCNF, inducing downregulation of GCNF expression (Stappert, 2015, doctoral thesis) (Figure 1.4 B).

The herein described miRNAs and transcription factors and their interactions, which regulate NSC proliferation and differentiation and by this overall brain development, are only a small fraction of already reported findings about the transcriptional regulation of brain development. However, many factors and their interplay in the complex networks are still under investigation or unknown. The wide use of cell models for human brain development based on human pluripotent stem cells (hPSCs) facilitates the research and investigation of important factors involved in human NSC maintenance and neuronal differentiation *in vitro.*

1.2 Modeling human brain development *in vitro*

Due to the unique features and complexity of the human brain across the entire animal kingdom, it is impossible to study molecular mechanisms of human brain development *in vivo* (Kelava and Lancaster, 2016). However, to study human development *in vitro*, reliable cell-based assays are essential. These

cells must be able to self-renew and maintain their properties over time, but also need to have the capability to differentiate into different more specific progeny. Therefore, hPSCs and their neural and neuronal progeny are commonly used for human brain development studies, as they are a close proxy for human neural development (Koch *et al.*, 2009; Shi *et al.*, 2012; Reinhardt *et al.*, 2013).
Proliferative NSCs derived from hPSCs and/or their more mature neuronal progeny can be used to analyze early human brain development or might be used for drug-screenings or cell replacement therapies (Armstrong and Svendsen, 2000; Kim and Jin, 2012). In the context of this study, human NSCs are utilized to study the distinct functions of transcription factors during neuronal differentiation.

1.2.2 Human pluripotent stem cells

In the past, cell culture-based research of development was often performed using cells derived from cancerous tissue (Sattler *et al.*, 2004; Hentschke *et al.*, 2006), which are easy to culture and to manipulate (Josephson *et al.*, 2007). Cancer cells are able to self-renew and differentiate (Jostock *et al.*, 1998; Coyle *et al.*, 2011). However, the missing genomic integrity of cancer cells makes them prone for mutations and they might not represent suitable models for physiological differentiation (Abbas *et al.*, 2013; Yao and Dai, 2014). Human PSCs overcome this issue and are nowadays commonly used to study human development *in vitro*. Human PSCs, such as human embryonic stem cells (hESCs) and human induced PSCs (hiPSCs), have the potential to self-renew and are able to differentiate upon certain clues into all cells of the three germ layers (Petros *et al.*, 2011). In 1998, the finding of maintaining hESCs, which were isolated from the human blastocyst, in culture and the development of protocols to differentiate them into more specified cell types were major achievements for cell-based research of developmental processes (Thomson *et al.*, 1998). Furthermore, nine years later, Takahashi and Yamanaka discovered that the forced expression of OCT3/4, SOX2, KLF4 and c-MYC in human somatic cells leads to their reprogramming into cells displaying pluripotency characteristics (Takahashi *et al.*, 2007). Thus, somatic cells can be reprogrammed into cells that display not only morphological similarities to ESCs, but are also highly similar regarding gene expression and chromatin state (Wernig *et al.*, 2007). Over the last years, various protocols were described to generate iPSCs from somatic cells, relying on forced transcription factor expression or altered miRNA expression mediated by inversive and non-inversive approaches or also induction with small molecules (Fusaki *et al.*, 2009; Anokye-Danso *et al.*, 2011; Kim *et al.*, 2020).
Both hESCs and hiPSCs are a valuable source for the generation of hNSCs. Detailed description and analysis of the molecular mechanisms driving differentiation of hPSCs towards defined human NSCs and then further into neuronal subtypes give insights into the molecular networks regulating human neurogenesis.

1.2.3 Neural stem cells derived from pluripotent stem cells

Various different types of NSCs can be generated from PSCs, that differ from each other with respect to their morphology, their abilities to form neural rosettes or their potential to differentiate into neurons (or preferentially glial cells), but also with respect to the mature neuronal types they are able to yield. These *in vitro* generated NSCs are supposed to display some similarities to the various *in vivo* NSCs which are populating the developing brain at different temporal phases and spatial regions and are

causing the complex and multicellular formation of the brain (Conti and Cattaneo, 2010). Human NSCs can be generated from hPSCs using different protocols (Galiakberova and Dashinimaev, 2020). For the generation of long-term self-renewing neuroepithelial-like stem (lt-NES) cells - a cell type, which was established in our institute - embryoid bodies of hPSCs were plated and the outgrowing neural rosette forming cells were isolated and cultured as neurospheres in the presence of fibroblast growth factor 2 (FGF2). These neurospheres were triturated and the obtained cells were cultured in FGF2 and epidermal growth factor (EGF) containing medium (Koch *et al.*, 2009).

Other neural differentiation protocols rely on specific culture conditions based on the molecular understanding of neural differentiation *in vivo*. In particular, neuroepithelial cells can be obtained from hPSCs by suppressing the Activin/TGFß/Nodal and BMP pathways (Chambers *et al.*, 2009), which are both described to inhibit neural fate decisions early during *in vivo* development (Meyers and Kessler, 2017; Manzari-Tavakoli *et al.*, 2022) (see Chapter 1.1). Both pathways rely on SMAD molecules for their downstream signaling, this is why the approach of suppressing the Activin/TGFß/Nodal and BMP pathways is named Dual-SMAD-inhibition (Chambers *et al.*, 2009; Ikushima and Miyazono, 2010; Wang *et al.*, 2014). The blockage of these two pathways by small molecules, in high density cultures of hPSCs leads to a highly effective differentiation of hPSCs into cortical stem and progenitor cells (Shi *et al.*, 2012).

Dual-SMAD-inhibition and activation of wingless-related integration site (WNT) and sonic hedgehog (SHH) signaling by using small molecules can be used to differentiate PSCs into a specific type of NSCs, into so called small molecule neuronal precursor cells (smNPCs), which have the potential to differentiate into cells of the neural crest lineage, as well as into neuronal and glial cells (Reinhardt *et al.*, 2013). WNT signaling regulates the development of cells at the lateral border of the neural plate, while SHH counteracts WNT signaling leading to the formation of ventral neural tube fates (Ulloa and Martí, 2009). SmNPCs are maintained under self-renewal conditions by adding WNT and SHH agonists to the medium. Under proliferating conditions, smNPCs grow as single colonies, displaying uniform expression of zonula occludens-1 (ZO1, a tight junction protein) and N-cadherin (a cell adhesion molecule). However, under FGF2 treatment, smNPCs form neural rosettes with apical expression of ZO1 and N-cadherin, which marks them as pre-rosette neuroepithelial cells (Reinhardt *et al.*, 2013). The formation of rosettes by neuroepithelial cells *in vitro* is a common feature of many other neural stem cells, such as neural rosette cells (R-NSCs) (Elkabetz *et al.*, 2008) or lt-NES (Koch *et al.*, 2009) (Figure 1.5). In contrast to smNPCs, R-NSCs, which also have the ability to differentiate into cells of the neural crest and neural tube linages, can only be expanded as proliferative cells for a limited time. Furthermore, smNPCs are claimed to have a bigger differentiation potential as lt-NES cells, since smNPCs can be robustly differentiated into motor neurons and midbrain dopaminergic neurons (Reinhardt *et al.*, 2013). Nevertheless, smNPCs differentiate into GABAergic neurons upon induction of NGN2 expression and NOTCH inhibition, similar to lt-NES cells after growth factor withdrawal (Strauß *et al.*, 2021; Falk *et al.*, 2012).

In this study, smNPCs derived from hiPSCs were used as reliable model for human neurogenesis.

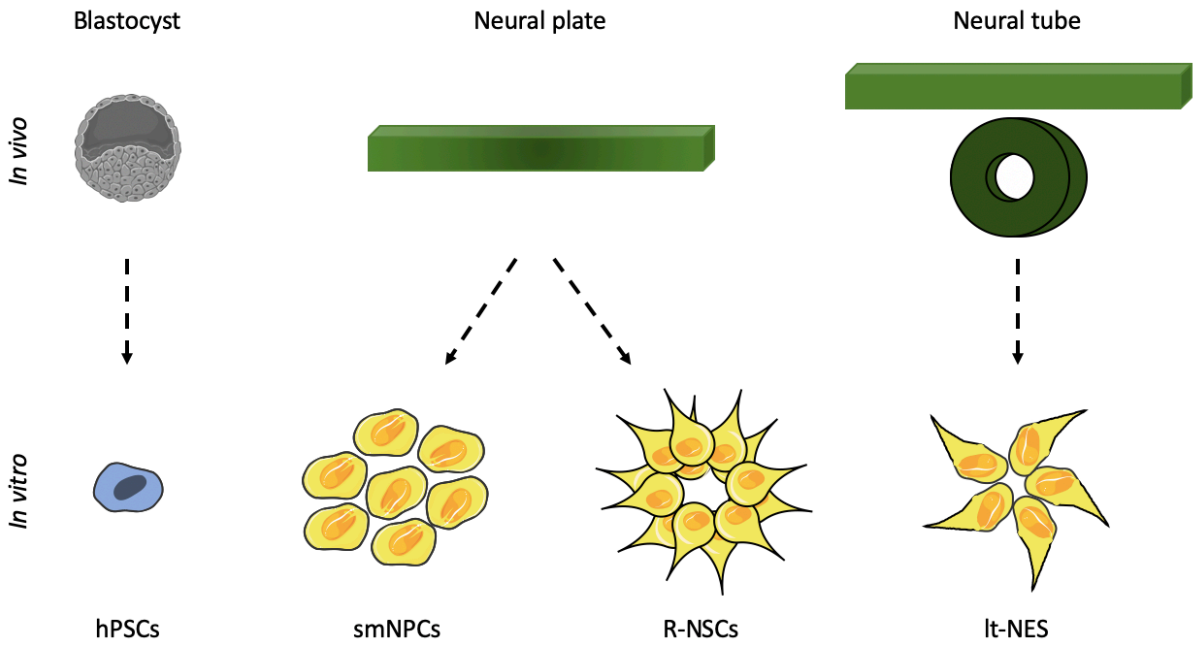

Figure 1.5: Overview of different types of *in vitro* generated stem cells and their developmental pendants. The *in vitro* generated human NSCs could be matched based on their morphology, gene expression and differentiation potential to different *in vivo* stages of neuronal development. Illustration is adapted from Conti and Cattaneo, 2010 and different elements of the figure were adapted from SMART Servier Medical Art.

1.2.4 iPSC-derived 3D cortical organoids

In comparison to 2D cultures of human iPSCs, NSCs and neurons, which are commonly used to analyze molecular mechanisms during human brain development, the utilization of 3D cultures, of so-called brain organoids, has certain advantages for studying cellular interactions during human brain development (Agboola *et al.*, 2021). The resemblance of the cytoarchitecture of brain organoids with the embryonic human brain make them ideal to study the development of the brain on cellular and structural level (Qian *et al.*, 2019). Initially, identical undifferentiated hPSCs aggregate into spherical structures. Upon neural induction clues, these hPSCs differentiate into various cell types of the human brain, which demonstrate positioning similar to the embryonic human brain (Renner *et al.*, 2017). Structurally, brain organoids display ventricular-like and subventricular zones, which are formed by neuroepithelial stem cells and ventricular radial glial cells (vRGs), and zones containing neuronal cells (Krefft *et al.*, 2018). During maturation of the brain organoids, primate specific outer radial glial cells (oRGs), that form the outer subventricular zone (Hansen *et al.*, 2010; Pollen *et al.*, 2015), as well as differentiated and mature neurons, which express specific cortical layer markers, emerge (Lancaster *et al.*, 2013; Camp *et al.*, 2015). Additionally, mature brain organoids could also contain glial cells (Dezonne *et al.*, 2017; Yakoub, 2019).

Thus, brain organoids mirror main characteristics of the embryonic brain on molecular, cellular and structural level. However, certain physiological features as gyrification and complex neuronal circuit formation are not yet fully recapitulated (Matsui *et al.*, 2020; Scott and Huang, 2022). Nevertheless, brain organoids are already widely and successfully used as model systems to understand human brain development and neural and neuronal disorders (Di Lullo and Kriegstein, 2017).

In summary, the complexity of brain organoids makes them promising *in vivo* models to study neurogenesis (Centeno *et al.*, 2018), however this complexity aggravates molecular studies of one specific gene involved in a particular step of neurogenesis (Iefremova *et al.*, 2017).

1.3 The role of GCNF in development

The molecular mechanisms of the various well-controlled steps of neurogenesis are still under investigation and many acting factors are not yet known (Mira and Morante, 2020). Experiments in different animal studies and various cell lines suggest that the nuclear receptor (NR) germ cell nuclear factor (GCNF) affects several steps of neural development as NSC specification, neuronal differentiation and brain regionalization (Barreto, Borgmeyer *et al.,* 2003; Sattler *et al.*, 2004; Chung *et al.*, 2006; Akamatsu *et al.*, 2009).

1.3.1 Structure of GCNF and its mode of action

Human GCNF (official gene symbol: *NR6A1*) is located on chromosome 9 (Agoulnik *et al.*, 1998), colocalizing with the MIR181A2 host gene (MIR181A2HG) (Mei *et al.*, 2017) and the nuclear receptor NR5A1 (Jiao *et al.*, 2013). This colocalization as well as its amino acid identity are conserved from mouse to human. Human GCNF is to 98.3 % and 82.7 % homolog to the according mouse and *Xenopus laevis* proteins, respectively (Kapelle *et al.*, 1997).

GCNF is described as one of the 48 members of the NR family of ligand-dependent transcription factors, which are involved in different physiological mechanisms, like embryonic development or NSC fate decisions (Stergiopoulos and Politis, 2013; Wagner and Cooney, 2013). The members of the NR family are sorted into six different subgroups according to their homology. GCNF is the only member of subgroup NR6, due to alterations in its structure that other NRs do not share. The majority of nuclear receptors consist of the following four domains, which are the N-terminal domain (NTD), the highly conserved DNA-binding domain (DBD) and a hinge region, which connects the DBD with the N-terminal ligand binding domain (LBD) (Figure 1.6 A). The NTD is highly unstructured and variable between the different nuclear receptors. It contains the activator function-1 region (AF-1), which interacts with various different co-regulatory proteins dependent on cell and promoter specificity (Weikum *et al.*, 2018). The DBD is highly conserved among the NR family and during evolution (Süsens and Borgmeyer, 2001; Weikum *et al.*, 2016). The actual DNA binding is mediated by two zinc finger (ZF) motifs. The first ZF interacts with the major groove of the DNA and allows base-specific binding. In case of GCNF, electrophoretic mobility assays (EMSA) demonstrated GCNF binding to an AGGTCA core motif, which is contained in extended half-sites, such as TCAAGGTCA or in a direct repeat with zero spacer (DR0) motif, AGGTCAAGGTCA (Figure 1.6 B) (Chen *et al.*, 1994; Yan *et al.*, 1997; Fuhrmann *et al.*, 2001). The second ZF motif mediates non-specific contacts with the DNA backbone and an additional peptide loop contains residues for dimerization of NRs. In contrast to other NRs, the DBD of GCNF contains a C-terminal extension (CTE), which mediates additional base-specific DNA binding within the minor DNA groove. The LBD structure varies among the NRs, which leads to a recognition of different ligands by different NRs. No ligand is identified for GCNF yet, which makes it an orphan NR. Additionally, the LBD of GCNF does not contain an activation function helix as the LBD of other NRs. The major alterations in its LBD structure cause that GCNF remains in its own category of subfamily 6 (Weikum *et al.*, 2018).

The AF-2 region is described to drive transcriptional activation after ligand binding and subsequent interaction with various co-regulatory proteins (Slagsvold *et al.*, 2000), whereas the interaction of GCNF with its DNA binding sequence leads to transcriptional repression of its target genes (Wang *et al.*, 2013). The mechanism how GCNF facilitates gene repression is still under investigation and may appear to be cell and context specific. It is suggested that GCNF binds to DNA as a homodimer (Figure 1.6 C) (Weikum *et al.*, 2016) or that GCNF interacts with the DNA as part of the transiently retinoid-inducer factor (TRIF) complex, forming hexameric GCNF structures, upon retinoic acid (RA) treatment (Figure 1.6 D) (Gu, Morgan, *et al.*, 2005). GCNF might exert its repressive function either by interacting with different co-repressors, such as nuclear receptor co-repressor-1 (NCoR1) and silencing mediator for retinoid or thyroid-hormone receptors (SMRT) (Yan and Jetten, 2000; Fuhrmann *et al.*, 2001) or by competing with other NRs and transcriptional activators (e.g. SF-1/NR5A1 or LRH-1/NR5A2) for the binding of the DR0 motif (Weikum *et al.*, 2016). Thus, GCNF mediated downregulation of octamer-binding transcription factor 4 (OCT4) expression is competing to liver receptor homolog-1 (LRH-1) binding. The OCT4 promoter consists of three DR0 motifs (Park *et al.*, 2018), which are bound by LRH-1, leading to transcriptional activation, or by GCNF, which represses *Oct4* expression via DNA methylation mediated by GCNF upon its DNA binding (Gu *et al.*, 2011).

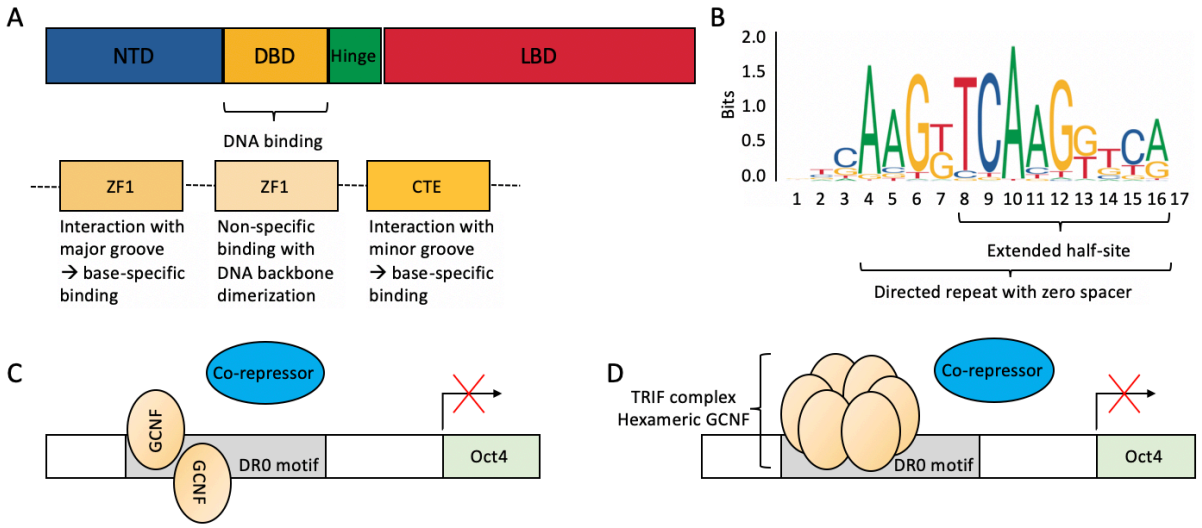

Figure 1.6: Structure of different domains of GCNF protein, its DNA binding site and the proposed function on gene transcription. (A) GCNF consists of the following four domains: N-terminal domain (NTD), the DNA-binding domain (DBD), a hinge region and the ligand binding domain (LBD). DNA binding is mediated via two zinc fingers (ZF) and a C-terminal extension (CTE) by binding to the **(B)** DR0 sites AAGTTCAAGGTCA (a directed repeat with zero spacer) or the extended half-site TCAAGGTCA (Bitscore model by JASPAR online tool). The schematic in A is adapted from Weikum et al., 2018. **(C)** GCNF is binding to DNA as homodimer at the DR0 motif within the regulatory region of its target genes, such as the Oct4 gene and leads to inhibition of its transcription by recruiting certain co-repressors. The illustration is modified from Weikum et al., 2016. **(D)** Upon treatment with retinoic acid, GCNF forms a hexameric complex – the TRIF complex – which binds DNA at the DR0 motif within the regulatory region of its target genes, e.g. Oct4 and recruits co-repressors to mediate transcriptional repression.

1.3.2 GCNF expression and its function during embryonic and neural development

GCNF is predominantly expressed in germ cells of different adult vertebrates (Chen *et al.*, 1994; Hirose *et al.*, 1995; Joos *et al.*, 1996; Süsens *et al.*, 1997). During the development of germ cells, GCNF is

expressed in spermatogonial cells and growing oocytes and in their common ancestors, the primordial germ cells (Zechel, 2005; Sabour *et al.*, 2014). GCNF might influence fertility and reduces *Oct4* expression in primordial germ cells, which stimulates retinoic acid gene 8 (*Stra8*) expression to induce meiosis and further development of primordial germ cells (Sabour *et al.*, 2014).

In the context of murine development, the expression pattern of GCNF and its proposed function were described. At embryonic day (E)6.5, GCNF is expressed in all three germ layers and also in the extraembryonic tissue (Fuhrmann *et al.*, 2001). With further embryonic development, the GCNF expression is more and more restricted. Thus at E8.5, GCNF expression is only detected in the proliferating neuroepithelium and in the underlying mesoderm (Süsens *et al.*, 1997; Fuhrmann *et al.*, 2001) and until E9.5, GCNF expression levels decrease further in the forebrain and midbrain (Chung *et al.*, 2006). It is widely assumed that GCNF expression, apart from its expression in the germ cells, declines even further from E10.5 (Chung and Cooney, 2001; Chung *et al.*, 2001). However, Bauer *et al.* demonstrated GCNF expression at E15 in the marginal zone of the neuroepithelium (Bauer *et al.*, 1997).

The knockout of GCNF in developing mouse embryos is lethal at E10.5 due to cardiovascular failure. From E8.5 on, gross morphological malformations are observed in GCNF knockout animals, such as failure of body axis turning, failure of neural tube closure, an impaired somitogenesis and the formation of a protruding tailbud, which is pushed out of the yolk sac (Chung and Cooney, 2001; Chung *et al.*, 2001). These malformations could be caused by persisting expression of *Oct4* and *Nanog* in the somatic tissue after gastrulation due to their missing repression by GCNF (Fuhrmann *et al.*, 2001; Gu, LeMenuet *et al.*, 2005). In *Xenopus laevis*, *GCNF* expression is enriched at the neurula stages (Joos *et al.*, 1996; David *et al.*, 1998) and its knockdown leads to inadequate neural plate cell migration and a failure of neural tube closure (David *et al.*, 1998; Barreto, Reintsch *et al.*, 2003). GCNF knockout mouse embryos display an underdeveloped midbrain, probably due to the reduced expression of various genes responsible for the formation of the midbrain-hindbrain boundary (Chung *et al.*, 2006). Along this line, altered expression of several important midbrain-hindbrain boundary marker genes leading to a caudal shift of the boundary was observed after GCNF knockdown in *Xenopus laevis* embryos (Song *et al.*, 1999; Barreto, Borgmeyer *et al.*, 2003).

Additionally, Oct4 repression by GCNF is required for full commitment of primitive neuroepithelial stem cells to neural-committed neuroepithelial stem cells, which can only differentiate into neural cell types (Akamatsu *et al.*, 2009). Experiments using murine pluripotent cells revealed induced GCNF expression upon treatment with RA (Sattler *et al.*, 2004; Gu, Morgan, *et al.*, 2005) to stimulate neuronal differentiation (Janesick *et al.*, 2015). Sattler *et al.* even demonstrated that overexpression of GCNF in mouse embryonic carcinoma cells could promote neuronal differentiation (Sattler *et al.*, 2004). Furthermore, GCNF expression was induced in *Xenopus laevis* embryos treated with RA, which might be stabilized in a feedback loop with RA signaling. GCNF downregulates the expression of the RA-degrading enzyme cytochrome P450 26A1 (CYP26), which leads to higher RA levels (Barreto, Borgmeyer *et al.*, 2003).

Only recently, expression of GCNF in murine hippocampal neurons was demonstrated. Increased expression of GCNF in these cells affects the cyclic adenosine monophosphate-response element binding protein (CREB)-brain-derived neurotrophic factor (BDNF) signaling, which leads to depression-like behavior in mice (Tan *et al.*, 2022).

In the context of human brain development, experiments using hPSCs demonstrated that GCNF is required to repress OCT4 and regulates differentiation of these stem cells (Wang *et al.*, 2016; Braun *et al.*, in revision). Human ESCs display prolonged OCT4 expression upon GCNF knockdown also under differentiating conditions, while the overexpression of GCNF could drive differentiation of hESCs by altering the expression of most of the pluripotency genes directly or indirectly (Wang *et al.*, 2016). Utilizing GCNF knockout iPSCs, Braun and colleagues demonstrated the importance of GCNF for iPSCs to exit from pluripotency and differentiate especially towards cells with neural identity (Braun *et al.*, in revision). An initial upregulation of GCNF expression upon RA treatment of human teratocarcinoma cells with subsequent decreasing mRNA and protein levels of GCNF was observed by Schmitz *et al.*, which led to the hypothesize that GCNF plays a crucial role in human neural determination and differentiation (Schmitz *et al.*, 1999). In the process of RA induced differentiation of this cell line, expression of CRIPTO-1, which is a negative regulator of neural development (Parisi *et al.*, 2003), is repressed by GCNF (Hentschke *et al.*, 2006).

In neural stem cells, GCNF expression is controlled by miR-181a (Stappert, 2015, doctoral thesis), which is demonstrated to promote the shift from hNSC self-renewal to neuronal differentiation (Stappert *et al.*, 2013). MiR181a might exert its neuronal differentiating promoting function by inhibiting GCNF, which is directly targeted and inhibited by miR181a, since overexpression of GCNF decreases the development of neurons from NSCs (Stappert, 2015, doctoral thesis) (Table 1.1).

Altered expression of GCNF is also linked to various types of cancer, e.g. prostate cancer (Mathieu *et al.*, 2013), gastric cancer (Zhou *et al.*, 2020) and liver cancer (Wang *et al.*, 2019). In testicular cancer cells, miR-196a-5p expression is downregulated, which increases GCNF expression in these cells. Additionally, GCNF directly targets and represses E-cadherin, while increasing microtubule-associated protein 2 (MAP2) expression upon RA-induced neuronal differentiation of cancer cells. Thus, the authors claim, that GCNF is involved in cell proliferation and cellular junction and aggregation (Liu *et al.*, 2020). Another molecular link of GCNF and cancer, was hypothesized by Gurtan and colleagues, since the tumor-suppressive miRNA let-7 is repressing GCNF and a mid-gastrulation developmental program in adult mesenchymal stem cells (Gurtan *et al.*, 2013).

Moreover, various studies describe modified GCNF expression in the context of donkey, sheep and swine growth (Fang *et al.*, 2019; Zhang *et al.*, 2019; Ijiri *et al.*, 2021). In sheep, as well as in swine, GCNF expression levels and the number of vertebrae, which influences the carcass length of the animals (King and Roberts, 1960), are associated (Mikawa *et al.*, 2007; Zhang *et al.*, 2019).

In summary, GCNF expression is involved at different levels in physiological and pathophysiological development. GCNF affects overall embryonic development and especially brain development, which could be demonstrate *in vivo* using mouse and *Xenopus laevis* models, as well as *in vitro* using murine and human cell lines. GCNF plays an important role as transcriptional regulator of various different genes involved in stem cell maintenance or differentiation.

Table 1.1: Overview of described GCNF target genes in the context of neural and neuronal development, which were identified as direct or indirect target genes in different *in vivo* and *in vitro* models.

In vivo/in vitro	System	Cell line	Target gene and identification method		Phenotypic observation	Reference
			indirect	direct		
Both	Mouse	PCC7-Mz1, mouse embryonal carcinoma cell line		Confirmed binding of GCNF to DR0 motif	GCNF expression is induced in PCC7-Mzl cells upon RA treatment, in embryonic mouse brains (E15) GCNF expression is displayed by post-mitotic cells of the neuronal lineage	Bauer *et al.* , 1997
Both	Mouse	P19, mouse embryonal carcinoma cell line		*Oct4* is bound by TRIF complex consisting of GCNF demonstrated with EMSA assays	GCNF knockdown abolishes Oct4 expression in certain differentiating somatic cells (anterior neuroepithelium of the head-fold or the presomatic mesoderm in the posterior, E8.5–E8.75)	Fuhrmann *et al.* , 2001
In vitro	Mouse	PCC7-Mz1, mouse embryonal carcinoma cell line	Delay in Nestin downregulation and Map2 and Synaptophysin upregulation upon GCNF downregulation		Impaired neuronal differentiation of neural progenitor cells upon downregulation of GCNF; GCNF KO NPCs require neuronal functionality with significant delay	Sattler *et al* ., 2004
Both	Mouse	Embryonic stem cells	*Stella, Sox2, Fgf4* expression upregulated in GCNF knockout cells during RA induced differentiation	*Oct4* and *Nanog* are upregulated in GCNF knockout cells, GCNF binding to their promotor region was confirmed in ChIP assays	Prolonged *Nanog* expression in GCNF KO mouse embryos, remaining *Nanog* expression in neural fold	Gu, LeMenuet *et al.* , 2005
In vivo	Mouse		Expression of *Gbx2, En1/2, Pax2/5, Fgf8* and *Wnt1* is altered in GCNF KO embryos		Alterated expression of midbrain/hindbrain marker genes due to GCNF KO, improper establishment of the isthamic organizer	Chung *et al.* , 2006
Both	Mouse	Embryonic stem cells and primitive neural stem cells		Oct4 via ChIP	Upon GCNF KO, impaired transition of primitive NSCs into definitive NSCs, Gcnf KO cells display prolonged Oct4 expression	Akamatsu *et al.*, 2009
Both	Mouse	Mouse adult unipotent germline stem cells	*Oct4* upregulated upon GCNF downregulation		Loss of GCNF leads to failure in spermatogonia and oocytes production in developing testes and ovaries, respectively	Sabour *et al* ., 2014
In vivo	*Xenopus laevis*		xRARγ2 expression was downregulated upon Gcnf knockdown		Overexpression of GCNF impaired postrior neural development, as somitogensis. Knockdown of Gcnf affects differentiation of the neural tube and anterior structures (e.g. cement gland and eyes)	David *et al* ., 1998
In vivo	*Xenopus laevis*		Altered spatial expression of fibronectin and overall reduced expresison of integrins α5 and α6 upon GCNF knockdown		GCNF knockdown embryos display impaired organogenesis including short and curved main body axis, failure of the neural tube closure, malformed proctodeum, highly irregular somite pattern and defective head differentiation	Barreto, Reintsch, *et al* ., 2003
In vivo	*Xenopus laevis*		xCYP26 expression is derepressed in xGCNF KO embryos, overexpression of antimorph xGCNF activates xCYP26		Knockdown of xGCNF impairs hindbrain patterning similar to reduced RA signaling	Barreto, Borgmeyer, *et al.*, 2003
In vitro	Human	NT2/D1 pluripotent embryonal carcinoma cell line		CRIPTO-1 and CRIPTO-3 are repressed by GCNF, which was confirmed by EMSA and ChIP assays		Hentschke *et al.* , 2006
In vitro	Human	Human neural stem cells (lt-NES)	Pro-neural bHLH transcription factors NEUROD1, NEUROD4 and NEUROG1 display putative GCNF binding sites in their promotor region, their expression is downregulated when GCNF is overexpressed		Overexpression of GCNF stabilizes neural rosette morphology and impairs neuronal differentiation	Laura Stappert, 2015, doctoral thesis
In vitro	Human	Human embryonic stem cells (H9)		*OCT4* is repressed by GCNF, binding confirmed by ChIP	Alteration of GCNF expression affects global gene expression, prolonged OCT4 expression in GCNF KO cells	Wang *et al.* , 2016
In vitro	Human	Human induced pluripotent stem cells	Altered expression of pluripotency genes in GCNF KO cells compared to parental cell line		Delayed differentiation of GCNF knockout iPSCs	Braun *et al* ., in preparation

Abbreviation: ChIP: Chromatin immunoprecipitation, E: Embryonic day, EMSA: Electrophoretic mobility shift assay, KO: Knockout, NPC: Neural progenitor cell, NSC: Neural stem cell, RA: Retinoid acid, TRIF: TIR-domain-containing adapter-inducing interferon-β.

1.4 The transcription factor BCL11A in the nervous system

B cell CLL/lymphoma 11a (BCL11A) is a transcriptional repressor and associates with the BAF (mammalian SWI/SNF) complex, that operates as an ATP-dependent chromatin remodeler (Figure ***1.7*** A) (Kadoch *et al.*, 2013; Simon *et al.*, 2020)

Different functions for BCL11A are reported. On one hand, BCL11A is expressed in various blood cells and plays a role during the transition from fetal to adult erythropoiesis (Sankaran and Orkin, 2013) and on the other hand BCL11A functions as a proto-oncogene in the immune system (Satterwhite *et al.*, 2001). Additionally, dysregulated BCL11A expression is also associated with neurological disorders and impaired neurogenesis (Simon *et al.*, 2020).

1.4.1 BCL11A protein structure and isoforms

The evolutionary conserved *BCL11A* gene is located on human chromosome 2 (Satterwhite *et al.*, 2001) and can be spliced differently after transcription, leading to the generation of four different isoforms (Liu *et al.*, 2006). All resulting proteins consist of a N-terminal C2HC ZF and nucleosome remodeling deacetylase (NuRD) domain, while the number of the C-terminal C2H2 ZF domain varies between the different isoforms (Figure 1.7 B) (Liu *et al.*, 2006; Simon *et al.*, 2020).

The C2HC motif is suspected to be responsible for dimerization and nuclear translocation, while the C2H2 ZF domain mediates DNA binding (Simon *et al.*, 2020).

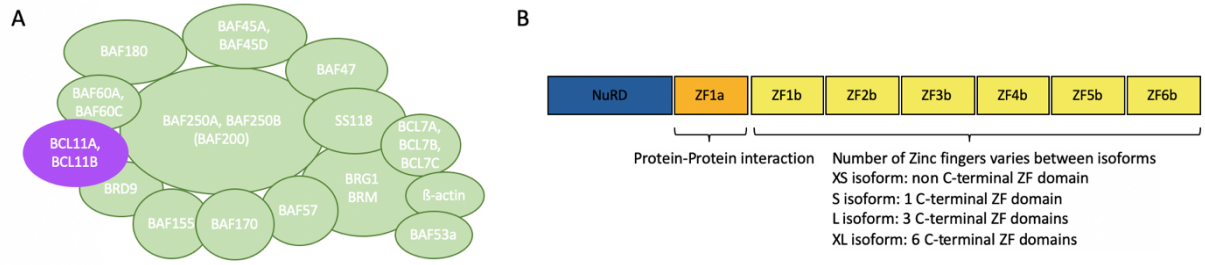

Figure 1.7: BCL11A as part of the SWI/SNF complex and its molecular structure. (A) Schematic of the transcription regulating SWI/SNF complex including BCL11A/B subunit. Figure is adapted from Kadoch et al., 2013. **(B)** The BCL11A protein exists in four different isoforms. All isoforms consist of the N-terminal C2HC zinc finger (ZF), which mediates protein-protein interactions and the nucleosome remodeling deacetylase (NuRD) domain. The number of ZFs responsible for DNA binding is dramatically different for the different isoforms.

1.4.2 Function of BCL11A in the central nervous system

Alterations of the *BCL11A* gene sequence or alterations in its expression are associated with neurological disorders. Thus, heterozygous mutations within the *BCL11A* sequence were identified in patients suffering from neurodevelopmental disorders like intellectual disabilities and behavioral problems (Basak *et al.*, 2015; Dias *et al.*, 2016; Peron *et al.*, 2019; Simon *et al.*, 2020). The deletion of *BCL11A* is a common feature in patients affected by 2p15-p16.1 microdeletion syndrome, who demonstrated autism spectrum disorder and developmental delay (Basak *et al.*, 2015). The brain of 2p15-p16.1 microdeletion syndrome patients displays abnormalities as hypoplasia of the corpus callosum, neocortex, amygdala and hippocampus (Simon *et al.*, 2020). Interestingly, impaired formation of the SWI/SNF complex, which consists of a BCL11A subunit, is also linked to autism spectrum

disorders (Dias *et al.*, 2016; Simon *et al.*, 2020). All these data suggest an important role of BCL11A in human neurodevelopment.

In mouse studies, the role of BCL11A during neurogenesis was studied in more detail. During murine spinal cord and cortex development, BCL11A regulates neuronal fate determination (Simon *et al.*, 2020). The knockout of *Bcl11a* in mice affects proper somatosensory circuit formation within the dorsal spinal horn, due to the defective regulation of the frizzled-related protein 3 (FRZB/SFRP3) (John *et al.*, 2012). Additionally, late born cortical neurons with *Bcl11a* deficiency demonstrate impairments in switching from multipolar to bipolar morphology, which leads to impaired radial migration and subsequent misdistribution. In this context semaphorin 3C (*Sema3c*) was identified as direct target gene of BCL11A through which BCL11a affects radial migration of cortical projection neurons (Wiegreffe *et al.*, 2015). Furthermore, two different studies revealed a role of BCL11A in the postmitotic development of different types of projection neurons, as corticothalamic, callosal and subcerebral projection neurons (Canovas *et al.*, 2015; Woodworth *et al.*, 2016). Additionally, Greig and colleagues demonstrated a function of BCL11A in the acquisition of the sensory area identity and the establishment of sensory input fields in the developing murine neocortex, since BCL11A regulates differentiation of layer IV neurons and the loss of BCL11A in the cortex leads to impaired organization of thalamocortical axons into properly configured sensory maps (Greig *et al.*, 2016). Moreover, a role of BCL11A in the midbrain dopaminergic system, where *Bcl11a* expressing neurons form specific subcircuits, could be demonstrated. Upon *Bcl11a* inactivation midbrain dopaminergic neurons display altered distribution, which negatively affects skilled motor behavior in mice. Furthermore, *Bcl11a* expressing neurons are highly vulnerable to neurodegeneration induced by α-synuclein overexpression or oxidative stress (Tolve et al., 2021) (Table 1.2).

Taken together, the association of BCL11A with neurological disorders in human patients, as well as the various described functions of BCL11A in the developing murine nervous system, emphasize the importance of BCL11A for proper brain development.

Table 1.2: Overview of reported functions of Bcl11a in the mouse neocortex and spinal cord.

Type of neuron	Function of BCL11A	Reference
Dorsal spinal neurons	Control of sensory circuit formation and neuronal morphogenesis	John *et al*., 2012
Cortical subcerebral projection neurons	BCL11A-mediated repression of *Tbr1* is crucial for subcerebral fate acquisiation	Cánovas *et al.*, 2015
Cortical projection neurons	Regulation of radial migration via control of *Sema3c* expression	Wiegreffe *et al.*, 2015
Neocortical neurons Neocortical layer IV neurons	Control of sensory area identity acquisition and sensory input fields establishment Regulation of differentiation	Greig *et al*., 2016
Deep-layer cortical projection neurons	Regulation of subtype identity	Woodworth *et al.*, 2016
Midbrain dopaminergic neurons	Formation of specific subcircuit and critical for establishment and maintenance of normal physiology	Tolve *et al.*, 2021

1.5 Neuronal forward programming

Neuronal differentiation is tightly regulated by complex networks of e.g. transcription factors and miRNAs (see Chapter 1.1.2). Transcription factors and miRNAs affect directly the expression of cell-type specific genes (Kageyama *et al.*, 1997; Liu and Zhao, 2009). Thus, transcriptional activators promote the expression of neuronal genes and drive neuronal differentiation positively, while transcriptional repressors inhibit the expression of neuronal genes in non-neuronal cells (Sun *et al.*, 2001; Gao *et al.*, 2011). The understanding of the specific roles of the transcription factors and their effects on neurogenesis led to the development of transcription factor-based neural and neuronal forward programming approaches to generate mature neurons in a short time-frame, which could then be used in drug-screening or cell replacement therapies (Flitsch *et al.*, 2020; Gu *et al.*, 2021; Hulme *et al.*, 2022).

1.5.1 Transcription factors to drive neuronal differentiation

Single transcription factors are able to convert non-neuronal cells into neurons upon their overexpression (Flitsch *et al.*, 2020). Prominent transcription factors in this context are ASCL1 and NGN2. The overexpression of both converts mouse astrocytes directly into neurons (Berninger *et al.*, 2007), while the overexpression of one of the two transcription factors is sufficient to convert hPSCs into neuronal cells (Thoma *et al.*, 2012; Chanda *et al.*, 2014).

The combination of ASCL1, POU domain class 3 homeobox 2 (BRN2) and myelin transcription factor 1 like (MYT1L) led to an efficient generation of mature neurons from fibroblasts (Vierbuchen *et al.*, 2010), while the combined overexpression of ASCL1 and SOX2 mediates conversion of human brain-resident pericytes into neurons (Karow *et al.*, 2012). Moreover, the overexpression of ASCL1 and distal less homeobox 2 (DLX2) triggers generation of GABAergic neurons from hiPSCs (Peitz *et al.*, 2020).

Many protocols for neuronal forward programming of stem cells are built upon NGN2 overexpression only. Human PSCs, which were transduced with a lentivirus carrying an inducible NGN2 overexpression construct, differentiated into mature neurons upon NGN2 induction, that could integrate into the synaptic networks of the mouse brain after transplantation (Zhang *et al.*, 2013). NSCs derived from hiPSCs formed more rapidly neurons, that demonstrated upregulated expression of glutamatergic genes and enhanced synaptogenesis upon NGN2 overexpression (Ho *et al.*, 2016). Recently established protocols, focus on the overexpression of NGN2 after targeted gene insertion into the safe harbor locus of hiPSC, which promises higher levels of protocol standardization (Meijer *et al.*, 2019).

1.5.2 Artificial proteins to accelerate neuronal differentiation

To activate expression of neuronal genes for accelerating neuronal differentiation, transcription activators could also be artificially designed. Potent transcriptional activator domains facilitate active gene expression upon gene targeting mediated by dead Cas9 (dCas9, a mutant variant of Cas9 protein (see below) with inactive nuclease activity) approaches (Balboa *et al.*, 2015) or by transcription factors directly (Naseri *et al.*, 2021).

There are several proteins with a strong transcriptional activator function, such as myoblast determination protein 1 (MYOD), forkhead-box protein A (FOXA) and herpes virus protein 16 (VP16).

One of the most extensively studied transactivators is VP16, which serves as a prototype to understand how transactivators control gene activity (Hirai *et al.*, 2010). The origin of the VP16 protein is the *Herpes Simplex* virus (HSV) type 1. Upon virus infection, VP16 is released into the host cell and is involved in the active expression of the viral immediate-early genes (Flint and Shenk, 1997; Wysocka and Herr, 2003). Gene expression activation is facilitated by two domains of the VP16 protein, a core domain that is required for indirect DNA binding (DBD) and a C-terminal transcriptional activation domain (TAD) (Triezenberg *et al.*, 1988; Greaves and O'Hare, 1989) (Figure 1.8 A). Subsequent to DNA binding within the promoter region of its target genes via the DBD, the TAD interacts with several host basal transcription factors and cofactors to mediate active gene expression (Lin *et al.*, 1991; Ge and Roeder, 1994; Kretzschmar *et al.*, 1994; Xiao *et al.*, 1994; Zhu *et al.*, 1994; Kobayashi *et al.*, 1995) (Figure ***1.8*** B). Additionally, the TAD of VP16 recruits histone acetyltransferases to target gene promoters and is involved in chromatin decondensation, which allows activation of gene expression (Utley *et al.*, 1998; Vignali, 2000; Carpenter *et al.*, 2005). These various interactions make the TAD of VP16 to a very potent transcriptional activator, which is used for fusion to dCas9 or transcription factors to amplify their activity (Kaneto *et al.*, 2005) or could be utilized to replace the repressor domain of repressive transcription factors to turn them into activating transcription factors (Immaneni *et al.*, 2000).

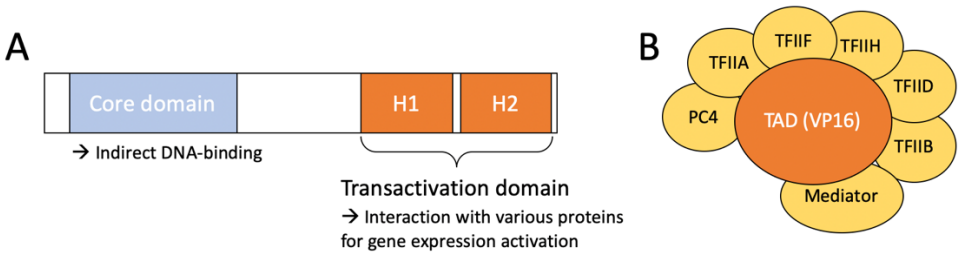

Figure 1.8: Structure of the VP16 protein and its involvement with different transcriptional activator proteins. (A) VP16 consists of a core domain, which mediates indirect DNA binding, and 2 transactivation domains, which facilitate interaction with **(B)** various different proteins, that are in involved in gene expression activation. Illustration is adapted from Hirai *et al.*, 2010.

In recent years, the use of the CRISPR/Cas9 system, originating from the defense system of bacteria and archaea against viruses, gained more and more importance for targeted genome editing (Cong *et al.*, 2013; Abdelnour *et al.*, 2021). The endonuclease Cas9 is directed by synthetic guide RNAs (gRNA) towards the DNA sequence, which is supposed to be cut (Jinek *et al.*, 2012). The thoughtful design of gRNAs and co-expression of gRNA and Cas9 enzyme facilitates targeted gene insertion or gene knockout (Ceasar *et al.*, 2016). Further development of the CRISPR/Cas9 system led to the generation of a dCas9 enzyme with inactivated endonuclease function to prevent DNA cleavage upon DNA binding (Xu and Qi, 2019). If these dCas9 enzymes are fused with transactivator domains, the expression of genes, targeted by the gRNA, will be activated (Park *et al.*, 2017). This system can be utilized to activate the expression of endogenous transcription factors, such as NGN2 or NEUROD1, which leads to rapid, neuronal differentiation of hiPSCs (Chavez *et al.*, 2015).

Another approach of forcing differentiation of cells into a desired cell type, is the use of modified transcriptional repressors. Timed differentiation or cell type specificity of non-neuronal cells is ensured

by the repression of neuronal genes by transcription factors, for instance (Schoenherr and Anderson, 1995). These transcriptional repressors could be used to induce or even accelerate neuronal differentiation, after reversing their function (Immaneni *et al.*, 2000).
The exchange of the repressor domain of repressor element 1 (RE1)-silencing transcription factor (REST) with the TAD domain of VP16 turned the actual transcriptional repressor into a transcriptional activator of neuronal genes (Immaneni *et al.*, 2000). In mouse NSCs, the expression of REST-VP16 leads to a rapid conversion of these stem cells into mature and electrophysiological active neurons, due to ectopic expression of REST target genes, which are required to activate neuronal traits (Chong *et al.*, 1995; Su *et al.*, 2004).
To sum up, various methods and protocols for the differentiation of non-neuronal cells into neuronal cells exist, which are based on the understanding of the molecular mechanisms of neural and neuronal development. These protocols are interesting tools for the fast generation of neurons, which could be used for e.g. drug-screening or cell replacement therapies.

1.6 Aims and objectives

The human brain represents the most complex construct of all biological systems. Consequently, the underlying regulatory molecular networks ensuring proper brain development are highly elaborate and entangled and not all involved players have yet been identified. A deeper understanding of the physiological mechanisms of neural development is not only desirable to increase knowledge about human brain development, but is also relevant for understanding developmental diseases.
A number of experimental observations in mouse and *Xenopus laevis* suggest that the orphan transcription factor GCNF plays a prominent role in neurogenesis. GCNF has been shown to be required for the development of definitive neural stem cells, neural tube closure, proper somitogenesis and correct brain regionalization. However, the role of GCNF during human brain development was not yet described. Hence, the aim of this study was to reveal more details about the mechanistic function of GCNF during human neuronal development.
Utilizing smNPCs derived from hiPSCs as proxy for human brain development, we aimed to explore the role of GCNF during human neurogenesis by addressing the following objectives:

1. GCNF expression pattern

Initially, the expression pattern of GCNF was analyzed to understand if GCNF might play a role in human NSCs and their neuronal differentiation. The RNA and protein level of GCNF in smNPCs and their neuronal progeny was determined to understand the temporal expression pattern. Additionally, the spatial expression pattern of GCNF was examined.

2. Role of GCNF during neuronal differentiation

To analyze the role of GCNF during neuronal differentiation, smNPC lines were generate, which carried different lentiviral constructs for e.g., GCNF overexpression or GCNF knockdown. Neuronal cultures derived from these smNPCs were evaluated for their proliferative capacity and neuronal differentiation status. Additionally, the overall architecture of formed neuronal cultures was examined and cluster formation was quantified.

3. GCNF mediated effects on the transcriptome and identification of a target gene

The transcriptome of smNPCs and their neuronal progeny was examined with regard to alteration in gene expression upon modulated GCNF expression to reach a better understanding of the molecular mechanisms of the observed changes in proliferation and differentiation of smNPCs after altered GCNF expression. Subsequently to the detailed transcriptomic analyses, a direct target gene of GCNF was identified by established ChIP-qRT-PCR assays.

4. Analysis of GCNF-VP16 as tool for accelerated differentiation

Based on the results of the first three objectives, we aimed to evaluate the fusion protein GCNF-VP16 as possible tool for accelerated neuronal differentiation. Since human neurons derived from hPSCs or hNSCs are well suited to identify disease-causing mechanisms or to execute drug-screening approaches, many protocols for accelerating the generation of such neurons were already designed. Unfortunately, these existing protocols have certain flaws, like time-consuming and labor-intensive re-plating steps or special treatment with antimitotic substances, which might be overcome by using ectopic expression of GCNF-VP16 to drive neuronal differentiation.

2 Material and Methods

2.1 Material

2.1.1 Plastic consumables, cell culture media, chemical reagents and kits

Table 2.1: Plastic consumables for various experiments

Consumable	Cat. number	Manufacturer
0.2 µm syringe filter	4610	Pall corporation
6 well plates	3506	Corning Costar
24 well plates	3524	Corning Costar
48 well plates	3548	Corning Costar
96 well imaging plates	655090	Greiner Bio-one
3.5 cm dish with 4 inserts	627170	Greiner Bio-one
6 cm tissue culture dishes	734-2318	VWR
10 cm tissue culture dishes	734-2321	VWR
1.5 mL Eppendorf tubes	0030120.086	Eppendorf
2 mL Eppendorf tubes	0030120.094	Eppendorf
15 mL Falcon tubes	352096	Falcon
50 mL Falcon tubes	352070	Falcon
40 µm Cell strainer	35240	Falcon
96 well plates qPCR	4ti-0760	4ti-tude
Bioruptor tubes (0.65 mL)	C30010011	Diagenode
Cell scraper	3008	Corning Costar
Cryovials 1.0 mL	710480	Biozym
Cryovials 1.8 mL	710482	Biozym
HybriSlip™ Hybridization Cover	H18202	Thermo Fisher Scientific
Immun-Blot PVDF Membrane	162-0177	Biorad
Low DNA-binding 0.6 mL tube	710136	Biozym
Low DNA-binding 1.5 mL tube	710176	Biozym
Microscope Cover glasses (∅ 10 mm)	0111500	Paul Marienfeld
Microscope Cover glasses (24 x 50 mm)	BR470819	Merck (Brand®)
Syringe (20 mL)	4616200V	B. Braun
Petri dish	351029	Falcon
qPCR sealing film	4ti-0500	4ti-tude
Whatman paper	GB005	GE Healthcare

Table 2.2: Media and cell culture solutions

Medium/Reagent	Cat. number	Manufacturer
Accutase	A11105-01	Gibco
B27 supplement - RA (50x)	12587-010	Gibco
B27 supplement + RA (50x)	17504-044	Gibco
BSA Fraction V (7.5 %)	15260-037	Gibco
DMEM-F12	11320-074	Gibco
DMEM high glucose	41965-039	Gibco
DPBS	14190-094	Gibco
Fetal bovine serum (FBS)	10270-106	Gibco
Geltrex (GT)	A14132-02	Gibco
Knockout Serum Replacement (SR)	10828-028	Gibco
L-Glutamine (200 mM)	25030-024	Gibco
MEM-NEAA	11140-035	Gibco
N2 supplement (100x)	T1129.2005	PAA
Neurobasal	21103-049	Gibco
OptiMEM	31985-062	Gibco
Penicillin Streptomycin (Pen/Strep)	15140-122	Gibco
Sodium pyruvate	11360-039	Gibco

Medium/Reagent	Cat. number	Manufacturer
Trypan Blue Stain (0.4 %)	15250-061	Gibco
Trypsin-EDTA	15400-054	Gibco

Table 2.3: Cell culture additives

Reagent	Cat. number	Manufacturer	Concentration (stock)	Solvent
Ascorbic acid	A8960-5G	Sigma-Aldrich	200 mM	H_2O
CHIR-99021	130-103-926	Miltenyi Biotec	10 mM	DMSO
Chloroquine	C6628	Sigma-Aldrich	50 mM	H_2O
DMSO	D4540-100ML	Sigma Aldrich		
DNase	LS002139	Worthington	10 mg/mL	PBS
Doxycycline	D9891-1G	Sigma-Aldrich	10 mg/mL	H_2O
G418	ALX-380-01	Enzo	200 mg/mL	H_2O
KCl	7447-40-7	Sigma Aldrich		
Lipofectamine 2000	11668-027	Invitrogen		
Polybrene	TR-1003-G	Millipore	10 mg/mL	H_2O
Purmorphamine	130-104-465	Miltenyi Biotec	10 mM	DMSO
Puromycin	6R312-0050	Enzo	10 mg/mL	H_2O
Rock-Inhibitor	SM02-10	Cell Guidance System	10 mM	H_2O

Table 2.4: Reagents for various experiments

Reagent	Cat. number	Manufacturer
100 µM fluorescein	170-8780	BioRad
1000x SYBR Green	S9430-5 ML	Sigma-Aldrich
1xDPBS	14190-094	Gibco
50 % Dextran sulfate	A4970.0250	AppliChem
50x Denhardt's	D2532	Merck
Acetic acid	3738.5	Roth
Acetic anhydride	320102	Sigma-Aldrich
Agar	5210.2	Roth
Agarose	35-1020	PeqGold
Ammonium Persulfate (APS)	A367.8	Sigma-Aldrich
Ampicillin	A9518	Sigma-Aldrich
Ampuwa H_2O	40676.00.00	Fresenius Kabi
BM purple AP substrate	11442074	Roche
Bromphenol blue	A1120.005	AppliChem
BSA	15260-037	Gibco
Chloroform	3313.1	Roth
Color Protein Standard Broad Range	P7712G	New England Biolabs
DAPI	D9542	Sigma-Aldrich
dATP	5100910-0250	VWR
dCTP	5100920-0250	VWR
ddH_2O		Millipore water purification system
Deoxycholic acid sodium salt (DOC)	30970	Fluka
DEPC	D5758	Sigma-Aldrich
dGTP	5100930-0250	VWR
DIG-labeled dNTPs	11277073910	Roche
dTTP	5100940-0250	VWR
D(+)-Glucose	HN06.3	Roth
EDTA	X986.3	Roth
Ethanol	5054.3	Roth
Ethidium bromide	2218.2	Roth
Formaldehyd (37 %, MeOH)	F8775-5ML	Sigma-Aldrich
Formamide (deionized)	155-15026	Thermo Fisher Scientific
GeneRuler 100bp Plus DNA ladder	SM0321	Thermo Fisher
Glycerol	G5516-500ML	Sigma-Aldrich
Glycine	3908.3	Roth
Glycogen	37-1810	Peqlab

Reagent	Cat. number	Manufacturer
HALT™ Protease-Inhibitor-Cocktail	78438	Thermo Fisher Scientific
HBSS	24020-083	Gibco
HCl	4625.1	Roth
IGEPAL CA-630	I3021-50ML	Sigma
Immobilon Classico western HRP substrate	WBLUC0500	Millipore
Isopropanol	CP41.3	Roth
KCl	6781.3	Roth
Levamisol	L-025	Sigma-Aldrich
Loading buffer	B7024S	New England Biolabs
Methanol	4627.5	Roth
$MgCl_2$	A537.5	Roth
$MgSO_4$	434183-500G	Sigma-Aldrich
Milk powder	T145.2	Roth
Mowiol	0713.2	Roth
NaCitrate	27833.294	VWR
NaCl	9265.2	Roth
NaOH	6771.3	Roth
$Na_3P_2O_7$	106591	Merck
Normal Goat Serum	S26-100ML	Millipore
Paraformaldehyd (PFA, 4 %)	J61899	Alfa Aesar
PEG6000 (Polyethylenglycol 6000)	0158.4	Sigma-Aldrich
Ponceau S solution	6226-79-5	VWR
Quick Extract DNA Extraction solution	QE09050	Lucigen
RNase Inhibitor	13398800	Roche
ROTIPHORESE® Gel 30 (37,5:1)	3029.1	Roth
Sarcosyl	L91150	Merck
Sodium lauryl sulfate (SDS)	2326.2	Roth
TEMED	T7024	Sigma-Aldrich
Triethanolamine	28746290	VWR
TriFast	30-2020	PeqGold
Tris	5429.2	Roth
Tris-HCl	9090.3	Roth
Triton X-100	T8787-100ML	Sigma-Aldrich
Tryptone	8952.2	Roth
Tween-20	P1379-500ML	Sigma-Aldrich
Vectashield	H-1000	Vector Laboratories
Yeast Extract	2363.5	Roth
Yeast tRNA (10 mg/mL)	R5636	Merck
β-Mercaptoethanol	63689-100ML	Sigma-Aldrich

Table 2.5: Kits used in various experiments

Used Kit	Cat. number	Manufacturer
Click-it Plus EdU Alexa Fluor 488	C10632	Invitrogen
DNeasy Blood&Tissue Kit	69504	Qiagen
Fluo-4 NW Calcium Assay kit	F36206	Invitrogen
LIVE/DEAD Fixable Near-IR Dead Cell Stain Kit	L34975	Invitrogen
peqGOLD Gel extraction kit	12-2501-02	Peqlab
peqGOLD Plasmid Miniprep kit I	12-6942-02	Peqlab
PerfeCTa SYBR Green SuperMix	95054-500	Quanta bio
Pierce BCA Protein Assay Kit	23277	Thermo Fisher
PureLink™ HiPure Plasmid-Filter-Midiprep-Kit	K210015	Invitrogen
qScript cDNA synthesis kit	95047-500	Quanta bio
RNA Clean & Concentrator-5	R1013	Zymo Research
Tag-ChIP-IT Kit	53022	Active Motif

2.1.2 Enzymes and antibodies

Table 2.6: Enzymes

Enzym	Cat. number	Manufacturer
DNase I	18068-015	Invitrogen
EcoR1	R0101S	New England Biolabs
Nhe1	R0131S	New England Biolabs
Not1	R0189L	New England Biolabs
Q5 High-fidelity DNA Polymerase	M0491S	New England Biolabs
RNase A	12091-021 (PureLink Kit)	Thermo Fisher Scientific
SP6 RNA Polymerase	10810274001	Roche
T4 DNA Ligase	M0202S	New England Biolabs
T7 RNA Polymerase	10881767001	Roche
Taq DNA Polymerase	10342-020	Invitrogen

Table 2.7: Primary antibodies

Antigen	Host/Isotype	Dilution	Cat. Number (clone)	Manufacturer
AM-tag	Mouse IgG2a recombinant	1:1000 (WB) 1:100 (ICC) 10 µg (ChIP)	91112	Active Motif
AP2a	Mouse IgG2b monoclonal	1:100 (ICC)	3B5	DSHB
CD200-APC	Mouse IgG1monoclonal	1:100 (FLC)	17-9200-42 (OX104)	Invitrogen
CD49f-PE	Rat IgG1 monoclonal	1:100 (FLC)	12-0495-81 (eBioGoH3)	Invitrogen
DACH1	Rabbit IgG polyclonal	1:100 (ICC)	19014-1-AP (lot 0010746)	Proteintech
DCX	Mouse IgG1 monoclonal	1:500 (ICC)	sc-271390 (E6)	Santa Cruz
DIG-AP Fab fragments	Sheep IgG polyclonal	1:5000 (ISH)	11093274910	Roche
GCNF	Mouse IgG monoclonal	1:1000 (WB)	PP-H7921 (H7921)	Perseus Proteomics
IgG	Mouse IgG polyclonal	10 µg (ChIP)	Sc-2025	Santa Cruz
KI67	Rabbit IgG monoclonal	1:100 (ICC)	KI68IR06 (SP6)	DCS
MAP2	Mouse IgG1 monoclonal	1:500 (ICC)	M1406-100µl (AP-20)	Sigma Aldrich
NESTIN	Mouse IgG1 monoclonal	1:500 (ICC)	BLD-656802 (10C2)	Biolegend
PAX6	Rabbit IgG polyclonal	1:200 (ICC)	poly19013/lot B277104	Biolegend
POL II	Mouse IgG1 monoclonal	5 µg (ChIP)	39097 (4H8)	Active Motif
PSD95	Mouse IgG monoclonal	1:500 (ICC)	AB2723 (6G6-1C9)	Abcam
SOX2	Rabbit IgG monoclonal	1:1000 (WB) 1:300 (ICC)	3579 (D6D9)	Cell Signaling
ßIIITUB	Mouse IgG2a monoclonal	1:500 (ICC)	801202 (TUJ1)	Biolegend
Synaptophysin	Guinea pig IgG polyclonal	1:1000 (ICC)	101 004	Synaptic Systems
β-actin	Mouse IgG monoclonal	1:5000 (WB)	MAB1501 (C4)	Merck Millipore

Table 2.8: Secondary antibodies

Name	Dilution	Cat. Number	Manufacturer
Alexa 488 goat α gp IgG	1:1000 (ICC)	A11073	Invitrogen
Alexa 488 goat α ms IgG	1:1000 (ICC)	A11001	Invitrogen
Alexa 488 goat α rb IgG	1:1000 (ICC)	A11008	Invitrogen
Alexa 555 goat α ms IgG	1:1000 (ICC)	A21424	Invitrogen
Alexa 555 goat α rb IgG	1:1000 (ICC)	A21428	Invitrogen
HRP-linked goat α rb	1:1000 (WB)	7074	Cell Signaling
HRP-linked horse α ms	1:1000 (WB)	7076	Cell Signaling
α ms IgG bridging	5 µg (ChIP)	53017	Active Motif

2.1.3 Plasmids and oligonucleotides

Table 2.9: Primers

Name	Sequence (5' → 3')	Used for which method
18S rRNA forward	TTC CTT GGA CCG GCG CAA G	qRT-PCR
18S rRNA reverse	GCC GCA TCG CCG GTC GG	qRT-PCR
BCL11A forward	GCA ACA CGC ACA GAA CAC TC	qRT-PCR
BCL11A reverse	GAG CTT CCA TCC GAA AAC TG	qRT-PCR
BCL11A pos forward	GGG AGA GAG AGA GAG AGA GAT GA	ChIP qRT-PCR
BCL11A pos reverse	TGT CTC TGT CCA TCC AGA CTC	ChIP qRT-PCR
BCL11A neg forward	TAT GAA GTA TGA GCC GCG TG	ChIP qRT-PCR
BCL11A neg reverse	TTC GAG CTG TTT GTT GAC CA	ChIP qRT-PCR
GAPDH	Supplied by Active Motif (71006)	ChIP qRT-PCR
GCNF forward	GAG GCC GGA ATA AGA GCA TT	qRT-PCR
GCNF reverse	CAG GGG AAC TGT GGT CAC TAT C	qRT-PCR
ISH hSOX2 forward	TGT ACA GCG GCC GCA TGT ACA TGA TGG AGA CGG	Cloning ISH probe
ISH hSOX2 reverse	TGT ACA GAA TTC TAG TGC TGG GAC ATG TGA AGT C	Cloning ISH probe
ISH mGCNF forward	TGT ACA GCG GCC GCC CCT GCC TTT TCT TAT GTA TGC	Cloning ISH probe
ISH mGCNF reverse	TGT ACA GAA TTC GAC TCC AAG TCC AGG AAA GAT G	Cloning ISH probe
MAP2 forward	CTG GCA CCC CAC CAA GTT AT	qRT-PCR
MAP2 reverse	AAC AAT TTG TAC CTG CCC CC	qRT-PCR
NC12	Supplied by Active Motif (71001)	ChIP qRT-PCR
NFIB forward	TGT GAC TGG ACC ATG AAT CAA	qRT-PCR
NFIB reverse	CCG GTA AGA TGG GTG TCC TA	qRT-PCR
NFIB pos forward	CCT CAT CAC TTA GGC AGG AA	ChIP qRT-PCR
NFIB pos reverse	GAA AGC TCT AGC GCT GAA AA	ChIP qRT-PCR
NFIB neg forward	CCT CAA CTT TAG CCC CTC TC	ChIP qRT-PCR
NFIB neg reverse	AAA ACG GAC TGT GTT TGA GC	ChIP qRT-PCR
PCYT1B forward	TGT GGA GGA AAG ATC AAA GGA	qRT-PCR
PCYT1B reserve	TCC TCT CCT GGA ACA TCT GC	qRT-PCR
PCYT1B pos forward	GCT AAG TCC GTC ACA CCT G	ChIP qRT-PCR
PCYT1B pos reverse	TGG AGC AGA ATT AGT GGG AAT G	ChIP qRT-PCR
PCYT1B neg forward	ACC AAC ATC AGC ATC ACC AG	ChIP qRT-PCR
PCYT1B neg reverse	CCA GAC CTG CAG CAT TAA CA	ChIP qRT-PCR
SP6 reverse	TAT TTA GGG TGA CAC TAT AG	Sequencing
T7 forward	TAA TAC GAC TCA CTA TAG G	Sequencing

Table 2.10: Plasmids for lentivirus production

Plasmid	Source or parental DNA origin	Antibiotic resistance
pMD2.G	Gift from Didier Trono (Wiznerowicz et al. 2003), Addgene plasmid # 12259	Ampicillin (Amp)
psPAX2	Gift from Didier Trono (Wiznerowicz et al. 2003) Addgene plasmid # 12260	Amp
pLVX-EtO	Modified from pLVX-Tet-ON-Advanced as described in Mertens et al. (2013) (Clontech, Cat. No. 632162),	Amp/G418
pLVX-Tight-Puro	From Clontech (part of the Lenti-X Tet-ON Advanced Inducible Expression System), Clontech, Cat. No. 632162	Amp/Puromycin
pCAG-mir30	Gift from Paddison et al. (2004) via Addgene (#14758)	Amp/Puromycin
pTight-miR30 ctrl	Into the pCAG-miR-30 backbone the miR-30: shRNA-ctr hybrid cassette, a scrambled non-targeting oligonucleotide sequence was cloned as described by Paddison et al., 2004 and from there transferred to the pLVX-Tight-Puro plasmid by Laura Stappert	Amp/Puromycin
pTight-GCNF	Amplified from cDNA generated from lt-NES cell's total RNA by Laura Stappert, GCNF/NR6A1 transcript variant ENST00000344523	Amp/Puromycin
pTight-mutDBD GCNF	GCNF variant with C60S, C63S, C112S and C115S mutations were introduced via PCR mutagenesis by Laura Stappert	Amp/Puromycin

Plasmid	Source or parental DNA origin	Antibiotic resistance
pTight-shRNA GCNF	The oligonucleotide[1] was cloned into miR30 backbone according to Fellmann et al., 2013 and transferred into pLVX-Tight-Puro plasmid by Laura Stappert	Amp/Puromycin
pTight-GCNF-VP16	GCNF cDNA from pLVX-Tight-GCNF-Puro and the VP16 sequence from mouse GCNF-VP16 construct (kind gift of Austin Cooney (Cooney et al., 1998)), cloned by Laura Stappert	Amp/Puromycin
pTight-NGN2	Generated as described in Ladewig et al., 2012	Amp/Puromycin
pTight-GCNF-AM	GCNF cDNA from pLVX-Tight-GCNF-Puro and the AM sequence[2] from Active Motif were combined, cloned by Laura Stappert	Amp/Puromycin

Table 2.11: Plasmids for RNA ISH probe preparation

Plasmid	Source or parental DNA origin	Antibiotic resistance
pCMV-SPORT6.1-hGCNF	hGCNF cDNA from C13f iPS cell total RNA cloned in pCMV-SPORT6.1 by Laura Stappert	Amp
pCMV-SPORT6.1-hSOX2	hSOX2 cDNA from I3 lt-NES cell total RNA cloned in pCMV-SPORT6.1 as described below, see chapter 2.2.6.4	Amp
pCMV-SPORT6.1-mGCNF	mGCNF cDNA cloned in pCMV-SPORT6.1 as described below, see chapter 2.2.6.4	Amp

Table 2.12: ISH RNA probes

Probe*	Sequence
hGCNF antisense	CACTCCACATCAACCTGCCTCTCACCTGCCACCCTTTTTCAGGGAGGTGAGTACCTGCCATGGTCACTGTTACCAGATCCTTA AAATCCTGGGCTTTGAGCTAGGTGCATTGCTCTGTTACCCATTTCCTACATTTGTTTGTTTGTTCTTGATTTCCTGGGGGAAT GGGACTGATGGAGACAGACAAACCCACTGTGGGCAGCATCTAAGCCATGTCCAAGGTTGGTCGAATTAAGGGAACCCTGG CCTCTCAGCAGGACAGAAAGCTGAGCTGTGGTTCCAGGCCCTCCTCTCTGGGCCCCTGGTGTGTATCTTTTTTCCTTGTTGCT TTTGAAATTTTTGCAATTATTTTAAGAATCCAGTCTTTCAGACCAGCCCTTTTATTAAGCTTTGAATTTTTAATTGATTTTTTTA AAGTAAAAAAAAAAAAAAACCCA
hSOX2 antisense	TGCTGGGGGCGGCGGGTTCCGGCACCTCGGCGCCGGGGAGATACATGCTGATCATGTCCCGGAGGTCCCCGGCCTGGCA GGGCGCCCTGGAGTGGGAGGAAGAGGTAACCACAGGGGGGCTGGAGCTGGCCTCGGACTTGACCACCGAACCCATGGA GCCAAGAGCCATGCCAGGGGTGCCCTGCTGCGAGTAGGACATGCTGTAGGTGGGCGAGCCGTTCATGTAGGTCTGCGAG CTGGTCATGGAGTTGTACTGCAGGGCGCTCACGTCGTAGCGGTGCATGGGCTGCATCTGCGCTGCGCCGTGCGCATTGAG GCCCGGGTGCTGCGGGTAGCCCAGCTGGTCCTGCATCATGCTGTAGCTGCCGTTGCTCCAGCCGTTCATGTGCGCGTAACT GTCCATGCGCTGGTTCACGCCCGCGCCCAGGCCGGCGCCCACCCCGACCCCGCTCGCCATGCTATTGCCGCCGGGGGCCAG CAGCCCGCCGGGCAGCGTGTACTTATCCTTCTTCATGAGCGTCTTGGTTTTCCGCCGGGGCCGGTATTTATAATCCGGGTGC TCCTTCATGTGCAGCGCTCGCAGCCGCTTAGCCTCGTCGATGAACGGCCGCTTCTCCGTCTCCGACAAAAGTTTCCACTCGG CGCCCAGGCGCTTGCTGATCTCCGAGTTGTGCATCTTGGGGTTCTCCTGGGCCATCTTGCGCCGCTGCCCGCGGGACCACA CCATGAAGGCATTCATGGGCCGCTTGACGCGGTCCGGGCTGTTTTTCTGGTTGCCGCCGGCCGCCGCCGCGGTGGAGTTG CCGCCGCCGCCCCCCGAAGTTTGCTGCGGGCCCGGCGGCTTCAGCT
mGCNF antisense	GACTCCAAGTCCAGGAAAGATGCTACTTGTGGCAGCCAAGAGAGGCTTTCTGGGGACCCTGTAATTAAATACACATCCCTG AGCTGTGGTCCCAGAAGTGCCTGCTTCAAGGCTGACCAGTTTCCAGCACCTGGTGGGATGATTGCCGTTTTTCATCCTAAGA AACAGATAAAACTACTTCACAGACACTGCATGAGGAGAAGGGAGGAGGATGGACGGCAGAGTGCGGGCGGGCATTCCCA CAGACCAAGGTGGGGGAGTCACTGAGTGCGCTTGCTTTCTTTCCTTTTTTTTCTTTTTTTTTTTTTTTTAGGTTTAAAAAAGC AGTAAAGAAAAAGAATCAAAGTTTAGTGGAAGGGCTGGTCTGAAAGGTTGAATTTCTTAAAACAACTGCAATTTAAAAAA CCAAAACCAAAACCCCAGTATTCTAAAGCTAGAGAGTGTGGGGTGTTCTTCACTTCCACTGTTCTAAGATCAGGACAGGGA GGTTCCTGCCTGCTTCCCTCTACCCTAGAGACCTGTCTCCTTCACTTGTAGGTTGGCCCTGGGGACTGGGTGTCCGGACCCA GGTAGAGTGCTTTGAGAGGAGTTGTAGGGAATTTCATCGAACTAAGGGTGAGACTACCAAACCTTGCAAAGGACAAAAAT GGCCTTTAAAGGGAGCCAGAGAACAGGAATTACAAAGCTCTAAGACTCCACACTTCTGCCTTGGGTCAAGAAAGCATACAT AAG

*As controls, sense probes were generated by IVT with T7

[1] Oligonucleotide sequence selected from the shRNA prediction from Fellmann et al., 2013:
TGCTGTTGACAGTGAGCGACCCATGTTGATTGAAGATGGATAGTGAAGCCACAGATGTATCCATCTTCAATCA
ACATGGGCTGCCTACTGCCTCGGA

[2] AM sequence from Active Motif:
GCCAAGATCCTCAACGCAAAGGCAACGTGATACTCTCTCAGGCTTACGGGTGCCAAGATCCTCAACGCAAAG
GCAACGTGATACTCTCTCAGGCTTA

2.1.4 Devices and software

Table 2.13: Technical devices for various experiments

Appliance	Model/ Cat. No.	Manufacturer
Blotting chamber and accessories	Mini TransBlot Cell 1703930	Biorad
Cell culture hood	HeraSafe	Heraeus
Centrifuge	5415 R	Eppendorf
Centrifuge (Cell culture)	Megafuge 1.0R	Heraeus
Centrifuge (Lentivirus prep)	Megafuge 16R	Heraeus
Centrifuge (Protein preparation)	Megafuge 40R	Heraeus
ChemiDOC	ChemiDOC XRS+	Biorad
Counting chamber	Neubauer	Marienfeld
Flow cytometer	BD FACSCanto™ II	Becton Dickinson
Fluorescence microscope	Axio Imager.Z1 with Apotome function	Zeiss
- Camera	AxioCam MRm	Zeiss
- Fluorescence lamp	HBO 100	Zeiss/LEJ (Leistungselektronik Jena)
Fluorescence microscope	Axio Observer.ZI SIP66732	Zeiss
- Camera	AxioCam MRm, AxioCam MRc	Zeiss
- Fluorescence lamp	Illuminator HXP120C	Zeiss
Freezing container	CoolCell	BioCision
Gel chamber	Compact M	Biometra
GelDOC	GelDoc XR+	Biorad
Glass douncer	FisherBrand 11582443	Thermo Fisher Scientific
Glass Staining Jar	Hellendhal type	VWR
Heating block	Thermomixer compact	Eppendorf
Heating oven (Western Blot)	UVP Minidizer Oven	Analytik Jena
Hybridization oven	Advantage ALO1-06-10	Advantage Lab
InCell analyzer 2200	InCell analyzer 2200	E Healthcare Life Science
Incubator (Bacteria)	TH15	Edmund Bühler
Incubator (Cell culture)	HeraCell	Heraeus
Inverse Light Microscope (Cell culture)	Axiovert 25	Zeiss
Inverse Light Microscope (Cell culture)	PAULA	Leica Microsystems
Leica LiveCell microscope	DMI6000 B with AFC	Leica Microsystems
- Camera	Orca -Flash 4.0	Hamamatsu
- CO_2 control	CO_2-Controller 2000	Pecon
- Lamp	Sola light engine	Lumencor
- Temperature control	TempController 2000-2	Pecon
Microwave	MW7809	Severin
NanoDrop	2000c	Thermo Scientific
Pipette Set (0.1-2.5 µL, 0.5-10 µL, 2-20 µL, 10-100 µL, 100-1000 µL)	General Lab Product Version	Eppendorf
Powerdecive (Gel electrophoresis)	Standard Power Pack P25	Biometra
Powerdecive (Western Blot)	PowerPac Universal	Bio-Rad
qRT-PCR cycler	Mastercycler REALPLEX^4	Eppendorf
SDS gel casting accessories and gel chamber (Western Blot)	Mini-PROTEAN Tetra Cell 1658001EDU	Biorad
Shaker	Rocking Platform	VWR
Sonication device	Bioruptor® PICO	Diagenode
Staining chamber	StainTray HA51.1	Roth
Thermocycler (PCR)	T3000	Biometra
Waterbath (Cell culture)	WNB14	Memmert

Table 2.14: Used software

Used Software	Producer
ApE (A plasmid Editor v2.0.61)	M. Wayne Davis
Axiovision Navigator	Zeiss
BD FACSDiva	Becton Dickinson
DAVID.ncifcrf.gov	NIAID (Huang *et al.*, 2009)

Used Software	Producer
FlowJo	Becton Dickinson
Geneontology.org, GO Enrichment Analysis	Ashburner *et al.*, 2000; Mi *et al.*, 2019; The Gene Ontology Consortium *et al.*, 2021
Genome studio V2011.1	Illumina
Image Lab	Bio-Rad
ImageJ2	NIH (Schindelin *et al.*, 2015)
Incell Analyzer	E Healthcare Life Science
LAS X 3.7.1	Leica Microsystems
JASPAR	Castro-Mondragon *et al.*, 2022
NCBI nucleotide blast	NIH
Primer3	Whitehead Institute for Biomedical Research (Untergasser *et al.*, 2012)
PRISM 9.0	Graphpad
SMART Servier Medical Art(https://smart.servier.com/)	Servier is licensed under a Creative Commons Attribution 3.0 Unported License
TAC 4.0	Thermo Fisher Scientific
TRANSFAC® Match Tool	geneXplain
ZEN blue	Zeiss

2.2 Methods

2.2.1 Cell Culture

Cell culture was performed under sterile conditions in a laminar flow hood (Table 2.13). The cells were cultivated at 37 °C in a humified incubator with 5 % CO_2.

Table 2.15: Cell lines

Abbreviation	Cell line	Source/generated by
smNPC	iLB-C-31F-r1 small molecule neural progenitor cells	Nils Christian Braun (Institute for Reconstructive Neurobiology, University Hospital Bonn)
HEK-293 FT	Human embryonic kidney 293 cells transformed with the SV40 large T antigen	LifeTechnologies

2.2.1.1 Reagents and media for cell culture work

All cell culture reagents and media were prepared under sterile conditions using the reagents listed above (Table 2.2, Table 2.3).

Table 2.16: Cell culture media for smNPCs

NPC maintenance N2B27 4CPL medium		Neuronal differentiation N2B27+RA, Diff medium		NPC freezing medium	
DMEM-F12	48.25 %	DMEM-F12	48.25 %	KSR	90 %
Neurobasal	48.25 %	Neurobasal	48.25 %	DMSO	10 %
B27 supplement - RA	1 %	B27 supplement + RA	1 %		
N2 supplement	0.5 %	N2 supplement	0.5 %		
L-Glutamine	1 %	L-Glutamine	1 %		
Pen/Strep	1 %	Pen/Strep	1 %		
Ascorbic acid	221 mM				
CHIR-99021	4 µM				
Purmorphamine	0.5 µM				

Table 2.17: Cell culture media for HEK cells

HEK maintenance medium		HEK transfection medium	
DMEM high glucose		DMEM high glucose	
FBS (heat inactivated)	10 %	FBS (heat inactivated)	2 %
Sodium pyruvate	1 mM	Sodium pyruvate	1 mM
NEAA	1 %	NEAA	1 %
Pen/Strep	1 %		

Table 2.18: Cell culture plate coating

Geltrex (GT)-coating
Dilute GT 1:30 or 1:60 in DMEM/F12, add to plastic ware and incubate overnight at 4 °C

2.2.1.2 Maintenance of smNPCs

SmNPCs were cultured according to previously established protocols (Reinhardt *et al.*, 2013; Roese-Koerner *et al.*, 2016). Cells were cultivated on 1:60 Geltrex (GT) coated 6 cm tissue culture (TC) dishes (Table 2.18) in N2B27 medium (Table 2.16) and daily controlled by visual assessment using phase contrast microscopy (PCM) (Table 2.13). Phase contrast images of cultures were taken by PAULA microscope (Table 2.13) to document cell morphology. SmNPCs were passaged approximately every third day in a ratio of 1:10 or 1:12 by incubation with Accutase for 10 min at 37 °C. The detached cells were washed with DMEM-F12 and transferred to a Falcon tube of appropriate volume. Next, the cells were centrifuged for 4 min at 250 xg, resuspended in fresh cell culture medium and seeded to new GT coated plates. For cell counting, 20 µL of the cell suspension were taken before centrifugation and diluted with 60 µL Trypan-Blue (Table 2.3). The 1:4 diluted cell suspension was added to a Neubauer chamber (Table 2.13). Each cell, which is not stained blue, within the four squares of the central grid was counted to determine the concentration of the cell suspension or the total cell number of detached cells. The cell pellet was then resuspended in fresh maintenance medium according to the counted and desired cell number.

2.2.1.3 Maintenance of HEK-293FT cells

HEK-293FT cells were cultivated on 1:60 GT coated (Table 2.18) 10 cm plates (Table 2.1) with HEK culture medium (Table 2.17) and were daily controlled by visual assessment (PCM). When the cells reached confluency, they were passaged utilizing Trypsin-EDTA (TE) (Table 2.3). To detach the cells, the medium was aspirated, the cells were washed with DPBS and 1 mL TE was added to 10 cm plates followed by incubation at 37 °C for 5 min. The cells were rinsed from the plate with DMEM and centrifuged for 5 min at 250 xg. The cell pellet was resuspended in fresh medium and the cells were seeded in appropriate number to fresh 1:60 GT coated plates.

2.2.1.4 Cryopreservation and thawing of cells

For cryopreservation, smNPC or HEK cells (Table 2.15) were detached with Accutase or TE, respectively, as described above. After completed incubation time, the cells were rinsed with DMEM-F12 or DMEM and transferred to a Falcon tube of appropriate volume. The cells were centrifuged and resuspended in DMSO-containing freezing medium (Table 2.16). The cell suspension was transferred to cryovials, which were then placed in freezing containers (Table 2.13). Initially, the freezing containers were frozen at -80 °C. For long-term storage, cryovials were transferred to -150 °C freezers or liquid nitrogen storage tanks. To thaw cells, cryovials were warmed-up at 37 °C in a water bath and the cell suspension was immediately diluted with 37 °C warm DMEM-F12 or DMEM and transferred to a Falcon tube containing 5 mL DMEM/F12 or DMEM. After centrifugation (250 xg, 4 min), the cell pellet was resuspended in culture medium (Table 2.16, Table 2.17) and seeded onto GT coated plates.

2.2.1.5 Quality control of generated smNPC lines

Quality control of cells was performed by immunocytochemistry staining for neural progenitor markers (see chapter 2.2.5.6), single-nucleotide polymorphism (SNP) analysis to validate genomic integrity of generated cells and regular mycoplasma testing, which was also performed for HEK cells.

2.2.1.5.1 SNP analysis

For SNP analysis, usually $1x10^6$ cells diluted in DMEM-F12 were taken during the passaging process and pelleted for 4 min at 250 xg. The genomic DNA of these harvested cells was purified using DNeasy Blood & Tissue kit (Qiagen) (Table 2.5) according to the kit's manual. The DNA was analyzed using an Infinium Global Screening Array-24 v.3.0 (Illumina) at the Institute of Human Genetics (University Hospital Bonn) and data analysis was performed by GenomeStudio (Illumina) (Table 2.14).

2.2.1.5.2 Mycoplasma testing

100 µL of smNPC or HEK suspension (usually a density of $2x10^6$ cells/mL) were taken during the passaging process and combined with 100 µL of QuickEx (Table 2.4) and incubated for 15 min at 68 °C and for 8 min at 95 °C in a thermocycler (Table 2.13). These samples were used to perform PCR using primers covering DNA sequences of most mycoplasma strains. The PCR was conducted by technicians from the working group Peitz (Tamara Bechler, Cornelia Thiele or Monika Veltel, Institute of Reconstructive Neurobiology, University Hospital Bonn).

2.2.1.6 Neuronal differentiation of smNPCs

SmNPCs were detached with Accutase, washed with DMEM-F12, transferred to Falcon tubes and counted with a Neubauer chamber (described above, see chapter 2.2.1.2). The cell pellet was resuspended in fresh maintenance medium according to the counted and desired cell number, which depends on the follow up experiment (see seeding plan below, Table 2.19). The following day, the medium was changed to neuronal differentiation medium (N2B27+RA medium, Table 2.16) containing 4 µg/mL doxycycline and no growth factors (Table 2.3). Differentiation medium was replaced every other day. Cells were harvested or fixed with 4 % PFA for various analyses after 2, 7, 14, 35 or 42 days of neuronal differentiation.

Table 2.19: Seeding cell number

Experiment			
RNA analysis	**Flow Cytometry**	**Immunostaining**	**Ca2+ imaging**
$2x10^6$ cells per 6 well	$2x10^6$ cells per 6 well	$5x10^4$ cells per insert on 3.5 cm dish	$1x10^4$ cells per 96 well
Life cell imaging			
$2.5x10^4$ cells per 24 well			

2.2.2 Lentiviral-based transgenesis

2.2.2.1 Preparation of plasmids for gene overexpression

In this work, we generated 8 different smNPC lines, which carried different lentiviral constructs for the induced overexpression of specific genes (EtO, miR30 ctr, GCNF, GCNF mutDBD, GCNF shRNA, GCNF-VP16, NGN2, GCNF-AM). Previously to the work, Dr. Laura Stappert performed the cloning steps and DNA plasmid preparation for the different constructs. For inducible transgene overexpression the Lenti-X Tet-ON Advanced Inducible Expression System from Clontech was utilized. To allow tetracycline/doxycycline dependable regulation, a modified version of the pLVX-Tet-On Advanced vector, which carries the EF1α promoter instead of the original CMV promoter as described by Mertens

et al. (2013) (Mertens *et al.*, 2013), was used (designated as EtO construct). For transgene delivery and expression, the genes of interest were cloned into the pLVX-Tight-Puro backbone (Table 2.10).

2.2.2.2 Lentivirus preparation

Lentiviral particle production and transfection of HEK-293FT cells were performed under S2 safety-conditions. The day before cell transfection, $7x10^6$ HEK-293FT cells were plated onto GT coated 10 cm TC dishes. At the day of transfection, the cells were incubated with medium containing no antibiotics, but 25 µM Chloroquine and only 2 % serum (Table 2.17). The transfection solutions were individually prepared as described in Table 2.20 and incubated for 5 min at room temperature (RT). Then both transfection solutions were mixed together and incubated for further 20 min at RT. After completed incubation time, the combined solutions were added dropwise to the HEK-293FT cells. Subsequent to 4 h incubation at 37 °C in a cell culture incubator at the S2 laboratory, the medium was changed to the usual culture medium (Table 2.17). The supernatant containing the produced lentiviral particles by the HEK-293FT cells was collected for three days in a row with daily medium change. The pooled supernatants were filtered through 0.45 µm syringe filters and the lentiviruses were collected using PEG6000 (Kutner *et al.*, 2009) (Table 2.21). The supernatants were mixed with PEG6000 (final conc. 8.5 %) and NaCl (final conc. 0.3 M) and incubated at 4 °C for 1.5 h, while they were inverted every 20 min. Then, the solution was centrifuged at 4,500 xg for 30 min at 4 °C. The pellets containing the lentiviral particles were resuspended in 1 mL HBSS buffer with 1 % BSA (Table 2.2, Table 2.3), distributed into 100 µL aliquots and stored at -80 °C.

Table 2.20: Transfection mixes

Transfection mix 1		Transfection mix 2	
psPAX2 (packaging plasmid)	6 µg	Lipofectamine 2000	60 µL
psMD2.G (envelope plasmid)	3 µg	OptiMEM	440 µL
Transfer vector containing the gene of interest (Table 2.10)	12 µg		
Add OptiMEM to 500 µL			

Table 2.21: PEG6000 precipitation mix

PEG6000 precipitation mix	
PEG6000 (50%)	6.8 mL
NaCl (4M)	3 mL
1xDPBS	5.2 mL

2.2.2.3 Lentiviral transduction and selection of smNPCs

Lentiviral transduction was performed under S2 laboratory conditions. For lentiviral transduction of smNPCs, $1x10^6$ cells were resuspended in 1.5 mL N2B27 4CPL medium supplemented with 10 µM ROCK inhibitor and 5 µg/mL polybrene (Table 2.3), and seeded to 1:60 GT coated 6 well TC plates. 100 µL of the concentrated viral particles were added to each well, while the cells were still in suspension. In the two following days, the cells were washed twice with DMEM/F12, after the old medium was aspirated and before fresh N2B27 4CPL medium was added. The enrichment for transduced cells was achieved by antibiotic selection. SmNPCs were treated with 200 µg/mL G418 and/or 5-2.5 µg/mL puromycin (Table 2.3). The selection started 72 h post-transduction and was maintained during further propagation of the cells for 7 days or 4 days, respectively. To generate cell lines transduced with the Lenti-X Tet-ON Advanced Inducible Expression System, cells were first transduced with the pLVX-EtO virus and thereafter propagated in the presence of G418. Subsequently,

pLVX-EtO cells were transduced with the different pLVX-Tight-Puro variants (Table 2.10) and treated with puromycin. To activate transgene expression, 4 µg/mL doxycycline was added to the cell culture medium.

2.2.3 Life cell imaging of smNPCs during neuronal differentiation

SmNPCs were seeded to a 24 well plate and differentiated for 2 days in the presence of doxycycline as described in chapter 2.2.1.6. During these days, phase contrast images of the cells were taken every 30 min using the Leica Live Cell microscope (Table 2.13). The cells were cultivated in a humid chamber, which is built around the microscope, at 5 % CO_2 and at 37 °C.

2.2.4 Calcium imaging of smNPC-derived neurons

The intracellular concentration of Ca^{2+} upon KCl induced depolarization indicates an electrophysiological activity of generated neurons. SmNPCs were seeded onto a 96 well microplate and differentiated for 5 to 6 weeks. The intracellular Ca^{2+} concentration was analyzed using the Fluo-4 NW Calcium assay kit (Table 2.5) and the InCell analyzer 2200 (Table 2.13). The culture medium was aspirated and without further washing step 1x dye loading solution was added to the cells and incubated for 30 min at 37 °C. During incubation time, the compounds used in this assay were prepared in a second 96 well plate. Three wells were filled with 120 mM KCl (1M KCl was diluted to 120 mM with assay buffer) and three different wells were filled with assay buffer as vehicle control. The cells were transferred to the InCell analyzer 2200. The plate holder of the microscope was warmed to 37 °C (bottom heater on, lid heater off) and the analyzing protocol was run semi-automatically. Each well was individually imaged and the area of interest had to be selected manually. Every 2 s a picture in the FITC channel was taken. A base line for the fluorescence intensity was established in the first 20 s of imaging. Then, 30 µL of reagent were added from the compound plate to the corresponding well of the cell culture plate and images for the next 100 s were taken. The fluorescence intensity of each image was determined by ImageJ2 (Table 2.14) and plotted relative to the mean of the base line fluorescence intensity over time course of signal assessment.

2.2.5 Analyses of protein expression

2.2.5.1 Protein preparation for Western Blot

Before protein lysate preparation, the cell culture medium was aspirated and the cells were washed twice with cold DPBS. A third time cold DPBS was added and the cells were detached by scraping them of the plate, while keeping the plates on ice. The cell suspension was centrifuged for 5 min at 2,000 xg and 4 °C (Table 2.13) and the cell pellet was resuspended in RIPA lysis buffer (Table 2.22), following by incubation for 1 h on ice while shaking. The lysates were cleared by centrifugation for 10 min at 13,200 xg and 4 °C and the supernatant containing the proteins was transferred to a new Eppendorf tube, which was stored at -80 °C.

Table 2.22: RIPA buffer recipe

Composition of RIPA buffer (1 mL)	
250 mM Tris-HCl, pH 7.5, 5 mM EDTA	200 µL
750 mM NaCl	200 µL
5 % Igepal in ddH_2O	200 µL
2.5 % Deoxycholic acid sodium salt in ddH_2O, 5 mM EDTA	200 µL
0.5 % Lauryl salt sodium salt in ddH_2O	200 µL
HALT protease inhibitor cocktail	1:100

2.2.5.2 BCA assay for protein concentration estimation

For protein concentration estimation, the Pierce BCA Protein Assay Kit (Table 2.5) was used following the manual instructions. The two reagents of the kit were mixed in a ratio of 50:1 (50x A, 1x B). The protein lysate, which was thawed on ice, was diluted 1:5 with RIPA buffer in a volume of 5 µL and 100 µL of BCA reaction mix was added. The samples were incubated for 30 min at 37 °C in a heating block (Table 2.13) and then cooled on ice. Utilizing a standard curve of protein concentrations from 0.125 to 2 mg/mL, the protein concentration of the individual protein samples could be determined by their measured absorbance intensity with the NanoDrop.

2.2.5.3 Sample preparation for Western Blot

The protein samples were adjusted to 60 µg (EtO, GCNF, GCNF-AM, GCNF mutDBD) or 90 µg (EtO, ctr, GCNF-VP16, GCNF shRNA) with RIPA buffer and 5x Laemmli buffer (Table 2.23) in a total volume of 30 to 45 µL for detection of GCNF signal. Protein samples of EtO cells for analyzing the protein level of GCNF and SOX2 during neuronal differentiation were adjusted to 90 µg, as well as GCNF-AM samples for detecting GCNF and AM upon DOX treatment. After heating the samples up for 10 min to 95 °C, they were stored at -20 °C.

Table 2.23: Reagents for preparing Laemmli buffer

Composition of Laemmli buffer	
Tris HCl	312.5 mM (pH 6.8)
SDS	10 %
Glycerol	50 %
Bromophenol blue	0.1 %
2-Mercaptoethanol (add fresh)	10 %

2.2.5.4 SDS-gel preparation

For protein separation, protein samples were run onto self-made SDS-gels. The hand-cast SDS-gels were prepared in two steps using the Mini PROTEAN casting chamber from Bio-Rad (Table 2.13). Initially, the separation gel was prepared (Table 2.24) and covered with isopropanol during the time of polymerization. After the separation gel was hardened, the isopropanol was aspirated and the stacking gel was added.

Table 2.24: Recipe for SDS gel

SDS gel for Western Blot			
10 % SDS separation gel (2x)		**SDS stacking gel (2x)**	
ddH_2O	8 mL	ddH_2O	2.3 mL
30 % Acrylamide	6.8 mL	30 % Acrylamide	0.66 mL
1.5 M Tris HCl (pH 8.8)	5.2 mL	0.5 M Tris HCl (pH 6.8)	1 mL
10 % SDS	200 µL	10 % SDS	40 µL
10 % APS	200 µL	10 % APS	40 µL
TEMED	8 µL	TEMED	4 µL

2.2.5.5 Western Blot

To separate individual proteins, the samples (see chapter 2.2.5.3) as well as 10 µL protein ladder (Table 2.4) were loaded onto self-made SDS gels. The gel was run for about 1.5 h at 100 to 120 V in Running buffer using the Mini PROTEAN electrophoresis chamber, before it was equilibrated in Transfer buffer (Table 2.25). The separated proteins were blotted onto a PVDF membrane using the Mini Trans-Blot Cell from Bio-Rad. The transfer sandwich was prepared as described in Table 2.26. The blotting was

performed for 2 h at 70 V under constant cooling. Next, the protein transfer was confirmed by Ponceau staining (Table 2.4). The blocking and antibody incubation were adapted accordingly to the different analyzed proteins in this work (Table 2.27). The membranes could be re-probed to extract as much as possible information from one performed blot. Therefore, membranes were incubated in stripping buffer (Table 2.25) for 30 min at 50 °C and washed five times for 5 to 10 min with TBS-T (Table 2.25) before the membrane could be blocked and incubated with another antibody. The chemiluminescence signal generated from the conversion of the used substrate (Immobilon Classico western HRP substrate, Table 2.4) by Horseradish peroxidase linked to the secondary antibody was detected with the ChemiDoc machine from Bio-Rad. Densiometric analyses of signals were performed using the Image lab software from Bio-Rad (Table 2.14). The lanes for each blot were defined as well as the detected signal bands. The signal intensity was determined and compared to each other after normalization to β-actin signal.

Table 2.25: Recipes for various Western Blot buffers

10x Running buffer (in H_2O)	
Trizma-Base	25 mM
Glycin	193 mM
SDS	0.1 % (w/v)

TBS-[T] (in H_2O)	
Tris HCl	10 mM (pH 7.5)
NaCl	150 mM (TBS_{50}: 50 mM)
[Tween-20]	0.1 %

Stripping buffer (in H_2O)	
SDS	2 % (w/v)
Tris HCl	62.5 mM (pH 6.7)
2-Mercap-toethanol	7 mM Add fresh

1x Transfer buffer (in H_2O)	
Trizma-Base	2.5 mM
Glycin	19.3 mM
Methanol	20 %

Table 2.26: Assembly of transfer sandwich

Transfer Sandwich
Cartridge (positioned to anode)
Sponge
Filter paper
SDS-gel with separated proteins
Membrane (PVDF or nitrocellulose)
Filter paper
Sponge
Cartidge (positioned to cathode)

Table 2.27: Conditions used for GCNF, SOX2, AM and β-actin Western Blot analysis

Condition	**GCNF**	**SOX2**
Blocking	5 % milk powder in TBS-T, 2 h at RT	5 % milk powder in TBS-T, 1 h at RT
1° antibody solution	GCNF mouse antibody, 1:1000 in 5 % milk powder in TBS-T, 4 °C overnight	SOX2 rabbit antibody, 1:1000 in 5 % milk powder in TBS-T, 4 °C overnight
Washing	TBS-T	TBS-T
2° antibody solution	HRP-goat anti-mouse, 1:1000 in 5 % milk powder in TBS-T, 2 h at RT	HRP-goat anti-rabbit, 1:1000 in 5 % milk powder in TBS-T, 1 h at RT
Condition	**AM-tag**	**β-actin**
Blocking	5 % milk powder in TBS-T, 2 h at RT	10 % milk powder in TBS-T, 1 h at RT
1° antibody solution	AM-tag mouse antibody, 1:1000 in 5 % milk powder in TBS-T, 2 h at RT	β-actin mouse antibody, 1:1000 in 5 % milk powder in TBS-T, 1 h at RT
Washing	TBS-T	TBS-T
2° antibody solution	HRP-goat anti-mouse, 1:1000 in 5 % milk powder in TBS-T, 2 h at RT	HRP-goat anti-mouse, 1:1000 in 5 % milk powder in TBS-T, 1 h at RT

2.2.5.6 Immunofluorescence staining

On the day of fixation (depending on experiment, mostly neuronal differentiation day (ND)7 or ND35), the culture medium was aspirated and the differentiated cells were carefully washed once with DPBS.

4 % PFA was added onto the cells and incubated for 10 min at RT. Fixed cultures were washed three times for 5 min with DPBS. Prior to staining a blocking step was performed to avoid unspecific binding of antibodies. The cells were incubated with 5 % FBS in 0.5 % Triton/DPBS for 2 h at RT. Cultures were stained with primary antibodies of interest (Table 2.7) in 5 % FBS in 0.5 % Triton/DPBS at 4 °C overnight. After three washing steps with DPBS the next day, the secondary antibodies (Table 2.8) were added for 2 h at RT in the dark followed by two further washing steps with DPBS. For immunofluorescence stainings of membrane associated proteins, the used buffers did not contain Triton. The cell nuclei were indirectly stained by counterstaining the DNA with 1:10,000 DAPI for 1 min at RT in the dark. The stained cells on 3.5 cm dishes with 4 inserts were mounted with Mowiol (Table 2.28) or Vectashield (Table 2.4) and glass covers and stored at 4 °C until imaging.

Table 2.28: Recipe of Mowiol

Mowiol solution	
Mowiol	2.49 g
Glycerol	6 g
ddH_2O	6 mL
→ dissolve	
0.2 M Tris HCl (pH 8.5)	12 mL
→ heat to 50 °C for 10 min, clarify by centrifugation, aliquot, store at -20 °C	

2.2.5.7 Image analysis and processing

The stained cells were imaged using Zeiss Apotome (stained cells cultivated on 3.5 cm dishes with 4 inserts) or Leica Live Cell (stained cell cultivated on 48 well plate). Three overview pictures at 10x magnification and five pictures at 20x magnification were taken per condition with the same exposure time for all cell lines to quantify the cells positive for neuronal or NSC markers. Automated adjustment of contrast and brightness was performed using ImageJ software (Table 2.14). Initially, DAPI-positive nuclei were scored and then cells positive for the markers of interest were manually counted using the cell counter plugin.

For the cell cluster analyses, cell clusters had to be defined initially. A cell cluster is an accumulation of five or more cells within less than one nucleus diameter away from each other. Only 10x overview images were used for cluster analyses. By determined the outer borders of each individual cluster the cluster area was measured, while their density was evaluated by counting each nucleus within each cluster.

2.2.5.8 Flow Cytometry assay and analysis

Flow cytometry analysis was performed using BD FACS Canto II Flow cytometer (FLC). Initially, forward scatter-area (FSC-A) and sideward scatter-area (SSC-A) were assessed to define the desired cell population. At least 2x10^4 single, living cells were analyzed by the following protocols.

2.2.5.8.1 EdU incorporation assay

SmNPC differentiated for 7 days were treated with 10 µM of 5-Ethynyl-2'-deoxyuridine (EdU) for 3 h at 37 °C, before the cells were dissociated with Accutase containing 1:100 DNase for 10 min incubation at 37 °C. The cell pellet formed after centrifugation at 180 xg was resuspended in 1:100 LIVE/DEAD reagent (Table 2.5) and incubated for 30 min at RT in the dark. The cell suspension was diluted with 1 mL DPBS and centrifuged for 5 min at 180 xg. The cells were fixed by adding 1 % BSA/DPBS and 4 % PFA for 10 min on ice and permeabilized in 0.5 % Triton/DPBS incubating 5 min on ice while

shaking. EdU was labelled by incubation for 30 min at RT with the EDU Click It-488 Kit reagents (Table 2.29, Table 2.5). Cells were washed in DPBS and resuspended in DPBS after centrifugation, followed by cell separation utilizing a cell strainer. The analysis was performed utilizing the flow cytometer as described above.

Table 2.29: Reaction cocktail for EdU Click It-488 reagents

Reaction cocktail for EdU detection	
PBS	218.75 µL
$CuSO_4$	5 µL
488 fluorescent dye	1.25 µL
Buffer additive	25 µL

2.2.5.8.2 Cluster of differentiation (CD) staining assay

7 day long differentiated smNPC cultures were dissociated with Accutase containing 1:100 DNase (10 min incubation at 37 °C), followed by centrifugation (180 xg for 5 min) and staining of dead cells by incubation the cells in 1:1000 LIVE/DEAD reagent (Table 2.5) for 30 min at RT in the dark. The cells were washed, pelleted and blocked by incubating the cells in 10 % FBS/DBPS for 30 min at RT. After another washing step and centrifugation, the cells were incubated in antibody solution (1:100 anti-CD200-APC and 1:100 anti-CD49f-PE in 2 % FBS/DPBS) for 30 min at RT. The stained cells were washed, resuspended and pushed to a cell strainer before analyzing by flow cytometer.

2.2.5.8.3 FLC analysis and processing

The raw data of the flow cytometry assays were analyzed by FlowJo software (Table 2.14). First, the cell population of interest was defined by applying FSC-A and SSC-A plots and SSC-A/SSC-H to exclude cell debris and cell duplets from the analyses. Secondly, the living cells within the population were determined according to the LIVE/DEAD staining. Among living cells, the signal for the stained marker of interest was examined by applicable channels in plots or histogram relying on unstained, secondary antibody or fluorescence-minus-one controls.

2.2.6 Analysis of gene expression on RNA level

2.2.6.1 RNA preparation

For gene expression analysis by quantitative real time PCR (qRT-PCR) or microarray analysis, adherent cells on the culture plate were washed twice with DPBS and lysed with 1 mL Trifast (Table 2.4). The lysate could be stored at -80 °C upon RNA extraction or directly used for RNA isolation. To separate RNA from DNA and protein, 200 µL chloroform was added to the Trifast lysate, mixed and incubated for 10 min at RT. After centrifugation at 12,000 xg for 10 min, three phases formed, of which the upper aqueous phase containing the RNA was transferred to a new 1.5 mL Eppendorf tube. The RNA was then precipitated by adding 500 µL isopropanol with 2 µL glycogen. After 1 h of incubation on ice (or incubation at -20 °C overnight) and subsequent centrifugation at 12,000 xg for 10 min at 4 °C, the RNA pellet was obtained. The RNA pellet was washed twice with ice-cold 75 % EtOH-DEPC-H_2O (Table 2.30) and air-dried for 30 min at RT, before it was solved in 20 µL DEPC-H_2O and treated with 2.5 µL DNase for 15 min at RT to acquire pure RNA. The DNase reaction was stopped by adding 2.5 µL of 25 mM EDTA solution and incubation for 10 min at 65 °C. The concentration and purity of the extracted RNA was measured by Nanodrop, prior to storage at -80 °C.

Table 2.30: Preparation of DEPC-H_2O

Preparation of DEPC-H_2O (1 L)	
DEPC	1 mL
H_2O	Up to 1000 mL
Stir under hood, lid open, overnight and light protected	
Next day, autoclaving	

2.2.6.2 qRT-PCR and cDNA synthesis

2.2.6.2.1 cDNA synthesis

To allow gene expression analysis by qRT-PCR the complementary DNA (cDNA) of the extracted RNA (see chapter 2.2.6.1) was synthesized using qScript cDNA Synthesis Kit (Table 2.5). 750 to 1000 ng RNA diluted in nuclease free water in a total volume of 15 µL were combined with 5 µL of master mix comprising qScript Reaction Mix 5x and qScript reverse transcriptase. Reverse transcription was performed using the following thermocycler program (Table 2.31). The concentration and purity of the yielded cDNA was determined by Nanodrop, prior to storage at 4 °C.

Table 2.31 cDNA synthesis thermocycler program

Step	Temperature [°C]	Time [min]
1	22	5
2	42	30
3	85	5
Pause	11	

2.2.6.2.2 qRT-PCR

For qRT-PCR 150 ng/µL of synthesized cDNA template was added to the qRT-PCR reaction mix (Table 2.32). The SYBR Green SuperMix 2x was prepared as presented below (Table 2.33). Each sample was prepared in three technical repeats on one 96 well plate. To analyze the expression level of the gene of interest, primers listed in Table 2.9 were designed and used in qRT-PCR reactions, which were run on the Mastercycler realplex[4] (Table 2.13). Cycling parameters established for qRT-PCR are listed in Table 2.34. The obtained data were analyzed using the $2^{-\Delta\Delta Ct}$ method (Livak and Schmittgen, 2001) and further normalized to the expression value of NPC or EtO samples.

Table 2.32: qRT-PCR reaction mix

Components	Amount [µL]
SYBR Green SuperMix 2x	10
Taq Polymerase	0.12
cDNA (150 ng/µL)	2
Forward/reverse primer mix (3 µM)	0.8
Add H_2O to final volume of 20 µL	

Table 2.33: SYBR Green SuperMix 2x recipe (40 mL)

Components	Amount [µL]
10x PCR buffer	8000
50 mM $MgCl_2$	4800
dNTPs (100 mM each)	160
1000x SYBR Green	60
100 µM fluorescein	8
Ampuwa H_2O	26492

Table 2.34: qRT-PCR thermocycler program

Step	Temperature [°C]	Time	Number of cycles
Pre-heating	95	3 min	1x
Denaturation	95	15 s	
Annealing	60	20 s	40x
Elongation	72	30 s	
Melting curve	55 - 95		1x
Hold	4		

2.2.6.3 Microarray-based gene expression analysis

For microarray-based gene expression analysis, isolated RNA samples (see chapter 2.2.6.1) were purified using the RNA Clean & Concentrator-5 Kit from Zymo Research (Table 2.5) and their integrity was examined on an Agilent 2100 BioAnalyzer (Agilent Technologies) at the Institute of Human Genetics (University Hospital Bonn). Subsequently, the cells were sent to ATLAS Biolabs for microarray-based gene expression analysis. There, biotinylated single stranded (ss)-cDNA was prepared according to the standard Affymetrix protocol using the GeneChip WT PLUS Reagent Kit User Manual (Affymetrix/Thermo Fisher Scientific). Fragmented and labeled ss-cDNA was then hybridized on a GeneChip Clariom S Array (Affymetrix/ThermoFisher Scientific). The raw data were processed with the Affymetrix Expression Console Software. All samples passed QC thresholds for hybridization and labeling. The analyses of differential gene expression as well as the principal component analysis (PCA) of these data were performed by using the Transcriptome Analysis Console Software (TAC 4.0, Table 2.14). Gene ontology enrichment for biological processes was performed using the web-based tool Geneonthology.org relying on the PANTHER classification system (Mi *et al.*, 2019). Functional annotation clustering was performed using DAVID Bioinformatics Resource 6.8 (Huang *et al.*, 2009).

2.2.6.4 RNA *in situ* hybridization

RNA *in situ* hybridization was carried out to analyze the spatial expression pattern of GCNF. Cryosections of E18.5 mouse brain coronal sections (provided from Marianna Tolve, Working group Blaess, Institute of Reconstructive Neurobiology, University Hospital Bonn) and of 20 days old human brain organoids (provided by Ammar Jabali, Working group Ladewig, Institute of Reconstructive Neurobiology, University Hospital Bonn) were treated with RNA probes against GCNF and SOX2. Therefore, single stranded, anti-sense DIG labeled RNA probes for GCNF and SOX2 mRNA were generated, initially.

2.2.6.4.1 Cloning of plasmids containing GCNF and SOX2 cDNA sequence

To generate specific RNA probes against GCNF and SOX2, plasmids containing their sequence as a template for *in vitro* transcription had to be prepared. The plasmid carrying human GCNF (hGCNF) sequence was prepared by Dr. Laura Stappert (Institute of Reconstructive Neurobiology, University Hospital Bonn). Oligonucleotides specific for mouse GCNF and hSOX2 were produced by performing Q5 polymerase-based PCR (Table 2.35, Table 2.36) using lt-NES cDNA generated from total lt-NES RNA and mouse cDNA provided by Working group Blaess. The samples were loaded on 1.5 % agarose gels (Table 2.37) and run for 30 min at 100 V. The bands of the generated DNA fragments were cut out and purified with the gel extraction kit (Table 2.5) according to the manufacturer's instructions.

Table 2.35: Q5 PCR reaction mix

Components	Amount [µL]
5x Q5 reaction buffer	4
10 mM dNTPs	0.4
Forward/reverse primer mix (10 µM)	2
Q5 polymerase	0.2
GC Enhancer	4
DNA template (50 ng/µL)	X according to conc. of template
Ampuwa H_2O	Fill up to 50

Table 2.36: Q5 PCR thermocycler program

Step	Temperature [°C]	Time	Number of cycles
Pre-heating	98	pause	1x
Denaturation	98	10 s	30x
Annealing	64 (mGCNF), 65 (hSOX2)	20 s	
Elongation	72	20 s	
Stop	72	2 min	1x
Hold	4		

Table 2.37: Buffer and recipe to prepare agarose gels

50 % TAE buffer	1.5 % agarose gel
242 g Tris 100 mL EDTA (0.5 M pH 8.5) 57 mL Acetic Acid (100 %) Add H_2O to 1000 mL	1.5 % agarose Add TAE buffer of desired volume Warm up in microwave until agarose dissolved, cool down to 50 °C Add 1:10,000 Ethidium bromide Fill in gel cast and wait until solidified

Afterwards, the PCR products were digested with EcoR1 and Not1 restriction enzymes according to NEB protocols to allow ligation into the CMV Sport 6 vector using T4 ligase (Table 2.38).

Table 2.38: Ligation into CMV Sport 6

Components	Amount [µL]
Ligation buffer	2
T4 ligase	1
CMV Sport 6 (50 ng)	0.95
PCR insert (26.44 ng)	1.57 (mGCNF), 1.21 (SOX2)
Ampuwa H_2O	Fill up to 20
Incubate for 2 h at 25 °C, 10 min at 65 °C	

The generated plasmids were inoculated into E. coli Stlb 3 competent bacteria. The bacteria were thawed on ice and 50 µL of bacteria were mixed carefully with 2 µL plasmid. After 30 min incubation on ice, a heat shock was applied for 45 s at 42 °C followed by cooling on ice for 2 min. Then 500 µL prewarmed SOC medium (Table 2.39) was added and the bacteria suspension was incubated for 1 h at 37 °C, while shaking. The cells were distributed on LB/Amp agar plates and incubated overnight at 37 °C.

Table 2.39: Media for bacteria and culture plates

LB medium		SOC medium		Agar plates
10 g	Tryptone	20 g	Tryptone	15 g agar dissolved in 1000 ml LB medium
5 g	Yeast Extract	5 g	Yeast Extract	→ autoclave
10 g	NaCl	0.5 g	NaCl	Heated agar (50 °C) + 1:1000 Amp
1 mL	NaOH (1 M)	0.186 g	KCl	→ pour into sterile petri dishes, let solidify at RT
Up to 1000 mL	ddH_2O	3.6 g	Glucose	→ store at 4 °C in sealed plastic bags
Autoclave and store at 4 °C		Up to 1 L ddH_2O		
		1 g	$MgCl_2$	
		1 g	$MgSO_4$	

The next day, 10 colonies of grown bacteria clones were picked with a sterile pipet tip and resuspended in 20 µL Ampuwa H_2O. This suspension is used as template in a colony PCR using T7 and SP6 primer (Table 2.9, Table 2.40, Table 2.41), which was performed to confirm transformation of bacteria.

Table 2.40: Colony Taq PCR reaction mix

Components	Amount [µL]
10x PCR buffer	2
10 mM dNTPs	0.4
Forward/reverse primer mix (10 µM)	2
Taq polymerase	0.1
50 mM $MgCl_2$	0.6
DNA template	1
Ampuwa H_2O	13.9

Table 2.41: Colony PCR thermocycler program

Step	Temperature [°C]	Time	Number of cycles
Pre-heating	95	6 min	1x
Denaturation	95	30 s	
Annealing	60	30 s	35x
Elongation	72	30 s	
Stop	72	10 min	1x
Hold	4		

The remaining bacteria suspension of clones, which show an integration of the PCR product into the vector were used to start a mini culture (5 mL LB medium + 1:1000 Amp), which was cultivated overnight at 37 °C. The plasmids expanded in the bacteria cultures were purified by mini prep kit (Table 2.5) according to manufacturer's instructions and sent for Sanger sequencing to MicroSynth using the same primers as before for the colony PCR (Table 2.9). The Sanger sequencing results were analyzed by ApE (A plasmid Editor v2.0.61, Table 2.14). 1 mL of mini cultures from clones carrying CMV Sport 6 plasmids with the correct sequence of PCR product were used to start midi cultures (200 mL LB medium + 1:1000 Amp), which were grown overnight at 37 °C while shaking. The next day, 300 µL of the bacteria culture was add to glycerol and stored at -80 °C. The desired plasmids from the remaining bacteria culture were harvested by midi prep kit (Table 2.5) according to kit's manual. The purified plasmids were stored at -20 °C.

2.2.6.4.2 Plasmid linearization and *in vitro* transcription to generate anti-sense RNA probes

Plasmids were linearized with the Nhe1 restriction enzyme according to NEB protocol and purification of linearized plasmids was carried out with the gel extraction kit according to the manufacturer's protocol. DIG-labeled RNA probes were transcribed from the linearized plasmid templates using DNA-dependent RNA polymerases from the bacteriophages SP6 (antisense probe) and T7 (sense probe for control) (Table 2.42).

Table 2.42: *In vitro* transcription protocol

Components	Amount [µL]
1 µg linearized plasmid	x
Polymerase (T7 or SP6)	1.5
10x transcription buffer	2
DIG-labeled dNTPs	2
RNase inhibitor	0.5
Ampuwa H_2O	Fill up to 20
Incubate for 3 h at 37 °C	

2.2.6.4.3 Hybridization

Cryosections of mouse telencephalon (E18.5) and human 20 days old brain organoids were post-fixed with 4 % PFA for 10 min. After rinsing them with DPBS, the sections were acetylated in 50 mL 0.1 M Triethanolamine (TEA)-HCl (Table 2.43) with 125 µL acetic anhydride for 5 min while stirring. Sections were rinsed again in DPBS and briefly dehydrated in EtOH and chloroform (70 % EtOH 1 min, 80 % EtOH 1 min, 95 % EtOH 2 min, 100 % EtOH 1 min, chloroform 5 min, 95 % EtOH 1 min, 100 % EtOH 1 min). The hybridization solution consists of 1 µg RNA probe and 1 mL hybridization buffer (Table 2.43), which was mixed together and incubated for 2 min at 80 °C. The prepared sections were air-dried and transferred to a humidified hybridization cassette, which was filled with a 1:1 mixture of formamide and ddH_2O. 300 µL of each hybridization solution was added to each slide, which were covered with RNAse-free coverslips and incubated at 55 °C overnight. On the next day, coverslips were removed in prewarmed 5x SSC (high stringency wash solution, Table 2.43) and to reduce unspecific hybridization, the sections were incubated in a 1:1 solution of formamide and 2x SSC for 30 min at 65 °C. Non-hybridized RNA was removed by incubating the sections with RNAse buffer (Table 2.43), containing 0.1 % RNase A, for 10 min at 37 °C. The sections were washed with 2x SSC for 20 min at 65 °C and then with 0.1x SSC for 15 min at 37 °C. Before the sections were stained with anti-DIG-AP Fab fragments (Table 2.7, 1:5000 in 1 % NGS 0.1 % DPBS-Tween-20) overnight at 4 °C, they were incubated with 10 % NGS in 0.1 % DPBS-Tween-20 for 1 h in a humidified chamber at RT to avoid unspecific binding of anti-DIG-AP Fab fragments. After staining, the sections were washed several times with 0.1 % DPBS-Tween-20, followed by two washing steps for 10 min at RT in NTMT buffer (Table 2.43) spiked with 1 mg/mL levamisole to diminish the background of endogenous alkaline phosphatase activity. The sections were incubated at RT with the AP substrate BM purple mixed with 0.5 mg/mL levamisole until signal was observed (4 days mouse cryosection, 3 days organoids). The reaction was stopped by incubating the sections in TE buffer (Table 2.43) for 10 min at RT. Finally, the sections were washed with DPBS and mounted with Vectashield and a glass coverslip.

Table 2.43: Solutions for RNA ISH

TEA-HCl 0.1 M	**SSC 20x pH 7.0**	**RNase A**
650 µL TEA 130 µL 12 M HCl Add Ampuwa H_2O (final volume 50 mL)	88.2 g NaCitrate ($C_6H_5Na_3O_7$) 174 g NaCl Add Ampuwa H_2O (final volume 1 L)	100 mg RNase A 100 µL Tris-HCl (pH 7.5 10 mM) 10 mL 0.5 M EDTA (pH 8.0 5 mM) 880 mL dH_2O
Hybridization buffer	**NTMT**	**TE buffer pH 8.0**
50 mL Formamide (deionized) 20 mL 50 % Dextran sulfate 2 mL 50x Denhardt's 2.5 mL yeast tRNA (10 mg/mL) 6 mL 5 M NaCl 2 mL 1 M Tris-HCl (pH 8.0) 1 mL 0.5 M EDTA 1 mL 1 M $Na_4P_2O_7$ (pH 8.0) 5 mL 20 % Sarcosyl 11.5 mL Ampuwa H_2O	2 mL 5 M NaCl 10 mL 1 M Tris-HCl (pH 9.5) 5 mL 1 M $MgCl_2$ 0.1 mL Tween-20 82.9 mL ddH_2O	1 mL 1 M Tris-HCl (pH 8.0) 200 µL 0.5 M EDTA Add ddH_2O (final volume 100 mL)

2.2.6.4.4 Image acquisition

The RNA in situ hybridized sections were imaged at an inverted Zeiss AxioObserver Z1 microscope equipped with an ApoTome (Table 2.13). At 5x and 20x magnifications, tile images were acquired with transillumination. Images were stitched with Zen blue software (Zeiss, 2012) (Table 2.14).

2.2.7 Analysis of GCNF binding sites

2.2.7.1 GCNF binding site prediction (TRANSFAC analysis)

For the prediction of GCNF binding sites in the regulatory region of suspected GCNF target genes, a list of these genes was uploaded to the TRANSFAC® (Table 2.14) database and analyzed using the Match Tool. The following parameters were applied to the analyses: For the genes on the list the best supported promotors in a region of -10,000 to 10,000 nucleotides were analyzed for the already published binding sites of GCNF (Figure 3.14). The cut-off was set at “minimize the sum of both error rates”. TRANSFAC Match Tool provides then a list of genes with predicted number of binding sites and genomic location.

2.2.7.2 Chromatin immunoprecipitation and analysis

2.2.7.2.1 ChIP sample preparation

Chromatin immunoprecipitation (ChIP) is a technique to study the interaction of proteins and DNA, which allows the physical confirmation of transcription factor binding. The overall processes of ChIP assays and its analyses by qRT-PCR is displayed in Figure 3.16. To analyze the binding of GCNF to DNA, GCNF-bound DNA fragments were immunoprecipitated. During this process, it was crucial that GCNF is targeted by a specific antibody. Since, no ChIP-grade antibodies for GCNF were available, a lentiviral overexpression for GCNF labeled with an AM-tag from Active Motif was designed and transduced into smNPCs (Table 2.10 and see Chapter 2.2.2.3). Thus, GCNF-bound DNA fragments were precipitated via an antibody against the AM-tag. The Tag-ChIP-It Kit from Active Motif (Table 2.5) was used for performing the ChIP assay. The manufacturer’s instructions were followed with some additional steps (see Chapter 6.1).

GCNF and GCNF-AM-overexpressing smNPCs were differentiated for 2 days in the presences of DOX on 6 cm dishes, then the cells were dissociated with Accutase for 10 min at 37 °C. The dissociated cells were transferred to a falcon tube and the 6 cm dishes were rinsed twice with DPBS to collect all cells. The cell number was determined by counting with a Neubauer chamber and the cells were centrifuged for 4 min at 250 xg. The cell pellet was resuspended in DPBS to prepare a cell suspension with a concentration of $5.4x10^6$ cells/mL. The first step of the ChIP assay is the crosslinking of all DNA bound protein with the DNA. Therefore, the cells in suspension were treated with 1/10 fixation buffer (Table 2.44) and incubated for 15 min at RT on a rolling device. To stop the crosslinking 1/20 of Stop solution was added and incubated for 5 min at RT on a rolling device.

Table 2.44: Recipe of fixation buffer

Components	Amount [µL]
Fixation reagent	90
Ampuwa H_2O	785
Formaldehyd (37% + MeOH)	375

During the incubation of crosslinking, the PBS-PP buffer was prepared according to the manual (Table 2.45) and stored on ice. The cells were centrifuged for 3 min at 1,300 xg at 4 °C and resuspended in PBS-PP buffer. This washing step was performed twice.

Table 2.45: Recipe for PBS-PP buffer

Components	Amount [mL]
10x PBS	2.4
Ampuwa H_2O	20.4
Detergent	1.2

In a next step the cells were lysed chemically by incubating them in Chromatin Prep Buffer supplemented with 1:1000 PI and PMSF (concentration of cell suspension $2.97x10^5$ cells/mL) for 10 min at 4 °C on a rolling device with regular applying mechanical force with a glass douncer (3x10 strokes with pauses in between). The cell lysis was confirmed by microscopic observation. The nuclei/cell debris suspension was centrifuged for 3 min at 4 °C at 1300 xg and the nuclei pellet was resuspended in ChIP buffer ($40x10^6$ cells/mL) supplemented with 1:100 PI and PMSF and snap frozen in liquid nitrogen. The nuclei suspension could be stored at -80 °C or used directly for ChIP. Before chromatin fragmentation using a Bioruptor Pico (Table 2.13), the nuclei suspension was thawed on ice and divided to Bioruptor tubes (100 µL per tube). Then, the nuclei suspension was sonicated at 4 °C for 60 min with 30 s off/on. Before the samples were used for ChIP assays the successful fragmentation of the samples was confirmed by taking a small fraction of the sample and performing reverse crosslinking, DNA purification and NaCl treatment of the DNA samples as described in the manual, followed by gel electrophoresis (1.5 % agarose gels, 15 min and additional 30 min, 100 V).
When successful chromatin fragmentation was confirmed and the DNA concentration was determined, the samples were used for ChIP.

2.2.7.2.2 ChIP and ChIP qRT-PCR

The ChIP itself was performed according to the manufacturer's instructions using POL II and IgG antibodies, as positive or isotype control, respectively, and AM-tag antibodies to target GCNF-AM (Table 2.7). Before the chromatin fragments, which were bound by the specific antibody (IP reaction), were pulled down by utilizing Protein G agarose beads, the beads (30 µL per IP reaction) were incubated with bridging antibody (5 µL per reaction) for 1 h at 4 °C on a rolling device to facilitate improved binding of mouse IgG to the beads. The beads were washed twice with ChIP buffer and added to the IP reaction. After the IP, reverse crosslinking and DNA purification were performed, the ChIP samples were analyzed by qRT-PCR using positive primers, which bind to the predicted GCNF binding site, and negative primer pairs, which bind to a DNA sequence 1,000 up- or downstream of the predicted binding site. As additional control for the qRT-PCR, samples, which were prepared after sonication to confirm the chromatin fragmentation, but which did not run through a ChIP reaction (Input samples), were used. Primer design was based on the predicted binding site from the TRANSFAC® analyses (see chapter 2.2.7.1) and performed using the web-based tools primer 3 and NCBI nucleotide blast (Table 2.14). The used primers are listed in Table 2.9. For the qRT-PCR, a commercial SYBR Green master mix was used (Table 2.5) in the following reaction (Table 2.46). The qRT-PCR program was the same as for qRT-PCR based on cDNA (Table 2.34).

The fold enrichment of chromatin fragments containing the GCNF binding site over DNA fragments 1,000 bp up- or downstream of the predicted binding site could be determined by dividing the fold change of the positive primer for a specific sample by the fold change of the negative primer for this sample.

Table 2.46: qRT-PCR reaction mix

Components	Amount [µL]
Quanta Master Mix	10
Forward/reverse primer mix (2.5 µM)	2.4
ChIP DNA	7.6

2.2.8 Statistical analysis

Statistical analysis of quantitative data, which were obtained in at least biological triplicates, were performed using GraphPad Prism 9 (Table 2.14). Initially, the normal distribution of the analyzed data was checked by Shapiro-Wilk test. Data distributed within the Gaussian distribution were analyzed by unpaired t-test, otherwise they were analyzed by non-parametric Mann-Whitney U test.
Results were represented in graphs with mean + SEM (standard error of mean), $p < 0.05$ was considered as statistically significant.

3. Results

Tight regulation of NSC proliferation and differentiation is crucial for the development and homeostasis of a functioning central nervous system. However, the molecular mechanisms regulating these processes are still under investigation. Various animal studies have indicated a critical role of the transcription factor GCNF in neural lineage development. GCNF displays a distinct expression pattern in the developing brain and reduction of its expression impairs neurogenesis in several species.

Nevertheless, little is known about the function of GCNF during human neurogenesis. The overall aim of this study was therefore to decipher the mechanistic role of GCNF during human neuronal development.

To this aim, the spatial and temporal expression pattern of GCNF were analyzed to gain first insights if GCNF might be involved in human neuronal differentiation. To understand the mechanistic role of GCNF during neuronal development, the proliferation capacity and differentiation status of differentiating smNPCs were analyzed upon modulation of GCNF expression. Additionally, the effect of altered GCNF expression on global gene expression at different timepoints of the neuronal differentiation was examined. Further, understanding of the molecular function of GCNF during neuronal differentiation was gained by being able to identify a direct target gene of GCNF.

During these studies, we discovered that reversing the function of GCNF towards a transcriptional activator by fusing the transactivator domain of VP16 with the GCNF protein had pronounced effects on neuronal differentiation and cell clustering. For that reason, GCNF-VP16 was investigated as tool for accelerated differentiation of hNSCs towards almost cluster-free neuronal cultures.

The following results are partially published in a patent application (Stappert, L., Klaus, F. and Brüstle, O., 2020. Rapid production of human neuronal cultures with single cell resolution. European Patent application No. 20192024.6-1118. Munich, Germany. European Patent Office).

3.1 Analysis of GCNF expression profile

3.1.1 GCNF expression is highest in neural progenitor cells

To gain first insights into the potential role of GCNF in human neurogenesis, the temporal and the spatial expression pattern of GCNF was analyzed and compared to the known NSC marker SOX2.

The temporal expression pattern of GCNF were analyzed in smNPCs and their neuronal progeny (Figure ***3.1***) and the spatial expression pattern was determined in the embryonic mouse brain and in human cortical organoids (Figure 3.2).

Protein samples from smNPCs and their neuronal progeny (ND7 and ND14, 7 days and 14 days old neurons) were analyzed by Western Blot to determine GCNF and SOX2 protein levels (Figure 3.1 A). Densitometric analyses of three independently performed Western Blots from independently generated protein samples revealed that GCNF is highest expressed at stem cell level and is downregulated during the process of neuronal differentiation with decreasing protein levels from ND7 to ND14 (Figure 3.1 B). A similar temporal expression pattern is displayed by SOX2 (Figure 3.1 C).

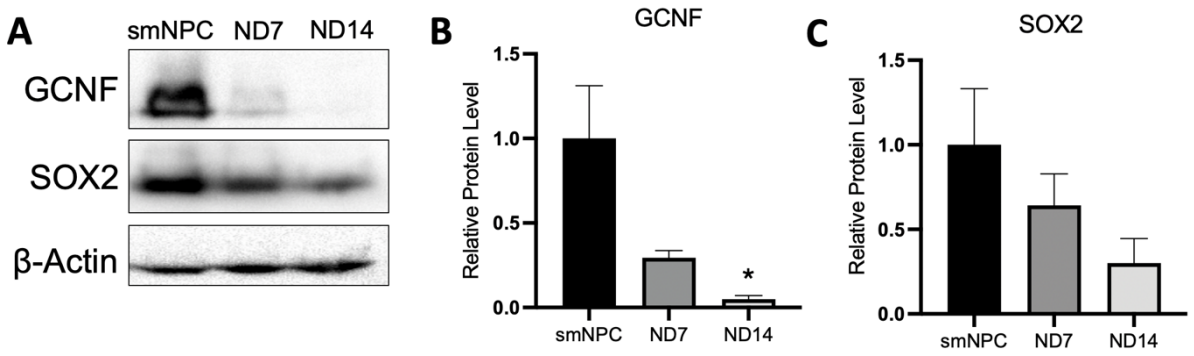

Figure 3.1: Temporal expression pattern of GCNF in smNPCs and their neuronal progeny. (A) Exemplary Western Blot for GCNF and neural stem cell marker SOX2 to determine their expression levels in smNPCs and their neuronal differentiated progeny (ND7 and ND14). β-actin was used as loading control. **(B)** Densitometric analysis of Western Blots displays a downregulation of GCNF protein levels during neuronal differentiation **(C)** similar to SOX2 expression pattern. The signal of GCNF/SOX2 was normalized to β-actin signal and smNPC samples. Data are presented as mean + SEM, n = 3, * $p \leq 0.05$, unpaired t-test, compared to smNPCs. ND7/ND14 = Neuronal differentiation day 7/14.

Next, the spatial expression pattern of GCNF was determined by using RNA *in situ* hybridization (ISH) of GCNF anti-sense probes on coronal E18.5 mouse brain sections and 20 days old human cortical organoids, which reproduce early stages of the developing human brain (Iefremova *et al.*, 2017). GCNF expression could be visualized by RNA ISH on E18.5 mouse brain sections in cells adjacent to the lateral ventricle, a region known for consisting of proliferating neural progenitor cells (NPCs) (Figure **3.2** A) (Conover and Todd, 2017). Furthermore, RNA ISH for GCNF and additionally for SOX2 on subsequent cortical organoid cryosections was performed and revealed a predominate expression of both genes in cells located at the apical surface of the neuroepithelial loops (Figure 3.2 B, C). These cortical loops resemble early developmental stages of the human cortex with cortical progenitor cells at the apical side of the loops, suggested to be reminiscent of the ventricular zone of the human brain (Iefremova *et al.*, 2017). Thus, GCNF is expressed in cells, which are considered to be cortical progenitor cells based on their locations and their expression of the NSC marker SOX2.

In summary, the temporal expression pattern as well as the spatial expression pattern of GCNF displayed high resemblance to the one of the NSC marker SOX2. Therefore, we hypothesized that GCNF might play a similar role in NSCs as the one described for SOX2. SOX2 is reported to be a NSC marker and its expression is necessary to maintain stem cell properties (Ellis *et al.*, 2004), which could also be a possible mechanistic function of GCNF.

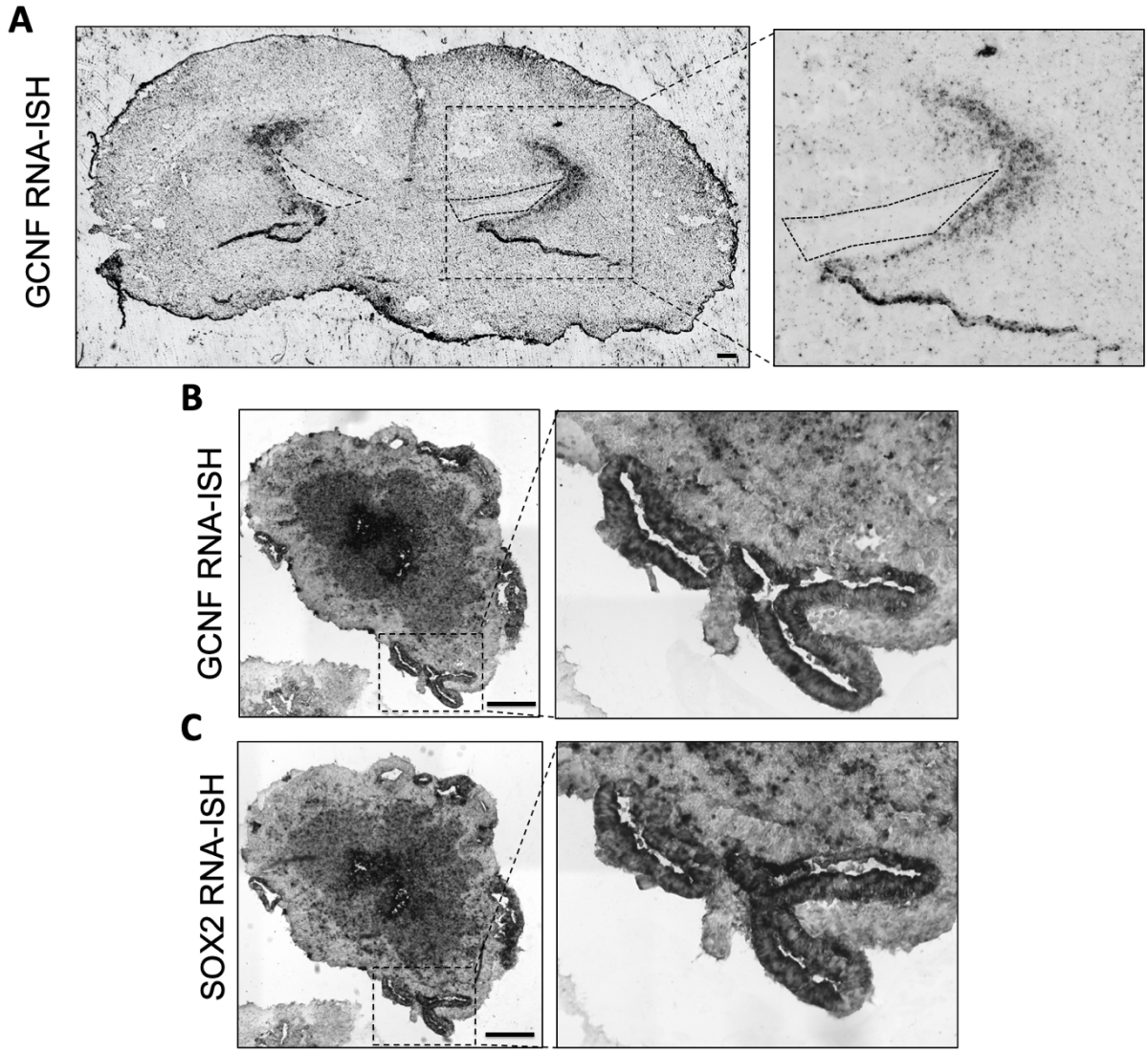

Figure 3.2: Spatial expression pattern of GCNF in E18.5 mouse brain and 20 days old human cortical organoids. (A) RNA *in situ* hybridization (ISH) using an antisense probe for GCNF on E18.5 old coronal mouse brain sections reveals expression of GCNF in neural progenitor cells located adjacent to the lateral ventricle. Scale bar = 100 µm. **(B)** RNA ISH of GCNF and **(C)** SOX2 on 20 days old human brain organoids displays GCNF and SOX expression in loop structures consisting of neural stem/progenitor cells. Scale bar = 100 µm.

3.2 GCNF inhibits neuronal differentiation, while increasing NSC proliferation and clustering

To understand the role of GCNF during human neuronal differentiation, smNPCs and their neuronal progeny were used as a proxy for human neuronal development. In a first step, smNPC lines were generated carrying different constructs to modulate GCNF expression in an inducable manner. Then, these smNPCs were differentiated for seven days and the effects of altered GCNF expression on proliferative capacity, neuronal differentiation status and overall cell culture architecture were analyzed.

3.2.1 Inducible expression of GCNF in NSCs

The modulation of GCNF expression during neuronal differentiation of smNPCs and the subsequent analysis of specific features of the generated, differentiated cell cultures could give valuable insights

into the mechanistic role of GCNF in neuronal development. Thus, we used the Tet-On Advanced system to modulate GCNF expression upon doxycycline (DOX) induction. This system includes two lentiviruses: One carries the Tet-On Advanced construct under an EF1α promotor (EtO virus) and the second lentivirus carries a plasmid coding for the cDNA of the gene of interest (GoI), which is controlled by the tetracycline response element (TRE). In the presence of DOX, the Tet-On Advanced fusion protein binds to the TRE and activates GoI expression.

Seven different smNPC lines were generated, which carried different lentiviral constructs (Figure 3.3 A). Two smNPC lines were used as controls: One cell line, that only carried the EtO virus and a second cell line, which carried an overexpression construct for the non-targeting miRNA miR30 (ctr), next to the EtO virus.

Four cell lines were generated, which carried different lentiviral constructs, that directly affected the GCNF expression: A GCNF-overexpressing construct, an overexpression construct of GCNF with a mutated, non-functional DNA-binding domain (GCNF mutDBD), a construct coding for a short hairpin RNA targeting the GCNF mRNA (GCNF shRNA) resulting in the knockdown of GCNF expression and a lentiviral construct for the inducible expression of GCNF fused with the transactivator domain of VP16 (GCNF-VP16) to reverse the function of GCNF from a transcriptional repressor to an transcriptional activator (Fuhrmann *et al.*, 2001). The different GCNF constructs made it possible to understand if observations of altered smNPC behavior in later performed experiments are a direct consequence of GCNF and its function. On one hand, smNPCs carrying the overexpression construct were assumed to show the opposite effects on smNPC behavior than smNPCs carrying the knockdown construct for GCNF. On the other hand, GCNF mutDBD carrying smNPCs could be used as control to understand if certain alterations in smNPC cell behavior were caused by GCNF and its role as transcription factor, since the form of the GCNF protein with the mutated DBD could not bind to DNA and therefore, it could not repress the expression of its target genes. Additionally, the smNPCs carrying the GCNF-VP16 construct should not only display opposite effects of smNPC behavior in later performed experiments compared to GCNF-overexpressing smNPCs. It could also be used to identify target genes of GCNF, as GCNF and GCNF-VP16 bind to the same target genes via their identical DBD. GCNF would naturally repress the expression of these direct target genes, while GCNF-VP16 would activate the expression of these genes via the fused transactivator domain of VP16. From previously performed experiments in our institute utilizing lt-NES as proxy for human brain development, we suggested that GCNF inhibits neuronal differentiation (Stappert, 2015, doctoral thesis). Hence, forced expression of GCNF-VP16 in smNPCs was suspected to promote neuronal differentiation. As control cell line for accelerated neuronal differentiation, smNPCs were transduced with a NGN2-overexpression construct. NGN2 is a transcription factor, which is well established as neuronal inducer (Thoma *et al.*, 2012).

Before, these generated smNPCs could be used for experiments to reveal the mechanistic role of GCNF during neuronal differentiation, the functionality of the generated and transduced constructs needed to be confirmed. For this reason, the seven different smNPC lines were cultivated in the presence of DOX for 48 h to induce transgene expression before the RNA and protein level of GCNF were analyzed.

On RNA level, the GCNF expression was significantly increased in smNPCs, in which GCNF, GCNF-mutDBD and GCNF-VP16 expression was induced, compared to the control cells, EtO and ctr. The expression of the shRNA targeting GCNF (GCNF shRNA) led to a significant decrease of GCNF mRNA

levels compared to control smNPC lines. Additionally, the overexpression of NGN2 in smNPCs resulted in decreased GCNF mRNA levels (Figure 3.3 B), which might be due to advanced neuronal differentiation of NGN2-overexpressing smNPCs and the natural downregulation of GCNF expression in the process of neuronal differentiation (Figure 3.1).

GCNF protein levels were determined by Western Blot and its densiometric analysis (Figure 3.3 C, D). On protein level, elevated GCNF levels could be demonstrated for GCNF, GCNF-mutDBD and GCNF-VP16 carrying smNPC lines after 48 h of DOX induction compared to control smNPC lines, EtO and ctr. The expression of the shRNA against GCNF mRNA led to a knockdown of GCNF also on protein level (Figure 3.3 C, D).

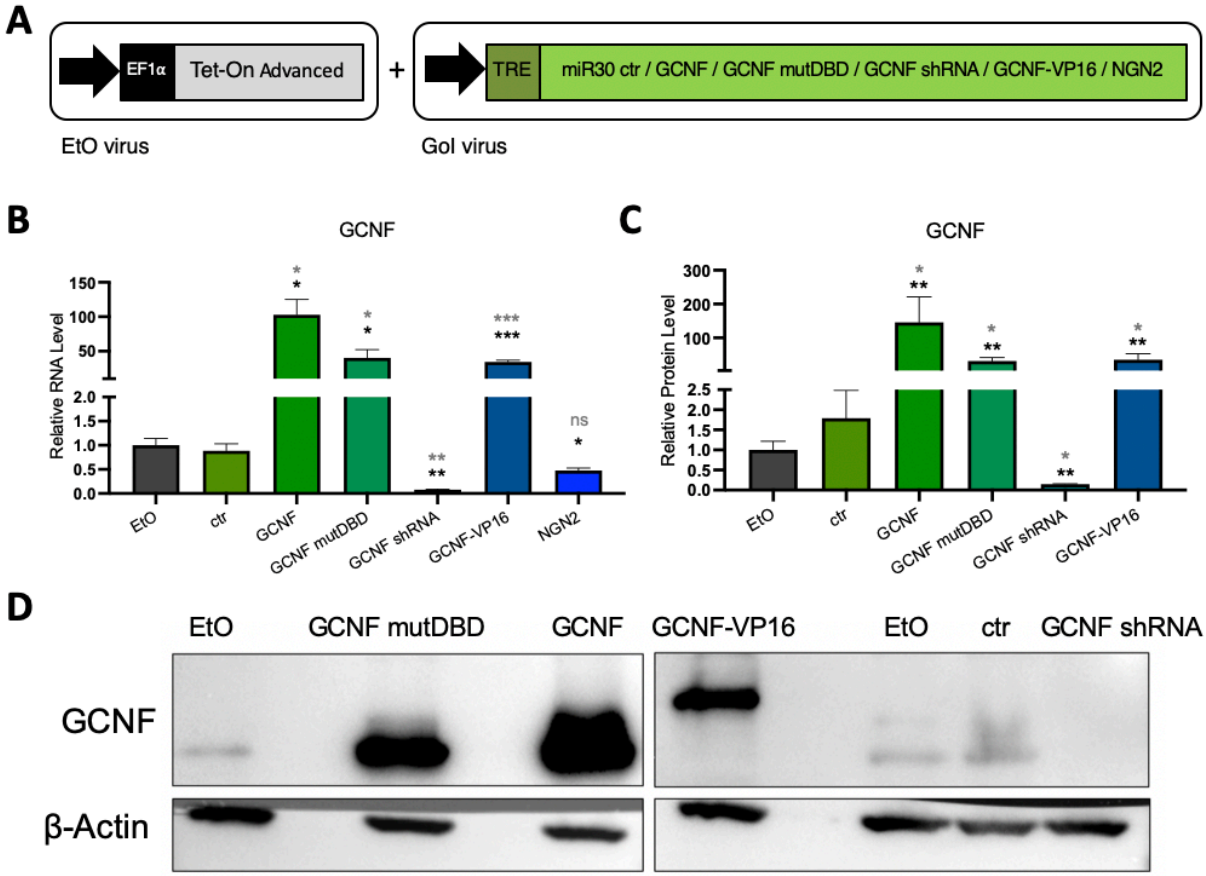

Figure 3.3: Modulation of GCNF expression in smNPCs. (A) Schematic of lentiviral constructs for inducible modulation of GCNF expression utilizing the Tet-On Advanced system. **(B)** Qualitative RT-PCRs and **(C)** Western Blots confirm the overexpression of GCNF in GCNF, GCNF mutDBD and GCNF-VP16 smNPC lines after 48 h treatment with doxycycline (DOX). (B) The GCNF-RNA level is decreased in GCNF shRNA cells and additionally also in the NGN2-overexpressing cell line. Data were normalized to 18S rRNA levels and are presented relative to EtO samples. Data are presented as mean + SEM, n = 3, * $p \leq 0.05$, ** $p \leq 0.01$, *** $p \leq 0.001$ (in black compared to EtO, in grey compared to ctr), unpaired t-test. (C) GCNF protein levels are normalized to β-actin protein levels. Data are presented relative to EtO samples as mean + SEM, n = 4, * $p \leq 0.05$, ** $p \leq 0.01$ (in black compared to EtO, in grey compared to ctr), Mann-Whitney test. **(D)** Exemplary Western Blot for GCNF for EtO, ctr, GCNF, GCNF mutDBD, GCNF shRNA and GCNF-VP16. β-actin was used as loading control. The samples were analyzed on two different blots due to technical feasibility.

To ensure quality of the generated smNPC lines, the NSC properties and genomic integrity of the cells after lentiviral transduction were analyzed. For this reason, expression of the NSC markers NESTIN, SOX2, PAX6 and DACH1 and of the neuronal markers β-III tubulin and MAP2 was confirmed in the

generated smNPC lines (Supplementary Figure 6.1) and SNP analysis of the generated smNPC lines was performed (Supplementary Figure 6.2). All cell lines passed this quality control and were used for downstream experiments to analyze the function of GCNF during neuronal differentiation.
Taken together, smNPC lines of high quality, carrying various constructs for inducible expression of GCNF, GCNF mutDBD, GCNF shRNA, GCNF-VP16 or NGN2, and two control lines were generated to enable experiments for investigating and analyzing the mechanistic function of GCNF during neuronal differentiation.

3.2.2 GCNF promotes NSC maintenance and proliferation

In the presence of DOX, all seven smNPC lines were spontaneously differentiated for seven days by withdrawal of small molecules needed for smNPC maintenance (Figure 3.4 A). The withdrawal of these small molecules induces smNPC differentiation into neuronal cells (Reinhardt *et al.*, 2013). After seven days, the number of remaining SOX2-positive cells and the proliferative capacity of the generated cell cultures were determined (Figure 3.4).
The differentiated cell cultures were stained for the NSC marker SOX2 and the number of remaining SOX2-positive smNPCs within the cultures was quantified (Figure 3.4 B, C). Additionally, the proliferative capacity of the different cell cultures was analyzed by 5-Ethynyl-2′-deoxyuridine (EdU) assays. EdU is a nucleotide analogue, which, when dividing cells are exposed to it, will be incorporated into the replicated DNA. Prior to cell harvest, the differentiated smNPCs were cultivated with EdU for 3 h, which was labeled with Alexa Fluor 488 via a Click-iT reaction. Utilizing flow cytometry, the percentage of Alexa 488-positive cells was quantified (Figure 3.4 D).
After seven days of differentiation, GCNF overexpression led to the increase of SOX2-positive cells within the cell cultures compared to EtO smNPC cultures. The overexpression of GCNF with mutated, non-functional DBD had no effect on the number of SOX2-positive cells, as well as the knockdown of GCNF by shRNA. However, overexpression of GCNF-VP16 decreased the number of remaining smNPCs in the cell culture significantly compared to control cultures. The effect of GCNF-VP16 expression was also stronger than the effect of NGN2 overexpression. NGN2 overexpression decreased the number of SOX2-positive smNPCs in seven days long differentiated smNPC cultures (54.4 % ± 3.7), but less than GCNF-VP16 overexpression (30.3 % ± 3.6) (Figure 3.4 B, C).
The immunostaining of the differentiated smNPC cultures already displayed differed cell density of these cultures (Figure 3.4 B), which hinted to differences in the proliferative capacity. To confirm this observation, the proliferation capacity of cells within the differentiated cell cultures was determined by flow cytometry-based EdU assay. A higher number of remaining SOX2-positive smNPCs in the cell cultures suggested a higher proliferation rate of these cultures, meaning a higher percentage of EdU-positive cells. Indeed, GCNF-overexpressing cell cultures exhibited 6.9 % ± 0.8 EdU-positive cells, which is almost double to proliferative cells in control cultures (EtO 3.6 % ± 0.4, ctr 4.1 % ± 0.3). Overexpression of GCNF mutDBD had no effect on the proliferation capacity, while the knockdown of GCNF decreased the proliferative capacity slightly compared to control cultures. GCNF-VP16 or NGN2 overexpression decreased the percentage of EdU-positive, proliferative cells (GCNF-VP16 1.7 % ± 0.7, NGN2 2.5 % ± 0.4) (Figure 3.4 D) in accordance to the significant reduction of SOX2-positive cells (Figure 3.4 C).

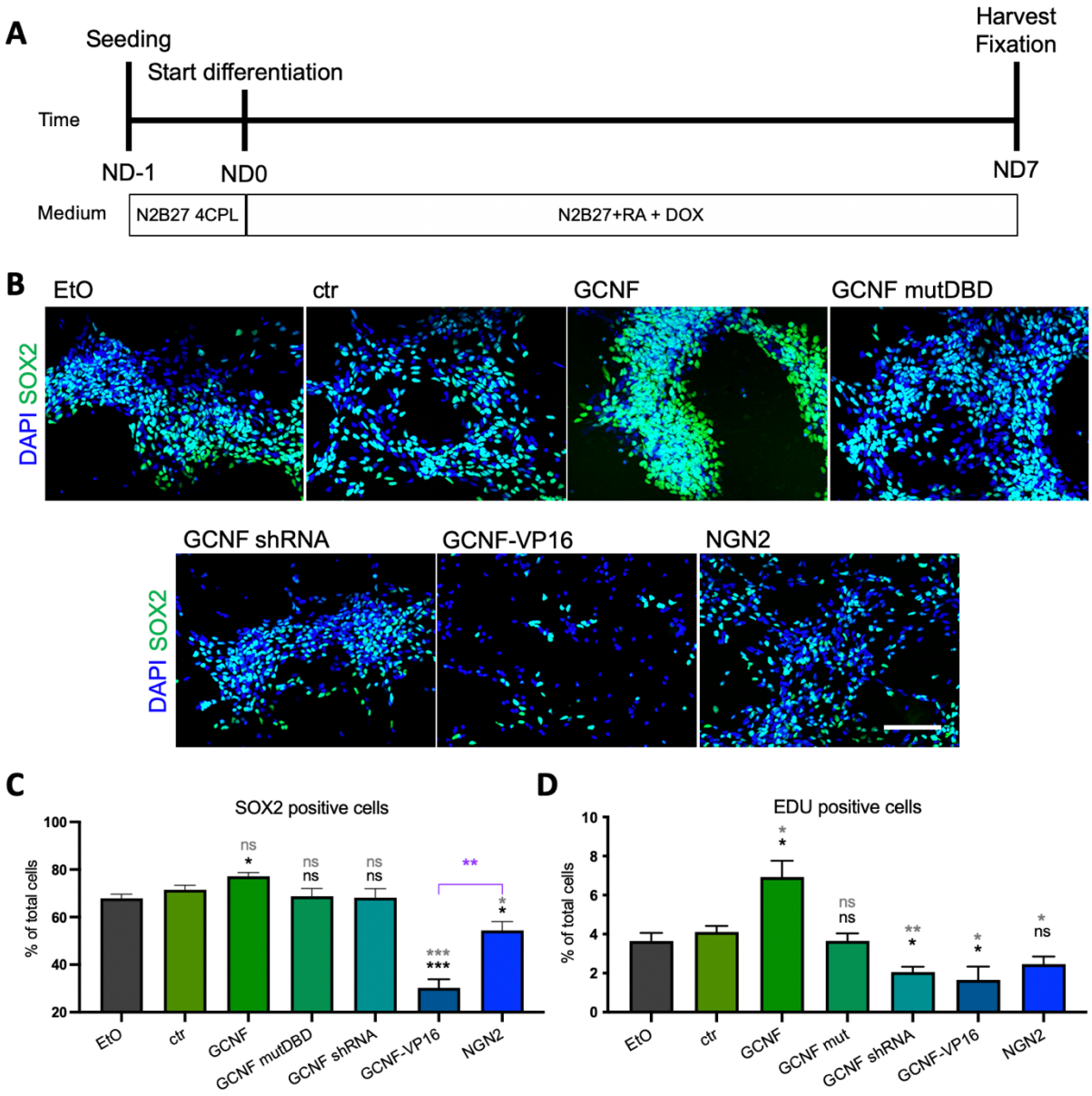

Figure 3.4: GCNF overexpression promotes stem cell proliferation. (A) Schematic displaying the differentiation of smNPCs. **(B)** Exemplary immunofluorescence images of smNPCs differentiated for seven days, stained for the neural stem cell marker (NSC) SOX2. Note the differences in cell density and cluster formation. DAPI labeled cell nuclei. Scale bar = 100 µm. **(C)** Quantification of SOX2-positive cells calculated as percentage from total cells suggest that GCNF-overexpressing cell cultures contain more SOX2-positive cells than cultures of control cell lines. Overexpression of GCNF mutDBD or GCNF shRNA has no effect on the number of SOX2-positive cells, however GCNF-VP16 expression and NGN2 overexpression significantly decrease the number of SOX2-positive stem cells. Data are presented as mean + SEM, n = 3, ns $p > 0.05$, * $p \leq 0.05$, ** $p \leq 0.01$, *** $p \leq 0.001$ (in black compared to EtO, in grey compared to ctr), unpaired t-test. In violet comparison between GCNF-VP16 and NGN2, ** $p \leq 0.01$, unpaired t-test. **(D)** EdU assays were performed to determine the percentage of proliferative cells within seven days old differentiated cultures. GCNF overexpression increases the number of proliferative cells, while the knockdown of GCNF (GCNF shRNA) or GCNF-VP16 expression inhibits proliferation. EdU assays were performed in collaboration with Dr. Laura Stappert (Institute of Reconstructive Neurobiology). Data are presented as mean + SEM, $n \geq 3$, ns $p > 0.05$, * $p \leq 0.05$, ** $p \leq 0.01$ (in black compared to EtO, in grey compared to ctr), unpaired t-test.

Both assays combined showed that GCNF is important for the maintenance of smNPCs. Its overexpression increased the number of SOX2-positive, proliferative cells within differentiated smNPC cultures. The knockdown of GCNF had no distinct effect on the expression of SOX2, however the knockdown of GCNF decreased the proliferative capacity of cells in the differentiated smNPC cultures.

Additionally, reversing the function of GCNF by fusion of the TAD of VP16 with GCNF and thus turning the transcriptional repressor GCNF into a transcriptional activator (Immaneni *et al.*, 2000), decreased the number of proliferating, SOX2-positive smNPCs in seven days old differentiating smNPC cultures. During differentiation, NSC cultures shift gradually from containing mostly proliferative progenitor cells to a higher percentage of neuronal cells. Thus, the effect of GCNF on the number of neuronal cells was determined, next.

3.2.3 GCNF inhibits neuronal differentiation

The number of neuronal cells within cell cultures could be quantified by counting cells positive for neuronal markers like β-III-Tubulin or MAP2. However, this method is time consuming and since most neuronal cell cultures form dense cell clusters, it is not reliable. For this reason, the number of MAP2-expressing neuronal cells was quantified by performing flow cytometry-based counting of CD200-positive and CD49f-negative cells (Turaç *et al.*, 2013). Additionally, the expression level of neuronal marker MAP2 determined by qRT-RNA analyses was used to support the indicated ratio of neuronal cells in seven days old differentiated smNPC cultures quantified by flow cytometry assay (Figure 3.5).

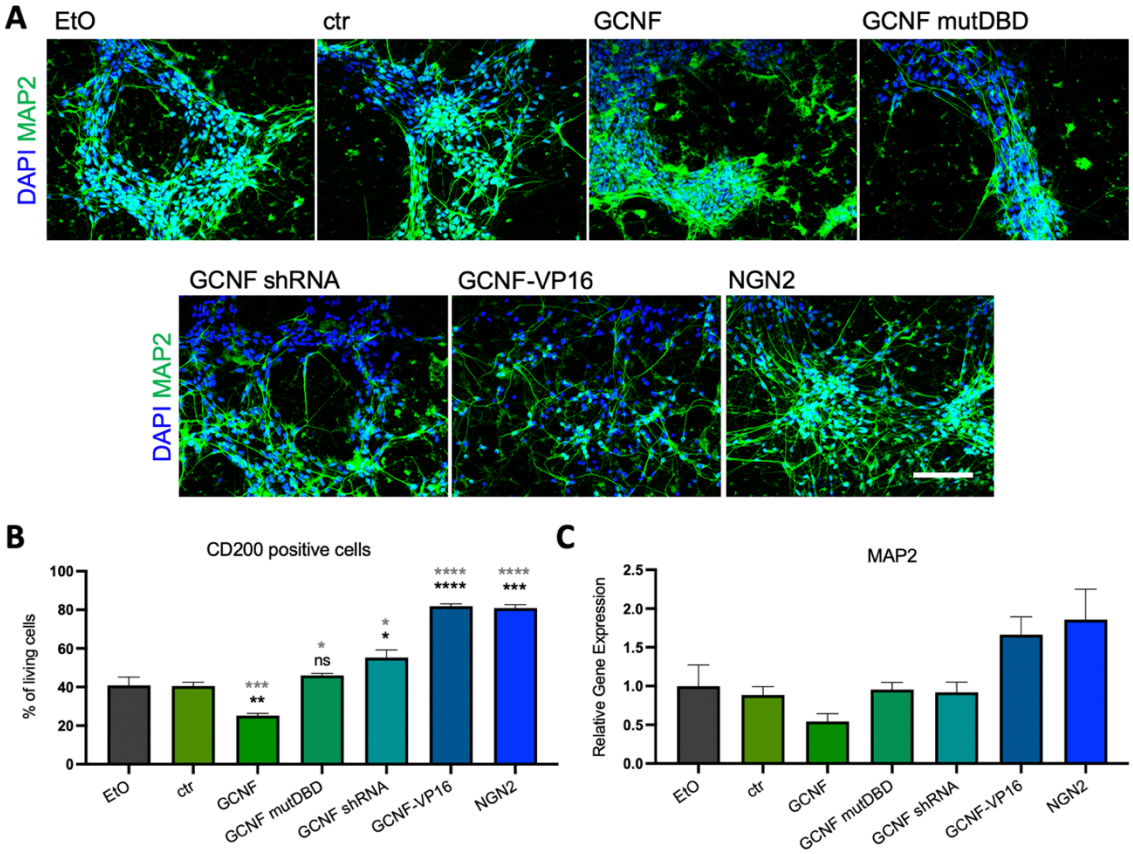

Figure 3.5: GCNF overexpression inhibits neuronal differentiation. (A) Exemplary immunofluorescence images for neuronal marker MAP2 of smNPCs differentiated for seven days. Note the differences in cell density and cluster formation. DAPI labels cell nuclei. Scale bar = 100 µm. **(B)** Flow cytometric assay to determinate the number of CD200-positive, neuronal cells and **(C)** quantitative RT-PCR for MAP2 indicate that GCNF decreases neuronal differentiation, while knockdown of GCNF as well as GCNF-VP16 expression and NGN2 overexpression increase neuronal differentiation of smNPCs. CD200 flow cytometric assays were performed in collaboration with Dr. Laura Stappert (Institute of Reconstructive Neurobiology). Flow cytometry data are presented as mean + SEM, n = 5, ns $p > 0.05$, * $p \leq 0.05$, ** $p \leq 0.01$, *** $p \leq 0.001$, **** $p \leq 0.0001$ (in black compared to EtO, in grey compared to ctr), unpaired t-test. Quantitative RT-PCR data were normalized to 18S rRNA levels and are presented relative to EtO samples. Data are presented as mean + SEM, n = 3, all samples: ns $p > 0.05$, Mann-Whitney test.

The immunostaining for MAP2 suggested differences in the number of MAP2-positive cells, but also revealed again a difference in the density and cluster formation of differentiated smNPC cultures depending on transgene expression. According to the MAP2 staining, it appears that GCNF decreased the number of MAP2-positive cells within the cell cultures, while GCNF-VP16 increased the rate of MAP2-positive cells (Figure 3.5 A). These observations could be confirmed by quantification of CD200-positive cells. GCNF overexpression significantly decreased the number of neuronal cells compared to control cells (GCNF 25.2 % ± 1.1 vs EtO 40.8 % ± 4.3, ctr 40.5 % ± 1.9). The overexpression of GCNF mutDBD had no influence on the ratio of neuronal cells within the differentiated smNPC cultures, however the knockdown of GCNF (GCNF shRNA) or reversing its function (GCNF-VP16) increased the number of CD200-positive, neuronal cultures significantly. Both, GCNF-VP16 expression and NGN2 overexpression, affected the amount of neuronal cells similarly yielding at around 80 % of CD200-positive cells (GCNF-VP16 81.9 % ± 1.3, NGN2 80.9 % ± 1.8), which is twice as high as in the control cultures (Figure 3.5 B). Analyses of the expression of the neuronal marker MAP2 on RNA level within the entire formed cell cultures showed non-significant alterations between the different cell lines, but the same trend as the CD200 quantification. MAP2 expression was decreased in GCNF-overexpressing cultures, while GCNF-VP16-expressing and NGN2-overexpressing cultures displayed higher MAP2 expression levels (Figure 3.5 C).

Together, these data indicate that GCNF promotes NSC maintenance and proliferation on the expense of neuronal cell formation. In contrast, GCNF-VP16 elevated neuronal differentiation similar to NGN2. NGN2 is known for driving stem cells into neurons and is often used for directed forward programming to generate neuronal cultures in a short time frame (Ho *et al.*, 2016).

3.2.4 GCNF increases cell cluster formation

When NSCs differentiate into neurons, they typically form cell clusters consisting of remaining NSCs and neuronal cell bodies, with outwardly orientated neurites (Yuan *et al.*, 2011; Reinhardt *et al.*, 2013; Zagoura *et al.*, 2017; Vitillo *et al.*, 2020). Altered overall morphology of differentiated smNPC cultures was observed depending on GCNF expression (Figure 3.4 A and Figure 3.5 A). To describe and quantify these alterations in cluster formation, the number of formed clusters, their area and their density was ascertained. A “cell cluster” was defined as an accumulation of five or more cells, whose nuclei are located within less than one nucleus diameter away from each other (Figure 3.6 A, B). The cluster area was measured by defining the outer border of each individual cluster and calculating the area (Figure 3.6 C) and their density was determined by counting each nucleus within each cluster (Figure 3.6 D).

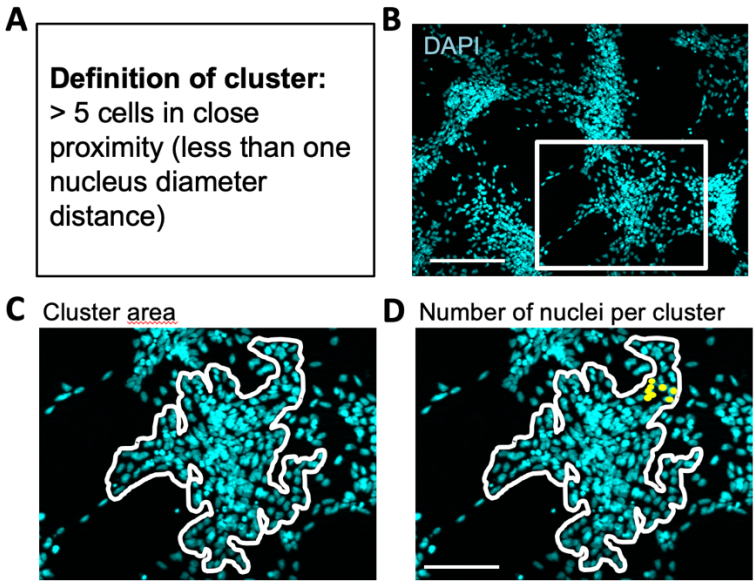

Figure 3.6: Strategy on how to quantify cell cluster formation. (A) A "cell cluster" was defined as five or more cells, which are less than one nuclei diameter away from each other. **(B)** Immunofluorescence images for DAPI taken with a 10x objective were analyzed. Scale bar = 200 µm. **(C) (D)** Zoom-in picture of cell cluster. (C) The cluster area was determined by outlining the outer cluster boarder and (D) the number of cells within each cluster was determined by counting each single cell within each individual cluster (each yellow dot presents one cell). Scale bar = 100 µm.

After defining the term "cell cluster" and developing a method for quantifying the observations in altered cell clustering, we evaluated cluster sizes and number of nuclei per cluster for seven days old neuronal cultures formed by differentiated smNPCs with modulated GCNF expression (Figure 3.7). Immunofluorescence staining of only DAPI, which labels the cell nuclei by intercalating in the cell's DNA, was sufficient to indicate alterations in cell clustering (Figure 3.7 A). GCNF overexpression increased significantly the area of formed clusters compared to EtO or ctr cells. GCNF mutDBD overexpression had no effect on the cluster size. Knockdown of GCNF by shRNA led to a decrease in cluster size, which was even more prominent by reversing GCNF function using GCNF-VP16. NGN2 overexpression also decreased cluster size, however this decrease was less prominent than in GCNF-VP16-expressing cultures (Figure 3.7 B). When pooling the percentage of clusters above an area of 4,000 µm^2 and below 4,000 µm^2, the promoting effect of GCNF on cluster area was even more obvious. In GCNF-overexpressing cultures, 53 % of formed clusters were bigger than 4,000 µm^2, which was compared to control cultures (EtO 29 % and ctr 32 %) more than 1.6 times higher. The knockdown of GCNF led to the formation of smaller cell clusters. Here, only 14 % of formed clusters were bigger than 4,000 µm^2, which was half of the clusters formed by EtO or ctr cells. However, this number was similar to NGN2-overexpressing cell cultures. Expression of GCNF-VP16 decreased the cell cluster area even further. Only 5 % of formed cell clusters occupied an area bigger than 4,000 µm^2 (Figure 3.7 C). The number of nuclei per cluster depended on cluster size and thus followed the same trend as cluster size. GCNF-overexpressing cell clusters contained significantly more nuclei than clusters formed by control cells. GCNF overexpression with a mutated DBD had no effect on number of nuclei per identified cell cluster. However, upon GCNF knockdown (GCNF shRNA) the number of nuclei was significantly decreased compared to ctr cell cultures. GCNF-VP16 expression led to an even smaller number of nuclei per cell cluster not only compared to control cell cultures, but also compared to NGN2-overexpressing cultures

(Figure 3.7 D). No significant changes in the cluster density (ratio of number of nuclei per cluster area) between the different cell lines could be detected (Figure 3.7 E). A qualitative observation of the immunofluorescence images for SOX2 and MAP2, suggested that the cell cluster consists of a mixture of remaining, SOX2-positive smNPCs and neuronal cell bodies (not quantified).

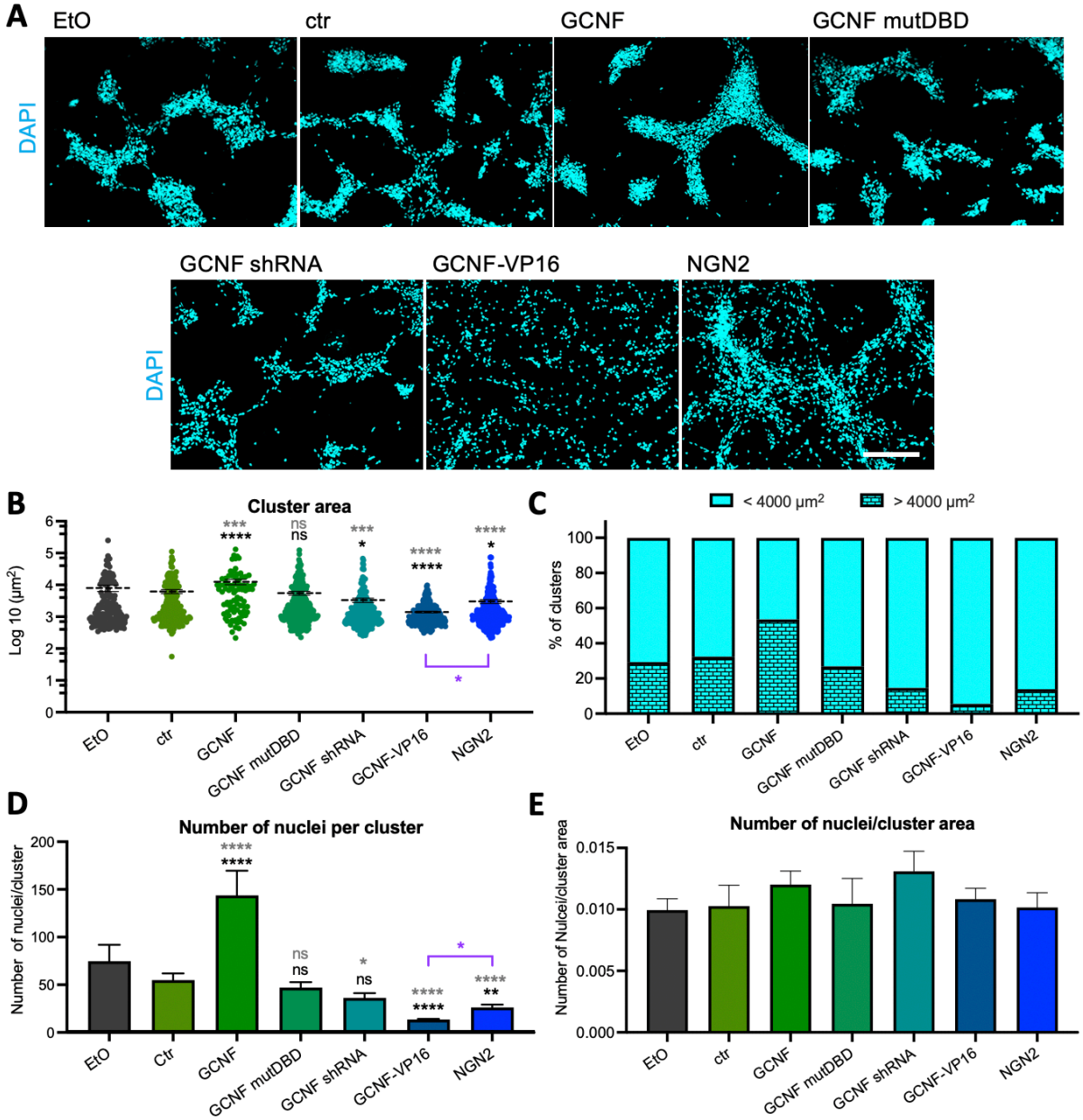

Figure 3.7: GCNF overexpression impacts cell cluster formation. (A) Exemplary immunofluorescence images for DAPI labeled cell nuclei of smNPCs, which were differentiated for seven days. Scale bar = 200 µm. **(B)** Quantification of areas of clusters within smNPC-derived neuronal cultures. GCNF overexpression increases the cluster area, whereas the knockdown of GCNF (GCNF shRNA), expression of GCNF-VP16 and NGN2 overexpression lead to a decrease of the cluster area. GCNF-VP16 decreases the cluster formation stronger than NGN2. Data are presented as mean + SEM, single values of n = 3, ns $p > 0.05$, * $p \leq 0.05$, **** $p \leq 0.0001$ (in black compared to EtO, in grey compared to ctr), Mann-Whitney test. In violet comparison of GCNF-VP16 and NGN2, * $p \leq 0.05$, Mann-Whitney test. **(C)** Summary of cluster quantification from (B). **(D)** Alterations of the number of nuclei per cell cluster follow the same trend as the cluster area. Data are presented as mean + SEM, single values of n = 3, ns $p > 0.05$, * $p \leq 0.05$, ** $p \leq 0.01$ **** $p \leq 0.0001$ (in black compared to EtO, in grey compared to ctr), Mann-Whitney test. In violet comparison of GCNF-VP16 and NGN2, * $p \leq 0.05$, Mann-Whitney test. **(E)** Ratio of number of nuclei per cluster normalized to the respective cluster area. The modulation of GCNF expression during neuronal differentiation of smNPC has no significant effect on the density of formed clusters. Data are presented as mean + SEM, n = 3, Mann-Whitney test.

GCNF was not only promoting smNPC maintenance and proliferation on the expense of neuronal differentiation, it also affected cell cluster formation in differentiated smNPC cultures to the effect that the area of formed clusters was prominently increased. In contrast, GCNF-VP16 overexpression interfered with cluster formation leading to decreased cluster areas.

To understand the molecular mechanism behind these phenotypical alterations of differentiated smNPC cultures upon modulated GCNF expression, the transcriptome of the different cell lines during the process of neuronal differentiation was analyzed.

3.3 Transcriptome analyses by microarray revealed that GCNF delays expression of neuronal genes

3.3.1 GCNF modulation affects temporal expression of differentiation-associated gene signature

To characterize the observed differences in smNPC differentiation upon modulation of GCNF expression on molecular level, transcriptome analyses of the different smNPC lines were conducted. Furthermore, since GCNF is described to act as a transcriptional repressor of its target genes and GCNF-VP16 as transcriptional activator of these target genes, gene expression analyses of both cell lines could provide first insights into potential GCNF target genes.

EtO, ctr, GCNF, GCNF-VP16 and NGN2-overexpressing cells were differentiated in the presence of DOX for 14 days. After 2 days, 7 days and 14 days of neuronal differentiation (ND2, ND7 and ND14, respectively), the RNA of the different cell cultures was harvested, purified and examined by microarray gene expression analysis (Figure 3.8 A).

The principal component analysis (PCA) revealed how similar the transcriptome of the samples was to each other and demonstrated the similarity or variance by arranging the samples in a coordinate system across three main principal components (PCA) (Jolliffe and Cadima, 2016). Depending on analyzed transgene status and time points, the examined RNA samples clustered together. The samples for ND2 of the EtO, ctr and GCNF cell lines clustered along PCA1, while ND2 samples for GCNF-VP16-expressing and NGN2-overexpressing cell cultures clustered closer to ND7 samples of control cell lines. This arrangement suggested that cell cultures of GCNF-VP16-expressing and NGN2-overexpressing cells have a similar differentiation level at ND2 as ND7 samples of control cell lines. In contrast, the ND7 samples of GCNF-overexpressing cells were less differentiated compared to control cell lines. At ND14, these observations were more dominant: ND14 samples of GCNF-overexpressing cells clustered along PCA1 between EtO and ctr ND7 and ND14 samples. ND7 samples of GCNF-VP16 and NGN2 were arranged together with ND14 samples of control cell lines. The ND14 samples of GCNF-VP16 and NGN2 were close to each other along PCA1 (Figure 3.8 B). Along PCA3 the samples were clustered mainly according to the transgenes.

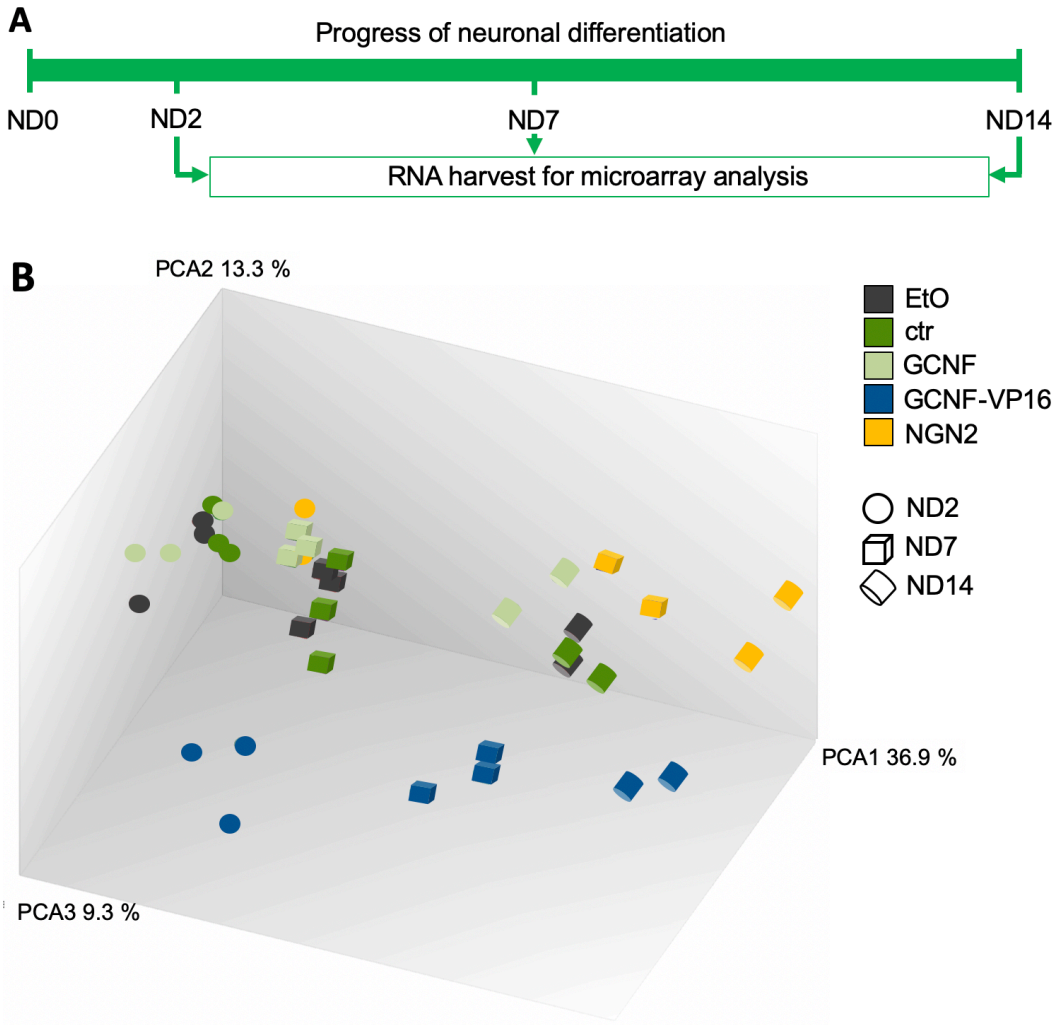

Figure 3.8: Principal component analysis reveals altered neuronal differentiation upon modulation of GCNF expression. (A) Schematic of differentiation and sample harvest. SmNPCs were seeded at ND-1 and treated with differentiation medium and DOX from ND0 on for 14 days. At ND2, ND7 and ND14 samples for RNA preparation and subsequent transcriptome microarray analysis were harvested. **(B)** Principal component analysis performed with TAC 4.0 reveals clustering of ND2 control samples and GCNF-overexpressing samples along PCA1, 2 and 3. ND2 samples of GCNF-VP16 and NGN2 cluster along PCA1 with ND7 samples of control and GCNF samples and ND7 samples of GCNF-VP16 and NGN2 cluster with ND14 samples of control and GCNF samples. Along PCA1 ND14 samples of NGN2 and GCNF-VP16 cluster together. However, GCNF-VP16 samples are clearly separated from all other samples along PCA3.

The top 100 genes, which were up- or downregulated during the process of neuronal differentiation were blotted and analyzed (Figure 3.9) to get more insights into the overall changes of the transcriptome. To that end, genes with a differential expression in EtO and ctr samples at ND2 and ND14 were extracted and sorted according to their changes in gene expression. The expression of the top 100 upregulated genes as well as the top 100 downregulated genes in control cell lines during neuronal differentiation ("differentiation-associated gene signature"), were analyzed for EtO, ctr, GCNF, GCNF-VP16 and NGN2 samples at ND2, ND7 and ND14. To better compare the fold change of the genes of the "differentiation-associated gene signature" among the five different cell lines, the fold change of each of these genes was normalized to the lowest fold change among the different cell lines at each time point for upregulated genes, or normalized to the highest fold change among the different cell lines at each time point for downregulated genes (listed in Supplementary Table 6.1-Table 6.12). The log2 of these calculated ratios for the "differentiation-associated gene signature" was visualized in a heatmap (Figure 3.9 A). The

biological process GO terms of the “differentiation-associated gene signature” were determined and sorted by fold enrichment. Only the top 10 of the found GO terms were listed (Figure 3.9 B, C). The top 100 upregulated genes from ND2 to ND14 were related to neuronal development and maturation as the majority of terms is linked to synapse development (Batool *et al.,* 2019). Additionally, the upregulated genes were involved in cerebellar cortex development (Figure 3.9 B), which suits the chosen neuronal differentiation model as smNPCs are suggested to mostly differentiate into GABAergic hindbrain neurons (Strauß *et al.*, 2021). The GO terms of the downregulated genes were linked to motor neuronal differentiation and cardiac development, which hinted to an increased restriction of smNPC differentiation potential from ND2 to ND14. Additionally, GO terms of different ion-related process were downregulated (Figure 3.9 C). It seems that processes in cell response to metal ions or inorganic compounds were altered in neuronal cells (ND14) compared to their smNPC ancestors (ND2), which fit to publications describing that differentiated neurons have a different metabolism as well as different detoxification systems than NSCs (Martinez *et al.*, 2019; Ludikhuize and Rodríguez Colman, 2021).

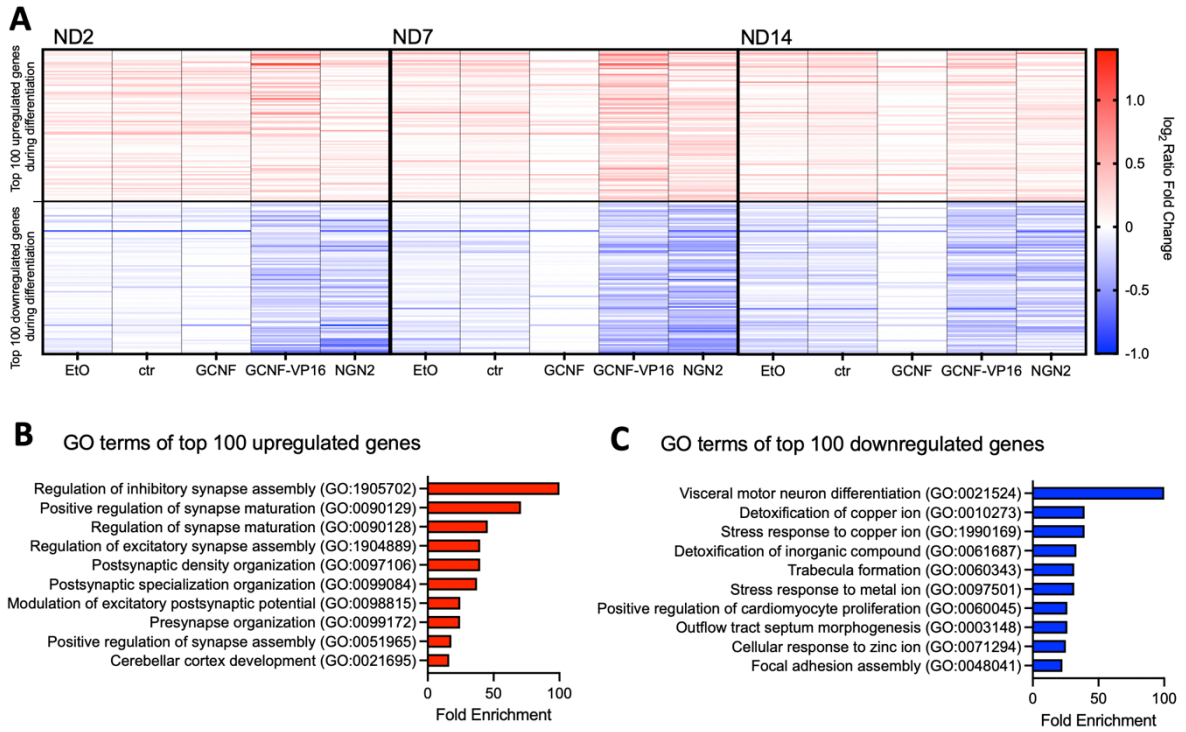

Figure 3.9: Heatmap and GO term analysis of top 100 up-or downregulated genes in EtO and ctr smNPCs from ND2 to ND14 display that GCNF delays neuronal maturation. (A) Heatmap displaying the relative expression of the top 100 genes, which are up- or downregulated in control smNPC lines during 14 days neuronal differentiation, at the three different analyzed time points (ND2, ND7, ND14) and in the five examined smNPC lines (EtO, ctr, GCNF, GCNF-VP16, NGN2). The fold change for each gene in the five different cell lines was normalized to the lowest fold change of the cell lines at the specific time point for upregulated genes and normalized to the highest fold change for downregulated genes. GCNF-VP16 expression and NGN2 overexpression lead to a stronger up- and downregulation of neuronal differentiation associated genes compared to EtO or ctr cell lines. GCNF overexpression reduces the up- and downregulation of these genes, which become more distinct at later time points (ND7 and ND14). **(B)** GO term analyses for the top 100 regulated genes during neuronal differentiation, reveal that most upregulated genes are involved in synapse development and cerebral cortex development. **(C)** Downregulated genes are related to the development of other mature cell types and detoxification mechanisms.

The heatmap revealed that the expression of genes, which were differently expressed at ND2, ND7 or ND14, were less altered in GCNF-overexpressing cell lines. At ND7 and ND14, this effect was even

stronger than at ND2, which fits to the arrangement of samples in the PCA. In contrast, GCNF-VP16-expression and NGN2-overexpression showed the strongest effects on the expression of the “differentiation-associated gene signature”. This suggested that the shift towards expression of the “differentiation-associated gene signature” was accelerated upon GCNF-VP16 or NGN2 expression, while it was downregulated in GCNF-overexpressing cultures. During the time course of neuronal differentiation, the expression of these genes in control cell lines became more aligned with the expression in GCNF-VP16-expressing and NGN2-overexpressing cell lines (Figure 3.9 A).

3.3.2 GCNF modulation affects widely the expression of genes related to cell membrane or membrane proteins

In a next step, genes, which are up- or downregulated in GCNF-overexpressing or GCNF-VP16-expressing cell cultures at ND2 and ND7 in comparison to EtO, ctr or both cell lines, were assessed to understand the molecular background of the observed phenotypical alterations upon GCNF overexpression (Figure 3.10, Figure 3.11, Figure 3.12 and Figure 3.13). Therefore, at ND2 or ND7, respectively, all differentially expressed genes (DEGs) in GCNF-overexpressing or GCNF-VP16-expresssing cells compared to EtO, ctr or both cell lines, were filtered out and the list of DEGs for each analysis were compared to each other. Subsequently, the GO terms (molecular function, biological process, cellular components) and annotation keywords regarding the DEGs, which were identified in all three comparative analyses, were determined and displayed in functional annotation clustering. Similar annotation terms were clustered together, which support the identification of major biological functions associated with the DEGs.

At ND2, the gene expression of only nine genes was upregulated in GCNF-overexpressing cells in all three comparative analyses (Figure 3.10 A). Functional annotation clustering of these upregulated genes revealed that the genes were linked to annotations like “membrane”, “Glycoprotein”, “Calcium ion binding” (Figure 3.10 B). 23 genes were downregulated in GCNF-overexpressing cells at day 2 of neuronal differentiation in comparison to EtO, ctr and both cell lines (Figure 3.10 C). The annotation clusters of the functional annotation clustering for the downregulated genes were linked to “membranes” and “cell surface” and indicated downregulation of genes linked to the cell surface, which could affect cell adhesion *(Khalili and Ahmad, 2015)*. Furthermore, genes linked to “metal ion binding”, such as transcription factors with zinc fingers *(Cassandri* et al*., 2017)*, as well as genes linked to “cytoplasm” were downregulated in GCNF-overexpression smNPCs. Other cluster annotations of the downregulated genes correlated with the overexpression of a transcriptional repressor, which affects subsequent transcription factors in a molecular network (“positive regulation of transcription from RNA Pol II promoter”, Figure 3.10 D).

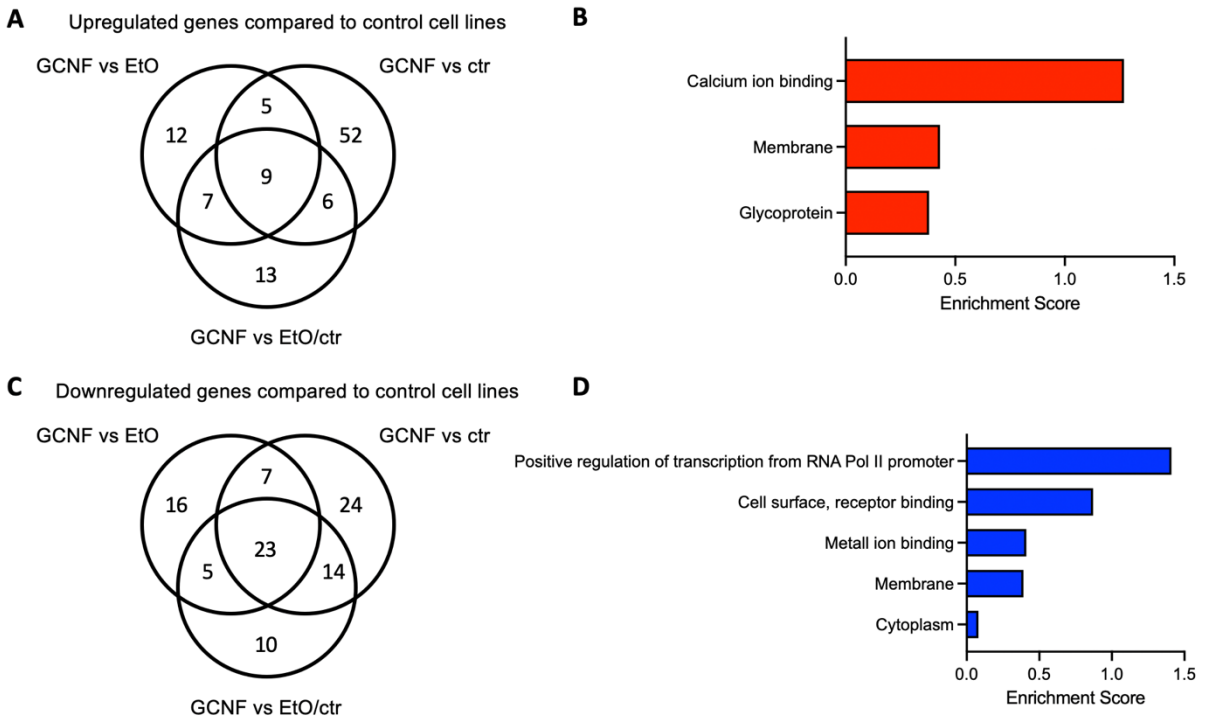

Figure 3.10: Functional annotation clustering of up- and downregulated genes in GCNF-overexpressing cell cultures at ND2. (A) (C) Venn-Diagram for genes, which are (A) upregulated or (C) down-regulated in GCNF-overexpressing cell cultures at ND2 compared to EtO, ctr or EtO and ctr cell lines. (**B) (D)** Functional annotation clustering for genes, which are (B) upregulated or (D) downregulated in all three comparative analyses.

At ND2 more genes were significantly differentially expressed in GCNF-VP16-expressing cells compared to EtO, ctr or both cell lines than in GCNF-overexpressing cells compared to controls (Figure **3.10**, Figure 3.11). This might be because the strong, efficient transactivator domain of VP16 affected gene expression stronger than the effect which is mediated by the transcriptional repressor GCNF (Immaneni *et al.*, 2000; Jonker *et al.*, 2005). 428 genes were upregulated in all three comparisons (Figure 3.11 A). Functional annotation clusters of these genes were linked to alterations of the cell membrane and surface and by this were involved in cell adhesion and cell-cell interactions (e.g. “cell membrane”, “transmembrane”, “cell junction and synapses” as well as “glycoprotein” and “GPI-anchor”) (Zanetta *et al.*, 1992; Armingol *et al.*, 2021). Furthermore, annotation clusters for upregulated genes were linked to changes in transcriptional regulation upon GCNF-VP16 expression (e.g. “DNA-binding region” and “activator (transcription)”) (Figure 3.11 B).

Moreover, 353 genes were downregulated in all three comparative analyses of GCNF-VP16-expressing cells (Figure 3.11 C). The annotation clusters of these downregulated genes were mostly related to processes regarding cell membrane and subsequent cell adhesion (“cell junction”, “glycoprotein”, “extracellular matrix, basement membrane”, “cell membrane, transmembrane”, “EGF-like domain”, “immunoglobulin domain”) (Wouters et al., 2005; Schwarz et al., 2009) or were involved in cellular maturation (“cell junction, synapse”, “retinoid metabolic process”, ”cellular response to cadmium ion”, “DNA damage and repair”) (Tan *et al.*, 2015; He and Yu, 2018). (Figure 3.11 D). Both processes were phenotypically highly affected by GCNF-VP16 expression in differentiated NSCs and was mirrored on transcriptional level.

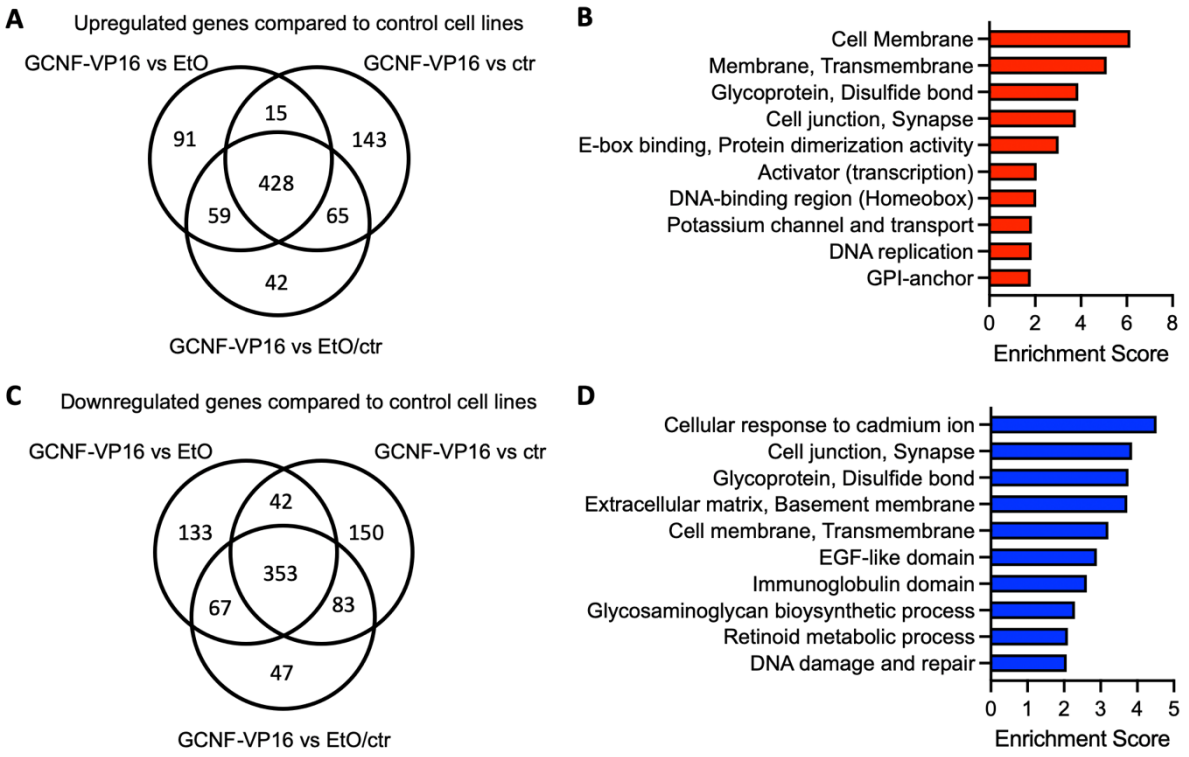

Figure 3.11: Functional annotation clustering of differentially expressed genes in GCNF-VP16-expressing cell cultures at ND2. (A) (C) Venn-Diagram for genes, which are (A) upregulated or (C) downregulated in GCNF-VP16-expressing cell cultures at ND2 compared to EtO smNPCs, ctr smNPCs or EtO and ctr. (**B) (D)** Functional annotation clustering for genes, which are (B) upregulated or (D) downregulated in all three comparative analyses (the 10 annotation clusters with the highest enrichment score are displayed).

After seven days of neuronal differentiation, the gene expression in GCNF-overexpressing cells compared to control cells was more prominent than at ND2 (Figure 3.10, Figure 3.12). The annotation clusters among the 37 upregulated genes were mostly related to cell membrane and adhesion ("plasma membrane, transmembrane", "calcium ion binding, cell adhesion", "extracellular space, basement membrane"), which could explain the alterations described in cell clustering (Solozobova *et al.*, 2012). Other listed terms were linked to "proteolysis" and "ubiquitination" (Figure 3.12 B). Functional annotation clustering of this list of downregulated genes, among which 25 displayed decreased expression in all three comparative analyses, revealed the association of these DEGs with the cell membrane ("plasma membrane, glycoprotein", "membrane", "extracellular space, developmental protein") and transcription ("nucleus, transcription regulation", "metal ion binding").

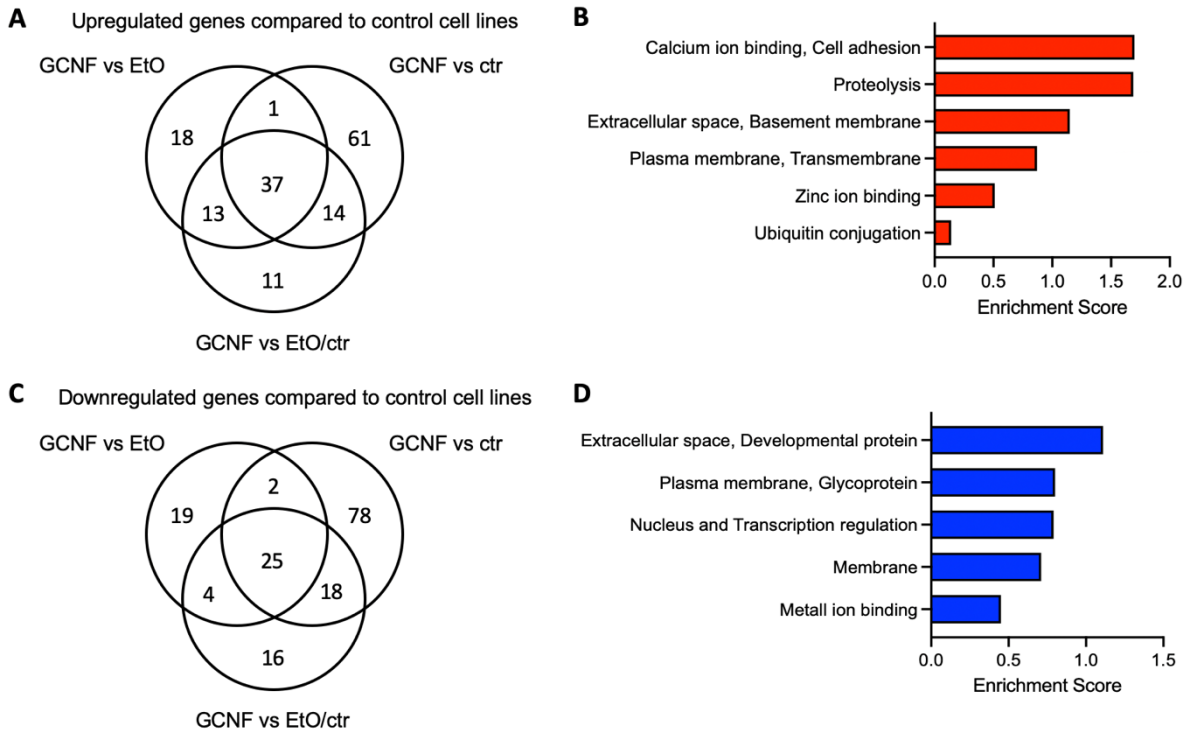

Figure 3.12: Functional annotation clustering of up- and downregulated genes in GCNF-overexpressing cell cultures at ND7. (A) (C) Venn-Diagram for genes, which are (A) upregulated or (C) downregulated in GCNF-overexpressing cell cultures at ND7 compared to EtO, ctr or EtO and ctr cell lines. (**B)** (**D)** Annotation clusters of functional annotation clustering for genes, which are (B) upregulated or (D) downregulated in all three comparative analyses.

Annotation clusters of 550 upregulated genes in GCNF-VP16-expressing cells showed terms, which were related to cell membrane, cell membrane proteins and cell-cell interactions (e.g. “cell adhesion, calcium”, “cell membrane”, “cell junction”, “glycoprotein”, “Pleckstrin homology (-like) domain”, “immunoglobulin domain”, “protocadherin gamma”) or were linked to the observed changes in neuronal differentiation (“synapse”, “ion channel, ion transport”, “long-term potentiation”) (Figure 3.13 B). Additionally, the functional annotation clustering of annotations for the 394 downregulated genes (Figure 3.13 C), which expression was decreased in all analysis of GCNF-VP16-expressing cells compared to control cultures, revealed that most of the annotation clusters might be related to the described phenotypical changes of GCNF-VP16 cell cultures in comparison to control cell cultures. The manifested alterations in cell clustering could be due to altered expression of genes involved in transmembrane proteins (e.g. “glycoprotein”, SHD/MHD domain”) and proliferation (e.g. “cell division”, “cyclin”, “G1/S transition of mitotic cell cycle” and “WNT signaling”). These alterations in the gene expression might build the mechanistic background of the decreased smNPC proliferation (Figure 3.13 D).

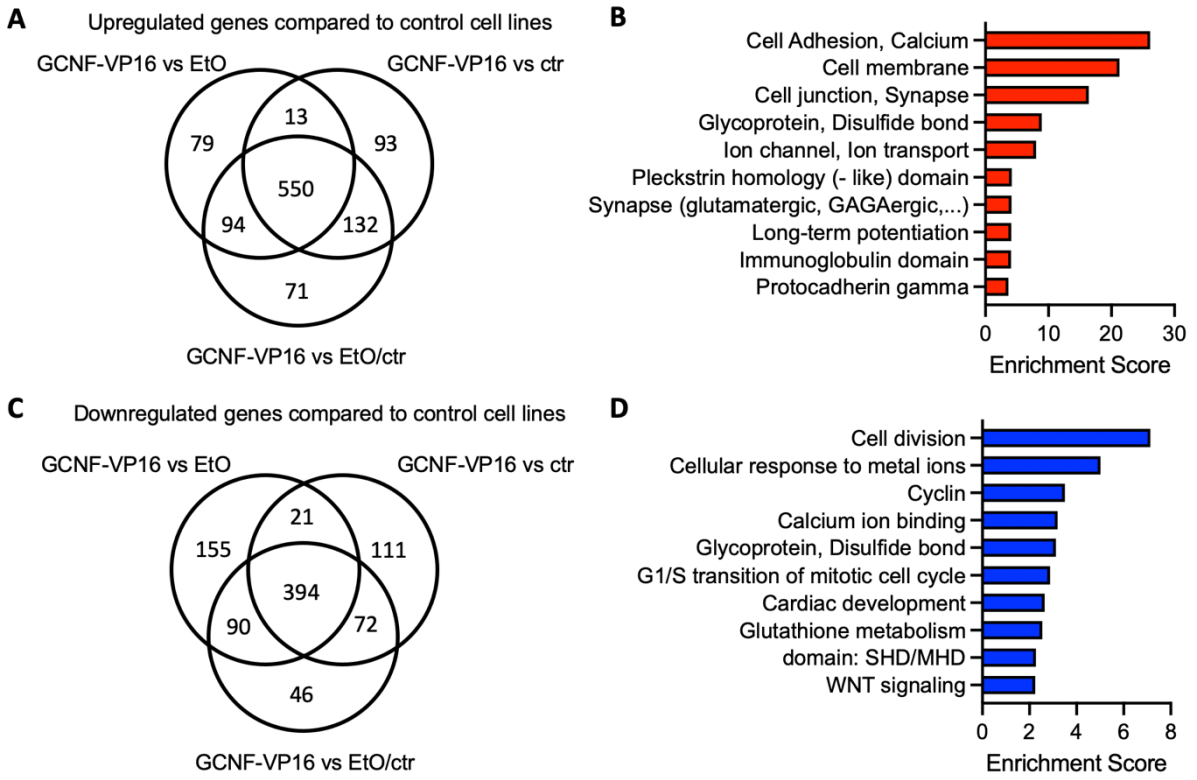

Figure 3.13: Functional annotation clustering of up- and downregulated genes in GCNF-VP16-expressing cell cultures at ND7. (A) (C) Venn-Diagram for genes, which are (A) upregulated or (C) down-regulated in GCNF-VP16-expressing cell cultures at ND7 compared to EtO cell line, ctr cell line or EtO and ctr. (**B) (D)** Functional annotation clustering for genes, which are (B) upregulated or (D) downregulated in all comparative analyses (the 10 with the highest enrichment score are displayed).

In summary, the detailed transcriptome analyses of GCNF-overexpressing and GCNF-VP16-expressing cell cultures at ND2 and ND7 in comparison to the control cultures revealed altered gene expression of genes linked to cell membrane, membrane proteins, proliferation and differentiation, which could lead to the described manifestation of changes in smNPC proliferation and maintenance, neuronal differentiation and cell clustering. However, it is necessary to narrow the list of DEGs down to find direct target genes of GCNF/GCNF-VP16.

3.3.3 BCL11A, NFIB and PCYT1B are predicted target genes of GCNF

At first, all performed transcriptome microarray analyses were combined to reduce the number of possible GCNF/GCNF-VP16 target genes. It was assumed that direct target genes of GCNF will be downregulated by GCNF overexpression, since GCNF acts classically as transcriptional repressor. However, the expression of the same genes would be upregulated in GCNF-VP16-expressing cells, because the fused TAD of VP16 transformed GCNF into a transcriptional activator. GCNF mediates DNA binding, but VP16 leads to upregulated expression of the bound target genes.

The lists of DEGs from the performed comparisons were examined in detailed. The downregulated genes from the comparison of the transcriptome of GCNF and EtO cell cultures at ND2 were matched with the list of upregulated genes in GCNF-VP16-overexpressing cell cultures compared to EtO at ND2. In this way, all other analyses were compared with each other (Figure 3.14 A). The resulting lists of

genes, whose expression is anticorrelated in GCNF-overexpressing and GCNF-VP16-expressing cells, were matched and checked for genes, which were listed in at least 5 of the 6 analyses.

A

Time point	Control of analysis	Down in GCNF	Up in GCNF-VP16
ND2	EtO	51	593
ND2	ctr	68	651
ND2	EtO + ctr	52	594
ND7	EtO	50	736
ND7	ctr	123	788
ND7	EtO + ctr	63	847

B

Anticorrelated Genes (at least 5 of 6 analyses)
MLC1
BCL11A
NFIB
PCYT1B

D

Predicted GCNF binding site
no
yes
yes
yes

C

Figure 3.14: Prediction of GCNF target genes. (A) Overview of genes, which were downregulated in GCNF-overexpressing smNPCs, but upregulated in GCNF-VP16-expressing cells at time points ND2 and ND7 for the three tested analyses per time point (compared each data set to EtO, ctr, or EtO and ctr). **(B)** Summary of anticorrelated genes in 5 of 6 comparative analyses. Only 4 genes were left. **(C)** Schematic of known GCNF response elements from TRANSFAC®. **(D)** Bioinformatic prediction of GCNF binding sites in the regulatory region of the four suggested GCNF target genes.

The comparison of the 12 microarray analyses, assuming that the expression of direct GCNF/GCNF-VP16 target genes were anticorrelated, reduced the list of DEGs down to 4 genes (MLC1, BCL11A, NFIB and PCYT1B) (Figure 3.14 B). Utilizing a bioinformatical tool (TRANSFAC®), binding sites for GCNF within the regulatory region of three of the four possible target genes could be predicted based on the published GCNF response elements (Figure 3.14 C and D). Thus, the list of genes, whose expression is directly regulated by the transcription factor GCNF, was reduced to three (BCL11A, NFIB and PCYT1B). All three of these genes were previously described to be involved in brain development or brain disorders. BCL11A is a transcriptional repressor, which is described to be involved in murine CNS development and neuro-psychological disorders (Simon *et al.,* 2020). Furthermore, altered expression of nuclear factor 1 B-type (NFIB) is linked to intellectual impairments and macrocephaly (Schanze *et al.*, 2018) and choline-phosphate cytidylyltransferase B (PCYT1B) might affect neuronal differentiation due its involvement in phosphatidylcholine synthesis (Paoletti *et al.*, 2011; McMaster, 2018).

Initially, we validated the results of the microarray for the three possible target genes by qRT-PCR (Figure 3.15). Since GCNF is a transcriptional repressor, a direct target gene of GCNF would display a reciprocal expression pattern compared to GCNF. GCNF was downregulated in the process of neuronal differentiation, while the expression of BCL11A, NFIB and PCYT1B was increased from the NSC stage to seven days and 14 days old neurons (Figure 3.15 A-C). The transcriptome microarray analyses showed that BCL11A, NFIB, PCYT1B expression was decreased upon GCNF overexpression and increased upon GCNF-VP16 expression.

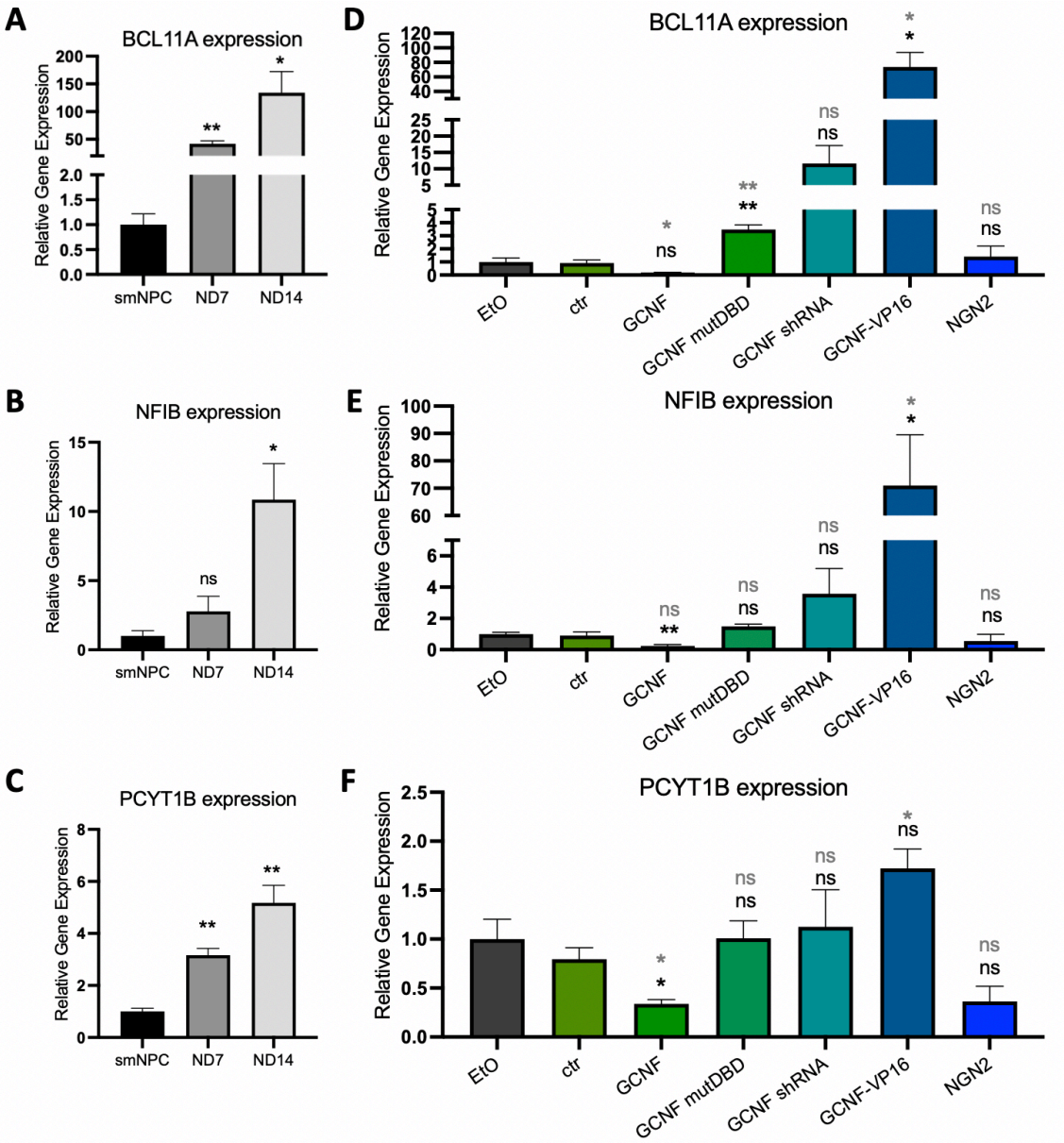

Figure 3.15: Gene expression analysis of BCL11A, NFIB and PCYT1B during neuronal differentiation and in the GCNF expression modulated cell lines. (A) BCL11A expression as well as **(B)** NFIB and **(C)** PCYT1B expression increases significantly during neuronal differentiation. Data were normalized to 18S rRNA levels and are presented relative to smNPC samples. Data are presented as mean + SEM, n = 3, ns $p > 0.05$, * $p \leq 0.05$, ** $p \leq 0.01$, unpaired t-test. **(D)** Altered BCL11A, **(E)** NFIB and **(F)** PCYT1B expression in GCNF-expression modulated cell lines. GCNF overexpression decreases BCL11A, NFIB and PCYT1B expression, while the knockdown of GCNF and GCNF-VP16 expression increase their expression. Data were normalized to 18S rRNA levels and are presented relative to EtO samples. Data are presented as mean + SEM, n = 3 (NGN2 n=2), ns $p > 0.05$, * $p \leq 0.05$, ** $p \leq 0.01$ (in black compared to EtO, in grey compared to ctr), unpaired t-test.

RNA samples of 7 days old neurons, which were differentiated from the seven different GCNF modulated cell lines (GCNF, GCNF mutDBD, GCNF shRNA, GCNF-VP16 and NGN2), were analyzed to determine the relative expression level of BCL11A, NFIB and PCYT1B. GCNF-overexpression led to downregulated expression of all three suspected target genes. The overexpression of a mutated version of GCNF had no influence on NFIB and PCYT1B expression, while it also increased BCL11A expression. The knockdown of GCNF resulted in an increased expression of BCL11A and NFIB, while the expression of PCYT1B was not affected. Expression of GCNF-VP16 increased the expression of all three genes, whereas NGN2 overexpression had no significant effect on their gene expression (Figure 3.15 D, E and F). This could explain why the enhanced differentiated cultures of GCNF-VP16 and NGN2 differed in regard to cell clustering or NSC maintenance and proliferation.

3.4 Establishment of ChIP assay to confirm BCL11A as target gene of GCNF

3.4.1 Establishment of ChIP assay for human NSCs

The three above described genes contained predicted GCNF binding sites in their regulatory region. Nonetheless, the physical binding of GCNF to these regulatory regions needed to be validated by e.g. chromatin immunoprecipitation (ChIP). Here, the first step is to crosslink DNA and all proteins, which bind to it, together. Next, the cells are lysed and the chromatin is fragmented. The chromatin fragments need to have a specific size, so that they can be recognized in later analyses by specific primers, but are not too long to give false positive signals (200-1200 bp, Kaufmann *et al.*, 2010). The fragmented chromatin was used for the actual immunoprecipitation. The DNA bound by the protein of interest and all DNA fragments crosslinked to it are precipitated and filtered from the remaining chromatin by using specific antibodies against the protein of interest. After the IP, the crosslinking is reserved and the DNA is purified. The pure DNA can then be used for sequencing or qRT-PCR to analyze which genes were bound by the protein of interest.

During this study, a ChIP assay for GCNF was established based on the ChIP-It kit from Active Motif. Even though the manual is detailed, the different steps, which are described above and visualized in the schematic (Figure 3.16 A), needed to be improved to ensure a reliable outcome.

However, a functional set-up for ChIP assays was finally established. Most steps were performed closely to the protocol of the ChIP-It kit from Active Motif, but in a modified way to achieve optimal results and to accommodate for the specific treatment requirement for NSCs (see chapters 2.2.7.2 and 6.1). Subsequent to the crosslinking with 4 % PFA, the cells were lysed not only by chemical degradation of the cell membrane, but also by applying mechanical force. The cells in suspension were sheared in a glass douncer. The douncing facilitated the generation of a suspension of single nuclei, which did not attach to each other (Figure 3.16 B). Before the chromatin fragmentation was performed using sonification, the cell nuclei suspension in ChIP buffer was snap-frozen in liquid nitrogen. Samples were compared before and after sonification to determine the quality of fragmentation. Chromatin fragmentation led to chromatin fragments of different sizes. The majority of fragments should have a size of 200 to 1,200 bp. Before sonification, chromatin fragments had a bigger size and formed a clear band close to the well, which indicated that the fragment size was too big to run through the agarose

gel. After sonification this band was smaller and even less distinct, when the samples were snap frozen before sonification (Figure 3.16 C, D). After snap-freezing and sonification, the size of the majority of generated chromatin fragments was between 200 and 1,200 bp (Figure 3.16 D). Additionally, the snap-freezing process improved lysis of cell nuclei and ensured higher chromatin concentration in the suspension. In conclusion, including a snap-freezing step before chromatin fragmentation improved the fragmentation and chromatin yield, which both ensured reliable sample analysis in later steps.

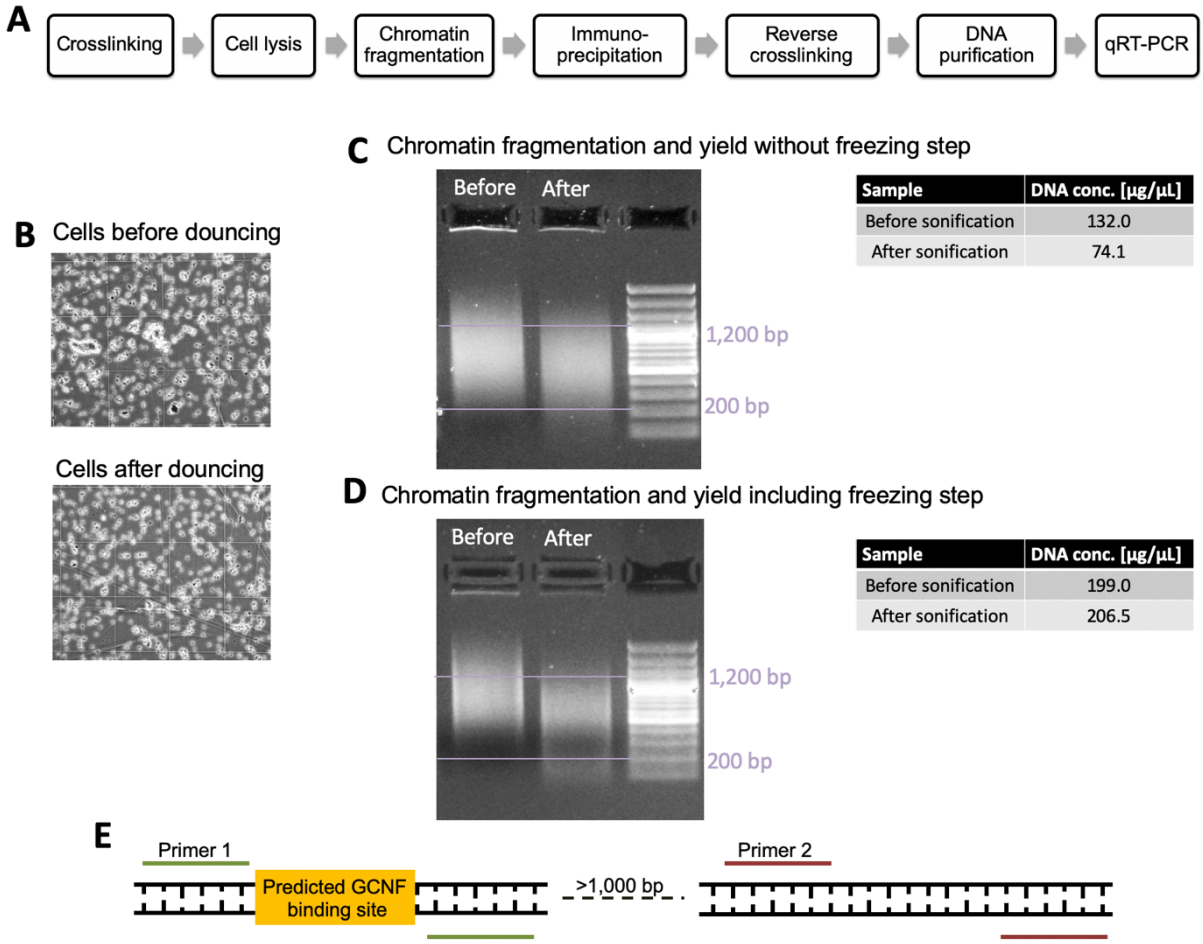

Figure 3.16: Establishing a chromatin immunoprecipitation assay for identifying GCNF target genes. (A) Schematic of steps, which need to be performed, for successful ChIP qRT-PCR. **(B)** Cell lysis was performed by incubating cells in lysis buffer from Active Motif and by mechanical force of 30 strokes in an ice-cooled cell douncer (3x10). Phase contrast images demonstrate the effect of douncing to generate single nuclei. **(C)** Gel image of chromatin samples before and after sonification for chromatin fragmentation. The sonification should cut the chromatin into 200 – 1,200 bp long fragments. Already before sonification a DNA smear between 200 and 1,200 bp is detectable, but also a clear band of DNA fragments with higher bp length close to the well is visible. After sonication this band is fainter and less broad. **(D)** To increase the sample concentration and improve chromatin fragmentation, a snap freezing step as part of sample preparation directly after cell lysis and before fragmentation was included. The gel image shows that the freezing step already improved chromatin fragmentation and increased sample concentration in the sample, which did not undergo sonification. However, the majority of chromatin fragments after sonification is 200 to 1,200 bp long and no clear band of longer chromatin fragments is visible. **(E)** Schematic to illustrate primer design for ChIP qRT-PCR. The potential binding sites of GCNF within the regulatory region of predicted GCNF target genes is shown. Primer pair 1 is covering the binding site, while primer pair 2 functions as a negative control and is binding to a DNA sequence 1,000 bp up- or downstream of the predicted binding site.

One method to analyze the DNA sequences, which were bound by the protein of interest, is qRT-PCR. Here, primers for possible binding sites, which were predicted by bioinformatical tools, were designed.

The first primer pair bound around the potential binding site of GCNF, while the second primer pair (negative control) was generated to bind around 1,000 bp up- or downstream of the predicted binding site (Figure 3.16 E). If GCNF bound to the predicted binding site, the chromatin fragment containing the sequence of the binding site and the sequence complementary to the primer, would be pulled down in the IP and this enrichment could later be analyzed by qRT-PCR. The fold change for the sequence of the binding site should be higher (Primer 1), than the fold change for the DNA sequence without GCNF binding site (Primer 2). If the chromatin fragmentation was not sufficient, the DNA fragment could be bound equally by both primer pairs. So, this primer design also ensured reliable analysis of ChIP samples by excluding false positive results due to insufficient chromatin fragmentation.
Other than optimized sample preparation the use of specific antibodies for the actual IP step is essential for performing ChIP assays with reliable results. Since there was no ChIP grade antibody against GCNF available, tagged-GCNF-overexpressing smNPCs were generated for which specific antibodies were available. Here, the AM-tag from Active Motif was used. The sequence of the AM-tag is derived from a 32 amino acid long peptide in the C-terminus of *Drosophila malanogaster* Histone variant H2Av, leading to almost no cross-reactivity with mammalian sequences and consequently reduced background signal. Additionally, the AM-tag is unstructured, which allowed the tag to extent from the coupled protein for maximum exposure during IP to increase enrichment efficiency (Tag-ChIP-IT Kit manual).

Before GCNF-AM-overexpressing cells were used for analyzing the binding of GCNF to the DNA, the existence of the AM-tag in the generated cells was confirmed and it was demonstrated that GCNF-AM overexpression had the same effect on BCL11A expression as GCNF (Figure 3.17). The GCNF-AM-overexpression construct was designed based on the Tet-On Advanced system (Figure 3.3) and transferred into the smNPCs via lentiviral transduction (Figure 3.17 A). To confirm expression of the GCNF-AM construct, smNPCs were cultivated for 48 h with or without DOX, followed by protein expression analysis by Western Blot and immunofluorescence staining (Figure 3.17 B, C). The Western Blot analysis displayed prominently the induction of GCNF-AM expression after DOX treatment. The signal for GCNF was distinctly stronger in the DOX-treated smNPCs compared to the endogenous GCNF signal in the non-DOX-treated smNPCs. The AM-tag signal was only visible after DOX treatment (Figure 3.17 B). Additionally, immunofluorescence stainings for AM confirmed AM expression only after DOX treatment. Accordingly, no signal for AM could be detected in smNPC cultures without DOX (Figure 3.17 C). Next, GCNF and GCNF-AM-overexpressing cells were compared regarding their expression level of GCNF and BCL11A. No significant difference in the GCNF level could be observed after GCNF- or GCNF-AM overexpression, respectively (Figure 3.17 D). Both, GCNF overexpression and GCNF-AM overexpression decreased BCL11A expression significantly (Figure 3.17 E).
These experiments showed that the GCNF-AM construct could be used to identify GCNF target genes. AM is only expressed when the GCNF-AM-smNPCs were treated with DOX and both, GCNF and GCNF-AM overexpression had the same effect on BCL11A expression.

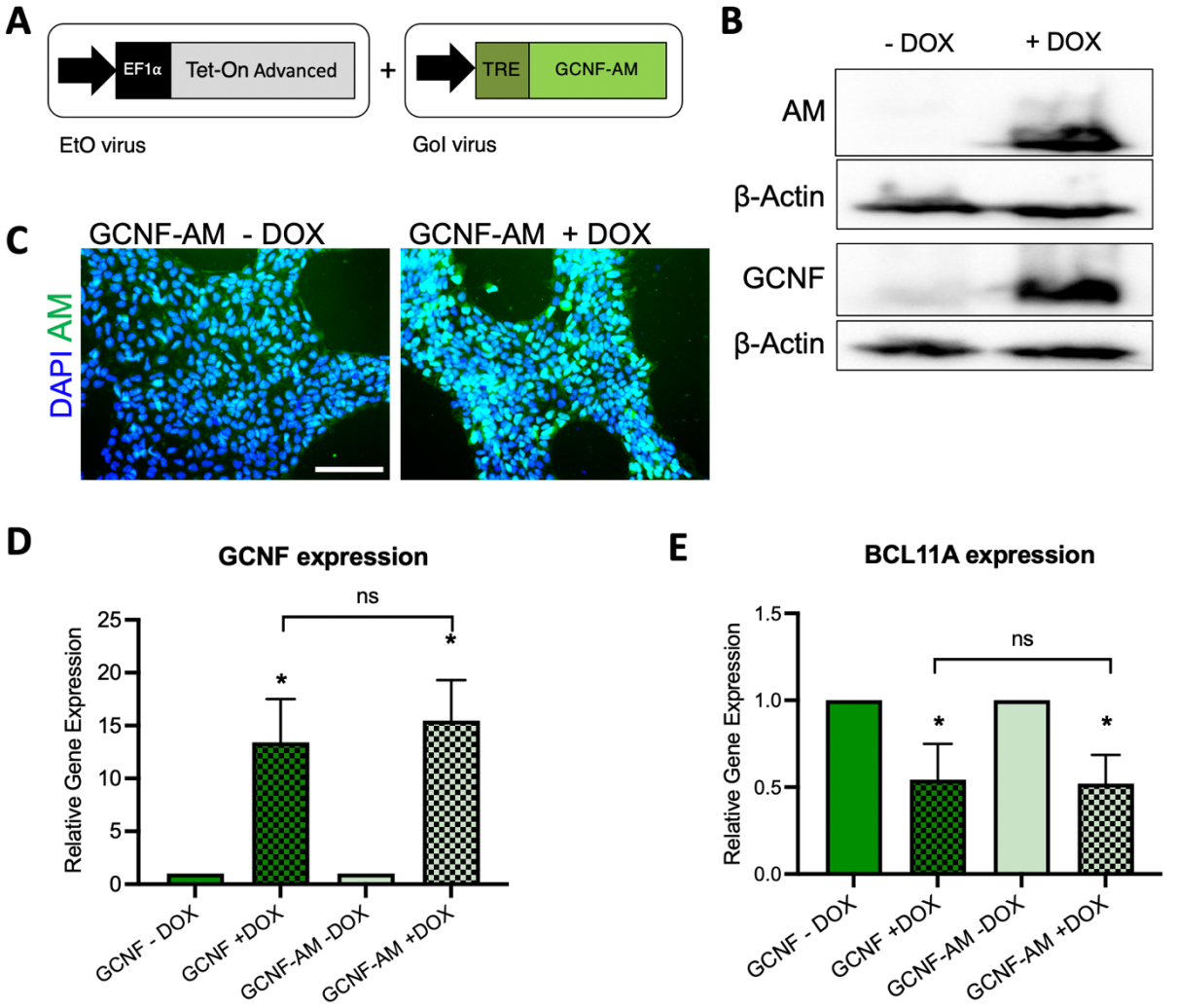

Figure 3.17: AM-tag of GCNF-overexpressing smNPCs to target GCNF during ChIP assay. (A) Schematic of inducible lentiviral construct, which is designed to target GCNF in ChIP assays. **(B)** Western Blot and **(C)** immunofluorescence stainings confirm expression of AM-tag in 48 h DOX treated smNPCs, which are transduced with EtO and GCNF-AM-viruses. The cells also overexpress GCNF. **(D) (E)** Quantitative RT-PCRs for GCNF and GCNF-AM cells after 48 h treatment with or without DOX display a significant overexpression of GCNF in GCNF cells and in GCNF-AM cells. (D) In both cell lines the overexpression level of GCNF is not significantly different from each other. (E) The repressing effect of GCNF and GCNF-AM on BCL11A expression is equal. Data were normalized to 18S rRNA levels and are presented relative to - DOX samples. Data are presented as mean + SEM, $n \leq 4$, ns $p > 0.05$, * $p \leq 0.05$, Mann-Whitney test.

3.4.2 Chromatin-Immunprecipitation confirms BCL11A as target gene of GCNF

For ChIP analyses, GCNF-AM and GCNF-overexpressing smNPCs were cultivated for 48 h in the presence of DOX and absence of small molecules used for smNPC expansion. The GCNF-overexpressing cells were used as control to ensure that the ChIP results were due to specific binding of the AM antibody against the AM tag rather than because of overexpression of any protein. After cell harvesting, the sample preparation was performed as described above including douncing of cells for cell lysis and additional snap-freezing step before sonification (Figure 3.16). As technical controls for reliably performed ChIP assays, ChIP was not only conducted with AM antibody, but also with Polymerase II (POL II) and IgG isotype control antibody. POL II binds to all actively expressed genes at the time of crosslinking (Tan and Wong, 2019), while IgG does not bind specifically to any protein. The ChIP qRT-PCRs were executed with the prepared ChIP samples and an input sample (DNA from

chromatin, which did not undergo ChIP) for the genes of interest (BCL11A, NFIB and PCYT1B) and for Glycerinaldehyd-3-phosphat-Dehydrogenase (GAPDH) as control. GAPDH is widely known as a house keeping gene and is ubiquitously expressed in all cell stages (Barber *et al.,* 2005).

The data generated by ChIP assays were analyzed by calculating the fold enrichment of the positive primers relative to negative control primers. The fold change of the positive primer for a specific sample was divided by the fold change of the negative primer for this sample. A fold enrichment above 1 indicated that the detected sequence was enriched in the previously performed ChIP assay due to binding of a protein of interest to the analyzed DNA sequence. The analyses of GAPDH by ChIP qRT-PCR should display a significantly higher fold enrichment for POL II ChIP samples than for IgG and AM ChIP samples and input samples. The fold enrichment for IgG ChIP samples should be around 1, since IgG as isotype control does not bind specifically to any protein and thus should not enrich specific DNA sequences in the ChIP assays. The input samples contain all DNA within the harvested and analyzed cells without any enrichment for specific sequences as these samples did not undergo ChIP. Hence, the fold enrichment for input samples should also not increase significantly above 1.

ChIP qRT-PCR for GAPDH confirmed that ChIP assays for GCNF-AM and GCNF samples worked technically. The fold enrichment for ChIP samples prepared with a POL II antibody was significantly higher than for AM and IgG ChIP samples or compared to the input sample (Figure 3.18 A, B). Binding of GCNF to the regulatory region of BCL11A was confirmed, since the fold enrichment was significantly higher in AM ChIP samples than in POL II and IgG ChIP samples or input samples (Figure 3.18 C). This binding was specific by GCNF-AM, as fold enrichment for ChIP samples derived from GCNF-overexpressing cells was not distinctly increased and was around 1 similar to the fold enrichment for controls (Figure 3.18 D). Unfortunately, binding of GCNF-AM to the predicted binding sites in the regulatory region of NFIB and PCYT1B could not be demonstrated. With the selected primer pairs, no significantly increased enrichment for NFIB and PCYT1B was deteced in the AM-ChIP samples from GCNF-AM-overexpressing cells (Figure 3.18 E-H).

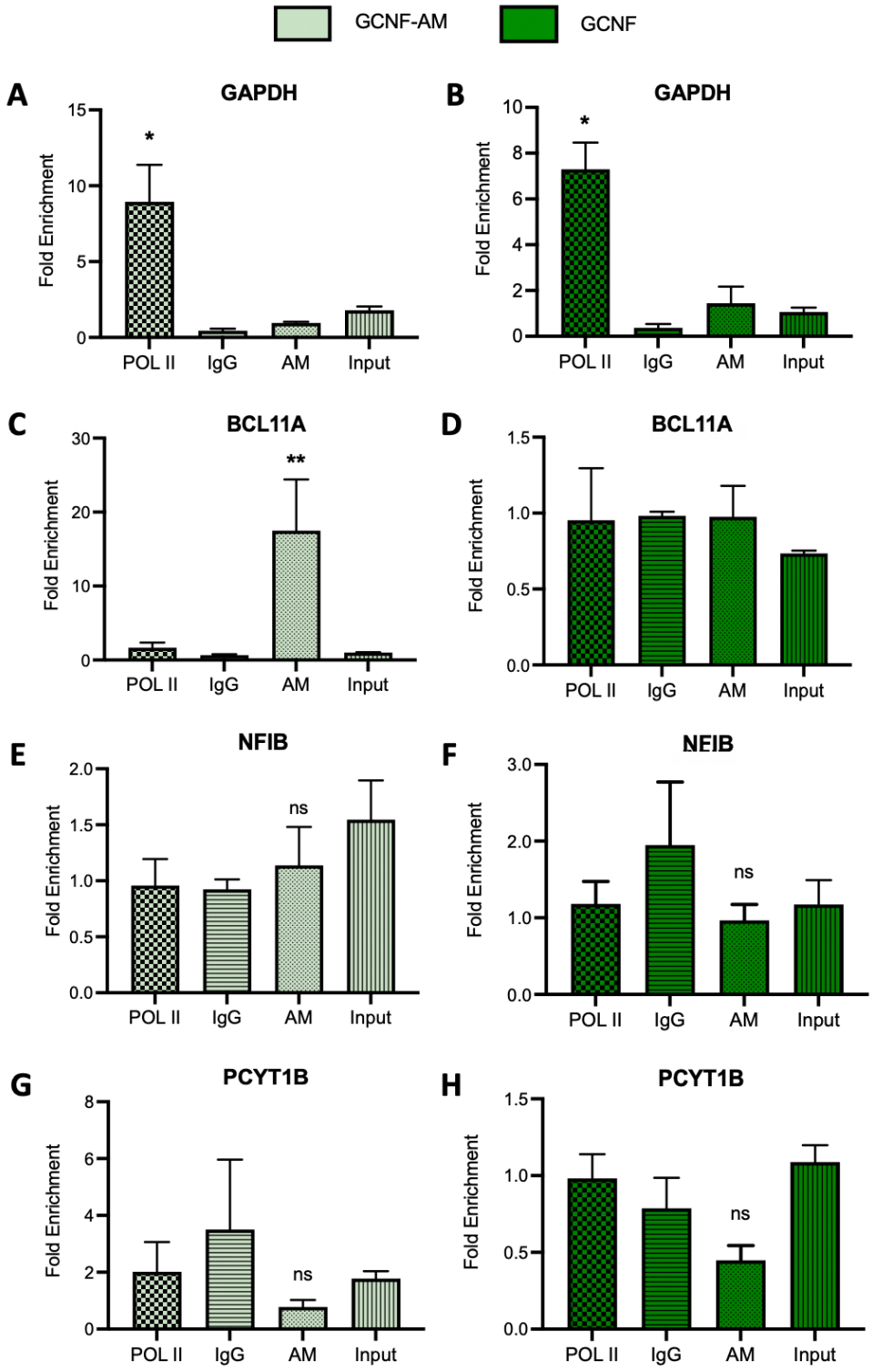

Figure 3.18: Results for ChIP assays to confirm binding of GCNF to the regulatory region of suspected target genes. (A) (B) As control for technically functioning ChIP assays, ChIP qRT-PCRs for GAPDH were performed. The enrichment of GAPDH is confirmed for (A) GCNF-AM and (B) GCNF cells in ChIP assays utilizing an antibody against POL II. Data are presented as mean + SEM, n = 3, * $p \leq 0.05$, unpaired t-test. **(C)** Binding of GCNF-AM to the regulatory region of BCL11A is confirmed. Data are presented as mean + SEM, n = 5, ** $p \leq 0.01$, Mann-Whitney test. **(D)** No enrichment for BCL11A is detected in ChIP assays using GCNF-overexpressing smNPCs. Data are presented as mean + SEM, n = 2. **(E) – (H)** Binding of GCNF to its predicted binding site within the regulatory region is neither confirmed for (E) NFIB in GCNF-AM or (F) GCNF samples, nor for (G) PCYT1B in GCNF-AM or (H) GCNF samples. Data are presented as mean + SEM, $n \geq 3$, ns $p > 0.05$, unpaired t-test.

To sum up, repeatable and reliably functioning ChIP assays were established, which was confirmed by several included controls. The binding of GCNF to the regulatory region of BCL11A to the bioinformatically predicted binding sites could be proven. However, binding of GCNF to the regulatory region of NFIB and PCYT1B could not be validated with the selected primer pairs. BCL11A could be established as direct target gene of GCNF, which might mediate on molecular level the effects of GCNF overexpression on smNPC maintenance and proliferation, neuronal differentiation and cell clustering.

3.5 Assessment of GCNF-VP16 as cell culture tool for advanced neuronal differentiation

The previous experiments revealed that GCNF-VP16 strongly induced a shift from NSC proliferation to neuronal differentiation (Figure 3.4, Figure 3.5 and Figure 3.8). Additionally, differentiated GCNF-VP16-expressing smNPCs displayed reduced cell cluster size compared to control cultures and compared to NGN2-overexpressing cell cultures (Figure 3.7).

To assess GCNF-VP16 as cell culture tool for accelerated neuronal differentiation, GCNF-VP16-expressing smNPCs and NGN2-overexpressing smNPCs were imaged using live-cell imaging and the generated neurons were analyzed with regard to maturity.

Live-cell imaging of EtO-smNPCs, GCNF-VP16-expressing and NGN2-overexpressing smNPCs for the first 2 days of neuronal differentiation illustrated that GCNF-VP16 expression strongly interfered with cluster formation (Figure 3.19). It was observed that GCNF-VP16-expressing cells seem to form neuronal processes earlier than EtO cells (Figure 3.19 A) and appear to be smaller and more motile than NGN2-overexpressing cells (Figure 3.19 B and C).

The natural formation of cell clusters in differentiating hNSC cultures makes reliable manual quantification or automated high throughput analysis of neuronal cultures difficult. For this reason, forced GCNF-VP16-expression could be an interesting tool to generate neuronal cultures with significantly reduced cluster areas compared to the gold standard – NGN2 overexpression.

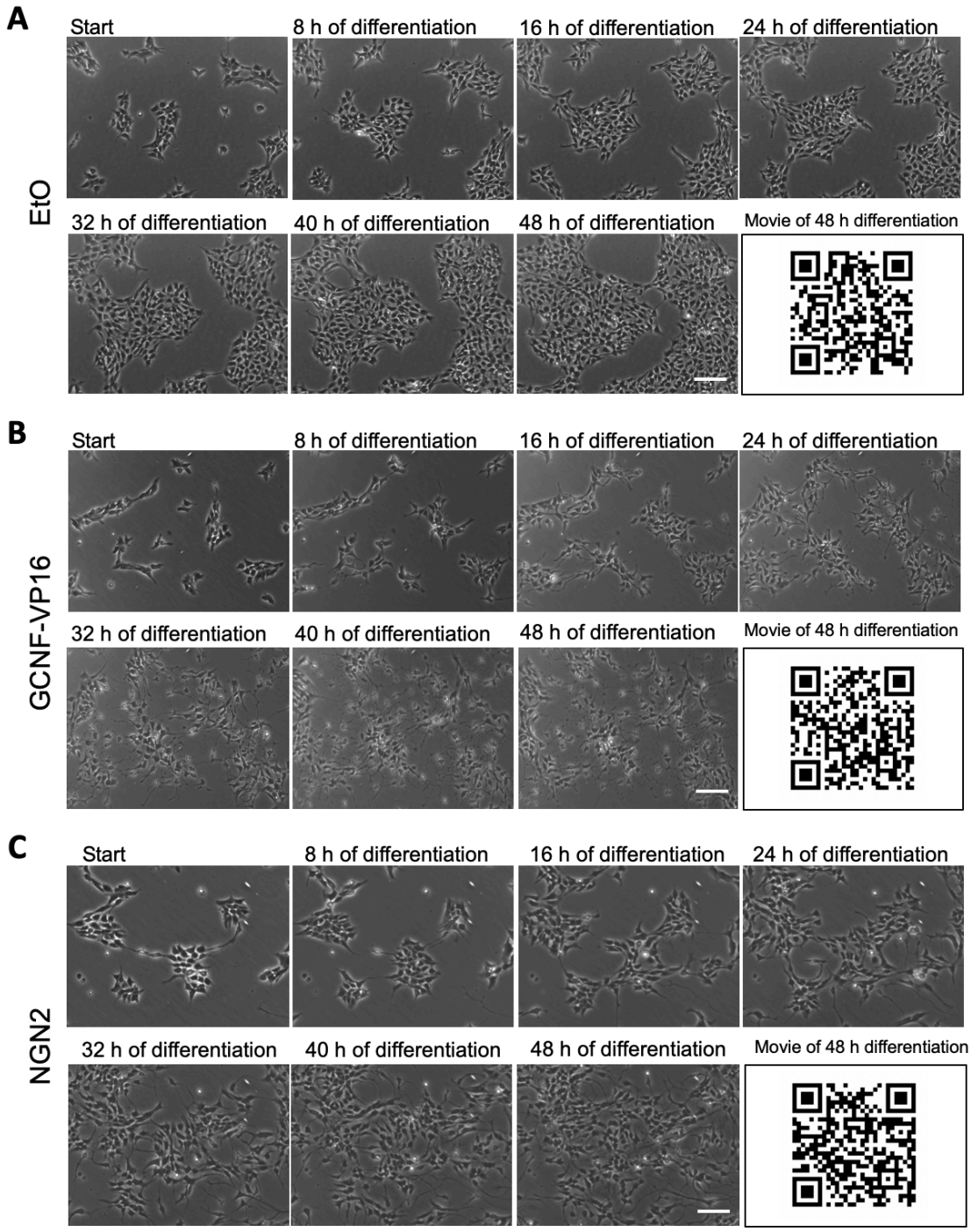

Figure 3.19: Phase contrast pictures taken during the first 48 h of differentiation in the presence of DOX displaying accelerated neuronal differentiation of GCNF-VP16-cells. (A) Exemplary pictures of EtO, **(B)** GCNF-VP16-expressing and **(C)** NGN2-overexpressing smNPCs taken during neuronal differentiation at time points 0 (start), 8 h, 16 h, 24 h, 32 h, 40 h and 48 h after DOX treatment and withdrawal of small molecules used for smNPC expansion. The QR codes lead to time lapse videos consisting of 96 single images taken every 30 min during 48 h neuronal differentiation in the presence of DOX. The videos are hosted on the online video platform YouTube (Google LLC). Scale bar 100 µm.

However, the question remained if GCNF-VP16 neurons reached maturity. One sign of neuronal maturity is the formation of synapses between neurons (He and Yu, 2018). GCNF-VP16-expressing and NGN2-overexpressing neurons were cultivated for 5 weeks before fixation and immediate staining for the presynaptic marker synaptophysin and the postsynaptic marker postsynaptic density protein 95

(PSD95). The detection of synaptophysin- and PSD95-positive puncta in 5-week-old GCNF-VP16- and NGN2-neurons (Figure 3.20 A, B) suggested that synapse formation prerequisites were present in these neuronal cultures.

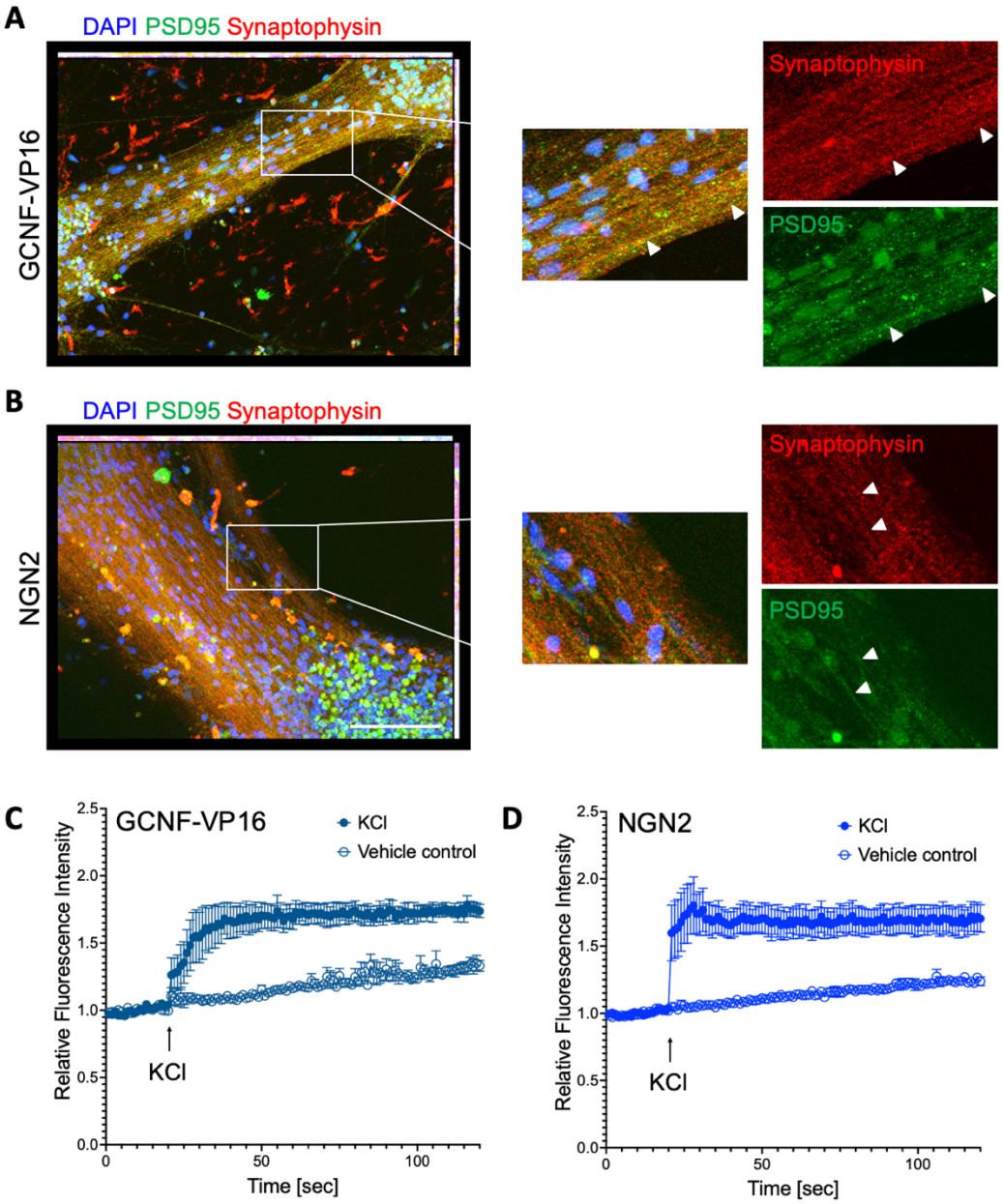

Figure 3.20: Immunofluorescence images of puncta expressing pre- and postsynaptic marker suggesting synapse development and calcium imaging indicate excitability of 5 and 6 weeks old GCNF-VP16- and NGN2-neurons. (A) (B) Staining for presynaptic marker synaptophysin and postsynaptic marker PSD95 of 5 weeks old (A) GCNF-VP16- or (B) NGN2-neurons displays expression of both markers along neuronal bundles. DAPI was used to counterstain nuclei. The enlargement and visualization of the single channels illustrate the presence of synaptophysin- and PSD95-positive puncta along axons (white arrow heads). Scale bar 100 µm. **(C) (D)** Calcium imaging of 5 and 6 weeks old (C) GCNF-VP16- and (D) NGN2-neurons indicate neuronal excitability. Upon treatment with KCl, the intracellular Ca^{2+} concentration in GCNF-VP16- or in NGN2-neurons cultivated for 5 to 6 weeks is elevated and by this the measured fluorescence intensity is increased. This increase is not observed in cells treated with vehicle control. n = 4, 2 independent technical repeats.

Calcium ions play important roles in different cellular processes, like proliferation and differentiation, but also in excitability (Vőfély *et al.*, 2018). This excitability could be confirmed by measuring the intracellular Ca^{2+} levels upon KCl treatment. This extracellular increase of potassium ions should lead to an unspecific depolarization and increasing intracellular Ca^{2+} levels (Patterson *et al.*, 2007). NGN2-

overexpressing neurons as well as GCNF-VP16-expressing neurons displayed a strong increase of fluorescence intensity after treatment with KCl, which indicated an increase of the intracellular Ca^{2+} (Figure 3.20 C, D).

In summary, neurons generated by GCNF-VP16 expression displayed the same maturity markers, such as synaptophysin- and PSD95-positive puncta and reaction to KCl depolarization with increased Ca^{2+} concentration, as neurons generated by NGN2 overexpression, which is the current gold standard for enhanced neuronal differentiation.

4. Discussion

In various animal studies, using mice or *Xenopus laevis*, the role of GCNF during embryonic development was described. These studies revealed that GCNF expression is important for proper cardiac development, body axis turning, neural tube closure and somitogenesis (Chung *et al.*, 2001; Barreto, Reintsch *et al.*, 2003). Additionally, in the developing brain of mice or *Xenopus laevis* regionalization is depended on GCNF expression. In *Xenopus laevis*, the midbrain-hindbrain identity of neural ectodermal cells is affected by GCNF (Song *et al.*, 1999) and in mice, GCNF expression is crucial for the establishment of midbrain structures (Chung *et al.*, 2006). Furthermore, GCNF controls the differentiation of primitive NSCs into definitive NSCs by repressing OCT4 (Akamatsu *et al.*, 2009).
GCNF is affecting all these processes by regulating and influencing the expression of downstream genes. During mouse development, it was demonstrated that GCNF controls OCT4 and NANOG expression (Gu, LeMenuet, *et al.*, 2005) and influences for example FGF8, WNT1, EN1/2 or GBX2 expression (Chung *et al.*, 2006). The studies, which describe the function of GCNF in human context, rely mostly on cancerous cells. Nevertheless, they suggest that GCNF may also play a role in human neural development (Schmitz *et al*, 1999; Hentschke *et al.*, 2006). Finally, it was confirmed that GCNF is crucial for downregulating OCT4 expression to ensure proper neural development of hPSCs (Wang *et al.*, 2016; Braun *et al.*, in revision).

In this study, the role of GCNF in human neuronal differentiation was analyzed using smNPCs and their neuronal progeny as proxy for human neuronal development. Initially, the temporal and spatial expression pattern of GCNF was described as similar to the expression pattern of the neural marker SOX2. Detailed analyses of the effects of altered GCNF expression on smNPC proliferation, maintenance and neuronal differentiation displayed that GCNF is promoting smNPC proliferation and maintenance on the expense of neuronal differentiation. Additionally, clustering of cells within seven days old, differentiated smNPC cultures was prominently affected by altered GCNF expression: GCNF overexpression increased cell clustering leading to the formation of larger cell clusters compared to control cells. GCNF-VP16 expression in smNPCs showed the opposite effect by strongly inducing neuronal differentiation and dissolving of cell clusters. On molecular level, GCNF overexpression delayed the expression of neuronal genes and altered the expression of genes, which are associated with the cell membrane or encode membrane proteins. In contrast, GCNF-VP16 accelerated the expression of genes linked to neuronal differentiation. Furthermore, BCL11A, a transcription factor involved in murine cortex development, could be confirmed by ChIP-qRT-PCR assays as novel, direct target gene of GCNF. The last part of this thesis focused on the evaluation of GCNF-VP16 as tool for accelerated neuronal differentiation resulting in neuronal cultures with significantly reduced cell cluster area. GCNF-VP16 expression in smNPCs led to the formation of neurons expressing synaptic marker and displaying rudimental electrophysical activity similar to neurons generated via forced NGN2 expression.

4.1 The spatial and temporal expression pattern of GCNF

To investigate the function of GCNF during neuronal differentiation, the temporal and spatial expression pattern of GCNF was analyzed in the context of human neuronal development.

In previous studies, GCNF expression was not only demonstrated in germ cells of adult vertebrates (Chen *et al.*, 1994; Hirose *et al.,* 1995; Joos *et al.*, 1996; Süsens *et al.*, 1997), but also during mouse development. Here, GCNF expression displays a dynamic pattern. Initially, GCNF is expressed in all three germ layers as well as in the extraembryonic tissue at E6.5 of mouse development. At E8.5, GCNF expression is only detectable in the proliferating neuroepithelium and in the underlying mesoderm and at E9.5 its expression is even further decreased in the forebrain and midbrain. It was reported, that GCNF expression declines further from E10.5 (Süsens *et al.*, 1997; Chung and Cooney, 2001; Chung *et al.*, 2001; Fuhrmann *et al.*, 2001). However, GCNF expression could be confirmed in the marginal zone of the neuroepithelium at E15 (Bauer *et al.*, 1997) and recently Tan et al., described GCNF expressing neurons in the adult mouse hippocampus (Tan *et al.*, 2022).

In this study, smNPCs and cerebral organoids derived from hiPSCs were utilized to analyze the expression pattern of GCNF. Additionally, the expression of GCNF in the developing mouse brain was examined, since previously performed expression studies of GCNF addressed the entire embryonic mouse body and did not focus on the developing brain especially.

For the temporal analysis of the GCNF expression pattern, smNPCs were differentiated for 14 days and protein samples were harvested at smNPC stage and at seven and 14 days of differentiation. GCNF is expressed in smNPCs with decreasing protein levels of GCNF in their neuronal progeny. Hence, GCNF is downregulated, while neuronal differentiation proceeded. The same pattern could be observed for the expression of the well-established NSC marker SOX2 (Suh *et al.*, 2007). Utilizing RNA ISH to determine GCNF expression in a tissue context, GCNF expression in cells adjacent to the lateral ventricle in the murine brain (coronal E18.5 mouse brain sections) and in the neuroepithelial loops of 20 days old human cortical organoids could be demonstrated. The region adjacent to the lateral ventricle yields proliferative NPCs (Conover and Todd, 2017), which keep their stem cell properties until adulthood (Fuentealba *et al.*, 2015). The ventricular-subventricular zone is therefore commonly described as neural stem cell niche (Redmond *et al.*, 2019). The neuroepithelial loops of 20 days old human cortical organoids, which resemble early stages of the human embryonic brain, are reported to consists of SOX2-positive neural progenitors (Iefremova *et al.*, 2017). GCNF expression, as well as SOX2 expression by cells located within these neuroepithelial loops could be confirmed. Thus, on temporal and on spatial level the GCNF expression pattern was similar to the expression pattern of SOX2. Hence, a similar function of GCNF in hNSCs and their neuronal differentiation as the one, which is described for SOX2, could be hypothesized.

SOX2 is a transcription factor, that is crucial for NSC maintenance and proliferation (Favaro *et al.*, 2009; Pagin *et al.*, 2021). The knockout of SOX2 diminishes the number of NSCs in the murine hippocampus by controlling the expression of Shh (Favaro *et al.*, 2009). Further analysis of the molecular mechanisms by which SOX2 controls proliferation of NSCs, revealed that SOX2 controls a network of genes, that is critical for NSC self-renewal and maintenance (Pagin *et al.*, 2021). The controlled downregulation of SOX2 expression is crucial for neural progenitor differentiation. Ectopic SOX2 expression inhibits differentiation of neural progenitor cells into neurons (Bylund *et al.*, 2003; Graham *et al.*, 2003)

Furthermore, overexpression of SOX2 is demonstrated in different human brain tumors such as medulloblastoma and glioblastoma, in which SOX2 drives cancer stem cell maintenance and proliferation (Mansouri *et al.*, 2016).
To understand the function of GCNF during human neuronal differentiation, the effect of modulated GCNF expression on smNPC proliferation, maintenance and differentiation was analyzed in more detail.

4.2 The role of GCNF hNSC maintenance, differentiation and clustering

Using the Tet-On Advanced system and lentiviral transduction, smNPCs were generated, which displayed modulated GCNF expression upon DOX induction. A classical GCNF overexpression construct was introduced into smNPCs as well as GCNF control constructs such as a shRNA for GCNF to facilitate its knockdown, a GCNF constructs with a mutated DBD to inhibit DNA binding of GCNF and its function as transcriptional repressor, and a GCNF-VP16 construct, which codes for a fusion protein of GCNF with the TAD of VP16 to turn GCNF into a strong transcriptional activator. Additionally, NGN2 overexpression in smNPCs was used as control for accelerated neuronal differentiation. The different GCNF-smNPCs as well as NGN2-overexpressing smNPCs and two different control smNPC lines with non-modulated GCNF expression were differentiated for seven days upon withdrawal of small molecules needed for smNPC expansion and in the presence of DOX. The differentiated cell cultures were analyzed for the number of remaining SOX2-positive smNPCs, the percentage of proliferative cells within the cultures and the neuronal differentiation status by assessing the fraction of CD200-positive cells. During these experiments, a difference in cell clustering was observed, which was subsequently quantified.
GCNF overexpression increased the number of SOX2-positive cells, as well as the number of proliferative cells on the expense of neuronal differentiation. Furthermore, differentiated smNPCs displayed increased cell cluster size, which consists of remaining smNPCs and the cell body of neuronal cells, upon GCNF overexpression. The increased cluster formation could either be an artifact of increased proliferation or could be caused by e.g., changes in the cell membrane, cell-adhesion or cell-cell interactions, which in turn could influence NSC maintenance and proliferation (Jiao *et al.*, 2017; Morante-Redolat and Porlan, 2019). The overexpression of GCNF with a mutated DBD, had no influence on the number of SOX2-positive or proliferative cells, nor on cluster area. The knockdown of GCNF did not alter the number of SOX2-positive cells, but decreased the proliferative capacity of cells within seven days old, differentiated smNPC cultures, while increasing the fraction of neuronal cells. Interestingly, not all SOX2-positive cells undergo proliferation and the status of SOX2 expression and proliferative capacity of a cell need to be evaluated separately (Kazanis *et al.*, 2010). The knockdown of GCNF hampered smNPC proliferation, but did not yet affect SOX2 expression. Differentiating NSCs exist the cell cycle and stop proliferation, while differentiating into neurons (Nguyen *et al.*, 2006). Thus, the lower number of proliferative cells and the higher fraction of neuronal cells complement each other. The GCNF shRNA-smNPCs did not self-renewal anymore, but instead differentiated into neuronal cells. The cluster area of formed clusters in shRNA GCNF-smNPC cultures was decreased compared to control cell lines, which could be caused by less cell proliferation and increased neuronal differentiation or altered cell properties regarding their cell membrane, adhesion and cell-cell interactions. Reversing the function of GCNF by fusing the TAD of VP16 to GCNF, led to opposite effects on smNPC maintenance, proliferation

and differentiation than those described for GCNF overexpression. GCNF-VP16 expression decreased the number of SOX2-positive and proliferative cells, while promoting the formation of neuronal cells. In GCNF-VP16-cell cultures the cluster area was prominently decreased. Concluding, GCNF expression strongly affects different important processes during human neuronal development such as hNSC maintenance, proliferation and differentiation. These processes need to be tightly controlled to ensure proper neurogenesis and the formation of a physiologically functional brain (Lancaster *et al.*, 2013; Iefremova *et al.*, 2017; Gomes *et al.*, 2020). GCNF might control the timing of neuronal differentiation by inhibiting premature differentiation and maintaining NSCs in their stem cell state.

Different studies describe an involvement of GCNF in controlling cell differentiation and proliferation. During mid-gastrulation in mice, GCNF represses the expression of actively transcribed genes during cell differentiation and mouse embryo maturation and its own expression is regulated by miRNA let-7. Let-7 and GCNF might function antagonistic to tightly control gene expression in the mid-gestation mouse embryo (Gurtan *et al.*, 2013). The importance for regulated GCNF expression during development was not only demonstrated in different animal studies based on mice or *Xenopus laevis* (Chung *et al.*, 2001; Barreto, Reintsch *et al.*, 2003), but also in studies, which investigated donkey and swine growth traits. Thus, the body length and height of donkeys are linked to a depletion within the intron 1 of the GCNF gene (Fang *et al.*, 2019), while mutations in the GCNF gene affect the number of vertebrae in swine and thus their size (Mikawa *et al.*, 2007; Ijiri *et al.*, 2021). Gain-of-function mutation in the GCNF gene correlates with larger body size (Mikawa *et al.*, 2007).

Interestingly, the number of formed vertebrae is depended on the number of somites generated during development, which is controlled by axis elongation of the presomatic mesoderm and somitogenesis. These two processes are in turn dependent on cell proliferation in the tail bud and tail bud movement (Gomez and Pourquié, 2009). Since, knockdown of GCNF in mice led to altered tail bud development (Chung *et al.*, 2001), it is likely that GCNF is involved in regulating cell proliferation in the tail bud.

Furthermore, altered GCNF expression is demonstrate to be responsible for germ cell cancer progression by increasing cancer cell proliferation and influencing cancer cell migration in prostate and ovarian cancers as well as in gastric cancers (Mathieu *et al.*, 2013; G. Cheng *et al.*, 2017; Zhou *et al.*, 2020; Daisuke *et al.*, 2021). Contradictory to the findings described in this study, a promoting function of GCNF on neuronal differentiation was reported by analyzing altered GCNF expression in cancer cells (Sattler *et al.*, 2004; Liu *et al.*, 2020). Sattler *et al.* showed that the repression of GCNF inhibited neuronal differentiation and maturation of mouse embryonic carcinoma cells, while its overexpression induced neuronal differentiation upon RA treatment (Sattler *et al.*, 2004). Additionally, GCNF induced MAP2 expression during RA-induced neurodifferentiation of testicular germ cell tumor cells (Liu *et al.*, 2020). Cancer cells and NSCs exhibit different molecular structures, even though both cell lines have the ability to self-renew and differentiate into multiple cell types. In fact, cancer cells show on molecular level more similarities with PSCs (Jostock *et al*, 1998). At the state of pluripotency, GCNF expression was described to be important for neural induction and differentiation of PSCs into cells of the neural lineage. In our institute, Braun and colleagues demonstrated that the knockout of GCNF impaired neural differentiation of hiPSCs (Braun et al., in revision), which might be due to the lost repression of OCT4 and NANOG by GCNF required for proper embryonic stem cell differentiation (Gu, LeMenuet, *et al.*, 2005). This differentiation promoting effect of GCNF might change to a differentiation inhibiting function

of GCNF on the level of multipotency, as GCNF overexpression inhibited neuronal differentiation of smNPCs and increased their maintenance and proliferation. A similar dual function was also described for SOX2. SOX2 expression is crucial for NSC maintenance and its timed repression is required for neuronal differentiation (Bylund *et al.*, 2003; Graham *et al.*, 2003). However, SOX2 promotes differentiation of PSCs into neuroectodermal cells (Thomson *et al.*, 1998; Zhao *et al.*, 2004).

Hence, in addition to the shared expression pattern of SOX2 and GCNF, GCNF might function similar to SOX2 in controlling temporal development.

Apart from the effect on smNPC proliferation and differentiation, modulated GCNF expression also altered the architecture of formed cell cultures: GCNF overexpression promoted the formation of large cell clusters within seven days old differentiating smNPC cultures. However, the knockdown of GCNF as well as reversing the function of GCNF (GCNF-VP16) decreased the area of formed clusters. Additionally, NGN2 overexpression led to a decrease of the cell cluster area. The cluster area might be influenced by the differences in smNPC proliferation. However, GCNF-VP16 expression diminished the cluster area more than NGN2 overexpression even though ectopic expression of both proteins had the same negative effect on cell proliferation. GCNF-VP16 expression had a more pronounced effect on the number of SOX2-positive smNPCs than NGN2 overexpression. The knockdown of GCNF had no influence on the number of remaining SOX2-positive smNPCs. These observations imply that the alterations in cell clustering could not only be a secondary effect of changes in smNPC proliferation or maintenance, but might rather directly influenced by modulated GCNF expression. It might also be that the changes observed in smNPC proliferation and differentiation might be consequences of different cell clustering. The differences in cell clustering might be a result of e.g., alteration in the cell membrane, cell adhesion and cell-cell interactions (Solozobova *et al.*, 2012).

Indeed, GCNF was described to be involved in gene expression regulation of important genes for cell adhesion. GCNF was demonstrated to regulate E-cadherin expression in tumor cells (Liu *et al.*, 2020) and cadherins are crucial proteins for cell adhesion and subsequent regulation of cell homeostasis (Yulis *et al.*, 2018). GCNF might influence E-cadherin expression not only under pathophysiological conditions, but also during neurogenesis, as GCNF also affects the distribution of fibronectin and the expression of integrin subunits that mediate cell-matrix interactions, during *Xenopus laevis* development. This interactions as well as cell-cell interactions via cadherins might regulate in cooperation morphogenetic cell movement (Barreto, Reintsch *et al.*, 2003). In a previous study using immortalized human cancer cells, GCNF was demonstrated to affect the lipogenesis of these cells. Here, the knockdown of GCNF led to accumulation of lipids and induced proliferation and migration via insulin signaling (Wang *et al.*, 2019). Cell membrane synthesis is directly influenced by alteration in lipogenesis, which in turn affects cadherin and integrin expression leading to changes in embryonic development, cell migration and cell clustering (Barcelona-Estaje *et al.*, 2021; Batchuluun *et al.*, 2022).

All these studies give evidence that GCNF affects different levels of cell adhesion and cell-cell interactions, which could ultimately result in differences in cell clustering, which then could alter NSC proliferation or differentiation. As demonstrated for the adult NSC niche, intact niche architecture is required for maintaining NSCs and their neurogenic potential. The extracellular matrix and adhesion molecules are involved in preserving niche architecture and the regulation of neural stemness and proliferation (Morante-Redolat and Porlan, 2019). Furthermore, adhesion molecules such as Neural cell

adhesion molecule (NCAM) and cell adhesion molecule L1 are involved in neural precursor cell proliferation, as well as in cell interactions and adhesion (Shin *et al.*, 2002; Dihné *et al.*, 2003)
Understanding changes in the transcriptome due to altered GCNF expression and identifying target genes of GCNF, would enhance knowledge of the molecular mechanisms leading to increased smNPC proliferation and clustering and decreased neuronal differentiation upon GCNF overexpression.

4.3 Effects of GCNF on transcriptome

Using microarray gene expression analyses, the gene expression of 20,000 genes in GCNF, GCNF-VP16, NGN2 and two control smNPC lines at differentiation day two, seven and 14 was analyzed. The initial analysis of transcriptomic alterations upon GCNF overexpression revealed that GCNF inhibited neuronal differentiation by delaying changes in the gene expression of genes, associated with neuronal differentiation, while GCNF-VP16 accelerated these changes in gene expression linked to neuronal differentiation.
A more detailed analysis of the genes, which are differentially expressed in GCNF and GCNF-VP16 smNPCs compared to control cells at ND2 and ND7 gave an impression of which biological processes, molecular function and cellular components were affected by GCNF overexpression or GCNF-VP16 expression.
Functional annotation clustering of the differential expressed genes (DEGs) in GCNF-overexpressing cells at ND2 revealed that the upregulated DEGs are associated with annotation clusters related to the “calcium ion binding”, “membrane”, “glycoprotein” and that the annotation clusters of downregulated DEGs include annotation clustered linked to “cell surface, receptor binding” and “membrane”. After seven days of differentiation, the majority of terms annotated for the DEGs were still linked to “calcium ion binding, cell adhesion”, “membrane” and “plasma membrane, glycoprotein”. The DEGs for GCNF-VP16 expressing cells at ND2 were also sorted into annotation clusters including “cell membrane” and “membrane, transmembrane”. At ND7 annotation clusters containing terms as “long-term potentiation” for upregulated DEGs or “cell division” for downregulated DEGs, hinted to altered expression of genes linked to neuronal differentiation and decreased proliferation (Cho *et al.*, 2013; Homem *et al.*, 2015). The alteration of expression of genes, which are associated with the cell membrane and membrane proteins, early in neuronal differentiation, might point to role of GCNF in e.g., cell adhesion. This could explain the observed alterations in cell clustering, which then affects cell proliferation and differentiation (Reichardt and Tomaselli, 1991; Shin *et al.*, 2002; Solozobova *et al.*, 2012). However, these analyses are not sufficient to confirm, whether the altered cell clustering of GCNF-overexpressing smNPCs is a consequence of alterations alteration in the cell membrane, cell adhesion and cell-cell interactions or whether the differences in cell clustering are results of changes in smNPC proliferation and differentiation.

4.4 BCL11A as target gene of GCNF

After the analysis of the broad effect of GCNF on gene expression, possible direct target genes of GCNF were identified. So far, little is known about target genes of GCNF in somatic stem cells. However, some target genes, which are directly repressed by binding of GCNF, are described at pluripotent level. For

instance, binding of GCNF to DR0 motifs in the regulatory region of OCT4 was demonstrated, which leads to its downregulation (Gu, LeMenuet, *et al.*, 2005; Park *et al.*, 2018). Furthermore, NANOG and CRIPTO-1 were reported as direct target gene of GCNF (Gu, LeMenuet *et al.*, 2005; Hentschke *et al.*, 2006). The repressing influence of GCNF on the gene expression of these pluripotency genes is crucial for proper neural differentiation of PSCs (Braun et al., in revision).

Profound effects of altered GCNF expression on NSC maintenance, proliferation and differentiation revealed an important role of GCNF on neural level, in addition to its importance at pluripotency level. Nevertheless, target genes of GCNF at this stage of developmental are not yet described and the molecular mechanism of the function of GCNF is unknown. The previously performed experiments demonstrated that GCNF and GCNF-VP16 had opposite effects on smNPC maintenance, proliferation, differentiation and clustering. This might be due to the fact that GCNF represses the expression of direct target genes, whereas GCNF-VP16 activates the expression of these genes (Fuhrmann *et al.*, 2001). Under the assumption that direct target genes of GCNF are targeted by GCNF and GCNF-VP16 with an opposite effect on their expression, the DEGs of GCNF-overexpressing and GCNF-V16-expressing genes were compared with each other at ND2 and ND7 to identify GCNF target genes. Only four genes met the set criteria. For three of this four genes a binding site of GCNF could be predicted by using bioinformatic tools – BCL11A, NFIB and PCYT1B. All three genes were previously reported to be linked to neuronal development. BCL11A is involved in murine CNS development and altered BCL11A expression is associated with neuro-psychological disorders (Simon et al., 2020). Furthermore, changes in NFIB expression are reported to cause intellectual impairments and macrocephaly (Schanze *et al.*, 2018), while PCYT1B is involved in phosphatidylcholine synthesis, which changes during neuronal differentiation (Paoletti *et al.*, 2011; McMaster, 2018).

The expression of all three genes was upregulated during the process of neuronal differentiation, meaning that the expression pattern of BCL11A, NFIB, PCYT1B displayed a reciprocal temporal expression pattern compared to GCNF. GCNF overexpression decreased, while GCNF-VP16 increased their mRNA levels. The knockdown of GCNF increased the expression of these genes, but not significantly. Overexpression of GCNF with mutated DBD, increased BCL11A expression levels, while it did not significantly affect the expression of the other two predicted target genes, NFIB and PCYT1B. The effect on BCL11A expression by GCNF mut could be explained by a dominant-negative effect (Veitia, 2008). Thus, mutated GCNF would bind to non-mutated, physiological GCNF protein and hinder GCNF binding to the DNA, which releases BCL11A repression by GCNF and increased BCL11A mRNA levels. However, the observed expression patterns of BCL11A, NFIB and PCYT1B during neuronal differentiation or in the different smNPC lines strengthen the suspicion that these three genes could be direct target genes of GCNF. Additionally, the expression of these genes was not altered upon NGN2-overexpression, which could be a reason for the significant phenotypic differences between GCNF-VP16-expressing and NGN2-overexpressing differentiated smNPC cultures.

To confirm the predicted target genes of GCNF as direct target genes, physical binding of GCNF to their regulatory region needed to be demonstrated. For this reason, ChIP-qRT-PCR assays were established and performed. Initially, a cell line was generated that overexpressed GCNF labeled with an AM-tag for antibody binding during immunoprecipitation, since no GCNF ChIP-grade antibodies were available. The level of GCNF and GCNF-AM overexpression was comparable, as well as their effect on repression

of BCL11A expression. Therefore, it was concluded that GCNF-AM cells could be used instead of GCNF cells to identify possible target genes of GCNF. The establishment of ChIP-qRT-PCR assays required small but important adaptations of a commercial protocol. Thus, the change from methanol-free formaldehyde to methanol containing formaldehyde might have increased cell permeability (Jamur and Oliver, 2010) and improved fixation of chromatin, while the addition of mechanical force (douncing) during the cell lysis step enhanced cell lysis and nuclei separation (DeCaprio and Kohl, 2019). Additionally, the snap-freezing step after cell lysis and before sonication, enhanced DNA concentration and improved chromatin fragmentation, possibly due to disruption of the nuclei envelope caused by freezing (Milani *et al.*, 2016).

By following the established protocol for ChIP-qRT-PCR assays, binding of GCNF to the predicted binding site in the regulatory region of BCL11A could be confirmed. Unfortunately, binding of GCNF to the predicted binding sites in the regulatory region of the NFIB or PCYT1B genes could not be proven. Nevertheless, NFIB and PCYT1B might still be direct target genes of GCNF, but could not be confirmed by using the established ChIP-qRT-PCR protocol. Even though, the chromatin fragmentation was improved during ChIP protocol establishment, some chromatin fragments, remain larger than 1,200 bp. If the fragments of the genomic DNA encoding NFIB or PCYT1B were too long, no enrichment of DNA fragments bound by the positive primer pair be detected relative to the fragments bound by the negative primer pair, since both primers would bind to the same DNA fragment. Further improvements of chromatin fragmentation and new primer design could overcome this issue and binding of GCNF to the predicted binding sites in the regulatory regions of NFIB or PCYT1B might be confirmed. Another method, which could be used to prove direct binding of GCNF to the NFIB or PCYT1B promoter, is a luciferase reporter assay (Pandolfi and Stecca, 2015). Here, the sequence of the regulatory region containing the predicted binding sites of NFIB or PCYT1B would be cloned into a luciferase reporter plasmid and binding of GCNF would be confirmed by modulated luciferase activity and altered luminescence.

To achieve unbiased identification of GCNF target genes, ChIP-sequencing assays could be performed. Here, all DNA fragments, which are bound during immunoprecipitation, are identified by next generation sequencing, which gives a broad overview of genes bound by GCNF, whether or not they have been shortlisted as target genes by previously performed transcriptome analysis or bioinformatic prediction. However, the sample requirements for ChIP-sequencing are high and could not be met with the protocol described in this study (Sullivan and Santos, 2020).

BCL11A was described in various studies to be involved in murine brain development and alterations in BCL11A expression are linked to neurophysiological disorders (Simon *et al.*, 2020). Interestingly, in the developing mouse brain, expression of BCL11A is described from E10.5 on (Dias *et al.*, 2016), at which GCNF expression diminishes (Chung *et al.*, 2001). BCL11A expression might be regulated by GCNF *in vivo*, since BCL11A expression increases after its transcriptional repressor GCNF is downregulated. BCL11A acts as transcriptional repressor (Seachrist *et al.*, 2020) and is part of the SWI/SNF complex, which regulates gene expression by altering the chromatin state (Kadoch *et al.*, 2013). Altered BCL11A expression is associated with various neurodevelopmental and neuropsychiatric disorders in human patients (Dias *et al.*, 2016; Peron *et al.*, 2019; Simon *et al.*, 2020). Additionally, BCL11A expression during mouse embryonic development could be demonstrated in the cerebral cortex, striatum, olfactory

bulb and dorsal spinal cord (Leid *et al.*, 2004) and different roles of BCL11A during murine CNS development were described. Thus, BCL11A expression is important for somatosensory circuit formation (John *et al.*, 2012), radial migration of late-born cortical projection neurons (Wiegreffe *et al.*, 2015), organization of thalamocortical axons into proper sensory maps (Greig *et al.*, 2016) and the formation of subcircuits of dopaminergic neurons, which are crucial for skilled motor behavior (Tolve *et al.*, 2021). Additionally, BCL11A is involved in axon branching and dendrite outgrowth (Kuo *et al.*, 2010) as demonstrated using hippocampal rat neurons. BCL11A is also involved in subtype specification of neurons. In mice, BCL11A is required for corticothalamic and callosal subtype acquisition of deep cortical layer neurons and repression of layer V subcerebral identity (Woodworth *et al.*, 2016). All these studies demonstrate importance of BCL11A in neuronal migration, organization, morphological changes or subtype specification, which are processes required for proper neuronal network formation (Ramakers, 2005). During the process of neuronal differentiation, the expression of BCL11A increased, which might be due to its crucial role in neuronal maturation. Furthermore, the role of BCL11A in neural stem/progenitor cells was described in previous studies. In *Drosophila malanogaster*, the BCL11A and BCL11B homolog was demonstrated to regulate temporal neuronal identity acquisition of differentiating neural stem cells (Fox *et al.*, 2022) and in murine cortical radial glial cells, the knockout of BCL11A induced premature differentiation of cortical projection neurons, while reducing neural progenitor cell proliferation (Du *et al.*, 2022). BCL11A does not only act as transcriptional repressor, but also as part of the mammalian SWI/SNF chromatin remodeling complex (Kadoch *et al.*, 2013). The SWI/SNF complex is crucial for proper neural development, as it is involved in neural fate establishment, maintenance and functionality (Sokpor *et al.*, 2017). Downregulation of BCL11A by GCNF, might affect the SWI/SNF complex and its regulation of neural development.

In this study, using smNPCs and their neuronal progeny as model for human neuronal development, reduced BCL11A expression is associated with increased hNSC proliferation and maintenance at the expense of neuronal differentiation as well as increased cell clustering. These oberserved effects are not directly linked with the previously reported function of BCL11A (e.g., neuronal spatial organization and migration, neuronal subtype acquisition). In addition, the knockdown of BCL11A in mouse cortical NSCs lead to premature neuronal differentiation (Du *et al.*, 2022), while in this study reduced BCL11A expression is linked to decreased neuronal differentiation and an increased neural proliferation. Since, the function of BCL11A in neuronal maturation processes is specific to the neuronal subtype, it is possible, that also the function of BCL11A in NSCs is subtype-specific. Thus, different effects of BCL11A with regard to cell proliferation and neuronal differentiation might be observed in different subtypes of NSCs. BCL11A is a transcription factor that affects cell behavior by altering the gene expression of its target genes, which might be different in the various NSC types as they show differences in their global gene expression levels (Cosacak *et al.*, 2019; Ding *et al.*, 2022).

In this study, only BCL11A could be confirmed as direct target gene of GCNF. However, whether altered BCL11A expression is solely responsible for the observed alterations in hNSC proliferation and differentiation has not been investigated and still remains to be proven. The alteration of GCNF expression affects the expression of various different genes and an interplay of different DEGs might be responsible for the observed phenotypic effects (Shi *et al.*, 2008).

Interestingly, GCNF-VP16 expression in smNPCs, which was used as control for GCNF mediated effects on gene expression and cell behavior, led to the accelerated generation of neuronal cultures with significantly reduced cluster areas.

4.5 GCNF-VP16 as tool for accelerated neuronal differentiation

GCNF-VP16 expression accelerated the formation of neuronal cells comparable to NGN2 overexpression, which is commonly used for forward programming of stem cells into neurons (Ho *et al.*, 2016; Flitsch *et al.*, 2020). NGN2 is a transcription factor, which activates the expression of proneuronal genes and promotes neuronal differentiation (Thoma *et al.*, 2012). However, GCNF acts as transcriptional repressor and seems to inhibit neuronal differentiation. By fusing the transactivator domain of VP16 to GCNF, the transcriptional repressor is turned into a transcriptional activator and drives neuronal differentiation. Immaneni and colleagues demonstrated similar effects by replacing the repressor domain of the transcription factor REST with the TAD of VP16 (Immaneni *et al.*, 2000). Under physiological conditions, REST inhibits the expression of neuronal genes in non-neuronal cells and maintains their non-neuronal identity (Ballas *et al.*, 2001; Kim *et al.*, 2015). However, REST-VP16 expression activated expression of neuronal (REST target) genes by mediating binding to the regulatory region of target genes via REST and activating transcription of these by TAD. The activation of REST target genes by REST-VP16 in mouse NSCs leads to the accelerated formation of mature and electrophysiological active neurons (Su *et al.*, 2004).

The neuronal accelerating effect of GCNF-VP16 follows the same idea. A transcriptional repressor, which inhibits neuronal differentiation, is turned into a transcriptional activator and drives by activating its target genes neuronal development of NSCs. GCNF-VP16 expression, as well as NGN2 overexpression in smNPCs led to the formation of neurons, that express synaptic markers and display increased intracellular Ca^{2+} concentration upon depolarization, which is both associated with neuronal maturity (Gingras *et al.*, 2007; Zheng *et al.*, 2012; Ali and Kwan, 2019). However, GCNF-VP16 significantly decreased the formation of cell clusters in differentiated smNPC cultures compared to NGN2 overexpression, which has advantages for e.g. automated image analysis of neuronal cultures (Schmuck *et al.*, 2020).

For automated high-throughput toxicity or drug-screenings in the context of brain development PSC derived neurons are of great interest (Boissart *et al.*, 2013; Wang *et al.*, 2017; Huang *et al.*, 2022) and in this context, an acceleration of neuronal differentiation and faster generation of neurons is preferred to save time and resources. Accelerated neuronal differentiation could be achieved by NGN2 overexpression (Kondo *et al.*, 2017). However, the generation of neuronal cell cultures, which could be used for automated high-content imaging is limited by cell density (Radio *et al.*, 2008; Schmuck *et al.*, 2020) and often requires replating steps (Dravid *et al.*, 2021) or treatment with anti-mitotic drugs (C. Cheng *et al.*, 2017). These time-consuming manipulation steps, could be overcome by GCNF-VP16 expression, which leads to the formation of almost cluster-free neuronal cultures and is therefore a promising tool to generate rapidly neuronal cultures, which could easily be used for high-content imaging.

4.6 Conclusion and outlook

To conclude, this study demonstrated that the transcriptional repressor GCNF plays a crucial role for hNSC maintenance and proliferation and inhibition of premature neuronal differentiation. Furthermore, GCNF affects cell clustering. Whether the altered cell clustering is a consequence of less differentiation and increased cell proliferation or whether the differences in cell clustering influence NSC proliferation and differentiation could not be clarified in this study.

In this study, a ChIP-qRT-PCR assay was established based on AM-tagged GCNF, which was used to confirmed bioinformatic prediction of GCNF target genes. Here, BCL11A could be identified as novel target gene of GCNF. In human, BCL11A was not yet described to be directly involved in NSC proliferation or differentiation and further experiments are required to prove if downregulated BCL11A expression leads to increased NSC proliferation and decreased neuronal differentiation. These experiments could be performed by utilizing a shRNA against BCL11A to reproduce the effects of GCNF overexpression leading to BCL11A knockdown or by rescuing the downregulation of BCL11A by reinstating BCL11A expression in GCNF-overexpressing smNPCs. However, it is also likely that the transcriptional repressor GCNF influences a network of genes, whose altered expression in combination causes the observations of increased smNPC cell clustering and proliferation and decreased differentiation. Therefore, ChIP-sequencing experiments could reveal an entire set of GCNF target genes, which could be examined to be responsible solely or in orchestra for the observed hNSC behavior.

Additionally, the artificial transcription factor GCNF-VP16 was identified as tool for accelerated neuronal differentiation of hNSCs. Ectopic expression of GCNF-VP16 in smNPCs promoted the formation of neuronal cell cultures in an almost cluster-free manner, which is favorable for automated high-content imaging in toxicity and drug-screening. Nonetheless, further experiments and cost-benefit analysis are necessary to generate a competitive product compared to already available products such as CutureOne™ form ThermoFisher (https://www.thermofisher.com/order/catalog/product/A3320201), which is a cell culture supplement that promotes neuronal differentiation of cells in a cluster free manner, or NGN2-neurons, which could be purchased with a seeding and differentiation protocol. Marketable products based on GCNF-VP16 could be, on one hand, frozen and pre-differentiated GCNF-VP16-neurons in combination with a thawing and seeding protocol, or on the other hand GCNF-VP16-hNSCs, which need to be treated and differentiated for a certain time by the costumer before use. However, the survival rate of GCNF-VP16-neurons after freezing and thawing still need to be determined and a more detailed understanding of the differentiation and maturity status of GCNF-VP16-induced neurons at different, early timepoints of differentiation is required to establish the before described products.

In summary, this study described a role of GCNF in hNSC cell clustering, proliferation and maintenance and inhibition of premature neuronal differentiation, which might be mediated by its target gene BCL11A. Additionally, GCNF-VP16 expression in hNSCs was introduced as tool for the rapid formation of almost cluster-free neuronal cultures.

5. References

Abbas, T., Keaton, M.A. and Dutta, A. (2013) 'Genomic Instability in Cancer', *Cold Spring Harbor Perspectives in Biology*, 5(3), pp. a012914–a012914. Available at: https://doi.org/10.1101/cshperspect.a012914.

Abdelnour, S.A. *et al.* (2021) 'The Potential of CRISPR/Cas9 Gene Editing as a Treatment Strategy for Inherited Diseases', *Frontiers in Cell and Developmental Biology*, 9, p. 699597. Available at: https://doi.org/10.3389/fcell.2021.699597.

Agboola, O.S. *et al.* (2021) 'Brain organoid: a 3D technology for investigating cellular composition and interactions in human neurological development and disease models in vitro', *Stem Cell Research & Therapy*, 12(1), p. 430. Available at: https://doi.org/10.1186/s13287-021-02369-8.

Agoulnik, I.Y. *et al.* (1998) 'Cloning, expression analysis and chromosomal localization of the human nuclear receptor gene GCNF', *FEBS Letters*, 424(1–2), pp. 73–78. Available at: https://doi.org/10.1016/S0014-5793(98)00142-2.

Akamatsu, W. *et al.* (2009) 'Suppression of Oct4 by Germ Cell Nuclear Factor Restricts Pluripotency and Promotes Neural Stem Cell Development in the Early Neural Lineage', *Journal of Neuroscience*, 29(7), pp. 2113–2124. Available at: https://doi.org/10.1523/JNEUROSCI.4527-08.2009.

Ali, F. and Kwan, A.C. (2019) 'Interpreting in vivo calcium signals from neuronal cell bodies, axons, and dendrites: a review', *Neurophotonics*, 7(01), p. 1. Available at: https://doi.org/10.1117/1.NPh.7.1.011402.

Anokye-Danso, F. *et al.* (2011) 'Highly Efficient miRNA-Mediated Reprogramming of Mouse and Human Somatic Cells to Pluripotency', *Cell Stem Cell*, 8(4), pp. 376–388. Available at: https://doi.org/10.1016/j.stem.2011.03.001.

Armingol, E. *et al.* (2021) 'Deciphering cell–cell interactions and communication from gene expression', *Nature Reviews Genetics*, 22(2), pp. 71–88. Available at: https://doi.org/10.1038/s41576-020-00292-x.
Armstrong, R.J.E. and Svendsen, C.N. (2000) 'Neural Stem Cells: From Cell Biology to Cell Replacement', *Cell Transplantation*, 9(2), pp. 139–152. Available at: https://doi.org/10.1177/096368970000900202.

Ashburner, M. *et al.* (2000) 'Gene Ontology: tool for the unification of biology', *Nature Genetics*, 25(1), pp. 25–29. Available at: https://doi.org/10.1038/75556.

Balboa, D. *et al.* (2015) 'Conditionally Stabilized dCas9 Activator for Controlling Gene Expression in Human Cell Reprogramming and Differentiation', *Stem Cell Reports*, 5(3), pp. 448–459. Available at: https://doi.org/10.1016/j.stemcr.2015.08.001.

Ballas, N. *et al.* (2001) 'Regulation of Neuronal Traits by a Novel Transcriptional Complex', *Neuron*, 31(3), pp. 353–365. Available at: https://doi.org/10.1016/S0896-6273(01)00371-3.

Bani-Yaghoub, M. *et al.* (2006) 'Role of Sox2 in the development of the mouse neocortex', *Developmental Biology*, 295(1), pp. 52–66. Available at: https://doi.org/10.1016/j.ydbio.2006.03.007.

Barber, R.D. *et al.* (2005) 'GAPDH as a housekeeping gene: analysis of GAPDH mRNA expression in a panel of 72 human tissues', *Physiological Genomics*, 21(3), pp. 389–395. Available at: https://doi.org/10.1152/physiolgenomics.00025.2005.

Barcelona-Estaje, E. *et al.* (2021) 'You Talking to Me? Cadherin and Integrin Crosstalk in Biomaterial Design', *Advanced Healthcare Materials*, 10(6), p. 2002048. Available at: https://doi.org/10.1002/adhm.202002048.

Barreto, G., Reintsch *et al.* (2003) 'The function of Xenopus germ cell nuclear factor (xGCNF) in morphogenetic movements during neurulation', *Developmental Biology*, 257(2), pp. 329–342. Available at: https://doi.org/10.1016/S0012-1606(03)00109-X.

Barreto, G., Borgmeyer, U. and Dreyer, C. (2003) 'The germ cell nuclear factor is required for retinoic acid signaling during Xenopus development', *Mechanisms of Development*, 120(4), pp. 415–428. Available at: https://doi.org/10.1016/S0925-4773(03)00018-2.

Barton, A. and Fendrik, A.J. (2013) 'Sustained vs. oscillating expressions of Ngn2, Dll1 and Hes1: A model of neural differentiation of embryonic telencephalon', *Journal of Theoretical Biology*, 328, pp. 1–8. Available at: https://doi.org/10.1016/j.jtbi.2013.03.004.

Basak, A. *et al.* (2015) 'BCL11A deletions result in fetal hemoglobin persistence and neurodevelopmental alterations', *Journal of Clinical Investigation*, 125(6), pp. 2363–2368. Available at: https://doi.org/10.1172/JCI81163.

Batchuluun, B., Pinkosky, S.L. and Steinberg, G.R. (2022) 'Lipogenesis inhibitors: therapeutic opportunities and challenges', *Nature Reviews Drug Discovery*, 21(4), pp. 283–305. Available at: https://doi.org/10.1038/s41573-021-00367-2.

Batool, S. *et al.* (2019) 'Synapse formation: from cellular and molecular mechanisms to neurodevelopmental and neurodegenerative disorders', *Journal of Neurophysiology*, 121(4), pp. 1381–1397. Available at: https://doi.org/10.1152/jn.00833.2018.

Bauer, U.-M. *et al.* (1997) 'Neuronal Cell Nuclear Factor. A Nuclear Receptor Possibly Involved in the Control of Neurogenesis and Neuronal Differentiation', *European Journal of Biochemistry*, 249(3), pp. 826–837. Available at: https://doi.org/10.1111/j.1432-1033.1997.t01-1-00826.x.

Belmonte-Mateos, C. and Pujades, C. (2022) 'From Cell States to Cell Fates: How Cell Proliferation and Neuronal Differentiation Are Coordinated During Embryonic Development', *Frontiers in Neuroscience*, 15, p. 781160. Available at: https://doi.org/10.3389/fnins.2021.781160.

Berninger, B. *et al.* (2007) 'Functional Properties of Neurons Derived from In Vitro Reprogrammed Postnatal Astroglia', *Journal of Neuroscience*, 27(32), pp. 8654–8664. Available at: https://doi.org/10.1523/JNEUROSCI.1615-07.2007.

Boissart, C. *et al.* (2013) 'Differentiation from human pluripotent stem cells of cortical neurons of the superficial layers amenable to psychiatric disease modeling and high-throughput drug screening', *Translational Psychiatry*, 3(8), pp. e294–e294. Available at: https://doi.org/10.1038/tp.2013.71.

Braun, N.C., et al. (in revision) 'Protracted pluripotency exit of differentiating GCNF-deficient human iPSCs'

Breunig, J.J., Haydar, T.F. and Rakic, P. (2011) 'Neural Stem Cells: Historical Perspective and Future Prospects', *Neuron*, 70(4), pp. 614–625. Available at: https://doi.org/10.1016/j.neuron.2011.05.005.

Bylund, M. *et al.* (2003) 'Vertebrate neurogenesis is counteracted by Sox1–3 activity', *Nature Neuroscience*, 6(11), pp. 1162–1168. Available at: https://doi.org/10.1038/nn1131.

Camp, J.G. *et al.* (2015) 'Human cerebral organoids recapitulate gene expression programs of fetal neocortex development', *Proceedings of the National Academy of Sciences*, 112(51), pp. 15672–15677. Available at: https://doi.org/10.1073/pnas.1520760112.

Canovas, J. *et al.* (2015) 'The Specification of Cortical Subcerebral Projection Neurons Depends on the Direct Repression of TBR1 by CTIP1/BCL11a', *Journal of Neuroscience*, 35(19), pp. 7552–7564. Available at: https://doi.org/10.1523/JNEUROSCI.0169-15.2015.

Carpenter, A.E. *et al.* (2005) 'Common Effects of Acidic Activators on Large-Scale Chromatin Structure and Transcription', *Molecular and Cellular Biology*, 25(3), pp. 958–968. Available at: https://doi.org/10.1128/MCB.25.3.958-968.2005.

Casas Gimeno, G. and Paridaen, J.T.M.L. (2022) 'The Symmetry of Neural Stem Cell and Progenitor Divisions in the Vertebrate Brain', *Frontiers in Cell and Developmental Biology*, 10, p. 885269. Available at: https://doi.org/10.3389/fcell.2022.885269.

Cassandri, M. *et al.* (2017) 'Zinc-finger proteins in health and disease', *Cell Death Discovery*, 3(1), p.

17071. Available at: https://doi.org/10.1038/cddiscovery.2017.71.

Castro-Mondragon, J.A. *et al.* (2022) 'JASPAR 2022: the 9th release of the open-access database of transcription factor binding profiles', *Nucleic Acids Research*, 50(D1), pp. D165–D173. Available at: https://doi.org/10.1093/nar/gkab1113.

Ceasar, S.A. *et al.* (2016) 'Insert, remove or replace: A highly advanced genome editing system using CRISPR/Cas9', *Biochimica et Biophysica Acta (BBA) - Molecular Cell Research*, 1863(9), pp. 2333–2344. Available at: https://doi.org/10.1016/j.bbamcr.2016.06.009.

Centeno, E.G.Z., Cimarosti, H. and Bithell, A. (2018) '2D versus 3D human induced pluripotent stem cell-derived cultures for neurodegenerative disease modelling', *Molecular Neurodegeneration*, 13(1), p. 27. Available at: https://doi.org/10.1186/s13024-018-0258-4.

Chambers, S.M. *et al.* (2009) 'Highly efficient neural conversion of human ES and iPS cells by dual inhibition of SMAD signaling', *Nature Biotechnology*, 27(3), pp. 275–280. Available at: https://doi.org/10.1038/nbt.1529.

Chanda, S. *et al.* (2014) 'Generation of Induced Neuronal Cells by the Single Reprogramming Factor ASCL1', *Stem Cell Reports*, 3(2), pp. 282–296. Available at: https://doi.org/10.1016/j.stemcr.2014.05.020.

Chavez, A. *et al.* (2015) 'Highly efficient Cas9-mediated transcriptional programming', *Nature Methods*, 12(4), pp. 326–328. Available at: https://doi.org/10.1038/nmeth.3312.

Chen, F. *et al.* (1994) 'Cloning of a novel orphan receptor (GCNF) expressed during germ cell development.', *Molecular Endocrinology*, 8(10), pp. 1434–1444. Available at: https://doi.org/10.1210/mend.8.10.7854358.

Cheng, C. *et al.* (2017) 'Highly Expandable Human iPS Cell–Derived Neural Progenitor Cells (NPC) and Neurons for Central Nervous System Disease Modeling and High-Throughput Screening', *Current Protocols in Human Genetics*, 92(1). Available at: https://doi.org/10.1002/cphg.33.

Cheng, G. *et al.* (2017) 'Positive expression of NR6A1/CT150 as a predictor of biochemical recurrence-free survival in prostate cancer patients', *Oncotarget*, 8(38), pp. 64427–64439. Available at: https://doi.org/10.18632/oncotarget.11749.

Cho, T. *et al.* (2013) 'Long-Term Potentiation Promotes Proliferation/Survival and Neuronal Differentiation of Neural Stem/Progenitor Cells', *PLoS ONE*. Edited by W. Hu, 8(10), p. e76860. Available at: https://doi.org/10.1371/journal.pone.0076860.

Chong, J.A. *et al.* (1995) 'REST: A mammalian silencer protein that restricts sodium channel gene expression to neurons', *Cell*, 80(6), pp. 949–957. Available at: https://doi.org/10.1016/0092-8674(95)90298-8.

Chung, A. and Cooney, A.J. (2001) 'Germ cell nuclear factor', *The International Journal of Biochemistry & Cell Biology*, 33(12), pp. 1141–1146. Available at: https://doi.org/10.1016/S1357-2725(01)00081-4.

Chung, A.C.-K. *et al.* (2001) 'Loss of Orphan Receptor Germ Cell Nuclear Factor Function Results in Ectopic Development of the Tail Bud and a Novel Posterior Truncation', *Molecular and Cellular Biology*, 21(2), pp. 663–677. Available at: https://doi.org/10.1128/MCB.21.2.663-677.2001.

Chung, A.C.-K. *et al.* (2006) 'Loss of orphan nuclear receptor GCNF function disrupts forebrain development and the establishment of the isthmic organizer', *Developmental Biology*, 293(1), pp. 13–24. Available at: https://doi.org/10.1016/j.ydbio.2005.12.017.

Clift, D. and Schuh, M. (2013) 'Restarting life: fertilization and the transition from meiosis to mitosis', *Nature Reviews Molecular Cell Biology*, 14(9), pp. 549–562. Available at: https://doi.org/10.1038/nrm3643.

Cong, L. *et al.* (2013) 'Multiplex Genome Engineering Using CRISPR/Cas Systems', *Science*, 339(6121), pp. 819–823. Available at: https://doi.org/10.1126/science.1231143.

Conover, J.C. and Todd, K.L. (2017) 'Development and aging of a brain neural stem cell niche', *Experimental Gerontology*, 94, pp. 9–13. Available at: https://doi.org/10.1016/j.exger.2016.11.007.

Conti, L. and Cattaneo, E. (2010) 'Neural stem cell systems: physiological players or in vitro entities?', *Nature Reviews Neuroscience*, 11(3), pp. 176–187. Available at: https://doi.org/10.1038/nrn2761.

Cosacak, M.I. *et al.* (2019) 'Single-Cell Transcriptomics Analyses of Neural Stem Cell Heterogeneity and Contextual Plasticity in a Zebrafish Brain Model of Amyloid Toxicity', *Cell Reports*, 27(4), pp. 1307-1318.e3. Available at: https://doi.org/10.1016/j.celrep.2019.03.090.

Coyle, D.E., Li, J. and Baccei, M. (2011) 'Regional Differentiation of Retinoic Acid-Induced Human Pluripotent Embryonic Carcinoma Stem Cell Neurons', *PLoS ONE*. Edited by M. Pera, 6(1), p. e16174. Available at: https://doi.org/10.1371/journal.pone.0016174.

Cui, C.-P. *et al.* (2018) 'Dynamic ubiquitylation of Sox2 regulates proteostasis and governs neural progenitor cell differentiation', *Nature Communications*, 9(1), p. 4648. Available at: https://doi.org/10.1038/s41467-018-07025-z.

Daisuke, H. *et al.* (2021) 'Novel *LAMC2* fusion protein has tumor-promoting properties in ovarian carcinoma', *Cancer Science*, 112(12), pp. 4957–4967. Available at: https://doi.org/10.1111/cas.15149.

David, R., Joos, T.O. and Dreyer, C. (1998) 'Anteroposterior patterning and organogenesis of Xenopus laevis require a correct dose of germ cell nuclear factor (xGCNF)', *Mechanisms of Development*, 79(1–2), pp. 137–152. Available at: https://doi.org/10.1016/S0925-4773(98)00181-6.

DeCaprio, J. and Kohl, T.O. (2019) 'Using Dounce Homogenization to Lyse Cells for Immunoprecipitation', *Cold Spring Harbor Protocols*, 2019(7), p. pdb.prot098574. Available at: https://doi.org/10.1101/pdb.prot098574.

Dezonne, R.S. *et al.* (2017) 'Derivation of Functional Human Astrocytes from Cerebral Organoids', *Scientific Reports*, 7(1), p. 45091. Available at: https://doi.org/10.1038/srep45091.

Di Lullo, E. and Kriegstein, A.R. (2017) 'The use of brain organoids to investigate neural development and disease', *Nature Reviews Neuroscience*, 18(10), pp. 573–584. Available at: https://doi.org/10.1038/nrn.2017.107.

Dias, C. *et al.* (2016) 'BCL11A Haploinsufficiency Causes an Intellectual Disability Syndrome and Dysregulates Transcription', *The American Journal of Human Genetics*, 99(2), pp. 253–274. Available at: https://doi.org/10.1016/j.ajhg.2016.05.030.

Dihné, M. *et al.* (2003) 'A New Role for the Cell Adhesion Molecule L1 in Neural Precursor Cell Proliferation, Differentiation, and Transmitter-Specific Subtype Generation', *The Journal of Neuroscience*, 23(16), pp. 6638–6650. Available at: https://doi.org/10.1523/JNEUROSCI.23-16-06638.2003.

Ding, C. *et al.* (2022) 'Short-read and long-read full-length transcriptome of mouse neural stem cells across neurodevelopmental stages', *Scientific Data*, 9(1), p. 69. Available at: https://doi.org/10.1038/s41597-022-01165-0.

Dravid, A. *et al.* (2021) 'Optimised techniques for high-throughput screening of differentiated SH-SY5Y cells and application for neurite outgrowth assays', *Scientific Reports*, 11(1), p. 23935. Available at: https://doi.org/10.1038/s41598-021-03442-1.

Du, H. *et al.* (2022) 'Transcription factors *Bcl11a* and *Bcl11b* are required for the production and differentiation of cortical projection neurons', *Cerebral Cortex*, 32(17), pp. 3611–3632. Available at: https://doi.org/10.1093/cercor/bhab437.

Duan, D. *et al.* (2013) 'Spatiotemporal expression patterns of Pax6 in the brain of embryonic, newborn, and adult mice', *Brain Structure and Function*, 218(2), pp. 353–372. Available at: https://doi.org/10.1007/s00429-012-0397-2.

Elkabetz, Y. *et al.* (2008) 'Human ES cell-derived neural rosettes reveal a functionally distinct early neural stem cell stage', *Genes & Development*, 22(2), pp. 152–165. Available at: https://doi.org/10.1101/gad.1616208.

Ellis, P. *et al.* (2004) 'SOX2, a Persistent Marker for Multipotential Neural Stem Cells Derived from Embryonic Stem Cells, the Embryo or the Adult', *Developmental Neuroscience*, 26(2–4), pp. 148–165. Available at: https://doi.org/10.1159/000082134.

Estivill-Torrus, G. *et al.* (2002) '*Pax6* is required to regulate the cell cycle and the rate of progression from symmetrical to asymmetrical division in mammalian cortical progenitors', *Development*, 129(2), pp. 455–466. Available at: https://doi.org/10.1242/dev.129.2.455.

Falk, A. *et al.* (2012) 'Capture of Neuroepithelial-Like Stem Cells from Pluripotent Stem Cells Provides a Versatile System for In Vitro Production of Human Neurons', *PLoS ONE*. Edited by M. Pera, 7(1), p. e29597. Available at: https://doi.org/10.1371/journal.pone.0029597.

Fang, X. *et al.* (2019) 'A Novel 13 bp Deletion within the NR6A1 Gene Is Significantly Associated with Growth Traits in Donkeys', *Animals*, 9(9), p. 681. Available at: https://doi.org/10.3390/ani9090681.

Favaro, R. *et al.* (2009) 'Hippocampal development and neural stem cell maintenance require Sox2-dependent regulation of Shh', *Nature Neuroscience*, 12(10), pp. 1248–1256. Available at: https://doi.org/10.1038/nn.2397.

Ferretti, E. and Hadjantonakis, A.-K. (2019) 'Mesoderm specification and diversification: from single cells to emergent tissues', *Current Opinion in Cell Biology*, 61, pp. 110–116. Available at: https://doi.org/10.1016/j.ceb.2019.07.012.

Flint, J. and Shenk, T. (1997) 'VIRAL TRANSACTIVATING PROTEINS', *Annual Review of Genetics*, 31(1), pp. 177–212. Available at: https://doi.org/10.1146/annurev.genet.31.1.177.

Flitsch, L.J., Laupman, K.E. and Brüstle, O. (2020) 'Transcription Factor-Based Fate Specification and Forward Programming for Neural Regeneration', *Frontiers in Cellular Neuroscience*, 14, p. 121. Available at: https://doi.org/10.3389/fncel.2020.00121.

Fox, P.M., Tang, J.L.Y. and Brand, A.H. (2022) 'The *Drosophila* homologue of CTIP1 (Bcl11a) and CTIP2 (Bcl11b) regulates neural stem cell temporal patterning', *Development*, 149(17), p. dev200677. Available at: https://doi.org/10.1242/dev.200677.

Fuentealba, L.C. *et al.* (2015) 'Embryonic Origin of Postnatal Neural Stem Cells', *Cell*, 161(7), pp. 1644–1655. Available at: https://doi.org/10.1016/j.cell.2015.05.041.

Fuhrmann, G. *et al.* (2001) 'Mouse Germline Restriction of Oct4 Expression by Germ Cell Nuclear Factor', *Developmental Cell*, 1(3), pp. 377–387. Available at: https://doi.org/10.1016/S1534-5807(01)00038-7.

Fusaki, N. *et al.* (2009) 'Efficient induction of transgene-free human pluripotent stem cells using a vector based on Sendai virus, an RNA virus that does not integrate into the host genome', *Proceedings of the Japan Academy, Series B*, 85(8), pp. 348–362. Available at: https://doi.org/10.2183/pjab.85.348.

Gage, F.H. (2000) 'Mammalian Neural Stem Cells', *Science*, 287(5457), pp. 1433–1438. Available at: https://doi.org/10.1126/science.287.5457.1433.

Galiakberova, A.A. and Dashinimaev, E.B. (2020) 'Neural Stem Cells and Methods for Their Generation From Induced Pluripotent Stem Cells in vitro', *Frontiers in Cell and Developmental Biology*, 8, p. 815. Available at: https://doi.org/10.3389/fcell.2020.00815.

Gao, Z. *et al.* (2011) 'The Master Negative Regulator REST/NRSF Controls Adult Neurogenesis by Restraining the Neurogenic Program in Quiescent Stem Cells', *Journal of Neuroscience*, 31(26), pp. 9772–9786. Available at: https://doi.org/10.1523/JNEUROSCI.1604-11.2011.

Ge, H. and Roeder, R.G. (1994) 'Purification, cloning, and characterization of a human coactivator, PC4, that mediates transcriptional activation of class II genes', *Cell*, 78(3), pp. 513–523. Available at:

https://doi.org/10.1016/0092-8674(94)90428-6.

Gingras, M., Champigny, M.-F. and Berthod, F. (2007) 'Differentiation of human adult skin-derived neuronal precursors into mature neurons', *Journal of Cellular Physiology*, 210(2), pp. 498–506. Available at: https://doi.org/10.1002/jcp.20889.

Gomes, A.R. *et al.* (2020) 'Modeling Rett Syndrome With Human Patient-Specific Forebrain Organoids', *Frontiers in Cell and Developmental Biology*, 8, p. 610427. Available at: https://doi.org/10.3389/fcell.2020.610427.

Gomez, C. and Pourquié, O. (2009) 'Developmental control of segment numbers in vertebrates', *Journal of Experimental Zoology Part B: Molecular and Developmental Evolution*, 312B(6), pp. 533–544. Available at: https://doi.org/10.1002/jez.b.21305.

Gómez-López, S. *et al.* (2011) 'Sox2 and Pax6 maintain the proliferative and developmental potential of gliogenic neural stem cells In vitro', *Glia*, 59(11), pp. 1588–1599. Available at: https://doi.org/10.1002/glia.21201.

Graham, V. *et al.* (2003) 'SOX2 Functions to Maintain Neural Progenitor Identity', *Neuron*, 39(5), pp. 749–765. Available at: https://doi.org/10.1016/S0896-6273(03)00497-5.

Greaves, R. and O'Hare, P. (1989) 'Separation of requirements for protein-DNA complex assembly from those for functional activity in the herpes simplex virus regulatory protein Vmw65', *Journal of Virology*, 63(4), pp. 1641–1650. Available at: https://doi.org/10.1128/jvi.63.4.1641-1650.1989.

Greig, L.C. *et al.* (2016) 'Ctip1 Controls Acquisition of Sensory Area Identity and Establishment of Sensory Input Fields in the Developing Neocortex', *Neuron*, 90(2), pp. 261–277. Available at: https://doi.org/10.1016/j.neuron.2016.03.008.

Gu, J., Cromer, B. and Sumer, H. (2021) 'Forward Programming of Pluripotent Stem Cells to Neurons', *Current Molecular Medicine*, 21(1), pp. 5–14. Available at: https://doi.org/10.2174/1566524020666200421115251.

Gu, P., Morgan, D.H., *et al.* (2005) 'Evolutionary Trace-based Peptides Identify a Novel Asymmetric Interaction That Mediates Oligomerization in Nuclear Receptors', *Journal of Biological Chemistry*, 280(36), pp. 31818–31829. Available at: https://doi.org/10.1074/jbc.M501924200.

Gu, P., LeMenuet, D., *et al.* (2005) 'Orphan Nuclear Receptor GCNF Is Required for the Repression of Pluripotency Genes during Retinoic Acid-Induced Embryonic Stem Cell Differentiation', *Molecular and Cellular Biology*, 25(19), pp. 8507–8519. Available at: https://doi.org/10.1128/MCB.25.19.8507-8519.2005.

Gu, P. *et al.* (2011) 'Differential Recruitment of Methyl CpG-Binding Domain Factors and DNA Methyltransferases by the Orphan Receptor Germ Cell Nuclear Factor Initiates the Repression and Silencing of *Oct4*', *STEM CELLS*, 29(7), pp. 1041–1051. Available at: https://doi.org/10.1002/stem.652.
Gurtan, A.M. *et al.* (2013) 'Let-7 represses *Nr6a1* and a mid-gestation developmental program in adult fibroblasts', *Genes & Development*, 27(8), pp. 941–954. Available at: https://doi.org/10.1101/gad.215376.113.

Hansen, D.V. *et al.* (2010) 'Neurogenic radial glia in the outer subventricular zone of human neocortex', *Nature*, 464(7288), pp. 554–561. Available at: https://doi.org/10.1038/nature08845.

He, Z. and Yu, Q. (2018) 'Identification and characterization of functional modules reflecting transcriptome transition during human neuron maturation', *BMC Genomics*, 19(1), p. 262. Available at: https://doi.org/10.1186/s12864-018-4649-2.

Hemmati-Brivanlou, A., Kelly, O.G. and Melton, D.A. (1994) 'Follistatin, an antagonist of activin, is expressed in the Spemann organizer and displays direct neuralizing activity', *Cell*, 77(2), pp. 283–295. Available at: https://doi.org/10.1016/0092-8674(94)90320-4.

Hentschke, M. *et al.* (2006) 'Germ Cell Nuclear Factor Is a Repressor of CRIPTO-1 and CRIPTO-3', *Journal of Biological Chemistry*, 281(44), pp. 33497–33504. Available at:

https://doi.org/10.1074/jbc.M606975200.

Herculano-Houzel, S. (2009) 'The human brain in numbers: a linearly scaled-up primate brain', *Frontiers in Human Neuroscience*, 3. Available at: https://doi.org/10.3389/neuro.09.031.2009.

Hirai, H., Tani, T. and Kikyo, N. (2010) 'Structure and functions of powerful transactivators: VP16, MyoD and FoxA', *The International Journal of Developmental Biology*, 54(11–12), pp. 1589–1596. Available at: https://doi.org/10.1387/ijdb.103194hh.

Hirose, T., O'Brien, D.A. and Jetten, A.M. (1995) 'RTR: a new member of the nuclear receptor superfamily that is highly expressed in murine testis', *Gene*, 152(2), pp. 247–251. Available at: https://doi.org/10.1016/0378-1119(94)00656-D.

Ho, S.-M. *et al.* (2016) 'Rapid Ngn2-induction of excitatory neurons from hiPSC-derived neural progenitor cells', *Methods*, 101, pp. 113–124. Available at: https://doi.org/10.1016/j.ymeth.2015.11.019.

Homem, C.C.F., Repic, M. and Knoblich, J.A. (2015) 'Proliferation control in neural stem and progenitor cells', *Nature Reviews Neuroscience*, 16(11), pp. 647–659. Available at: https://doi.org/10.1038/nrn4021.

Huang, C.Y. *et al.* (2022) 'Population-based high-throughput toxicity screen of human iPSC-derived cardiomyocytes and neurons', *Cell Reports*, 39(1), p. 110643. Available at: https://doi.org/10.1016/j.celrep.2022.110643.

Huang, D.W., Sherman, B.T. and Lempicki, R.A. (2009) 'Systematic and integrative analysis of large gene lists using DAVID bioinformatics resources', *Nature Protocols*, 4(1), pp. 44–57. Available at: https://doi.org/10.1038/nprot.2008.211.

Hulme, A.J. *et al.* (2022) 'Making neurons, made easy: The use of Neurogenin-2 in neuronal differentiation', *Stem Cell Reports*, 17(1), pp. 14–34. Available at: https://doi.org/10.1016/j.stemcr.2021.11.015.

Iefremova, V. *et al.* (2017) 'An Organoid-Based Model of Cortical Development Identifies Non-Cell-Autonomous Defects in Wnt Signaling Contributing to Miller-Dieker Syndrome', *Cell Reports*, 19(1), pp. 50–59. Available at: https://doi.org/10.1016/j.celrep.2017.03.047.

Ijiri, M. *et al.* (2021) '*NR6A1* Allelic Frequencies as an Index for both Miniaturizing and Increasing Pig Body Size', *In Vivo*, 35(1), pp. 163–167. Available at: https://doi.org/10.21873/invivo.12244.

Ikushima, H. and Miyazono, K. (2010) 'TGFβ signalling: a complex web in cancer progression', *Nature Reviews Cancer*, 10(6), pp. 415–424. Available at: https://doi.org/10.1038/nrc2853.

Immaneni, A. *et al.* (2000) 'REST-VP16 activates multiple neuronal differentiation genes in human NT2 cells', *Nucleic Acids Research*, 28(17), pp. 3403–3410. Available at: https://doi.org/10.1093/nar/28.17.3403.

Jamur, M.C. and Oliver, C. (2010) 'Permeabilization of Cell Membranes', in C. Oliver and M.C. Jamur (eds) *Immunocytochemical Methods and Protocols*. Totowa, NJ: Humana Press (Methods in Molecular Biology), pp. 63–66. Available at: https://doi.org/10.1007/978-1-59745-324-0_9.

Janesick, A., Wu, S.C. and Blumberg, B. (2015) 'Retinoic acid signaling and neuronal differentiation', *Cellular and Molecular Life Sciences*, 72(8), pp. 1559–1576. Available at: https://doi.org/10.1007/s00018-014-1815-9.

Jiao, Q. *et al.* (2017) 'Cell-Cell Connection Enhances Proliferation and Neuronal Differentiation of Rat Embryonic Neural Stem/Progenitor Cells', *Frontiers in Cellular Neuroscience*, 11, p. 200. Available at: https://doi.org/10.3389/fncel.2017.00200.

Jiao, X. *et al.* (2013) 'Novel NR5A1 Missense Mutation in Premature Ovarian Failure: Detection in Han Chinese Indicates Causation in Different Ethnic Groups', *PLoS ONE*. Edited by Q.-Y. Sun, 8(9), p. e74759. Available at: https://doi.org/10.1371/journal.pone.0074759.

Jinek, M. *et al.* (2012) 'A Programmable Dual-RNA–Guided DNA Endonuclease in Adaptive Bacterial Immunity', *Science*, 337(6096), pp. 816–821. Available at: https://doi.org/10.1126/science.1225829.

John, A. *et al.* (2012) 'Bcl11a is required for neuronal morphogenesis and sensory circuit formation in dorsal spinal cord development', *Development*, 139(10), pp. 1831–1841. Available at: https://doi.org/10.1242/dev.072850.

Jolliffe, I.T. and Cadima, J. (2016) 'Principal component analysis: a review and recent developments', *Philosophical Transactions of the Royal Society A: Mathematical, Physical and Engineering Sciences*, 374(2065), p. 20150202. Available at: https://doi.org/10.1098/rsta.2015.0202.

Jonker, H.R.A. *et al.* (2005) 'Structural Properties of the Promiscuous VP16 Activation Domain', *Biochemistry*, 44(3), pp. 827–839. Available at: https://doi.org/10.1021/bi0482912.

Joos, T.O., David, R. and Dreyer, C. (1996) 'xGCNF, a nuclear orphan receptor is expressed during neurulation in Xenopus laevis', *Mechanisms of Development*, 60(1), pp. 45–57. Available at: https://doi.org/10.1016/S0925-4773(96)00599-0.

Josephson, R. *et al.* (2007) 'Qualification of Embryonal Carcinoma 2102Ep As a Reference for Human Embryonic Stem Cell Research', *Stem Cells*, 25(2), pp. 437–446. Available at: https://doi.org/10.1634/stemcells.2006-0236.

Jostock, R., Rentrop, M. and Maelicke, A. (1998) 'Cell fate specification in an in vitro model of neural development', *European Journal of Cell Biology*, 76(1), pp. 63–76. Available at: https://doi.org/10.1016/S0171-9335(98)80018-6.

Kadoch, C. *et al.* (2013) 'Proteomic and bioinformatic analysis of mammalian SWI/SNF complexes identifies extensive roles in human malignancy', *Nature Genetics*, 45(6), pp. 592–601. Available at: https://doi.org/10.1038/ng.2628.

Kageyama, R. *et al.* (1997) 'bHLH Transcription factors and mammalian neuronal differentiation', *The International Journal of Biochemistry & Cell Biology*, 29(12), pp. 1389–1399. Available at: https://doi.org/10.1016/S1357-2725(97)89968-2.

Kaneto, H. *et al.* (2005) 'PDX-1/VP16 Fusion Protein, Together With NeuroD or Ngn3, Markedly Induces Insulin Gene Transcription and Ameliorates Glucose Tolerance', *Diabetes*, 54(4), pp. 1009–1022. Available at: https://doi.org/10.2337/diabetes.54.4.1009.

Kapelle, M. *et al.* (1997) 'cDNA cloning of two closely related forms of human germ cell nuclear factor (GCNF)', *Biochimica et Biophysica Acta (BBA) - Gene Structure and Expression*, 1352(1), pp. 13–17. Available at: https://doi.org/10.1016/S0167-4781(97)00043-2.

Karow, M. *et al.* (2012) 'Reprogramming of Pericyte-Derived Cells of the Adult Human Brain into Induced Neuronal Cells', *Cell Stem Cell*, 11(4), pp. 471–476. Available at: https://doi.org/10.1016/j.stem.2012.07.007.

Kaufmann, K. *et al.* (2010) 'Chromatin immunoprecipitation (ChIP) of plant transcription factors followed by sequencing (ChIP-SEQ) or hybridization to whole genome arrays (ChIP-CHIP)', *Nature Protocols*, 5(3), pp. 457–472. Available at: https://doi.org/10.1038/nprot.2009.244.

Kazanis, I. *et al.* (2010) 'Quiescence and Activation of Stem and Precursor Cell Populations in the Subependymal Zone of the Mammalian Brain Are Associated with Distinct Cellular and Extracellular Matrix Signals', *Journal of Neuroscience*, 30(29), pp. 9771–9781. Available at: https://doi.org/10.1523/JNEUROSCI.0700-10.2010.

Kelava, I. and Lancaster, M.A. (2016) 'Stem Cell Models of Human Brain Development', *Cell Stem Cell*, 18(6), pp. 736–748. Available at: https://doi.org/10.1016/j.stem.2016.05.022.

Keller, G. (2005) 'Embryonic stem cell differentiation: emergence of a new era in biology and medicine', *Genes & Development*, 19(10), pp. 1129–1155. Available at: https://doi.org/10.1101/gad.1303605.

Khalili, A. and Ahmad, M. (2015) 'A Review of Cell Adhesion Studies for Biomedical and Biological

Applications', *International Journal of Molecular Sciences*, 16(8), pp. 18149–18184. Available at: https://doi.org/10.3390/ijms160818149.

Kim, H.J. *et al.* (2015) 'REST Regulates Non-Cell-Autonomous Neuronal Differentiation and Maturation of Neural Progenitor Cells via Secretogranin II', *Journal of Neuroscience*, 35(44), pp. 14872–14884. Available at: https://doi.org/10.1523/JNEUROSCI.4286-14.2015.

Kim, H.-J. and Jin, C.Y. (2012) 'Stem Cells in Drug Screening for Neurodegenerative Disease', *The Korean Journal of Physiology & Pharmacology*, 16(1), p. 1. Available at: https://doi.org/10.4196/kjpp.2012.16.1.1.

Kim, Y., Jeong, J. and Choi, D. (2020) 'Small-molecule-mediated reprogramming: a silver lining for regenerative medicine', *Experimental & Molecular Medicine*, 52(2), pp. 213–226. Available at: https://doi.org/10.1038/s12276-020-0383-3.

King, J.W.B. and Roberts, R.C. (1960) 'Carcass length in the bacon pig; its association with vertebrae numbers and prediction from radiographs of the young pig', *Animal Production*, 2(01), pp. 59–65. Available at: https://doi.org/10.1017/S0003356100033493.

Kobayashi, N., Boyer, T.G. and Berk, A.J. (1995) 'A class of activation domains interacts directly with TFIIA and stimulates TFIIA-TFIID-promoter complex assembly', *Molecular and Cellular Biology*, 15(11), pp. 6465–6473. Available at: https://doi.org/10.1128/MCB.15.11.6465.

Koch, P. *et al.* (2009) 'A rosette-type, self-renewing human ES cell-derived neural stem cell with potential for in vitro instruction and synaptic integration', *Proceedings of the National Academy of Sciences*, 106(9), pp. 3225–3230. Available at: https://doi.org/10.1073/pnas.0808387106.

Kondo, T. *et al.* (2017) 'iPSC-Based Compound Screening and In Vitro Trials Identify a Synergistic Anti-amyloid β Combination for Alzheimer's Disease', *Cell Reports*, 21(8), pp. 2304–2312. Available at: https://doi.org/10.1016/j.celrep.2017.10.109.

Krefft, O. *et al.* (2018) 'Generation of Standardized and Reproducible Forebrain-type Cerebral Organoids from Human Induced Pluripotent Stem Cells', *Journal of Visualized Experiments*, (131), p. 56768. Available at: https://doi.org/10.3791/56768.

Kretzschmar, M. *et al.* (1994) 'A novel mediator of class II gene transcription with homology to viral immediate-early transcriptional regulators', *Cell*, 78(3), pp. 525–534. Available at: https://doi.org/10.1016/0092-8674(94)90429-4.

Kuo, T.-Y., Chen, C.-Y. and Hsueh, Y.-P. (2010) 'Bcl11A/CTIP1 mediates the effect of the glutamate receptor on axon branching and dendrite outgrowth: Glutamate receptors control Bcl11A in axonogenesis', *Journal of Neurochemistry*, p. no-no. Available at: https://doi.org/10.1111/j.1471-4159.2010.06852.x.

Kutner, R.H., Zhang, X.-Y. and Reiser, J. (2009) 'Production, concentration and titration of pseudotyped HIV-1-based lentiviral vectors', *Nature Protocols*, 4(4), pp. 495–505. Available at: https://doi.org/10.1038/nprot.2009.22.

Lancaster, M.A. *et al.* (2013) 'Cerebral organoids model human brain development and microcephaly', *Nature*, 501(7467), pp. 373–379. Available at: https://doi.org/10.1038/nature12517.

Lang, M.-F. and Shi, Y. (2012) 'Dynamic Roles of microRNAs in Neurogenesis', *Frontiers in Neuroscience*, 6. Available at: https://doi.org/10.3389/fnins.2012.00071.

Lasky, J.L. and Wu, H. (2005) 'Notch Signaling, Brain Development, and Human Disease', *Pediatric Research*, 57(5 Part 2), pp. 104R-109R. Available at: https://doi.org/10.1203/01.PDR.0000159632.70510.3D.

Leid, M. *et al.* (2004) 'CTIP1 and CTIP2 are differentially expressed during mouse embryogenesis', *Gene Expression Patterns*, 4(6), pp. 733–739. Available at: https://doi.org/10.1016/j.modgep.2004.03.009.

Lin, Y.-S. *et al.* (1991) 'Binding of general transcription factor TFIIB to an acidic activating region', *Nature*, 353(6344), pp. 569–571. Available at: https://doi.org/10.1038/353569a0.

Liu, C. and Zhao, X. (2009) 'MicroRNAs in Adult and Embryonic Neurogenesis', *NeuroMolecular Medicine*, 11(3), pp. 141–152. Available at: https://doi.org/10.1007/s12017-009-8077-y.

Liu, H. *et al.* (2006) 'Functional studies of BCL11A: characterization of the conserved BCL11A-XL splice variant and its interaction with BCL6 in nuclear paraspeckles of germinal center B cells', *Molecular Cancer*, 5(1), p. 18. Available at: https://doi.org/10.1186/1476-4598-5-18.

Liu, X. *et al.* (2020) 'microRNA-196a-5p inhibits testicular germ cell tumor progression via NR6A1/E-cadherin axis', *Cancer Medicine*, 9(23), pp. 9107–9122. Available at: https://doi.org/10.1002/cam4.3498.

Livak, K.J. and Schmittgen, T.D. (2001) 'Analysis of Relative Gene Expression Data Using Real-Time Quantitative PCR and the 2−ΔΔCT Method', *Methods*, 25(4), pp. 402–408. Available at: https://doi.org/10.1006/meth.2001.1262.

Llorca, A. *et al.* (2019) 'A stochastic framework of neurogenesis underlies the assembly of neocortical cytoarchitecture', *eLife*, 8, p. e51381. Available at: https://doi.org/10.7554/eLife.51381.

Ludikhuize, M.C. and Rodríguez Colman, M.J. (2021) 'Metabolic Regulation of Stem Cells and Differentiation: A Forkhead Box O Transcription Factor Perspective', *Antioxidants & Redox Signaling*, 34(13), pp. 1004–1024. Available at: https://doi.org/10.1089/ars.2020.8126.

Ma, D.K. *et al.* (2009) 'Adult neural stem cells in the mammalian central nervous system', *Cell Research*, 19(6), pp. 672–682. Available at: https://doi.org/10.1038/cr.2009.56.

Ma, T.C., Vong, K.I. and Kwan, K.M. (2020) 'Spatiotemporal Decline of BMP Signaling Activity in Neural Progenitors Mediates Fate Transition and Safeguards Neurogenesis', *Cell Reports*, 30(11), pp. 3616-3624.e4. Available at: https://doi.org/10.1016/j.celrep.2020.02.089.

Mansouri, S. *et al.* (2016) 'Sox2: regulation of expression and contribution to brain tumors', *CNS Oncology*, 5(3), pp. 159–173. Available at: https://doi.org/10.2217/cns-2016-0001.

Manzari-Tavakoli, A. *et al.* (2022) 'The Cross-Talks Among Bone Morphogenetic Protein (BMP) Signaling and Other Prominent Pathways Involved in Neural Differentiation', *Frontiers in Molecular Neuroscience*, 15, p. 827275. Available at: https://doi.org/10.3389/fnmol.2022.827275.

Martinez, A.M. *et al.* (2019) 'NSC -34 motor neuron-like cells are sensitized to ferroptosis upon differentiation', *FEBS Open Bio*, 9(4), pp. 582–593. Available at: https://doi.org/10.1002/2211-5463.12577.

Martynoga, B., Drechsel, D. and Guillemot, F. (2012) 'Molecular Control of Neurogenesis: A View from the Mammalian Cerebral Cortex', *Cold Spring Harbor Perspectives in Biology*, 4(10), pp. a008359–a008359. Available at: https://doi.org/10.1101/cshperspect.a008359.

Mathieu, R. *et al.* (2013) 'Expression screening of cancer/testis genes in prostate cancer identifies nr6a1 as a novel marker of disease progression and aggressiveness', *The Prostate*, 73(10), pp. 1103–1114. Available at: https://doi.org/10.1002/pros.22659.

Matsui, T.K., Tsuru, Y. and Kuwako, K. (2020) 'Challenges in Modeling Human Neural Circuit Formation via Brain Organoid Technology', *Frontiers in Cellular Neuroscience*, 14, p. 607399. Available at: https://doi.org/10.3389/fncel.2020.607399.

McMaster, C.R. (2018) 'From yeast to humans – roles of the Kennedy pathway for phosphatidylcholine synthesis', *FEBS Letters*, 592(8), pp. 1256–1272. Available at: https://doi.org/10.1002/1873-3468.12919.

Mei, Q. *et al.* (2017) 'Genetic and Methylation-Induced Loss of miR-181a2/181b2 within chr9q33.3 Facilitates Tumor Growth of Cervical Cancer through the PIK3R3/Akt/FoxO Signaling Pathway', *Clinical Cancer Research*, 23(2), pp. 575–586. Available at: https://doi.org/10.1158/1078-0432.CCR-16-0303.

Meijer, M. *et al.* (2019) 'A Single-Cell Model for Synaptic Transmission and Plasticity in Human iPSC-Derived Neurons', *Cell Reports*, 27(7), pp. 2199-2211.e6. Available at: https://doi.org/10.1016/j.celrep.2019.04.058.

Mertens, J. *et al.* (2013) 'Embryonic Stem Cell–Based Modeling of Tau Pathology in Human Neurons', *The American Journal of Pathology*, 182(5), pp. 1769–1779. Available at: https://doi.org/10.1016/j.ajpath.2013.01.043.

Meyers, E.A. and Kessler, J.A. (2017) 'TGF-β Family Signaling in Neural and Neuronal Differentiation, Development, and Function', *Cold Spring Harbor Perspectives in Biology*, 9(8), p. a022244. Available at: https://doi.org/10.1101/cshperspect.a022244.

Mi, H. *et al.* (2019) 'PANTHER version 14: more genomes, a new PANTHER GO-slim and improvements in enrichment analysis tools', *Nucleic Acids Research*, 47(D1), pp. D419–D426. Available at: https://doi.org/10.1093/nar/gky1038.

Mikawa, S. *et al.* (2007) 'Fine mapping of a swine quantitative trait locus for number of vertebrae and analysis of an orphan nuclear receptor, germ cell nuclear factor (NR6A1)', *Genome Research*, 17(5), pp. 586–593. Available at: https://doi.org/10.1101/gr.6085507.

Milani, P. *et al.* (2016) 'Cell freezing protocol suitable for ATAC-Seq on motor neurons derived from human induced pluripotent stem cells', *Scientific Reports*, 6(1), p. 25474. Available at: https://doi.org/10.1038/srep25474.

Mira, H. and Morante, J. (2020) 'Neurogenesis From Embryo to Adult – Lessons From Flies and Mice', *Frontiers in Cell and Developmental Biology*, 8, p. 533. Available at: https://doi.org/10.3389/fcell.2020.00533.

Morante-Redolat, J.M. and Porlan, E. (2019) 'Neural Stem Cell Regulation by Adhesion Molecules Within the Subependymal Niche', *Frontiers in Cell and Developmental Biology*, 7, p. 102. Available at: https://doi.org/10.3389/fcell.2019.00102.

Murry, C.E. and Keller, G. (2008) 'Differentiation of Embryonic Stem Cells to Clinically Relevant Populations: Lessons from Embryonic Development', *Cell*, 132(4), pp. 661–680. Available at: https://doi.org/10.1016/j.cell.2008.02.008.

Naseri, G. *et al.* (2021) 'Artificial Transcription Factors for Tuneable Gene Expression in Pichia pastoris', *Frontiers in Bioengineering and Biotechnology*, 9, p. 676900. Available at: https://doi.org/10.3389/fbioe.2021.676900.

Nguyen, L. *et al.* (2006) 'Coupling Cell Cycle Exit, Neuronal Differentiation and Migration in Cortical Neurogenesis', *Cell Cycle*, 5(20), pp. 2314–2318. Available at: https://doi.org/10.4161/cc.5.20.3381.

Nishikawa, S., Goldstein, R.A. and Nierras, C.R. (2008) 'The promise of human induced pluripotent stem cells for research and therapy', *Nature Reviews Molecular Cell Biology*, 9(9), pp. 725–729. Available at: https://doi.org/10.1038/nrm2466.

Nowotschin, S., Hadjantonakis, A.-K. and Campbell, K. (2019) 'The endoderm: a divergent cell lineage with many commonalities', *Development*, 146(11), p. dev150920. Available at: https://doi.org/10.1242/dev.150920.

Pagin, M. *et al.* (2021) 'Sox2 Controls Neural Stem Cell Self-Renewal Through a Fos -Centered Gene Regulatory Network', *Stem Cells*, 39(8), pp. 1107–1119. Available at: https://doi.org/10.1002/stem.3373.

Pandolfi, S. and Stecca, B. (2015) 'Luciferase Reporter Assays to Study Transcriptional Activity of Hedgehog Signaling in Normal and Cancer Cells', in N.A. Riobo (ed.) *Hedgehog Signaling Protocols*. New York, NY: Springer New York (Methods in Molecular Biology), pp. 71–79. Available at: https://doi.org/10.1007/978-1-4939-2772-2_7.

Paoletti, L. *et al.* (2011) 'Role of Phosphatidylcholine during Neuronal differentiation', *IUBMB Life*, p.

n/a-n/a. Available at: https://doi.org/10.1002/iub.521.

Parisi, S. *et al.* (2003) 'Nodal-dependent Cripto signaling promotes cardiomyogenesis and redirects the neural fate of embryonic stem cells', *Journal of Cell Biology*, 163(2), pp. 303–314. Available at: https://doi.org/10.1083/jcb.200303010.

Park, J.-J. *et al.* (2017) 'RNA-guided transcriptional activation via CRISPR/dCas9 mimics overexpression phenotypes in Arabidopsis', *PLOS ONE*. Edited by S. Maas, 12(6), p. e0179410. Available at: https://doi.org/10.1371/journal.pone.0179410.

Park, S. *et al.* (2018) 'GCNF regulates OCT4 expression through its interactions with nuclear receptor binding elements in NCCIT cells', *Journal of Cellular Biochemistry*, 119(3), pp. 2719–2730. Available at: https://doi.org/10.1002/jcb.26438.

Patterson, M., Sneyd, J. and Friel, D.D. (2007) 'Depolarization-induced Calcium Responses in Sympathetic Neurons: Relative Contributions from Ca2+ Entry, Extrusion, ER/Mitochondrial Ca2+ Uptake and Release, and Ca2+ Buffering', *Journal of General Physiology*, 129(1), pp. 29–56. Available at: https://doi.org/10.1085/jgp.200609660.

Peitz, M., Krutenko, T. and Brüstle, O. (2020) 'Protocol for the Standardized Generation of Forward Programmed Cryopreservable Excitatory and Inhibitory Forebrain Neurons', *STAR Protocols*, 1(1), p. 100038. Available at: https://doi.org/10.1016/j.xpro.2020.100038.

Periyasamy, S. and Mowry, B. (2022) 'BrainDevo: Spatio-Temporal Gene Regulation Repository of Brain Development', *Frontiers in Molecular Neuroscience*, 15, p. 799801. Available at: https://doi.org/10.3389/fnmol.2022.799801.

Peron, A. *et al.* (2019) 'BCL11A-Related Intellectual Disability', in M.P. Adam et al. (eds) *GeneReviews®*. Seattle (WA): University of Washington, Seattle. Available at: http://www.ncbi.nlm.nih.gov/books/NBK547048/ (Accessed: 29 September 2022).

Petros, T.J., Tyson, J.A. and Anderson, S.A. (2011) 'Pluripotent Stem Cells for the Study of CNS Development', *Frontiers in Molecular Neuroscience*, 4. Available at: https://doi.org/10.3389/fnmol.2011.00030.

Pollen, A.A. *et al.* (2015) 'Molecular Identity of Human Outer Radial Glia during Cortical Development', *Cell*, 163(1), pp. 55–67. Available at: https://doi.org/10.1016/j.cell.2015.09.004.

Qian, X., Song, H. and Ming, G. (2019) 'Brain organoids: advances, applications and challenges', *Development*, 146(8), p. dev166074. Available at: https://doi.org/10.1242/dev.166074.

Radio, N.M. *et al.* (2008) 'Assessment of Chemical Effects on Neurite Outgrowth in PC12 cells Using High Content Screening', *Toxicological Sciences*, 105(1), pp. 106–118. Available at: https://doi.org/10.1093/toxsci/kfn114.

Ramakers, G.J.A. (2005) 'Neuronal network formation in human cerebral cortex', in *Progress in Brain Research*. Elsevier, pp. 1–14. Available at: https://doi.org/10.1016/S0079-6123(04)47001-0.

Redmond, S.A. *et al.* (2019) 'Development of Ependymal and Postnatal Neural Stem Cells and Their Origin from a Common Embryonic Progenitor', *Cell Reports*, 27(2), pp. 429-441.e3. Available at: https://doi.org/10.1016/j.celrep.2019.01.088.

Reichardt, L.F. and Tomaselli, K.J. (1991) 'Extracellular Matrix Molecules and their Receptors: Functions in Neural Development', *Annual Review of Neuroscience*, 14(1), pp. 531–570. Available at: https://doi.org/10.1146/annurev.ne.14.030191.002531.

Reinhardt, P. *et al.* (2013) 'Derivation and Expansion Using Only Small Molecules of Human Neural Progenitors for Neurodegenerative Disease Modeling', *PLoS ONE*. Edited by M. Daadi, 8(3), p. e59252. Available at: https://doi.org/10.1371/journal.pone.0059252.

Renner, M. *et al.* (2017) 'Self-organized developmental patterning and differentiation in cerebral organoids', *The EMBO Journal*, 36(10), pp. 1316–1329. Available at:

https://doi.org/10.15252/embj.201694700.

Roese-Koerner, B. *et al.* (2016) 'Reciprocal Regulation between Bifunctional miR-9/9∗ and its Transcriptional Modulator Notch in Human Neural Stem Cell Self-Renewal and Differentiation', *Stem Cell Reports*, 7(2), pp. 207–219. Available at: https://doi.org/10.1016/j.stemcr.2016.06.008.

Sabour, D. *et al.* (2014) 'Germ Cell Nuclear Factor Regulates Gametogenesis in Developing Gonads', *PLoS ONE*. Edited by Q. Wu, 9(8), p. e103985. Available at: https://doi.org/10.1371/journal.pone.0103985.

Sakamoto, M. *et al.* (2003) 'The Basic Helix-Loop-Helix Genes Hesr1/Hey1 and Hesr2/Hey2 Regulate Maintenance of Neural Precursor Cells in the Brain', *Journal of Biological Chemistry*, 278(45), pp. 44808–44815. Available at: https://doi.org/10.1074/jbc.M300448200.

Sankaran, V.G. and Orkin, S.H. (2013) 'The Switch from Fetal to Adult Hemoglobin', *Cold Spring Harbor Perspectives in Medicine*, 3(1), pp. a011643–a011643. Available at: https://doi.org/10.1101/cshperspect.a011643.

Sansom, S.N. *et al.* (2009) 'The Level of the Transcription Factor Pax6 Is Essential for Controlling the Balance between Neural Stem Cell Self-Renewal and Neurogenesis', *PLoS Genetics*. Edited by J.M. Hébert, 5(6), p. e1000511. Available at: https://doi.org/10.1371/journal.pgen.1000511.

Sasai, Y. (1994) 'Xenopus chordin: A novel dorsalizing factor activated by organizer-specific homeobox genes', *Cell*, 79(5), pp. 779–790. Available at: https://doi.org/10.1016/0092-8674(94)90068-X.

Sasai, Y. and De Robertis, E.M. (1997) 'Ectodermal Patterning in Vertebrate Embryos', *Developmental Biology*, 182(1), pp. 5–20. Available at: https://doi.org/10.1006/dbio.1996.8445.

Satterwhite, E. *et al.* (2001) 'The BCL11 gene family: involvement of BCL11A in lymphoid malignancies', *Blood*, 98(12), pp. 3413–3420. Available at: https://doi.org/10.1182/blood.V98.12.3413.

Sattler, U. *et al.* (2004) 'The Expression Level of the Orphan Nuclear Receptor GCNF (Germ Cell Nuclear Factor) Is Critical for Neuronal Differentiation', *Molecular Endocrinology*, 18(11), pp. 2714–2726. Available at: https://doi.org/10.1210/me.2004-0251.

Schanze, I. *et al.* (2018) 'NFIB Haploinsufficiency Is Associated with Intellectual Disability and Macrocephaly', *The American Journal of Human Genetics*, 103(5), pp. 752–768. Available at: https://doi.org/10.1016/j.ajhg.2018.10.006.

Schindelin, J. *et al.* (2015) 'The ImageJ ecosystem: An open platform for biomedical image analysis: T HE I MAGEJ E COSYSTEM', *Molecular Reproduction and Development*, 82(7–8), pp. 518–529. Available at: https://doi.org/10.1002/mrd.22489.

Schmitz, T.P., Süsens, U. and Borgmeyer, U. (1999) 'DNA binding, protein interaction and differential expression of the human germ cell nuclear factor', *Biochimica et Biophysica Acta (BBA) - Gene Structure and Expression*, 1446(3), pp. 173–180. Available at: https://doi.org/10.1016/S0167-4781(99)00079-2.

Schmuck, M.R. *et al.* (2020) 'Automated high content image analysis of dendritic arborization in primary mouse hippocampal and rat cortical neurons in culture', *Journal of Neuroscience Methods*, 341, p. 108793. Available at: https://doi.org/10.1016/j.jneumeth.2020.108793.

Schoenherr, C.J. and Anderson, D.J. (1995) 'The Neuron-Restrictive Silencer Factor (NRSF): A Coordinate Repressor of Multiple Neuron-Specific Genes', *Science*, 267(5202), pp. 1360–1363. Available at: https://doi.org/10.1126/science.7871435.

Schwarz, V. *et al.* (2009) 'IgCAMs redundantly control axon navigation in Caenorhabditis elegans', *Neural Development*, 4(1), p. 13. Available at: https://doi.org/10.1186/1749-8104-4-13.

Scott, G. and Huang, Y. (2022) 'Engineering cerebral folding in brain organoids', *Neural Regeneration Research*, 17(11), p. 2420. Available at: https://doi.org/10.4103/1673-5374.335789.

Seachrist, D.D. *et al.* (2020) 'The transcriptional repressor BCL11A promotes breast cancer metastasis',

Journal of Biological Chemistry, 295(33), pp. 11707–11719. Available at: https://doi.org/10.1074/jbc.RA120.014018.

Shahbazi, M.N. (2020) 'Mechanisms of human embryo development: from cell fate to tissue shape and back', *Development*, 147(14), p. dev190629. Available at: https://doi.org/10.1242/dev.190629.

Shi, Y. *et al.* (2008) 'Neural stem cell self-renewal', *Critical Reviews in Oncology/Hematology*, 65(1), pp. 43–53. Available at: https://doi.org/10.1016/j.critrevonc.2007.06.004.

Shi, Y., Kirwan, P. and Livesey, F.J. (2012) 'Directed differentiation of human pluripotent stem cells to cerebral cortex neurons and neural networks', *Nature Protocols*, 7(10), pp. 1836–1846. Available at: https://doi.org/10.1038/nprot.2012.116.

Shimojo, H., Ohtsuka, T. and Kageyama, R. (2011) 'Dynamic Expression of Notch Signaling Genes in Neural Stem/Progenitor Cells', *Frontiers in Neuroscience*, 5. Available at: https://doi.org/10.3389/fnins.2011.00078.

Shin, M.H. *et al.* (2002) 'Neural cell adhesion molecule (NCAM) promotes the differentiation of hippocampal precursor cells to a neuronal lineage, especially to a glutamatergic neural cell type', *Experimental & Molecular Medicine*, 34(6), pp. 401–410. Available at: https://doi.org/10.1038/emm.2002.57.

Simon, R., Wiegreffe, C. and Britsch, S. (2020) 'Bcl11 Transcription Factors Regulate Cortical Development and Function', *Frontiers in Molecular Neuroscience*, 13, p. 51. Available at: https://doi.org/10.3389/fnmol.2020.00051.

Slagsvold, T. *et al.* (2000) 'Mutational Analysis of the Androgen Receptor AF-2 (Activation Function 2) Core Domain Reveals Functional and Mechanistic Differences of Conserved Residues Compared with Other Nuclear Receptors', *Molecular Endocrinology*, 14(10), pp. 1603–1617. Available at: https://doi.org/10.1210/mend.14.10.0544.

Smith, W.C. and Harland, R.M. (1992) 'Expression cloning of noggin, a new dorsalizing factor localized to the Spemann organizer in Xenopus embryos', *Cell*, 70(5), pp. 829–840. Available at: https://doi.org/10.1016/0092-8674(92)90316-5.

Sokpor, G. *et al.* (2017) 'Chromatin Remodeling BAF (SWI/SNF) Complexes in Neural Development and Disorders', *Frontiers in Molecular Neuroscience*, 10, p. 243. Available at: https://doi.org/10.3389/fnmol.2017.00243.

Solozobova, V., Wyvekens, N. and Pruszak, J. (2012) 'Lessons from the Embryonic Neural Stem Cell Niche for Neural Lineage Differentiation of Pluripotent Stem Cells', *Stem Cell Reviews and Reports*, 8(3), pp. 813–829. Available at: https://doi.org/10.1007/s12015-012-9381-8.

Song, K., Takemaru, K.-I. and Moon, R.T. (1999) 'A Role for xGCNF in Midbrain–Hindbrain Patterning in Xenopus laevis', *Developmental Biology*, 213(1), pp. 170–179. Available at: https://doi.org/10.1006/dbio.1999.9368.

Stappert, L. *et al.* (2013) 'MicroRNA-Based Promotion of Human Neuronal Differentiation and Subtype Specification', *PLoS ONE*. Edited by P. Rameshwar, 8(3), p. e59011. Available at: https://doi.org/10.1371/journal.pone.0059011.

Stappert, L. (2015) 'MicroRNAs and orphan nuclear receptor GCNF as novel regulators of human neural stem cell differentiation and neuronal subtype specification', doctorel thesis.

Stappert, L., Klaus, F. and Büstle, O., 2020. Rapid production of human neuronal cultures with single cell resolution. European Patent application No. 20192024.6-1118. Munich, Germany. European Patent Office.

Stergiopoulos, A. and Politis, P.K. (2013) 'The role of nuclear receptors in controlling the fine balance between proliferation and differentiation of neural stem cells', *Archives of Biochemistry and Biophysics*, 534(1–2), pp. 27–37. Available at: https://doi.org/10.1016/j.abb.2012.09.009.

Strauß, T. *et al.* (2021) 'iPS Cell-Based Model for MAPT Haplotype as a Risk Factor for Human Tauopathies Identifies No Major Differences in TAU Expression', *Frontiers in Cell and Developmental Biology*, 9, p. 726866. Available at: https://doi.org/10.3389/fcell.2021.726866.

Su, X. *et al.* (2004) 'Activation of REST/NRSF Target Genes in Neural Stem Cells Is Sufficient To Cause Neuronal Differentiation', *Molecular and Cellular Biology*, 24(18), pp. 8018–8025. Available at: https://doi.org/10.1128/MCB.24.18.8018-8025.2004.

Suh, H. *et al.* (2007) 'In Vivo Fate Analysis Reveals the Multipotent and Self-Renewal Capacities of Sox2+ Neural Stem Cells in the Adult Hippocampus', *Cell Stem Cell*, 1(5), pp. 515–528. Available at: https://doi.org/10.1016/j.stem.2007.09.002.

Sullivan, A.E. and Santos, S.D.M. (2020) 'An Optimized Protocol for ChIP-Seq from Human Embryonic Stem Cell Cultures', *STAR Protocols*, 1(2), p. 100062. Available at: https://doi.org/10.1016/j.xpro.2020.100062.

Sun, Y. *et al.* (2001) 'Neurogenin Promotes Neurogenesis and Inhibits Glial Differentiation by Independent Mechanisms', *Cell*, 104(3), pp. 365–376. Available at: https://doi.org/10.1016/S0092-8674(01)00224-0.

Süsens, U. *et al.* (1997) 'The Germ Cell Nuclear Factor mGCNF Is Expressed in the Developing Nervous System', *Developmental Neuroscience*, 19(5), pp. 410–420. Available at: https://doi.org/10.1159/000111238.

Süsens, U. and Borgmeyer, U. (2001) 'Genomic structure of the gene for mouse germ-cell nuclear factor (GCNF). II. Comparison with the genomic structure of thhe human GCNF gene', *Genome Biology*, 2(5), p. research0017.1. Available at: https://doi.org/10.1186/gb-2001-2-5-research0017.

Takahashi, K. *et al.* (2007) 'Induction of Pluripotent Stem Cells from Adult Human Fibroblasts by Defined Factors', *Cell*, 131(5), pp. 861–872. Available at: https://doi.org/10.1016/j.cell.2007.11.019.

Takahashi, K. and Yamanaka, S. (2006) 'Induction of Pluripotent Stem Cells from Mouse Embryonic and Adult Fibroblast Cultures by Defined Factors', *Cell*, 126(4), pp. 663–676. Available at: https://doi.org/10.1016/j.cell.2006.07.024.

Tan, B.-T. *et al.* (2015) 'Retinoic acid induced the differentiation of neural stem cells from embryonic spinal cord into functional neurons in vitro', *International Journal of Clinical and Experimental Pathology*, 8(7), pp. 8129–8135.

Tan, K. and Wong, K.H. (2019) 'RNA polymerase II ChIP-seq—a powerful and highly affordable method for studying fungal genomics and physiology', *Biophysical Reviews*, 11(1), pp. 79–82. Available at: https://doi.org/10.1007/s12551-018-00497-9.

Tan, P. *et al.* (2022) 'Hippocampal NR6A1 impairs CREB-BDNF signaling and leads to the development of depression-like behaviors in mice', *Neuropharmacology*, 209, p. 108990. Available at: https://doi.org/10.1016/j.neuropharm.2022.108990.

The Gene Ontology Consortium *et al.* (2021) 'The Gene Ontology resource: enriching a GOld mine', *Nucleic Acids Research*, 49(D1), pp. D325–D334. Available at: https://doi.org/10.1093/nar/gkaa1113.

Thoma, E.C. *et al.* (2012) 'Ectopic Expression of Neurogenin 2 Alone is Sufficient to Induce Differentiation of Embryonic Stem Cells into Mature Neurons', *PLoS ONE*. Edited by V. Laudet, 7(6), p. e38651. Available at: https://doi.org/10.1371/journal.pone.0038651.

Thomson, J.A. *et al.* (1998) 'Embryonic Stem Cell Lines Derived from Human Blastocysts', *Science*, 282(5391), pp. 1145–1147. Available at: https://doi.org/10.1126/science.282.5391.1145.

Tolve, M. *et al.* (2021) 'The transcription factor BCL11A defines distinct subsets of midbrain dopaminergic neurons', *Cell Reports*, 36(11), p. 109697. Available at: https://doi.org/10.1016/j.celrep.2021.109697.

Triezenberg, S.J., Kingsbury, R.C. and McKnight, S.L. (1988) 'Functional dissection of VP16, the trans-activator of herpes simplex virus immediate early gene expression.', *Genes & Development*, 2(6), pp.

718–729. Available at: https://doi.org/10.1101/gad.2.6.718.

Turaç, G. *et al.* (2013) 'Combined Flow Cytometric Analysis of Surface and Intracellular Antigens Reveals Surface Molecule Markers of Human Neuropoiesis', *PLoS ONE*. Edited by E. Mezey, 8(6), p. e68519. Available at: https://doi.org/10.1371/journal.pone.0068519.

Ulloa, F. and Martí, E. (2009) 'Wnt won the war: Antagonistic role of Wnt over Shh controls dorso-ventral patterning of the vertebrate neural tube', *Developmental Dynamics*, p. NA-NA. Available at: https://doi.org/10.1002/dvdy.22058.

Untergasser, A. *et al.* (2012) 'Primer3—new capabilities and interfaces', *Nucleic Acids Research*, 40(15), pp. e115–e115. Available at: https://doi.org/10.1093/nar/gks596.

Utley, R.T. *et al.* (1998) 'Transcriptional activators direct histone acetyltransferase complexes to nucleosomes', *Nature*, 394(6692), pp. 498–502. Available at: https://doi.org/10.1038/28886.

Veitia, R.A. (2008) 'Exploring the Molecular Etiology of Dominant-Negative Mutations', *The Plant Cell*, 19(12), pp. 3843–3851. Available at: https://doi.org/10.1105/tpc.107.055053.

Vierbuchen, T. *et al.* (2010) 'Direct conversion of fibroblasts to functional neurons by defined factors', *Nature*, 463(7284), pp. 1035–1041. Available at: https://doi.org/10.1038/nature08797.

Vignali, M. (2000) 'Distribution of acetylated histones resulting from Gal4-VP16 recruitment of SAGA and NuA4 complexes', *The EMBO Journal*, 19(11), pp. 2629–2640. Available at: https://doi.org/10.1093/emboj/19.11.2629.

Vitillo, L. *et al.* (2020) 'GMP-grade neural progenitor derivation and differentiation from clinical-grade human embryonic stem cells', *Stem Cell Research & Therapy*, 11(1), p. 406. Available at: https://doi.org/10.1186/s13287-020-01915-0.

Vőfély, G. *et al.* (2018) 'Characterization of calcium signals in human induced pluripotent stem cell-derived dentate gyrus neuronal progenitors and mature neurons, stably expressing an advanced calcium indicator protein', *Molecular and Cellular Neuroscience*, 88, pp. 222–230. Available at: https://doi.org/10.1016/j.mcn.2018.02.003.

Wagner, R.T. and Cooney, A.J. (2013) 'Minireview: The Diverse Roles of Nuclear Receptors in the Regulation of Embryonic Stem Cell Pluripotency', *Molecular Endocrinology*, 27(6), pp. 864–878. Available at: https://doi.org/10.1210/me.2012-1383.

Wang, C. *et al.* (2017) 'Scalable Production of iPSC-Derived Human Neurons to Identify Tau-Lowering Compounds by High-Content Screening', *Stem Cell Reports*, 9(4), pp. 1221–1233. Available at: https://doi.org/10.1016/j.stemcr.2017.08.019.

Wang, H. *et al.* (2013) 'Epigenetic Reprogramming of the Germ Cell Nuclear Factor Gene Is Required for Proper Differentiation of Induced Pluripotent Cells', *Stem Cells*, 31(12), pp. 2659–2666. Available at: https://doi.org/10.1002/stem.1367.

Wang, H. *et al.* (2016) 'Germ Cell Nuclear Factor (GCNF) Represses Oct4 Expression and Globally Modulates Gene Expression in Human Embryonic Stem (hES) Cells', *Journal of Biological Chemistry*, 291(16), pp. 8644–8652. Available at: https://doi.org/10.1074/jbc.M115.694208.

Wang, R.N. *et al.* (2014) 'Bone Morphogenetic Protein (BMP) signaling in development and human diseases', *Genes & Diseases*, 1(1), pp. 87–105. Available at: https://doi.org/10.1016/j.gendis.2014.07.005.

Wang, Yinfang *et al.* (2019) 'NR6A1 regulates lipid metabolism through mammalian target of rapamycin complex 1 in HepG2 cells', *Cell Communication and Signaling*, 17(1), p. 77. Available at: https://doi.org/10.1186/s12964-019-0389-4.

Weikum, E.R. *et al.* (2016) 'A Structural Investigation into Oct4 Regulation by Orphan Nuclear Receptors, Germ Cell Nuclear Factor (GCNF), and Liver Receptor Homolog-1 (LRH-1)', *Journal of Molecular Biology*, 428(24), pp. 4981–4992. Available at: https://doi.org/10.1016/j.jmb.2016.10.025.

Weikum, E.R., Liu, X. and Ortlund, E.A. (2018) 'The nuclear receptor superfamily: A structural perspective: The Nuclear Receptor Superfamily', *Protein Science*, 27(11), pp. 1876–1892. Available at: https://doi.org/10.1002/pro.3496.

Wernig, M. *et al.* (2007) 'In vitro reprogramming of fibroblasts into a pluripotent ES-cell-like state', *Nature*, 448(7151), pp. 318–324. Available at: https://doi.org/10.1038/nature05944.

Wiegreffe, C. *et al.* (2015) 'Bcl11a (Ctip1) Controls Migration of Cortical Projection Neurons through Regulation of Sema3c', *Neuron*, 87(2), pp. 311–325. Available at: https://doi.org/10.1016/j.neuron.2015.06.023.

Woodworth, M.B. *et al.* (2016) 'Ctip1 Regulates the Balance between Specification of Distinct Projection Neuron Subtypes in Deep Cortical Layers', *Cell Reports*, 15(5), pp. 999–1012. Available at: https://doi.org/10.1016/j.celrep.2016.03.064.

Wouters, M.A. *et al.* (2005) 'Evolution of distinct EGF domains with specific functions', *Protein Science*, 14(4), pp. 1091–1103. Available at: https://doi.org/10.1110/ps.041207005.

Wysocka, J. and Herr, W. (2003) 'The herpes simplex virus VP16-induced complex: the makings of a regulatory switch', *Trends in Biochemical Sciences*, 28(6), pp. 294–304. Available at: https://doi.org/10.1016/S0968-0004(03)00088-4.

Xiao, H. *et al.* (1994) 'Binding of basal transcription factor TFIIH to the acidic activation domains of VP16 and p53', *Molecular and Cellular Biology*, 14(10), pp. 7013–7024. Available at: https://doi.org/10.1128/mcb.14.10.7013-7024.1994.

Xu, X. and Qi, L.S. (2019) 'A CRISPR–dCas Toolbox for Genetic Engineering and Synthetic Biology', *Journal of Molecular Biology*, 431(1), pp. 34–47. Available at: https://doi.org/10.1016/j.jmb.2018.06.037.
Yakoub, A. (2019) 'Cerebral organoids exhibit mature neurons and astrocytes and recapitulate electrophysiological activity of the human brain', *Neural Regeneration Research*, 14(5), p. 757. Available at: https://doi.org/10.4103/1673-5374.249283.

Yan, Z. and Jetten, A.M. (2000) 'Characterization of the Repressor Function of the Nuclear Orphan Receptor Retinoid Receptor-related Testis-associated Receptor/Germ Cell Nuclear Factor', *Journal of Biological Chemistry*, 275(45), pp. 35077–35085. Available at: https://doi.org/10.1074/jbc.M005566200.

Yan, Z.H. *et al.* (1997) 'Characterization of the Response Element and DNA Binding Properties of the Nuclear Orphan Receptor Germ Cell Nuclear Factor/Retinoid Receptor-related Testis-associated Receptor', *Journal of Biological Chemistry*, 272(16), pp. 10565–10572. Available at: https://doi.org/10.1074/jbc.272.16.10565.

Yao, Y. and Dai, W. (2014) 'Genomic Instability and Cancer', *Journal of Carcinogenesis & Mutagenesis*, 05(02). Available at: https://doi.org/10.4172/2157-2518.1000165.

Yuan, S.H. *et al.* (2011) 'Cell-Surface Marker Signatures for the Isolation of Neural Stem Cells, Glia and Neurons Derived from Human Pluripotent Stem Cells', *PLoS ONE*. Edited by M. Pera, 6(3), p. e17540. Available at: https://doi.org/10.1371/journal.pone.0017540.

Yulis, M., Kusters, D.H.M. and Nusrat, A. (2018) 'Cadherins: cellular adhesive molecules serving as signalling mediators: Cadherins as signalling mediators', *The Journal of Physiology*, 596(17), pp. 3883–3898. Available at: https://doi.org/10.1113/JP275328.

Zagoura, D. *et al.* (2017) 'Evaluation of the rotenone-induced activation of the Nrf2 pathway in a neuronal model derived from human induced pluripotent stem cells', *Neurochemistry International*, 106, pp. 62–73. Available at: https://doi.org/10.1016/j.neuint.2016.09.004.

Zanetta, J.-P. *et al.* (1992) 'Glycoproteins and lectins in cell adhesion and cell recognition processes', *The Histochemical Journal*, 24(11), pp. 791–804. Available at: https://doi.org/10.1007/BF01046351.

Zechel, C. (2005) 'The germ cell nuclear factor (GCNF)', *Molecular Reproduction and Development*, 72(4), pp. 550–556. Available at: https://doi.org/10.1002/mrd.20377.

Zechner, C., Nerli, E. and Norden, C. (2020) ‘Stochasticity and determinism in cell fate decisions’, *Development*, 147(14), p. dev181495. Available at: https://doi.org/10.1242/dev.181495.

Zhai, J. *et al.* (2022) ‘Human embryonic development: from peri-implantation to gastrulation’, *Trends in Cell Biology*, 32(1), pp. 18–29. Available at: https://doi.org/10.1016/j.tcb.2021.07.008.

Zhang, X. *et al.* (2019) ‘Association analysis of polymorphism in the NR6A1 gene with the lumbar vertebrae number traits in sheep’, *Genes & Genomics*, 41(10), pp. 1165–1171. Available at: https://doi.org/10.1007/s13258-019-00843-5.

Zhang, Y. *et al.* (2013) ‘Rapid Single-Step Induction of Functional Neurons from Human Pluripotent Stem Cells’, *Neuron*, 78(5), pp. 785–798. Available at: https://doi.org/10.1016/j.neuron.2013.05.029.

Zhao, S. *et al.* (2004) ‘SoxB transcription factors specify neuroectodermal lineage choice in ES cells’, *Molecular and Cellular Neuroscience*, 27(3), pp. 332–342. Available at: https://doi.org/10.1016/j.mcn.2004.08.002.

Zheng, S. *et al.* (2012) ‘PSD-95 is post-transcriptionally repressed during early neural development by PTBP1 and PTBP2’, *Nature Neuroscience*, 15(3), pp. 381–388. Available at: https://doi.org/10.1038/nn.3026.

Zhou, W. *et al.* (2020) ‘hsa_circ_001653 up-regulates NR6A1 expression and elicits gastric cancer progression by binding to microRNA-377’, *Experimental Physiology*, 105(12), pp. 2141–2153. Available at: https://doi.org/10.1113/EP088399.

Zhu, H., Joliot, V. and Prywes, R. (1994) ‘Role of transcription factor TFIIF in serum response factor-activated transcription’, *The Journal of Biological Chemistry*, 269(5), pp. 3489–3497.

6. Appendix

6.1 Step-by-Step protocol for ChIP

For sample preparation and subsequent ChIP, the Tag-ChIP-IT Kit from Active Motif (Catalog No. 53022) was used. To optimize the ChIP results, the protocol was slightly modified. These altered or additional steps are depicted in blue.

Chromatin preparation – Cell harvest, crosslinking and cell lysis

- GCNF-AM smNPCs, which were cultivated without small molecules used for smNPC expansion and with DOX for 48 h, were harvested with Accutase
    - Aspirate medium
    - Add Accutase and incubate for 10 min at 37 °C
    - Add DPBS, wash cell from plate (repeat this step two times)
    - Collect cell suspension in 50 mL Falcon tube
    - Take 20 µL of cell suspension and mix with 20 µL of Trypan Blue
    - Load the mixture onto a Neubauer chamber and count all living cells
    - Centrifuge cells at 250 xg for 4 min
    - Resuspend cell pellet in DPBS (5.4x10^6 cells/mL)

- Add 1/10 fixation buffer

Fixation buffer	1250 µL
Fixation reagent	90 µL
Ampuwa H_2O	785 µL
Formaldehyd (37 % **+ MeOH**, Sigma Aldrich)	375 µL

- Incubate for 15 min at RT on rolling device
- Add 1/20 of Stop solution
- Incubate 5 min at RT on rolling device
- Prepare PBS-PP Wash Buffer, store on ice

PBS-PP	12 mL
PBS (10x)	1.2 mL
Ampuwa H_2O	10.2 mL
Detergent	0.6 mL

- Centrifuge at 1,300 xg for 3 min at 4 °C
- Aspirate supernatant and resuspend in 5 mL cold PBS-PP
- Centrifuge at 1,300 xg for 3 min at 4 °C
- Aspirate supernatant and resuspend in 5 mL cold PBS-PP
- Centrifuge at 1,300 xg for 3 min at 4 °C
- Resuspend cell pellet in Chromatin Prep Buffer (**3x10^6 cell/mL**)

Chromatin Prep Buffer	
Chromatin Prep Buffer	1x
Protein Inhibitor Cocktail	1:000
PMSF	1:1000

- Incubate for 10 min at 4 °C on rolling device
- Take 10 µL of cell suspension and add 10 µL Trypan blue and set a side
- Transfer solution to cooled glass douncer and dounce 3x10 times on ice with 20 s break within each cycle

- Take 10 µL of cell suspension and add 10 µL Trypan blue and compare under microscope with the sample before douncing: Are cells lysed? Continue with the following steps, if the cells were lysed. If cells were not lysed, add another cycle of douncing and check again
- Centrifuge at 1,300 xg for 3 min at 4 °C
- Resuspend in 1 mL ChIP buffer

ChIP Buffer	
ChIP Buffer	1x
Protein Inhibitor Cocktail	1:00
PMSF	1:100

- Centrifuge at 1,300 xg for 3 min at 4 °C
- Aspirate supernatant
- Freeze cell pellet in liquid nitrogen and store at -80 °C

Chromatin fragmentation

- Thaw nuclei pellet on ice for 10 min
- Resuspend in freshly prepare ChIP buffer (30x10^6 cells/mL)
- Incubate for 10 min on ice
- Divide to 12x 100 µL Bioruptor tubes (take 25 µL suspension a side, store on ice and use later as “pre-sonication” control)
- Sonicate for 60 cycles (30 s on/off) at 4° C (Bioruptor® PICO from Diagenode)
- Pool suspension of all tubes
- Centrifuge at highest speed for 2 min at 4 °C
- Take 25 µL for reverse crosslinking and chromatin fragmentation size determination, freeze remaining suspension in liquid nitrogen and store at -80 °C

DNA purification to confirm fragmentation (Input preparation)

- Add 25 µL of chromatin solution to 175 µL TE buffer, add 1 µL RNase A, incubate 30 min at 37 °C
- Add 2 µL Proteinase K and incubate for 2 h at 55 °C, following by incubation for 30 min at 80 °C
- Add Precipitation buffer, Carrier and 100 % EtOH
- Store overnight at -80 °C
- Next day, centrifuge at 16,100 xg for 15 min at 4 °C
- Aspirate supernatant and wash pellet with 70% EtOH
- Centrifuge at 16,100 xg for 10 min at 4 °C
- Dry pellet for 10 min with open lid
- Re-suspend pellet in 25 µL DNA purification buffer and shake for 10 min at RT
- Determine DNA concentration with Nanodrop
- Use 500 ng DNA of each sample, treat with 500 mM NaCl

Reaction	
DNA	500 ng
500 mM NaCl	1 µL
Ampuwa H_2O	Add up to 10 µL

- Incubate samples for 20 min at 100 °C and cool down in ramping to 50 °C (10 min at 90 °C, 10 min at 80°C, 10 min at 70° C, 10 min at 60 °C, 10 min at 50 °C)
- Transfer samples on ice for 5 min, add 6x loading buffer form ThermoFisher
- Prepare 1.5 % agarose gel
- Load 12 µL of Input sample onto agarose gel and run at 100 V for 15 min, take a picture, then run for further 30 min and take another picture

- Determine the size of the fragmented chromatin, if chromatin fragmentation is sufficient – majority of chromatin cut into 200 – 1200 bp long fragments, go on with ChIP reaction

ChIP

- Thaw sonicated chromatin on ice
- Spin chromatin in a microcentrifuge at 16,100 xg for 2 min at 4 °C
- Set up the ChIP reactions by adding the components in the order shown below to 1.5 mL microcentrifuge tubes (DNA low bind tubes)

    - Prepare first part of the ChIP-reaction-mix and store on ice, while preparing the antibody/blocker mix

ChIP-reaction-mix	Pol II (antibody sample)	AM (antibody sample)	IgG (antibody sample)
Chromatin	30 µg*	30 µg*	30 µg*
ChIP Buffer	Add up to 240 µL	Add up to 240 µL	Add up to 240 µL
PIC	5 µL	5 µL	5 µL

*To calculate the volume of chromatin, use the DNA concentration measured during „DNA purification and fragmentation confirmation" of the specific samples

    - Prepare antibody/blocker mix and incubate for 1 min at RT, then add to ChIP-reaction-mix

Antibody/blocker mix	Pol II (antibody sample)	AM (antibody sample)	IgG (antibody sample)
Antibody	5 µg	10 µg	10 µg
Blocker	5 µL	5 µL	5 µL

    - Add to ChIP-reaction mix

- Cap tubes and incubate on rotator overnight at 4°C
- Prepare Protein G agarose beads before adding to ChIP mix, use Bridging AB from Active Motif (53017) to facilitate better binding of mouse IgG to Protein G beads
- Follow instructions of manual from Active Motif
- Pipet 30 µL for each ChIP reaction in a 1.7 mL microcentrifuge tube and add 5 µg of Bridging Antibody per IP reaction
- Mix well by pipetting up and down
- Cap the tubes and incubate for 1 h at 4 °C on a rotator
- Briefly spin tubes in a microcentrifuge to collect liquid from caps
- Pellet the beads at 1,000 xg for 1 min
- Carefully remove the supernatant and discard
- Add 200 µL of TE per IP and completely resuspend pellet by pipetting up and down several times: Take care to ensure that beads are not clinging to the pipet tips after pipetting
- Pellet the beads at 1,000 xg for 1 min
- Carefully remove the supernatant and discard

- Spin the ChIP reactions at 1,250 xg for 1 min
- Using a cut pipet tip, add 30 µL washed and prepared Protein G agarose beads to each immunoprecipitation reaction
- Cap tubes and incubate on a shaker at 4 °C for 3 h
- Remove the tab from the bottom of a ChIP Filtration Column for each ChIP reaction and place in a holder
- Remove ChIP reactions from rotator and spin at 1,250 xg for 1 min
- Add 600 µL ChIP Buffer to each ChIP reaction and transfer the entire reaction (including the protein G agarose beads) to the ChIP Filtration Column
- Allow flow-through to occur by gravity

- During the gravity flow, transfer 100 µL per ChIP reaction of Elution Buffer AM4 to a 1.5 mL microcentrifuge tube and allow to pre-warm at 37 °C during the wash steps
- Add 900 µL Wash Buffer AM1 to each ChIP Filtration Column, wait for 3 min
- Add 900 µL Wash Buffer AM1 to each ChIP Filtration Column, wait for 3 min
- Add 900 µL Wash Buffer AM1 to each ChIP Filtration Column, wait for 3 min
- Add 900 µL Wash Buffer AM1 to each ChIP Filtration Column, wait for 3 min
- Add 900 µL Wash Buffer AM1 to each ChIP Filtration Column, wait for 3 min
- Transfer columns to a new 1.5 mL microcentrifuge tube and spin in microcentrifuge at 1,250 xg for 3 min at RT to remove residual Wash Buffer
- Transfer the ChIP Filtration Columns to new 1.5 mL microcentrifuge tubes (low binding DNA tubes)
- Add 50 µl of 37 °C warm Elution Buffer AM4 to each column
- Incubate for 5 min at RT and spin at 1,250 xg for 3 min at RT
- Add another 50 µL of 37°C Elution Buffer AM4 to each column
- Incubate for 5 min at RT and spin at 1,250 xg for 3 min at RT
- Discard the ChIP Filtration Columns
  →The flow-through (~100 µL volume) contains the ChIP DNA

Reverse Crosslinking and DNA purification

- Transfer each eluted ChIP DNA to a 250 µL PCR tube and add 2 µL Proteinase K
- Vortex to mix and heat for 30 min at 55 °C in a thermocycler and then for 2 h at 80 °C (Lid temperature 99 °C)
- Transfer the DNA to a 1.5 mL microcentrifuge tube (low DNA binding tube) and add 500 µL DNA Purification Binding Buffer to each tube
- Vortex to mix
- Adjust the pH with 5 µL 3M Sodium Acetate (sample should be bright yellow in color to indicate a proper pH. If your sample is not bright yellow, add another 5 µL of 3M Sodium Acetate)
- For each sample, place a DNA purification column in the collection tube and add each pH adjusted sample to its own column
- Close the cap on each column and spin at 16,100 xg for 1 min at RT
- Remove the column from the collection tube, remove and discard the flow through from the collection tube
- Return the column to the collection tube and add 750 µL DNA Purification Wash Buffer (add 40 mL of 100 % EtOH before first use)
- Add 200 µL of DNA Purification Elution Buffer per ChIP reaction into a microcentrifuge tube and heat up to 37 °C
- Cap the column and spin at 14,000 rpm for 1 min at RT
- Remove the column from the collection tube, remove and discard the flow through from the collection tube
- Return the column to the collection tube and spin at 16,100 xg for 2 min with the column cap open
- Transfer the column to a clean microcentrifuge tube
- Add 100 µL of warm DNA Purification Elution Buffer (to the center of the column matrix and incubate for 5 min at RT
- Spin at 16,100 xg for 1 min
- Add additional 100 µL warm DNA Purification Elution Buffer to the column and incubate for 5 min at RT
- Spin at 16,100 xg for 1 min in a microcentrifuge
- Total elution volume is 200 µL.
- Store samples at -20 °C

6.2 Supplementary figures

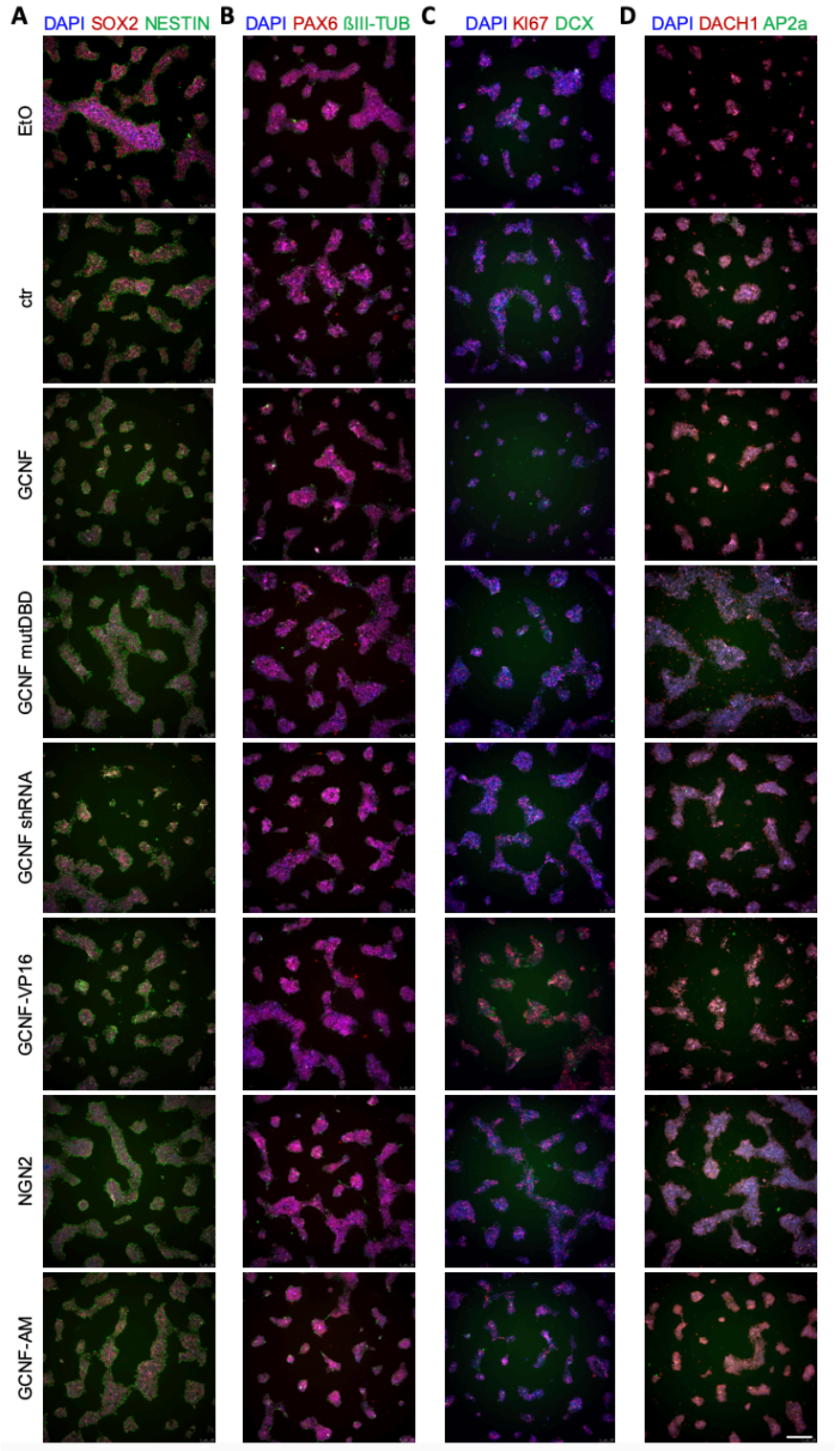

Supplementary Figure 6.1: Immunofluorescence staining of NSC and neuronal markers for quality control of used smNPC lines. **(A)** All eight cell lines are positive stained for the NSC markers SOX2 and NESTIN. **(B)** The cell lines display a strong staining of NSC marker PAX6, less cells were positive for neuronal marker βIII-TUB. **(C)** Most of the stained cells are positive for proliferation marker KI67 and only a small number of cells is positive for neuronal marker DCX. **(D)** The majority of smNPCs of all eight lines is positive for NSC marker DACH1. Staining of AP2α, a neural crest marker, is not detectable. Scale bar 200 µm.

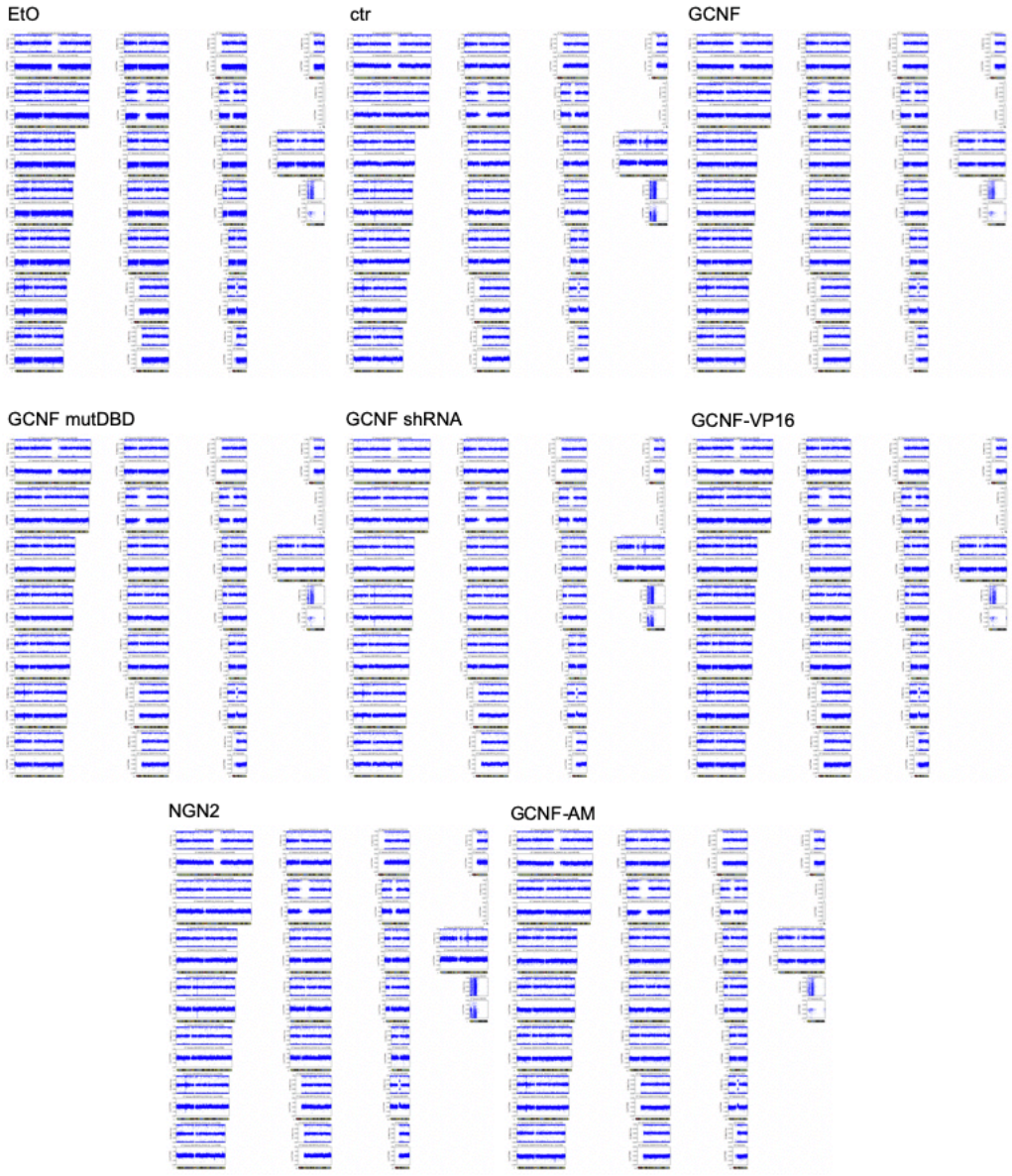

Supplementary Figure 6.2: SNP analyses of smNPC lines. SNP analysis results showing B allele frequency (upper) and logR ratio (lower) plots for all chromosomes of the eight generated cell lines.

6.3 Supplementary tables

Table 6.1: Fold Change (log2) for top 100 upregulated genes during the process of neuronal differentiation at ND2.

ID	Eto 48h Avg (log2)	ctr 48h Avg (log2)	GCNF 48h Avg (log2)	GCNFVP16 48h Avg (log2)	NGN2 48h Avg (log2)	Gene Symbol
TC1100007064.hg.1	5,21	5,59	5,92	5,71	5,58	SLC17A6
TC1300008602.hg.1	6,88	7,1	6,93	7,74	6,67	MAB21L1
TC0700011658.hg.1	5,02	4,89	4,6	5,78	5,67	SEMA3E
TC0100018511.hg.1	6,89	6,11	6,22	11,48	6,85	C1orf61
TC0500013266.hg.1	7,72	7,52	8,01	10,47	8,67	HMP19
TC2200006945.hg.1	6,54	6,32	6,87	9,4	6,35	SEZ6L
TC1200009997.hg.1	4,4	4,3	4,21	5,35	4,2	GRIN2B
TC0300013469.hg.1	4,74	5,55	5,13	5,08	5,92	SST
TC1100007056.hg.1	5,67	5,03	6,63	4,69	5,63	NELL1
TC0200012713.hg.1	7,47	7,43	5,93	15,71	8,47	BCL11A
TC0900011370.hg.1	5,67	5,9	5,09	9,06	5,86	BRINP1
TC0800010936.hg.1	4,83	4,25	4,56	4,37	5,04	PMP2
TC0400008725.hg.1	5,05	5,58	5,55	6,75	4,73	PCDH10
TC1500007062.hg.1	5,15	5,07	5,72	5,06	5,36	CKMT1B; CKMT1A
TC0300012935.hg.1	8,65	9,22	8,87	9,13	6,56	SHOX2
TC0400008977.hg.1	10,2	11,01	11,31	11,17	10,77	MAB21L2
TC0300013022.hg.1	6,19	5,9	6,07	5,05	4,89	SLITRK3
TC0700012126.hg.1	5,83	5,58	5,62	5,84	6,65	RELN
TC1200011438.hg.1	6,42	7,21	6,72	6,8	5,43	MGAT4C
TC0800011509.hg.1	7,95	8,5	7,41	7,86	6,73	CSMD3
TC0700011924.hg.1	6,55	6,49	6,74	6,23	7,45	TMEM130
TC1000008670.hg.1	7,2	6,87	6,62	7,71	7,03	TLX1
TC0400010867.hg.1	6,16	6,41	6,59	8,62	5,8	EPHA5
TC0200013042.hg.1	5,75	5,97	6,08	4,41	5,26	CYP26B1
TC1100012583.hg.1	6,58	7,5	6,77	9,62	6,66	BLID; MIR100HG
TC1900008637.hg.1	6,45	6,74	6,76	7,51	6,78	IGLON5
TC1300009165.hg.1	7,8	8,29	8,89	7,95	8,19	PCDH9
TC2000009813.hg.1	6,85	6,94	6,96	8,07	6,5	EEF1A2
TC0200009865.hg.1	7,19	7,72	7,67	7,7	5,55	SCN2A
TC0X00011126.hg.1	8,26	8,87	8,51	7,61	7,05	GABRA3
TC0600009439.hg.1	8,05	8,42	8,29	11,08	7,29	TMEM200A
TC0400009110.hg.1	9,9	10,36	10,54	10,18	9,34	GRIA2
TC1600010239.hg.1	5,2	4,43	4,92	9	5,37	CBLN1
TC0300007973.hg.1	7,69	7,83	8,05	9,26	7,73	CADM2
TC1800008487.hg.1	6,52	7,07	6,51	8,54	6,58	CELF4
TC1500007838.hg.1	5,65	6,1	5,73	5	6,29	ISLR2
TC1000008668.hg.1	6,33	6,46	6,66	9,18	6,31	SFXN3
TC2000006676.hg.1	9,1	9,49	9,25	9,12	9,21	LAMP5
TC0200016556.hg.1	4,97	5,14	4,75	4,96	5,36	SLC4A10
TC0700006690.hg.1	6,03	6,32	6,52	6,84	5,84	NXPH1
TC1300009646.hg.1	6,07	6,2	6,39	6,41	6,34	NALCN
TC1500007739.hg.1	5,7	5,96	4,64	6,88	5,55	THSD4
TC0400012288.hg.1	5,24	5,59	5,68	8,78	5,1	FSTL5
TC1500008470.hg.1	8,43	8,56	8,5	7,94	8,28	ARRDC4
TC0600013160.hg.1	4,94	4,33	4,64	5,37	5,8	SAMD3
TC0300008082.hg.1	5,34	5,28	5,19	5,4	6,03	EPHA6
TC1500007067.hg.1	7,24	7,03	6,85	6,44	6,41	CKMT1A
TC0500010265.hg.1	8,19	9,1	8,71	8,64	6,55	CDH18
TC0500009055.hg.1	5,49	5,37	6,12	6,36	6,22	ABLIM3
TC0600010707.hg.1	8,6	8,77	9,4	7,2	7,92	NRN1
TC0100018367.hg.1	5,12	5,37	5,6	5,3	5,13	CHRM3
TC0700012011.hg.1	7,52	7,28	7,93	8,6	6,81	ACTL6B
TC0300006437.hg.1	7,32	7,47	7,46	9,94	6,99	CHL1
TC0500007820.hg.1	6,48	7,16	7,24	6,64	9,93	SV2C
TC1100009561.hg.1	9,51	9,55	10,07	7,22	7,67	NTM
TC0100016755.hg.1	6,33	6,84	6,57	5,56	4,67	BRINP3
TC1900010005.hg.1	8,59	9,22	8,68	11,22	8,72	RAB3A
TC0300008853.hg.1	7,45	7,6	7,87	8,82	7,69	TMEM108
TC1100012633.hg.1	9,13	9,41	9,05	9,2	8,8	SCN3B
TC0200014814.hg.1	6,47	6,66	6,42	6,57	6,01	SCN1A
TC1100010531.hg.1	9,1	9,45	9,05	9,71	11,21	SLC1A2
TC1700008082.hg.1	9,46	10,25	9,61	9,39	9,25	MAPT
TC1600007240.hg.1	5,95	5,92	5,68	6,41	6,78	PRKCB
TC1900010334.hg.1	8,07	7,86	8,57	8,14	7,62	TSHZ3
TC1900008902.hg.1	6,99	6,94	7,18	6,83	7,69	BRSK1
TC1600009949.hg.1	9,59	9,4	9,82	10,12	9,42	FAM57B
TC0100010155.hg.1	6,29	6,2	6,42	6,42	7,02	SEMA4A
TC1900007025.hg.1	9,49	9,07	9,38	10,17	9,28	PLPPR2
TC1300009169.hg.1	6	6,29	5,5	5,46	5,85	PCDH9
TC1600009943.hg.1	6,11	6,72	6,53	6,24	6,6	SEZ6L2
TC1600011349.hg.1	8,07	8,22	8,24	8,23	8,83	RBFOX1
TC2000008367.hg.1	8,76	9,13	7,81	9,29	8,48	PAK7
TC1700011143.hg.1	4,9	4,96	4,74	5,06	5,83	CA10
TC1100007095.hg.1	7,07	7,25	7,03	6,11	5,96	LUZP2
TC0300007529.hg.1	9,06	9,17	9,27	9,1	10,07	CACNA2D3
TC0900008784.hg.1	8,21	8,02	8,28	8,18	8,11	LMX1B
TC0200015958.hg.1	9,06	9,54	8,4	10,97	8,92	DNER
TC0100015042.hg.1	6,17	6,08	6,11	4,78	5,64	PLPPR5
TC1800008437.hg.1	5,87	6,07	5,78	7,54	5,81	NOL4
TC0500009400.hg.1	6,49	6,79	6,49	8,28	7,57	KCNIP1
TC0200012559.hg.1	9,47	10,44	10,35	9,95	8,57	NRXN1
TC1500010768.hg.1	6,44	6,3	6,15	6,92	7,05	SCAMP5
TC0100011621.hg.1	7,51	7,79	9,19	7,06	7,99	TGFB2; TGFB2-OT1
TC1900009808.hg.1	7,94	7,83	7,84	8,21	7,77	ADGRL1
TC0100013072.hg.1	8,79	8,91	8,88	9,19	9,31	ATP13A2
TC2000007760.hg.1	8,67	8,93	9,44	9,2	7,1	TSHZ2
TC1200011393.hg.1	8,49	8,14	8,13	9,08	8,01	PPFIA2
TC1000007833.hg.1	6,88	6,31	6,91	6,58	7,05	LRRTM3
TC1000008658.hg.1	9,85	9,71	9,9	7,88	11,11	PAX2
TC0200016482.hg.1	6,47	7,14	6,85	7,62	6,28	CTNNA2
TC0900009145.hg.1	11,72	12,14	11,7	12,06	12,08	OLFM1
TC0100017018.hg.1	8,31	9,11	8,79	7,21	7,96	ETNK2
TC1200007359.hg.1	8,16	8,48	8,27	9,92	8,91	CNTN1
TC0400008137.hg.1	7,93	8,72	8,44	9,93	7,24	CCSER1
TC0100009364.hg.1	6,92	6,95	7,57	6,89	6,9	CSF1
TC1300009204.hg.1	6,56	6,67	7,2	5,95	6,28	KLHL1
TC1000011640.hg.1	8,46	8,22	8,28	8,76	9,24	LBX1
TC1700009303.hg.1	5,51	5,73	5,76	6,53	5,96	DOC2B
TC1000009104.hg.1	5,53	5,83	5,21	6,03	5,79	PLPP4
TC1100009242.hg.1	5,51	5,8	6,09	5,35	6,21	ABCG4

Table 6.2: To lowest fold change normalized fold changes (log2) for top 100 upregulated genes during the process of neuronal differentiation at ND2.

ID	Eto 48h Avg (log2)	ctr 48h Avg (log2)	GCNF 48h Avg (log2)	GCNFVP16 48h Avg (log2)	NGN2 48h Avg (log2)	Gene Symbol
TC1100007064.hg.1	0,00	0,10	0,18	0,13	0,10	SLC17A6
TC1300008602.hg.1	0,04	0,09	0,06	0,21	0,00	MAB21L1
TC0700011658.hg.1	0,13	0,09	0,00	0,33	0,30	SEMA3E
TC0100018511.hg.1	0,17	0,00	0,03	0,91	0,16	C1orf61
TC0500013266.hg.1	0,04	0,00	0,09	0,48	0,21	HMP19
TC2200006945.hg.1	0,05	0,00	0,12	0,57	0,01	SEZ6L
TC1200009997.hg.1	0,07	0,03	0,00	0,35	0,00	GRIN2B
TC0300013469.hg.1	0,00	0,23	0,11	0,10	0,32	SST
TC1100007056.hg.1	0,27	0,10	0,50	0,00	0,26	NELL1
TC0200012713.hg.1	0,33	0,33	0,00	1,41	0,51	BCL11A
TC0900011370.hg.1	0,16	0,21	0,00	0,83	0,20	BRINP1
TC0800010936.hg.1	0,18	0,00	0,10	0,04	0,25	PMP2
TC0400008725.hg.1	0,09	0,24	0,23	0,51	0,00	PCDH10
TC1500007062.hg.1	0,03	0,00	0,18	0,00	0,08	CKMT1B; CKMT1A
TC0300012935.hg.1	0,40	0,49	0,44	0,48	0,00	SHOX2
TC0400008977.hg.1	0,00	0,11	0,15	0,13	0,08	MAB21L2
TC0300013022.hg.1	0,34	0,27	0,31	0,05	0,00	SLITRK3
TC0700012126.hg.1	0,06	0,00	0,01	0,07	0,25	RELN
TC1200011438.hg.1	0,24	0,41	0,31	0,32	0,00	MGAT4C
TC0800011509.hg.1	0,24	0,34	0,14	0,22	0,00	CSMD3
TC0700011924.hg.1	0,07	0,06	0,11	0,00	0,26	TMEM130
TC1000008670.hg.1	0,12	0,05	0,00	0,22	0,09	TLX1
TC0400010867.hg.1	0,09	0,14	0,18	0,57	0,00	EPHA5
TC0200013042.hg.1	0,38	0,44	0,46	0,00	0,25	CYP26B1
TC1100012583.hg.1	0,00	0,19	0,04	0,55	0,02	BLID; MIR100HG
TC1900008637.hg.1	0,00	0,06	0,07	0,22	0,07	IGLON5
TC1300009165.hg.1	0,00	0,09	0,19	0,03	0,07	PCDH9
TC2000009813.hg.1	0,08	0,09	0,10	0,31	0,00	EEF1A2
TC0200009865.hg.1	0,37	0,48	0,47	0,47	0,00	SCN2A
TC0X00011126.hg.1	0,23	0,33	0,27	0,11	0,00	GABRA3
TC0600009439.hg.1	0,14	0,21	0,19	0,60	0,00	TMEM200A
TC0400009110.hg.1	0,08	0,15	0,17	0,12	0,00	GRIA2
TC1600010239.hg.1	0,23	0,00	0,15	1,02	0,28	CBLN1
TC0300007973.hg.1	0,00	0,03	0,07	0,27	0,01	CADM2
TC1800008487.hg.1	0,00	0,12	0,00	0,39	0,02	CELF4
TC1500007838.hg.1	0,18	0,29	0,20	0,00	0,33	ISLR2
TC1000008668.hg.1	0,00	0,03	0,08	0,54	0,00	SFXN3
TC2000006676.hg.1	0,00	0,06	0,02	0,00	0,02	LAMP5
TC0200016556.hg.1	0,07	0,11	0,00	0,06	0,17	SLC4A10
TC0700006690.hg.1	0,05	0,11	0,16	0,23	0,00	NXPH1
TC1300009646.hg.1	0,00	0,03	0,07	0,08	0,06	NALCN
TC1500007739.hg.1	0,30	0,36	0,00	0,57	0,26	THSD4
TC0400012288.hg.1	0,04	0,13	0,16	0,78	0,00	FSTL5
TC1500008470.hg.1	0,09	0,11	0,10	0,00	0,06	ARRDC4
TC0600013160.hg.1	0,19	0,00	0,10	0,31	0,42	SAMD3
TC0300008082.hg.1	0,04	0,02	0,00	0,06	0,22	EPHA6
TC1500007067.hg.1	0,18	0,13	0,10	0,01	0,00	CKMT1A
TC0500010265.hg.1	0,32	0,47	0,41	0,40	0,00	CDH18
TC0500009055.hg.1	0,03	0,00	0,19	0,24	0,21	ABLIM3
TC0600010707.hg.1	0,26	0,28	0,38	0,00	0,14	NRN1
TC0100018367.hg.1	0,00	0,07	0,13	0,05	0,00	CHRM3
TC0700012011.hg.1	0,14	0,10	0,22	0,34	0,00	ACTL6B
TC0300006437.hg.1	0,07	0,10	0,09	0,51	0,00	CHL1
TC0500007820.hg.1	0,00	0,14	0,16	0,04	0,62	SV2C
TC1100009561.hg.1	0,40	0,40	0,48	0,00	0,09	NTM
TC0100016755.hg.1	0,44	0,55	0,49	0,25	0,00	BRINP3
TC1900010005.hg.1	0,00	0,10	0,02	0,39	0,02	RAB3A
TC0300008853.hg.1	0,00	0,03	0,08	0,24	0,05	TMEM108
TC1100012633.hg.1	0,05	0,10	0,04	0,06	0,00	SCN3B
TC0200014814.hg.1	0,11	0,15	0,10	0,13	0,00	SCN1A
TC1100010531.hg.1	0,01	0,06	0,00	0,10	0,31	SLC1A2
TC1700008082.hg.1	0,03	0,15	0,06	0,02	0,00	MAPT
TC1600007240.hg.1	0,07	0,06	0,00	0,17	0,26	PRKCB
TC1900010334.hg.1	0,08	0,04	0,17	0,10	0,00	TSHZ3
TC1900008902.hg.1	0,03	0,02	0,07	0,00	0,17	BRSK1
TC1600009949.hg.1	0,03	0,00	0,06	0,11	0,00	FAM57B
TC0100010155.hg.1	0,02	0,00	0,05	0,05	0,18	SEMA4A
TC1900007025.hg.1	0,07	0,00	0,05	0,17	0,03	PLPPR2
TC1300009169.hg.1	0,14	0,20	0,01	0,00	0,10	PCDH9
TC1600009943.hg.1	0,00	0,14	0,10	0,03	0,11	SEZ6L2
TC1600011349.hg.1	0,00	0,03	0,03	0,03	0,13	RBFOX1
TC2000008367.hg.1	0,17	0,23	0,00	0,25	0,12	PAK7
TC1700011143.hg.1	0,05	0,07	0,00	0,09	0,30	CA10
TC1100007095.hg.1	0,25	0,28	0,24	0,04	0,00	LUZP2
TC0300007529.hg.1	0,00	0,02	0,03	0,01	0,15	CACNA2D3
TC0900008784.hg.1	0,03	0,00	0,05	0,03	0,02	LMX1B
TC0200015958.hg.1	0,11	0,18	0,00	0,39	0,09	DNER
TC0100015042.hg.1	0,37	0,35	0,35	0,00	0,24	PLPPR5
TC1800008437.hg.1	0,02	0,07	0,00	0,38	0,01	NOL4
TC0500009400.hg.1	0,00	0,07	0,00	0,35	0,22	KCNIP1
TC0200012559.hg.1	0,14	0,28	0,27	0,22	0,00	NRXN1
TC1500010768.hg.1	0,07	0,03	0,00	0,17	0,20	SCAMP5
TC0100011621.hg.1	0,09	0,14	0,38	0,00	0,18	TGFB2; TGFB2-OT1
TC1900009808.hg.1	0,03	0,01	0,01	0,08	0,00	ADGRL1
TC0100013072.hg.1	0,00	0,02	0,01	0,06	0,08	ATP13A2
TC2000007760.hg.1	0,29	0,33	0,41	0,37	0,00	TSHZ2
TC1200011393.hg.1	0,08	0,02	0,02	0,18	0,00	PPFIA2
TC1000007833.hg.1	0,12	0,00	0,13	0,06	0,16	LRRTM3
TC1000008658.hg.1	0,32	0,30	0,33	0,00	0,50	PAX2
TC0200016482.hg.1	0,04	0,19	0,13	0,28	0,00	CTNNA2
TC0900009145.hg.1	0,00	0,05	0,00	0,04	0,05	OLFM1
TC0100017018.hg.1	0,20	0,34	0,29	0,00	0,14	ETNK2
TC1200007359.hg.1	0,00	0,06	0,02	0,28	0,13	CNTN1
TC0400008137.hg.1	0,13	0,27	0,22	0,46	0,00	CCSER1
TC0100009364.hg.1	0,01	0,01	0,14	0,00	0,00	CSF1
TC1300009204.hg.1	0,14	0,16	0,28	0,00	0,08	KLHL1
TC1000011640.hg.1	0,04	0,00	0,01	0,09	0,17	LBX1
TC1700009303.hg.1	0,00	0,06	0,06	0,25	0,11	DOC2B
TC1000009104.hg.1	0,09	0,16	0,00	0,21	0,15	PLPP4
TC1100009242.hg.1	0,04	0,12	0,19	0,00	0,22	ABCG4

Table 6.3: Fold Change (log2) for top 100 upregulated genes during the process of neuronal differentiation at ND7.

ID	Eto ND7 Avg (log2)	ctr ND7 Avg (log2)	GCNF ND7 Avg (log2)	GCNFVP16 ND7 Avg (log2)	NGN2 ND7 Avg (log2)	Gene Symbol
TC1100007064.hg.1	7,61	6,92	7,7	7,95	7,95	SLC17A6
TC1300008602.hg.1	11,14	11	11,57	12,83	11,65	MAB21L1
TC0700011658.hg.1	8,66	8,09	5,41	7,69	9,56	SEMA3E
TC0100018511.hg.1	6,92	7,21	5,92	11,72	6,38	C1orf61
TC0500013266.hg.1	10,37	10,49	10,17	14	12,84	HMP19
TC2200006945.hg.1	7,63	7,68	6,89	9,1	7,81	SEZ6L
TC1200009997.hg.1	5,88	5,5	5,32	8,13	6,06	GRIN2B
TC0300013469.hg.1	7,77	7,53	7,02	7,74	5,43	SST
TC1100007056.hg.1	7,45	7,9	7,89	7,09	8,92	NELL1
TC0200012713.hg.1	10,43	10,29	7,62	16,06	10,7	BCL11A
TC0900011370.hg.1	7,23	7,94	6,05	10,85	9,36	BRINP1
TC0800010936.hg.1	5,05	5,34	4,95	5,56	5,29	PMP2
TC0400008725.hg.1	7,19	6,86	6,96	10,07	6,05	PCDH10
TC1500007062.hg.1	6,04	6,78	6,18	5,38	8,02	CKMT1B; CKMT1A
TC0300012935.hg.1	11,37	11,9	10,55	9,86	9,49	SHOX2
TC0400008977.hg.1	13,41	13,47	12,65	13,39	13,87	MAB21L2
TC0300013022.hg.1	7,14	6,44	7,13	9,93	5,91	SLITRK3
TC0700012126.hg.1	6,52	7,19	5,73	7,35	7,37	RELN
TC1200011438.hg.1	8,46	8,77	8,18	9,5	8,74	MGAT4C
TC0800011509.hg.1	9,08	9,52	9,34	10,11	9,33	CSMD3
TC0700011924.hg.1	7,68	7,78	7,4	8,9	10,21	TMEM130
TC1000008670.hg.1	7,83	7,19	6,77	8,22	6,77	TLX1
TC0400010867.hg.1	7,87	8,29	8,49	10,66	7,94	EPHA5
TC0200013042.hg.1	7,3	6,76	7,64	7,87	5,47	CYP26B1
TC1100012583.hg.1	8,94	9,22	8,4	12,19	8,06	BLID; MIR100HG
TC1900008637.hg.1	7,61	7,44	7,5	7,77	8,61	IGLON5
TC1300009165.hg.1	9,7	9,49	10,55	10,81	11,5	PCDH9
TC2000009813.hg.1	7,77	8,49	7,18	8,44	7,98	EEF1A2
TC0200009865.hg.1	8,85	9,45	9,3	9,82	9,37	SCN2A
TC0X00011126.hg.1	8,82	9,72	9,57	11,06	8,45	GABRA3
TC0600009439.hg.1	9,33	9,65	9,38	11,04	10,33	TMEM200A
TC0400009110.hg.1	11,85	12,28	12,24	13,44	13,12	GRIA2
TC1600010239.hg.1	6,46	5,82	5,76	9,98	7,72	CBLN1
TC0300007973.hg.1	10,07	9,92	9,62	11,87	10,2	CADM2
TC1800008487.hg.1	7,18	7,58	7,57	8,39	9,65	CELF4
TC1500007838.hg.1	7,13	7,36	6,44	8,6	8,49	ISLR2
TC1000008668.hg.1	7,2	7,43	7,32	10,39	9,27	SFXN3
TC2000006676.hg.1	12,31	12,53	11,72	10,89	12,39	LAMP5
TC0200016556.hg.1	5,86	5,78	5,24	8,21	5,99	SLC4A10
TC0700006690.hg.1	8,01	7,83	6,75	8,08	8,61	NXPH1
TC1300009646.hg.1	7,34	7,41	6,65	7,13	7,35	NALCN
TC1500007739.hg.1	8,19	7,9	4,82	7,35	5,64	THSD4
TC0400012288.hg.1	5,8	6,36	6,03	7,75	6,13	FSTL5
TC1500008470.hg.1	10,54	10,48	10,43	9,52	10,33	ARRDC4
TC0600013160.hg.1	5,42	5,31	5,21	6,17	5,87	SAMD3
TC0300008082.hg.1	6,18	6,12	5,25	7,3	7,07	EPHA6
TC1500007067.hg.1	8,61	9,18	8,78	8,23	10,14	CKMT1A
TC0500010265.hg.1	9,79	10,3	10,51	12,13	8,43	CDH18
TC0500009055.hg.1	5,83	6,28	5,85	6,88	6,38	ABLIM3
TC0600010707.hg.1	11,01	11,19	12,47	9,52	10,83	NRN1
TC0100018367.hg.1	6,5	6,77	5,47	6,28	5,52	CHRM3
TC0700012011.hg.1	8,9	8,57	8,54	11,22	10,56	ACTL6B
TC0300006437.hg.1	7,82	8,24	8,33	10,81	9,34	CHL1
TC0500007820.hg.1	7,87	8,11	8,04	8,02	9,74	SV2C
TC1100009561.hg.1	10,88	11,2	11,73	11,43	10,56	NTM
TC0100016755.hg.1	7,57	8,46	8,64	8,07	5,8	BRINP3
TC1900010005.hg.1	10,31	10,03	9,79	12,63	11,82	RAB3A
TC0300008853.hg.1	8,44	8,98	8,38	10,54	9,93	TMEM108
TC1100012633.hg.1	9,91	10	9,53	11,06	10,67	SCN3B
TC0200014814.hg.1	6,8	7,15	7,14	8,31	7,64	SCN1A
TC1100010531.hg.1	10,37	11,04	9,82	11,45	13	SLC1A2
TC1700008082.hg.1	10,46	10,38	10,22	12,13	12,12	MAPT
TC1600007240.hg.1	7,21	7,43	7,02	7,14	9,61	PRKCB
TC1900010334.hg.1	8,48	8,59	8,96	9,43	9,85	TSHZ3
TC1900008902.hg.1	7,52	7,58	7,4	8,11	8,96	BRSK1
TC1600009949.hg.1	10,11	10,19	10	11,46	12,3	FAM57B
TC0100010155.hg.1	6,41	6,69	6,52	7,11	7,58	SEMA4A
TC1900007025.hg.1	10,44	10,81	9,94	12,22	11,09	PLPPR2
TC1300009169.hg.1	7,35	7,9	7,87	8,8	9,13	PCDH9
TC1600009943.hg.1	7,57	6,76	6,8	7,42	9,12	SEZ6L2
TC1600011349.hg.1	9,46	10,09	9,48	9,76	10,04	RBFOX1
TC2000008367.hg.1	9,99	9,86	9,62	11,33	10,86	PAK7
TC1700011143.hg.1	5,29	5,56	5,26	5,68	5,77	CA10
TC1100007095.hg.1	8,54	8,49	8,06	7,46	6,09	LUZP2
TC0300007529.hg.1	10,65	11,02	10,27	10,16	11,39	CACNA2D3
TC0900008784.hg.1	8,66	8,2	8,11	8,8	8,37	LMX1B
TC0200015958.hg.1	10,89	11,02	10,12	11,81	12,91	DNER
TC0100015042.hg.1	7,38	7,5	6,9	8,86	7,42	PLPPR5
TC1800008437.hg.1	6,93	7,47	7,19	11,77	7,69	NOL4
TC0500009400.hg.1	8,53	8,36	8,04	8,72	10,06	KCNIP1
TC0200012559.hg.1	10,85	11,16	10,99	12,36	11,91	NRXN1
TC1500010768.hg.1	7,4	7,39	7,18	8,95	9,31	SCAMP5
TC0100011621.hg.1	9,45	9,45	10,07	8,48	7,28	TGFB2; TGFB2-OT1
TC1900009808.hg.1	8,46	8,62	8,19	10,69	9,2	ADGRL1
TC0100013072.hg.1	9,24	9,14	9,31	10,75	10,75	ATP13A2
TC2000007760.hg.1	9,59	9,43	9,69	12,54	8,09	TSHZ2
TC1200011393.hg.1	9,24	9,19	9,74	12,23	11,31	PPFIA2
TC1000007833.hg.1	7,37	7,73	7,81	7,12	8,05	LRRTM3
TC1000008658.hg.1	11,51	10,73	10,45	11,17	11,3	PAX2
TC0200016482.hg.1	7,78	8,13	8	10,18	9,2	CTNNA2
TC0900009145.hg.1	12,66	12,75	12,34	12,96	14,48	OLFM1
TC0100017018.hg.1	9,31	9,06	9,43	8,63	10,04	ETNK2
TC1200007359.hg.1	9,51	9,89	10,34	14,09	12,82	CNTN1
TC0400008137.hg.1	9,61	9,7	9,49	11,48	11,66	CCSER1
TC0100009364.hg.1	6,93	7,15	6,98	6,63	5,73	CSF1
TC1300009204.hg.1	7,64	7,3	7,6	7,53	8,78	KLHL1
TC1000011640.hg.1	10,08	8,9	8,44	9,99	11,43	LBX1
TC1700009303.hg.1	6,43	5,84	5,59	7,58	7,07	DOC2B
TC1000009104.hg.1	6,09	6,75	5,86	7,53	7	PLPP4
TC1100009242.hg.1	5,74	5,92	5,78	5,47	7,29	ABCG4

Table 6.4: To lowest fold change normalized fold changes (log2) for top 100 upregulated genes during the process of neuronal differentiation at ND7.

ID	Eto ND7 Avg (log2)	ctr ND7 Avg (log2)	GCNF ND7 Avg (log2)	GCNFVP16 ND7 Avg (log2)	NGN2 ND7 Avg (log2)	Gene Symbol
TC1100007064.hg.1	0,14	0,00	0,15	0,20	0,20	SLC17A6
TC1300008602.hg.1	0,02	0,00	0,07	0,22	0,08	MAB21L1
TC0700011658.hg.1	0,68	0,58	0,00	0,51	0,82	SEMA3E
TC0100018511.hg.1	0,23	0,28	0,00	0,99	0,11	C1orf61
TC0500013266.hg.1	0,03	0,04	0,00	0,46	0,34	HMP19
TC2200006945.hg.1	0,15	0,16	0,00	0,40	0,18	SEZ6L
TC1200009997.hg.1	0,14	0,05	0,00	0,61	0,19	GRIN2B
TC0300013469.hg.1	0,52	0,47	0,37	0,51	0,00	SST
TC1100007056.hg.1	0,07	0,16	0,15	0,00	0,33	NELL1
TC0200012713.hg.1	0,45	0,43	0,00	1,08	0,49	BCL11A
TC0900011370.hg.1	0,26	0,39	0,00	0,84	0,63	BRINP1
TC0800010936.hg.1	0,03	0,11	0,00	0,17	0,10	PMP2
TC0400008725.hg.1	0,25	0,18	0,20	0,74	0,00	PCDH10
TC1500007062.hg.1	0,17	0,33	0,20	0,00	0,58	CKMT1B; CKMT1A
TC0300012935.hg.1	0,26	0,33	0,15	0,06	0,00	SHOX2
TC0400008977.hg.1	0,08	0,09	0,00	0,08	0,13	MAB21L2
TC0300013022.hg.1	0,27	0,12	0,27	0,75	0,00	SLITRK3
TC0700012126.hg.1	0,19	0,33	0,00	0,36	0,36	RELN
TC1200011438.hg.1	0,05	0,10	0,00	0,22	0,10	MGAT4C
TC0800011509.hg.1	0,00	0,07	0,04	0,16	0,04	CSMD3
TC0700011924.hg.1	0,05	0,07	0,00	0,27	0,46	TMEM130
TC1000008670.hg.1	0,21	0,09	0,00	0,28	0,00	TLX1
TC0400010867.hg.1	0,00	0,08	0,11	0,44	0,01	EPHA5
TC0200013042.hg.1	0,42	0,31	0,48	0,52	0,00	CYP26B1
TC1100012583.hg.1	0,15	0,19	0,06	0,60	0,00	BLID; MIR100HG
TC1900008637.hg.1	0,03	0,00	0,01	0,06	0,21	IGLON5
TC1300009165.hg.1	0,03	0,00	0,15	0,19	0,28	PCDH9
TC2000009813.hg.1	0,11	0,24	0,00	0,23	0,15	EEF1A2
TC0200009865.hg.1	0,00	0,09	0,07	0,15	0,08	SCN2A
TC0X00011126.hg.1	0,06	0,20	0,18	0,39	0,00	GABRA3
TC0600009439.hg.1	0,00	0,05	0,01	0,24	0,15	TMEM200A
TC0400009110.hg.1	0,00	0,05	0,05	0,18	0,15	GRIA2
TC1600010239.hg.1	0,17	0,01	0,00	0,79	0,42	CBLN1
TC0300007973.hg.1	0,07	0,04	0,00	0,30	0,08	CADM2
TC1800008487.hg.1	0,00	0,08	0,08	0,22	0,43	CELF4
TC1500007838.hg.1	0,15	0,19	0,00	0,42	0,40	ISLR2
TC1000008668.hg.1	0,00	0,05	0,02	0,53	0,36	SFXN3
TC2000006676.hg.1	0,18	0,20	0,11	0,00	0,19	LAMP5
TC0200016556.hg.1	0,16	0,14	0,00	0,65	0,19	SLC4A10
TC0700006690.hg.1	0,25	0,21	0,00	0,26	0,35	NXPH1
TC1300009646.hg.1	0,14	0,16	0,00	0,10	0,14	NALCN
TC1500007739.hg.1	0,76	0,71	0,00	0,61	0,23	THSD4
TC0400012288.hg.1	0,00	0,13	0,06	0,42	0,08	FSTL5
TC1500008470.hg.1	0,15	0,14	0,13	0,00	0,12	ARRDC4
TC0600013160.hg.1	0,06	0,03	0,00	0,24	0,17	SAMD3
TC0300008082.hg.1	0,24	0,22	0,00	0,48	0,43	EPHA6
TC1500007067.hg.1	0,07	0,16	0,09	0,00	0,30	CKMT1A
TC0500010265.hg.1	0,22	0,29	0,32	0,52	0,00	CDH18
TC0500009055.hg.1	0,00	0,11	0,00	0,24	0,13	ABLIM3
TC0600010707.hg.1	0,21	0,23	0,39	0,00	0,19	NRN1
TC0100018367.hg.1	0,25	0,31	0,00	0,20	0,01	CHRM3
TC0700012011.hg.1	0,06	0,01	0,00	0,39	0,31	ACTL6B
TC0300006437.hg.1	0,00	0,08	0,09	0,47	0,26	CHL1
TC0500007820.hg.1	0,00	0,04	0,03	0,03	0,31	SV2C
TC1100009561.hg.1	0,04	0,08	0,15	0,11	0,00	NTM
TC0100016755.hg.1	0,38	0,54	0,57	0,48	0,00	BRINP3
TC1900010005.hg.1	0,07	0,03	0,00	0,37	0,27	RAB3A
TC0300008853.hg.1	0,01	0,10	0,00	0,33	0,24	TMEM108
TC1100012633.hg.1	0,06	0,07	0,00	0,21	0,16	SCN3B
TC0200014814.hg.1	0,00	0,07	0,07	0,29	0,17	SCN1A
TC1100010531.hg.1	0,08	0,17	0,00	0,22	0,40	SLC1A2
TC1700008082.hg.1	0,03	0,02	0,00	0,25	0,25	MAPT
TC1600007240.hg.1	0,04	0,08	0,00	0,02	0,45	PRKCB
TC1900010334.hg.1	0,00	0,02	0,08	0,15	0,22	TSHZ3
TC1900008902.hg.1	0,02	0,03	0,00	0,13	0,28	BRSK1
TC1600009949.hg.1	0,02	0,03	0,00	0,20	0,30	FAM57B
TC0100010155.hg.1	0,00	0,06	0,02	0,15	0,24	SEMA4A
TC1900007025.hg.1	0,07	0,12	0,00	0,30	0,16	PLPPR2
TC1300009169.hg.1	0,00	0,10	0,10	0,26	0,31	PCDH9
TC1600009943.hg.1	0,16	0,00	0,01	0,13	0,43	SEZ6L2
TC1600011349.hg.1	0,00	0,09	0,00	0,05	0,09	RBFOX1
TC2000008367.hg.1	0,05	0,04	0,00	0,24	0,17	PAK7
TC1700011143.hg.1	0,01	0,08	0,00	0,11	0,13	CA10
TC1100007095.hg.1	0,49	0,48	0,40	0,29	0,00	LUZP2
TC0300007529.hg.1	0,07	0,12	0,02	0,00	0,16	CACNA2D3
TC0900008784.hg.1	0,09	0,02	0,00	0,12	0,05	LMX1B
TC0200015958.hg.1	0,11	0,12	0,00	0,22	0,35	DNER
TC0100015042.hg.1	0,10	0,12	0,00	0,36	0,10	PLPPR5
TC1800008437.hg.1	0,00	0,11	0,05	0,76	0,15	NOL4
TC0500009400.hg.1	0,09	0,06	0,00	0,12	0,32	KCNIP1
TC0200012559.hg.1	0,00	0,04	0,02	0,19	0,13	NRXN1
TC1500010768.hg.1	0,04	0,04	0,00	0,32	0,37	SCAMP5
TC0100011621.hg.1	0,38	0,38	0,47	0,22	0,00	TGFB2; TGFB2-OT1
TC1900009808.hg.1	0,05	0,07	0,00	0,38	0,17	ADGRL1
TC0100013072.hg.1	0,02	0,00	0,03	0,23	0,23	ATP13A2
TC2000007760.hg.1	0,25	0,22	0,26	0,63	0,00	TSHZ2
TC1200011393.hg.1	0,01	0,00	0,08	0,41	0,30	PPFIA2
TC1000007833.hg.1	0,05	0,12	0,13	0,00	0,18	LRRTM3
TC1000008658.hg.1	0,14	0,04	0,00	0,10	0,11	PAX2
TC0200016482.hg.1	0,00	0,06	0,04	0,39	0,24	CTNNA2
TC0900009145.hg.1	0,04	0,05	0,00	0,07	0,23	OLFM1
TC0100017018.hg.1	0,11	0,07	0,13	0,00	0,22	ETNK2
TC1200007359.hg.1	0,00	0,06	0,12	0,57	0,43	CNTN1
TC0400008137.hg.1	0,02	0,03	0,00	0,27	0,30	CCSER1
TC0100009364.hg.1	0,27	0,32	0,28	0,21	0,00	CSF1
TC1300009204.hg.1	0,07	0,00	0,06	0,04	0,27	KLHL1
TC1000011640.hg.1	0,26	0,08	0,00	0,24	0,44	LBX1
TC1700009303.hg.1	0,20	0,06	0,00	0,44	0,34	DOC2B
TC1000009104.hg.1	0,06	0,20	0,00	0,36	0,26	PLPP4
TC1100009242.hg.1	0,07	0,11	0,08	0,00	0,41	ABCG4

Table 6.5: Fold Change (log2) for top 100 upregulated genes during the process of neuronal differentiation at ND14.

ID	Eto ND15 Avg (log2)	ctr ND15 Avg (log2)	GCNF ND15 Avg (log2)	GCNFVP16 ND15 Avg (log2)	NGN2 ND15 Avg (log2)	Gene Symbol
TC1100007064.hg.1	11,66	10,72	10,06	9,71	9,57	SLC17A6
TC1300008602.hg.1	13,08	13,12	13,53	12,78	12,6	MAB21L1
TC0700011658.hg.1	10,66	10,83	7,06	9,13	13,56	SEMA3E
TC0100018511.hg.1	12,22	11,76	9,43	13,01	10,04	C1orf61
TC0500013266.hg.1	13,26	13,39	13	14,28	14,1	HMP19
TC2200006945.hg.1	11,84	12,3	10,58	11,66	11,69	SEZ6L
TC1200009997.hg.1	9,98	10,4	9,08	12,29	8,48	GRIN2B
TC0300013469.hg.1	10,74	10,26	9,28	9,38	8,48	SST
TC1100007056.hg.1	9,89	11,02	10,39	10,84	11,29	NELL1
TC0200012713.hg.1	12,79	12,84	10,7	15,51	12,73	BCL11A
TC0900011370.hg.1	11,06	11,25	9,57	11,7	11,64	BRINP1
TC0800010936.hg.1	9,48	9,73	10,51	9,65	6,55	PMP2
TC0400008725.hg.1	10,17	10,68	9,91	11,9	9,66	PCDH10
TC1500007062.hg.1	10,06	10,38	10,14	9,43	11,72	CKMT1B; CKMT1A
TC0300012935.hg.1	13,89	14,01	13,32	13,15	12,43	SHOX2
TC0400008977.hg.1	15,85	15,54	15,05	14,83	14,97	MAB21L2
TC0300013022.hg.1	10,98	10,85	10,39	11,28	10,47	SLITRK3
TC0700012126.hg.1	9,82	11,01	7,85	10,05	10,52	RELN
TC1200011438.hg.1	11,19	11,66	11,03	11,36	11,49	MGAT4C
TC0800011509.hg.1	11,82	12,67	11,69	13,26	11,99	CSMD3
TC0700011924.hg.1	11,19	11,43	11,62	11,94	12,4	TMEM130
TC1000008670.hg.1	11,62	11,28	9,33	10,65	7,32	TLX1
TC0400010867.hg.1	10,06	10,98	10,35	11,98	10,5	EPHA5
TC0200013042.hg.1	10,75	10,5	10,95	10,94	9,07	CYP26B1
TC1100012583.hg.1	11,95	11,63	11,9	11,64	11,97	BLID; MIR100HG
TC1900008637.hg.1	11,06	11,12	11,33	10,64	11,58	IGLON5
TC1300009165.hg.1	12,02	12,46	12,67	12,68	13,81	PCDH9
TC2000009813.hg.1	11,14	11,4	11,34	11,61	11,54	EEF1A2
TC0200009865.hg.1	10,81	11,63	11,04	12,13	12,2	SCN2A
TC0X00011126.hg.1	12,12	12,81	12	14,05	11,52	GABRA3
TC0600009439.hg.1	12,43	12,37	11,74	11,72	13,14	TMEM200A
TC0400009110.hg.1	13,56	14,16	13,5	14,56	14,94	GRIA2
TC1600010239.hg.1	9,44	8,61	7,7	9,61	8,37	CBLN1
TC0300007973.hg.1	11,67	12,2	11,84	12,85	11,68	CADM2
TC1800008487.hg.1	10,67	11,3	10,4	11,46	11,69	CELF4
TC1500007838.hg.1	9,82	10,27	9,61	9,79	10,12	ISLR2
TC1000008668.hg.1	10,64	10,6	10,05	11,17	11,92	SFXN3
TC2000006676.hg.1	13,64	13,06	13,8	11,63	13,26	LAMP5
TC0200016556.hg.1	8,57	9,41	8,86	11,16	10,25	SLC4A10
TC0700006690.hg.1	10,1	10,59	9,74	9,85	11,76	NXPH1
TC1300009646.hg.1	9,78	10,46	10,18	9,92	10,74	NALCN
TC1500007739.hg.1	10,51	9,98	6,9	8,62	7,59	THSD4
TC0400012288.hg.1	8,38	9,64	8,5	9,23	8,57	FSTL5
TC1500008470.hg.1	12,5	11,5	12,77	10,8	12,3	ARRDC4
TC0600013160.hg.1	8,79	8,85	8,38	8,34	9,52	SAMD3
TC0300008082.hg.1	9,28	9,3	7,95	10,22	10,3	EPHA6
TC1500007067.hg.1	10,93	11,17	11,12	10,85	12,31	CKMT1A
TC0500010265.hg.1	12,24	12,52	11,94	13,34	12,46	CDH18
TC0500009055.hg.1	9,28	9,21	8,52	10,66	9,52	ABLIM3
TC0600010707.hg.1	12,56	12,36	13,57	11,56	12,65	NRN1
TC0100018367.hg.1	8,72	9,4	7,65	8,87	8,75	CHRM3
TC0700012011.hg.1	11,23	11,38	10,58	12,11	11,68	ACTL6B
TC0300006437.hg.1	10,65	11,31	10,45	12,42	11,4	CHL1
TC0500007820.hg.1	10,45	10,45	9,84	9,77	9,33	SV2C
TC1100009561.hg.1	13,27	13,35	13,48	13,14	13,49	NTM
TC0100016755.hg.1	10,23	10,31	10,39	10,19	8,23	BRINP3
TC1900010005.hg.1	12,69	12,92	12,41	13,4	13,31	RAB3A
TC0300008853.hg.1	11,53	11,12	10,64	11,23	10,62	TMEM108
TC1100012633.hg.1	12,72	12,93	12,44	13,5	13,1	SCN3B
TC0200014814.hg.1	9,67	10,17	9,43	10,9	9,49	SCN1A
TC1100010531.hg.1	12,92	12,67	11,88	12,8	12,81	SLC1A2
TC1700008082.hg.1	13,25	13,57	13,01	14,22	14,02	MAPT
TC1600007240.hg.1	9,61	9,9	9,51	9,2	11,06	PRKCB
TC1900010334.hg.1	11,62	11,62	11,25	11,26	10,57	TSHZ3
TC1900008902.hg.1	10,57	10,56	10,5	10,7	10,61	BRSK1
TC1600009949.hg.1	12,99	13,15	12,85	12,99	13,43	FAM57B
TC0100010155.hg.1	9,73	9,95	9,89	10,45	9,15	SEMA4A
TC1900007025.hg.1	12,87	12,95	12,69	13,45	12,48	PLPPR2
TC1300009169.hg.1	9,39	9,87	9,3	10,76	10,83	PCDH9
TC1600009943.hg.1	9,89	9,77	9,86	9,43	10,03	SEZ6L2
TC1600011349.hg.1	11,3	11,74	11,47	11,6	11,9	RBFOX1
TC2000008367.hg.1	12,14	12,3	11,88	13,08	12,47	PAK7
TC1700011143.hg.1	8,02	8,88	8,87	8,87	8,63	CA10
TC1100007095.hg.1	10,43	11,09	10,67	9,83	9,45	LUZP2
TC0300007529.hg.1	12,58	12,72	12,13	12,44	13,69	CACNA2D3
TC0900008784.hg.1	11,45	10,64	9,79	10,19	8,47	LMX1B
TC0200015958.hg.1	12,82	12,87	12,43	12,78	13,62	DNER
TC0100015042.hg.1	9,12	9,85	9,22	10,93	10,07	PLPPR5
TC1800008437.hg.1	9,07	9,39	8,77	12,07	9,9	NOL4
TC0500009400.hg.1	10,01	9,96	10,59	9,86	11,68	KCNIP1
TC0200012559.hg.1	12,62	12,91	12,73	13,82	13,25	NRXN1
TC1500010768.hg.1	9,71	9,84	9,91	10,02	10,81	SCAMP5
TC0100011621.hg.1	11,07	11,04	12,07	8,91	8,04	TGFB2; TGFB2-OT1
TC1900009808.hg.1	11,38	11,36	10,86	12,2	11,08	ADGRL1
TC0100013072.hg.1	12,28	12,27	12,13	12,33	12,15	ATP13A2
TC2000007760.hg.1	12,23	12,01	10,76	13,54	10,75	TSHZ2
TC1200011393.hg.1	10,96	11,7	11,03	12,85	12,57	PPFIA2
TC1000007833.hg.1	9,54	10,27	9,73	9,85	10,19	LRRTM3
TC1000008658.hg.1	13,62	13	12,77	12,54	11,98	PAX2
TC0200016482.hg.1	9,97	10,52	9,99	11,28	10,54	CTNNA2
TC0900009145.hg.1	14,8	15,09	14,56	14,8	15,6	OLFM1
TC0100017018.hg.1	11,63	11,91	12,08	11,16	11,79	ETNK2
TC1200007359.hg.1	10,9	11,9	12,12	14,52	14,18	CNTN1
TC0400008137.hg.1	11,35	11,92	11,23	11,98	13,04	CCSER1
TC0100009364.hg.1	10,38	10,13	9,91	7,65	6,57	CSF1
TC1300009204.hg.1	9,89	9,8	9,44	8,88	10,07	KLHL1
TC1000011640.hg.1	11,72	11,45	10,25	10,64	11,38	LBX1
TC1700009303.hg.1	9,1	8,78	7,23	8,88	9,29	DOC2B
TC1000009104.hg.1	8,35	9,01	7,29	9,17	9,5	PLPP4
TC1100009242.hg.1	8,99	8,56	8,74	8,44	9,19	ABCG4

Table 6.6: To lowest fold change normalized fold changes (log2) for top 100 upregulated genes during the process of neuronal differentiation at ND14.

ID	Eto ND15 Avg (log2)	ctr ND15 Avg (log2)	GCNF ND15 Avg (log2)	GCNFVP16 ND15 Avg (log2)	NGN2 ND15 Avg (log2)	Gene Symbol
TC1100007064.hg.1	0,28	0,16	0,07	0,02	0,00	SLC17A6
TC1300008602.hg.1	0,05	0,06	0,10	0,02	0,00	MAB21L1
TC0700011658.hg.1	0,59	0,62	0,00	0,37	0,94	SEMA3E
TC0100018511.hg.1	0,37	0,32	0,00	0,46	0,09	C1orf61
TC0500013266.hg.1	0,03	0,04	0,00	0,14	0,12	HMP19
TC2200006945.hg.1	0,16	0,22	0,00	0,14	0,14	SEZ6L
TC1200009997.hg.1	0,23	0,29	0,10	0,54	0,00	GRIN2B
TC0300013469.hg.1	0,34	0,27	0,13	0,15	0,00	SST
TC1100007056.hg.1	0,00	0,16	0,07	0,13	0,19	NELL1
TC0200012713.hg.1	0,26	0,26	0,00	0,54	0,25	BCL11A
TC0900011370.hg.1	0,21	0,23	0,00	0,29	0,28	BRINP1
TC0800010936.hg.1	0,53	0,57	0,68	0,56	0,00	PMP2
TC0400008725.hg.1	0,07	0,14	0,04	0,30	0,00	PCDH10
TC1500007062.hg.1	0,09	0,14	0,10	0,00	0,31	CKMT1B; CKMT1A
TC0300012935.hg.1	0,16	0,17	0,10	0,08	0,00	SHOX2
TC0400008977.hg.1	0,10	0,07	0,02	0,00	0,01	MAB21L2
TC0300013022.hg.1	0,08	0,06	0,00	0,12	0,01	SLITRK3
TC0700012126.hg.1	0,32	0,49	0,00	0,36	0,42	RELN
TC1200011438.hg.1	0,02	0,08	0,00	0,04	0,06	MGAT4C
TC0800011509.hg.1	0,02	0,12	0,00	0,18	0,04	CSMD3
TC0700011924.hg.1	0,00	0,03	0,05	0,09	0,15	TMEM130
TC1000008670.hg.1	0,67	0,62	0,35	0,54	0,00	TLX1
TC0400010867.hg.1	0,00	0,13	0,04	0,25	0,06	EPHA5
TC0200013042.hg.1	0,25	0,21	0,27	0,27	0,00	CYP26B1
TC1100012583.hg.1	0,04	0,00	0,03	0,00	0,04	BLID; MIR100HG
TC1900008637.hg.1	0,06	0,06	0,09	0,00	0,12	IGLON5
TC1300009165.hg.1	0,00	0,05	0,08	0,08	0,20	PCDH9
TC2000009813.hg.1	0,00	0,03	0,03	0,06	0,05	EEF1A2
TC0200009865.hg.1	0,00	0,11	0,03	0,17	0,17	SCN2A
TC0X00011126.hg.1	0,07	0,15	0,06	0,29	0,00	GABRA3
TC0600009439.hg.1	0,08	0,08	0,00	0,00	0,16	TMEM200A
TC0400009110.hg.1	0,01	0,07	0,00	0,11	0,15	GRIA2
TC1600010239.hg.1	0,29	0,16	0,00	0,32	0,12	CBLN1
TC0300007973.hg.1	0,00	0,06	0,02	0,14	0,00	CADM2
TC1800008487.hg.1	0,04	0,12	0,00	0,14	0,17	CELF4
TC1500007838.hg.1	0,03	0,10	0,00	0,03	0,07	ISLR2
TC1000008668.hg.1	0,08	0,08	0,00	0,15	0,25	SFXN3
TC2000006676.hg.1	0,23	0,17	0,25	0,00	0,19	LAMP5
TC0200016556.hg.1	0,00	0,13	0,05	0,38	0,26	SLC4A10
TC0700006690.hg.1	0,05	0,12	0,00	0,02	0,27	NXPH1
TC1300009646.hg.1	0,00	0,10	0,06	0,02	0,14	NALCN
TC1500007739.hg.1	0,61	0,53	0,00	0,32	0,14	THSD4
TC0400012288.hg.1	0,00	0,20	0,02	0,14	0,03	FSTL5
TC1500008470.hg.1	0,21	0,09	0,24	0,00	0,19	ARRDC4
TC0600013160.hg.1	0,08	0,09	0,01	0,00	0,19	SAMD3
TC0300008082.hg.1	0,22	0,23	0,00	0,36	0,37	EPHA6
TC1500007067.hg.1	0,01	0,04	0,04	0,00	0,18	CKMT1A
TC0500010265.hg.1	0,04	0,07	0,00	0,16	0,06	CDH18
TC0500009055.hg.1	0,12	0,11	0,00	0,32	0,16	ABLIM3
TC0600010707.hg.1	0,12	0,10	0,23	0,00	0,13	NRN1
TC0100018367.hg.1	0,19	0,30	0,00	0,21	0,19	CHRM3
TC0700012011.hg.1	0,09	0,11	0,00	0,19	0,14	ACTL6B
TC0300006437.hg.1	0,03	0,11	0,00	0,25	0,13	CHL1
TC0500007820.hg.1	0,16	0,16	0,08	0,07	0,00	SV2C
TC1100009561.hg.1	0,01	0,02	0,04	0,00	0,04	NTM
TC0100016755.hg.1	0,31	0,33	0,34	0,31	0,00	BRINP3
TC1900010005.hg.1	0,03	0,06	0,00	0,11	0,10	RAB3A
TC0300008853.hg.1	0,12	0,07	0,00	0,08	0,00	TMEM108
TC1100012633.hg.1	0,03	0,06	0,00	0,12	0,07	SCN3B
TC0200014814.hg.1	0,04	0,11	0,00	0,21	0,01	SCN1A
TC1100010531.hg.1	0,12	0,09	0,00	0,11	0,11	SLC1A2
TC1700008082.hg.1	0,03	0,06	0,00	0,13	0,11	MAPT
TC1600007240.hg.1	0,06	0,11	0,05	0,00	0,27	PRKCB
TC1900010334.hg.1	0,14	0,14	0,09	0,09	0,00	TSHZ3
TC1900008902.hg.1	0,01	0,01	0,00	0,03	0,02	BRSK1
TC1600009949.hg.1	0,02	0,03	0,00	0,02	0,06	FAM57B
TC0100010155.hg.1	0,09	0,12	0,11	0,19	0,00	SEMA4A
TC1900007025.hg.1	0,04	0,05	0,02	0,11	0,00	PLPPR2
TC1300009169.hg.1	0,01	0,09	0,00	0,21	0,22	PCDH9
TC1600009943.hg.1	0,07	0,05	0,06	0,00	0,09	SEZ6L2
TC1600011349.hg.1	0,00	0,06	0,02	0,04	0,07	RBFOX1
TC2000008367.hg.1	0,03	0,05	0,00	0,14	0,07	PAK7
TC1700011143.hg.1	0,00	0,15	0,15	0,15	0,11	CA10
TC1100007095.hg.1	0,14	0,23	0,18	0,06	0,00	LUZP2
TC0300007529.hg.1	0,05	0,07	0,00	0,04	0,17	CACNA2D3
TC0900008784.hg.1	0,43	0,33	0,21	0,27	0,00	LMX1B
TC0200015958.hg.1	0,04	0,05	0,00	0,04	0,13	DNER
TC0100015042.hg.1	0,00	0,11	0,02	0,26	0,14	PLPPR5
TC1800008437.hg.1	0,05	0,10	0,00	0,46	0,17	NOL4
TC0500009400.hg.1	0,02	0,01	0,10	0,00	0,24	KCNIP1
TC0200012559.hg.1	0,00	0,03	0,01	0,13	0,07	NRXN1
TC1500010768.hg.1	0,00	0,02	0,03	0,05	0,15	SCAMP5
TC0100011621.hg.1	0,46	0,46	0,59	0,15	0,00	TGFB2; TGFB2-OT1
TC1900009808.hg.1	0,07	0,06	0,00	0,17	0,03	ADGRL1
TC0100013072.hg.1	0,02	0,02	0,00	0,02	0,00	ATP13A2
TC2000007760.hg.1	0,19	0,16	0,00	0,33	0,00	TSHZ2
TC1200011393.hg.1	0,00	0,09	0,01	0,23	0,20	PPFIA2
TC1000007833.hg.1	0,00	0,11	0,03	0,05	0,10	LRRTM3
TC1000008658.hg.1	0,19	0,12	0,09	0,07	0,00	PAX2
TC0200016482.hg.1	0,00	0,08	0,00	0,18	0,08	CTNNA2
TC0900009145.hg.1	0,02	0,05	0,00	0,02	0,10	OLFM1
TC0100017018.hg.1	0,06	0,09	0,11	0,00	0,08	ETNK2
TC1200007359.hg.1	0,00	0,13	0,15	0,41	0,38	CNTN1
TC0400008137.hg.1	0,02	0,09	0,00	0,09	0,22	CCSER1
TC0100009364.hg.1	0,66	0,62	0,59	0,22	0,00	CSF1
TC1300009204.hg.1	0,16	0,14	0,09	0,00	0,18	KLHL1
TC1000011640.hg.1	0,19	0,16	0,00	0,05	0,15	LBX1
TC1700009303.hg.1	0,33	0,28	0,00	0,30	0,36	DOC2B
TC1000009104.hg.1	0,20	0,31	0,00	0,33	0,38	PLPP4
TC1100009242.hg.1	0,09	0,02	0,05	0,00	0,12	ABCG4

Table 6.7: Fold Change (log2) for top 100 downregulated genes during the process of neuronal differentiation at ND2.

ID	Eto 48h Avg (log2)	ctr 48h Avg (log2)	GCNF 48h Avg (log2)	GCNFVP16 48h Avg (log2)	NGN2 48h Avg (log2)	Gene Symbol
TC0700008263.hg.1	11,54	11,84	11,91	10,74	11,29	DBF4
TC1500009795.hg.1	15,25	15,27	15,22	13,82	15,46	IGDCC3
TC2100007821.hg.1	7,32	7,08	7,55	5,91	6,26	ADAMTS1
TC0200006677.hg.1	12,4	12,1	12,51	11,59	12,08	RRM2
TC1000007885.hg.1	8,71	9,12	8,47	9,51	7,96	SRGN
TC1200009913.hg.1	11,76	11,89	11,47	11,82	10,34	YBX3
TC1800007298.hg.1	9,72	9,48	8,66	7,5	9,61	LIPG
TC0300009524.hg.1	11,31	10,83	10,71	9,9	10,31	ECT2
TC0300012164.hg.1	9,55	9,37	9,61	9,06	9,38	POLQ
TC0300006968.hg.1	8,79	9,48	9,63	7,94	11,21	CMTM7
TC1000006880.hg.1	7,56	6,93	7	6,27	7,19	PTER
TC0200013912.hg.1	10,94	11,12	11,25	10,2	10,42	CKAP2L
TC0300009119.hg.1	6,86	7,78	6,69	5,02	4,58	AGTR1
TC0100007243.hg.1	7,22	7,15	7,8	8,42	7,48	ALPL
TC0X00007936.hg.1	9,93	10,13	10,04	8,88	8,85	CENPI
TC0X00010851.hg.1	9,62	9,47	9,75	7,73	8,51	GPC3
TC0400011920.hg.1	9,67	9,68	9,8	7,49	7,34	SLC7A11
TC0100012328.hg.1	7,95	7,93	7,97	8,02	6,65	TRIM58
TC0800006869.hg.1	7,28	7,14	6,97	6,67	6,34	SLC7A2
TC1200006604.hg.1	6,83	6,59	6,84	12,49	7,11	CD9
TC0100012172.hg.1	10,51	10,32	10,81	9,34	9,71	EXO1
TC1300006919.hg.1	6,48	6,66	6,24	5,61	6,05	FREM2
TC1000012477.hg.1	12,73	12,62	12,73	11,65	12,1	HELLS
TC0X00007537.hg.1	10,46	10,45	10,44	9,25	10,1	KIF4A
TC0700007345.hg.1	9,75	9,98	9,75	9,38	11,16	STK17A
TC1000010758.hg.1	12,64	12,16	12,66	11,51	12,24	RTKN2
TC2100007198.hg.1	7,51	7,18	6,91	6,69	5,89	BACE2
TC1200012597.hg.1	12,65	12,28	13,23	11,91	10,82	MGST1
TC0500007415.hg.1	8,6	8,66	8,49	7,14	7,5	GPX8
TC0700008875.hg.1	9,2	9,23	9,83	6,67	6,13	MET
TC1500009756.hg.1	8,95	8,77	8,39	7,83	7,99	RBPMS2
TC0600007282.hg.1	11,82	11,71	11,85	10,59	9,44	HIST1H2BF
TC0400008134.hg.1	9,94	9,3	9,81	8,36	6,76	MMRN1
TC1000012011.hg.1	7,02	7,2	7,69	6,4	7,33	RGS10
TC1800007316.hg.1	8,11	8,35	7,95	7,65	7,8	SKA1
TC0600008630.hg.1	12,23	12,29	12,44	11,83	12,02	TTK
TC0600013431.hg.1	9,96	9,67	9,96	9,73	9,31	PLAGL1; HYMAI
TC1200011470.hg.1	10,12	9,95	10,04	8,19	8,81	DUSP6
TC0600007377.hg.1	15,19	15,2	15,53	14,31	13,8	HIST1H2BM
TC1600007958.hg.1	12,59	12,82	12,88	10,52	10,59	MT1L
TC0300010476.hg.1	11,08	10,86	11,09	10,53	10,25	SGOL1
TC1600011399.hg.1	14,02	14,24	14,37	11,29	12,51	MT1X
TC1200009397.hg.1	9,27	8,72	8,49	10	8,66	FZD10
TC0600007700.hg.1	11,25	11,14	11,14	10,05	10,83	KIFC1
TC1500009738.hg.1	10,7	10,29	11,13	8,66	9,71	KIAA0101; CSNK1G1
TC1100012229.hg.1	9,35	8,96	9,73	7,85	7,5	KDELC2
TC1600011405.hg.1	9,95	9,58	9,83	8,06	8,88	GINS3
TC0600011635.hg.1	10,75	11,14	10,89	9,03	9,68	FKBP5
TC1800009268.hg.1	9,06	9,03	8,91	5,96	7,7	DSC2
TC1800006484.hg.1	11,01	11,16	11,76	10,05	10,46	NDC80
TC1200010493.hg.1	11,58	11,08	11,66	10,09	11,99	DBX2
TC1400010715.hg.1	10,81	10,65	11,06	7,54	8,49	AJUBA
TC1200006946.hg.1	9,19	9,05	9,09	8,04	6,73	H2AFJ
TC0X00010512.hg.1	9,05	9,17	9,6	8,71	9,86	CHRDL1
TC0700007596.hg.1	8,36	8,78	8,74	7,04	7,66	EGFR
TC1100006525.hg.1	8	8,11	8,23	8,5	7,07	KRTAP5-5
TC0500007368.hg.1	8,03	6,64	6,88	6,24	5,54	ITGA2
TC0100008807.hg.1	8,78	8,57	8,78	6,92	7,33	NEXN
TC0400012903.hg.1	13,76	13,48	13,82	12,28	13,69	PROM1
TC0600011130.hg.1	8,77	10,46	10,15	8,59	8,08	HIST1H4C
TC0600007290.hg.1	14,33	14,33	14,48	13,52	12,99	HIST1H2BH
TC0200009189.hg.1	9,69	9,69	9,81	9,18	9,22	GYPC
TC1100009097.hg.1	7,78	8,01	7,49	6,4	5,76	HTR3B
TC1100010418.hg.1	12,02	11,88	12,15	10,92	11,01	KIF18A
TC2000009462.hg.1	12,32	12,22	12,28	10,08	12,35	SALL4
TC1700011364.hg.1	10,82	10,88	10,6	9,08	9,63	BRIP1
TC0100015049.hg.1	8,49	8,52	8,63	7,05	7,25	FRRS1
TC0300012367.hg.1	10,66	10,48	10,55	8,93	7,77	KIAA1257
TC0100006881.hg.1	9,83	10,1	9,8	8,84	9,5	TNFRSF1B; MIR4632; MIR7846
TC0100014910.hg.1	9,39	9,22	9,13	7,94	7,18	TGFBR3
TC1100010792.hg.1	8,83	9,43	9,21	9,56	9,8	FOLH1
TC0200008502.hg.1	11,74	11,56	11,57	10	10,61	NCAPH
TC2100007816.hg.1	11,47	11,26	11,61	11,47	10,4	CYYR1
TC0700010604.hg.1	7,8	7,5	8,29	6,89	7,76	CPVL
TC0400012620.hg.1	12,64	12,41	12,51	11,08	11,59	CENPU
TC1300006802.hg.1	10,64	10,83	10,82	9,26	10,47	BRCA2
TC0100017733.hg.1	7,12	7,14	7,22	6,49	5,99	TSNAX
TC0600011818.hg.1	10,3	10,49	10,11	10,9	8,62	C6orf132
TC1800007014.hg.1	8,69	8,48	8,94	7,85	6,65	DSG2
TC0800010234.hg.1	10,39	10,39	11,02	8,23	9,75	SFRP1
TC0X00010837.hg.1	10	10,26	10,41	9,97	9,68	MBNL3
TC0100016254.hg.1	6,95	7,9	6,44	9,35	4,67	RXRG
TC1100007727.hg.1	11,81	11,59	11,76	10,13	10,86	FAM111B
TC0400008237.hg.1	12,16	11,95	12,34	9,11	9,04	MTTP
TC0100014202.hg.1	10,68	10,42	10,62	8,73	9,76	ORC1
TC0600007293.hg.1	9,99	10,25	10,8	8,42	7,96	HIST1H2BI
TC1200008041.hg.1	9,59	9,1	10,17	8,31	8,02	HMGA2
TC1100007453.hg.1	14,25	14,22	14,48	12,82	13,71	MDK
TC1500009505.hg.1	14,93	14,86	15,32	11,3	14,25	PRTG
TC0400011548.hg.1	12,2	12,14	11,97	10,84	12,03	LEF1
TC1700008511.hg.1	8,15	9,44	9,42	7,69	6,06	TBX2
TC0800012388.hg.1	7,56	8,23	7,4	6,54	5,18	DLC1
TC1600007965.hg.1	10,71	11,08	11,43	8,89	7,65	MT1F
TC0400007371.hg.1	10,21	10,23	10,14	10,81	7,39	SHISA3
TC0200008793.hg.1	9,81	10,65	10,67	6,67	6	SLC5A7
TC0300011956.hg.1	9,73	10,24	10,77	9,49	6,87	DPPA4
TC0100007457.hg.1	10,61	10,72	11,23	8,09	9,4	LIN28A
TC0500010651.hg.1	11,59	12,01	11,9	9,21	8,63	FGF10
TC0500007349.hg.1	9,34	10,85	10,35	6,68	6,68	ISL1
TC0700010719.hg.1	12,74	13,4	12,94	8,84	8,32	TBX20

Table 6.8: To highest fold change normalized fold changes (log2) for top 100 downregulated genes during the process of neuronal differentiation at ND2.

ID	Eto 48h Avg (log2)	ctr 48h Avg (log2)	GCNF 48h Avg (log2)	GCNFVP16 48h Avg (log2)	NGN2 48h Avg (log2)	Gene Symbol
TC0700008263.hg.1	-0,05	-0,01	0,00	-0,15	-0,08	DBF4
TC1500009795.hg.1	-0,02	-0,02	-0,02	-0,16	0,00	IGDCC3
TC2100007821.hg.1	-0,04	-0,09	0,00	-0,35	-0,27	ADAMTS1
TC0200006677.hg.1	-0,01	-0,05	0,00	-0,11	-0,05	RRM2
TC1000007885.hg.1	-0,13	-0,06	-0,17	0,00	-0,26	SRGN
TC1200009913.hg.1	-0,02	0,00	-0,05	-0,01	-0,20	YBX3
TC1800007298.hg.1	0,00	-0,04	-0,17	-0,37	-0,02	LIPG
TC0300009524.hg.1	0,00	-0,06	-0,08	-0,19	-0,13	ECT2
TC0300012164.hg.1	-0,01	-0,04	0,00	-0,09	-0,03	POLQ
TC0300006968.hg.1	-0,35	-0,24	-0,22	-0,50	0,00	CMTM7
TC1000006880.hg.1	0,00	-0,13	-0,11	-0,27	-0,07	PTER
TC0200013912.hg.1	-0,04	-0,02	0,00	-0,14	-0,11	CKAP2L
TC0300009119.hg.1	-0,18	0,00	-0,22	-0,63	-0,76	AGTR1
TC0100007243.hg.1	-0,22	-0,24	-0,11	0,00	-0,17	ALPL
TC0X00007936.hg.1	-0,03	0,00	-0,01	-0,19	-0,19	CENPI
TC0X00010851.hg.1	-0,02	-0,04	0,00	-0,33	-0,20	GPC3
TC0400011920.hg.1	-0,02	-0,02	0,00	-0,39	-0,42	SLC7A11
TC0100012328.hg.1	-0,01	-0,02	-0,01	0,00	-0,27	TRIM58
TC0800006869.hg.1	0,00	-0,03	-0,06	-0,13	-0,20	SLC7A2
TC1200006604.hg.1	-0,87	-0,92	-0,87	0,00	-0,81	CD9
TC0100012172.hg.1	-0,04	-0,07	0,00	-0,21	-0,15	EXO1
TC1300006919.hg.1	-0,04	0,00	-0,09	-0,25	-0,14	FREM2
TC1000012477.hg.1	0,00	-0,01	0,00	-0,13	-0,07	HELLS
TC0X00007537.hg.1	0,00	0,00	0,00	-0,18	-0,05	KIF4A
TC0700007345.hg.1	-0,19	-0,16	-0,19	-0,25	0,00	STK17A
TC1000010758.hg.1	0,00	-0,06	0,00	-0,14	-0,05	RTKN2
TC2100007198.hg.1	0,00	-0,06	-0,12	-0,17	-0,35	BACE2
TC1200012597.hg.1	-0,06	-0,11	0,00	-0,15	-0,29	MGST1
TC0500007415.hg.1	-0,01	0,00	-0,03	-0,28	-0,21	GPX8
TC0700008875.hg.1	-0,10	-0,09	0,00	-0,56	-0,68	MET
TC1500009756.hg.1	0,00	-0,03	-0,09	-0,19	-0,16	RBPMS2
TC0600007282.hg.1	0,00	-0,02	0,00	-0,16	-0,33	HIST1H2BF
TC0400008134.hg.1	0,00	-0,10	-0,02	-0,25	-0,56	MMRN1
TC1000012011.hg.1	-0,13	-0,09	0,00	-0,26	-0,07	RGS10
TC1800007316.hg.1	-0,04	0,00	-0,07	-0,13	-0,10	SKA1
TC0600008630.hg.1	-0,02	-0,02	0,00	-0,07	-0,05	TTK
TC0600013431.hg.1	0,00	-0,04	0,00	-0,03	-0,10	PLAGL1; HYMAI
TC1200011470.hg.1	0,00	-0,02	-0,01	-0,31	-0,20	DUSP6
TC0600007377.hg.1	-0,03	-0,03	0,00	-0,12	-0,17	HIST1H2BM
TC1600007958.hg.1	-0,03	-0,01	0,00	-0,29	-0,28	MT1L
TC0300010476.hg.1	0,00	-0,03	0,00	-0,07	-0,11	SGOL1
TC1600011399.hg.1	-0,04	-0,01	0,00	-0,35	-0,20	MT1X
TC1200009397.hg.1	-0,11	-0,20	-0,24	0,00	-0,21	FZD10
TC0600007700.hg.1	0,00	-0,01	-0,01	-0,16	-0,05	KIFC1
TC1500009738.hg.1	-0,06	-0,11	0,00	-0,36	-0,20	KIAA0101; CSNK1G1
TC1100012229.hg.1	-0,06	-0,12	0,00	-0,31	-0,38	KDELC2
TC1600011405.hg.1	0,00	-0,05	-0,02	-0,30	-0,16	GINS3
TC0600011635.hg.1	-0,05	0,00	-0,03	-0,30	-0,20	FKBP5
TC1800009268.hg.1	0,00	0,00	-0,02	-0,60	-0,23	DSC2
TC1800006484.hg.1	-0,10	-0,08	0,00	-0,23	-0,17	NDC80
TC1200010493.hg.1	-0,05	-0,11	-0,04	-0,25	0,00	DBX2
TC1400010715.hg.1	-0,03	-0,05	0,00	-0,55	-0,38	AJUBA
TC1200006946.hg.1	0,00	-0,02	-0,02	-0,19	-0,45	H2AFJ
TC0X00010512.hg.1	-0,12	-0,10	-0,04	-0,18	0,00	CHRDL1
TC0700007596.hg.1	-0,07	0,00	-0,01	-0,32	-0,20	EGFR
TC1100006525.hg.1	-0,09	-0,07	-0,05	0,00	-0,27	KRTAP5-5
TC0500007368.hg.1	0,00	-0,27	-0,22	-0,36	-0,54	ITGA2
TC0100008807.hg.1	0,00	-0,03	0,00	-0,34	-0,26	NEXN
TC0400012903.hg.1	-0,01	-0,04	0,00	-0,17	-0,01	PROM1
TC0600011130.hg.1	-0,25	0,00	-0,04	-0,28	-0,37	HIST1H4C
TC0600007290.hg.1	-0,02	-0,02	0,00	-0,10	-0,16	HIST1H2BH
TC0200009189.hg.1	-0,02	-0,02	0,00	-0,10	-0,09	GYPC
TC1100009097.hg.1	-0,04	0,00	-0,10	-0,32	-0,48	HTR3B
TC1100010418.hg.1	-0,02	-0,03	0,00	-0,15	-0,14	KIF18A
TC2000009462.hg.1	0,00	-0,02	-0,01	-0,29	0,00	SALL4
TC1700011364.hg.1	-0,01	0,00	-0,04	-0,26	-0,18	BRIP1
TC0100015049.hg.1	-0,02	-0,02	0,00	-0,29	-0,25	FRRS1
TC0300012367.hg.1	0,00	-0,02	-0,01	-0,26	-0,46	KIAA1257
TC0100006881.hg.1	-0,04	0,00	-0,04	-0,19	-0,09	TNFRSF1B; MIR4632; MIR7846
TC0100014910.hg.1	0,00	-0,03	-0,04	-0,24	-0,39	TGFBR3
TC1100010792.hg.1	-0,15	-0,06	-0,09	-0,04	0,00	FOLH1
TC0200008502.hg.1	0,00	-0,02	-0,02	-0,23	-0,15	NCAPH
TC2100007816.hg.1	-0,02	-0,04	0,00	-0,02	-0,16	CYYR1
TC0700010604.hg.1	-0,09	-0,14	0,00	-0,27	-0,10	CPVL
TC0400012620.hg.1	0,00	-0,03	-0,01	-0,19	-0,13	CENPU
TC1300006802.hg.1	-0,03	0,00	0,00	-0,23	-0,05	BRCA2
TC0100017733.hg.1	-0,02	-0,02	0,00	-0,15	-0,27	TSNAX
TC0600011818.hg.1	-0,08	-0,06	-0,11	0,00	-0,34	C6orf132
TC1800007014.hg.1	-0,04	-0,08	0,00	-0,19	-0,43	DSG2
TC0800010234.hg.1	-0,08	-0,08	0,00	-0,42	-0,18	SFRP1
TC0X00010837.hg.1	-0,06	-0,02	0,00	-0,06	-0,10	MBNL3
TC0100016254.hg.1	-0,43	-0,24	-0,54	0,00	-1,00	RXRG
TC1100007727.hg.1	0,00	-0,03	-0,01	-0,22	-0,12	FAM111B
TC0400008237.hg.1	-0,02	-0,05	0,00	-0,44	-0,45	MTTP
TC0100014202.hg.1	0,00	-0,04	-0,01	-0,29	-0,13	ORC1
TC0600007293.hg.1	-0,11	-0,08	0,00	-0,36	-0,44	HIST1H2BI
TC1200008041.hg.1	-0,08	-0,16	0,00	-0,29	-0,34	HMGA2
TC1100007453.hg.1	-0,02	-0,03	0,00	-0,18	-0,08	MDK
TC1500009505.hg.1	-0,04	-0,04	0,00	-0,44	-0,10	PRTG
TC0400011548.hg.1	0,00	-0,01	-0,03	-0,17	-0,02	LEF1
TC1700008511.hg.1	-0,21	0,00	0,00	-0,30	-0,64	TBX2
TC0800012388.hg.1	-0,12	0,00	-0,15	-0,33	-0,67	DLC1
TC1600007965.hg.1	-0,09	-0,04	0,00	-0,36	-0,58	MT1F
TC0400007371.hg.1	-0,08	-0,08	-0,09	0,00	-0,55	SHISA3
TC0200008793.hg.1	-0,12	0,00	0,00	-0,68	-0,83	SLC5A7
TC0300011956.hg.1	-0,15	-0,07	0,00	-0,18	-0,65	DPPA4
TC0100007457.hg.1	-0,08	-0,07	0,00	-0,47	-0,26	LIN28A
TC0500010651.hg.1	-0,05	0,00	-0,01	-0,38	-0,48	FGF10
TC0500007349.hg.1	-0,22	0,00	-0,07	-0,70	-0,70	ISL1
TC0700010719.hg.1	-0,07	0,00	-0,05	-0,60	-0,69	TBX20

Table 6.9: Fold Change (log2) for top 100 downregulated genes during the process of neuronal differentiation at ND7.

ID	Eto ND7 Avg (log2)	ctr ND7 Avg (log2)	GCNF ND7 Avg (log2)	GCNFVP16 ND7 Avg (log2)	NGN2 ND7 Avg (log2)	Gene Symbol
TC0700008263.hg.1	10,93	11,31	11,4	9,83	10,19	DBF4
TC1500009795.hg.1	14,67	14,58	15,17	12,81	14,82	IGDCC3
TC2100007821.hg.1	6,51	6,34	6,56	5,42	5,14	ADAMTS1
TC0200006677.hg.1	11,33	11,74	11,49	9,97	8,88	RRM2
TC1000007885.hg.1	9,19	8,67	9,09	9,62	8,56	SRGN
TC1200009913.hg.1	11,52	11,33	11,36	9,89	8,22	YBX3
TC1800007298.hg.1	9,37	9,35	9,01	6,66	6,95	LIPG
TC0300009524.hg.1	10,63	10,84	11,02	9,47	8,75	ECT2
TC0300012164.hg.1	8,83	8,61	8,79	7,58	7,33	POLQ
TC0300006968.hg.1	8,15	8,04	8,75	6,65	8,9	CMTM7
TC1000006880.hg.1	6,2	5,83	6,15	5,59	5,58	PTER
TC0200013912.hg.1	10,75	10,82	11,13	9,77	8,06	CKAP2L
TC0300009119.hg.1	6,08	6,15	5,59	4,83	4,75	AGTR1
TC0100007243.hg.1	6,01	6,37	6,73	5,99	6,14	ALPL
TC0X00007936.hg.1	8,44	8,64	9,46	8,14	7,46	CENPI
TC0X00010851.hg.1	8,12	8,36	8,39	7,17	8,36	GPC3
TC0400011920.hg.1	8,37	8,77	8,94	6,83	7,05	SLC7A11
TC0100012328.hg.1	7,34	7,34	7,94	7,62	6,43	TRIM58
TC0800006869.hg.1	6,73	6,67	6,38	6,16	5,43	SLC7A2
TC1200006604.hg.1	5,74	5,4	5,82	9,51	5,47	CD9
TC0100012172.hg.1	9,69	9,35	10,33	8,77	7,86	EXO1
TC1300006919.hg.1	5,58	5,69	5,74	5,59	4,84	FREM2
TC1000012477.hg.1	11,5	11,37	12,03	10,41	9,68	HELLS
TC0X00007537.hg.1	9,81	9,82	10,82	8,28	6,89	KIF4A
TC0700007345.hg.1	9,15	9,21	9,41	8,44	8,91	STK17A
TC1000010758.hg.1	11,84	11,63	12,04	10,88	9,96	RTKN2
TC2100007198.hg.1	5,91	6,11	7,19	5,98	4,95	BACE2
TC1200012597.hg.1	10,78	9,89	11,71	9,43	8,76	MGST1
TC0500007415.hg.1	7,18	6,98	8,03	5,48	5,69	GPX8
TC0700008875.hg.1	7,46	8,74	8,36	6,03	6,08	MET
TC1500009756.hg.1	7,87	7,78	8,37	6,33	6,06	RBPMS2
TC0600007282.hg.1	11,11	10,79	11,47	10,86	8,56	HIST1H2BF
TC0400008134.hg.1	8,45	7,74	8,98	6,22	5,94	MMRN1
TC1000012011.hg.1	6,84	6,42	7,37	5,45	8,17	RGS10
TC1800007316.hg.1	7,61	7,69	7,77	6,69	5,96	SKA1
TC0600008630.hg.1	11,9	12,01	12,45	10,69	9,33	TTK
TC0600013431.hg.1	8,08	8,62	8,44	8,34	8,03	PLAGL1; HYMAI
TC1200011470.hg.1	9,09	9,35	9,56	9,24	9,59	DUSP6
TC0600007377.hg.1	13,86	13,67	14,79	13,61	10,8	HIST1H2BM
TC1600007958.hg.1	13,1	13,24	12,87	12,06	10,42	MT1L
TC0300010476.hg.1	10,36	10,5	10,84	9,25	8,09	SGOL1
TC1600011399.hg.1	14,18	14,67	14,43	12,73	12,43	MT1X
TC1200009397.hg.1	8,26	7,48	8,38	8,37	7,43	FZD10
TC0600007700.hg.1	10,83	10,44	10,78	9,26	8,07	KIFC1
TC1500009738.hg.1	9,54	9,77	10,06	8,53	7,32	KIAA0101; CSNK1G1
TC1100012229.hg.1	8,13	8,26	8,83	7,53	5,67	KDELC2
TC1600011405.hg.1	8,9	8,54	9,4	8,26	7,17	GINS3
TC0600011635.hg.1	9,96	10,01	10,53	8,09	9,25	FKBP5
TC1800009268.hg.1	7,46	7,68	7,81	5,85	7,98	DSC2
TC1800006484.hg.1	10,59	10,63	10,69	9,26	8,06	NDC80
TC1200010493.hg.1	10,89	10,44	11,26	8,51	10,44	DBX2
TC1400010715.hg.1	10,09	9,72	10,5	7,07	6,02	AJUBA
TC1200006946.hg.1	9,06	8,54	8,91	8,83	6,64	H2AFJ
TC0X00010512.hg.1	8,39	8,56	8,64	7,66	8,85	CHRDL1
TC0700007596.hg.1	7,01	7,04	7,82	5,92	7,83	EGFR
TC1100006525.hg.1	8,05	8,16	7,59	8,11	6,91	KRTAP5-5
TC0500007368.hg.1	6,55	6,2	6,32	5,46	4,81	ITGA2
TC0100008807.hg.1	7,63	7,53	8,02	5,98	6,32	NEXN
TC0400012903.hg.1	12,67	12,17	13,1	10,73	10,37	PROM1
TC0600011130.hg.1	9,57	9,89	10,44	9,87	6,84	HIST1H4C
TC0600007290.hg.1	13,61	13,44	14,19	13,29	11,61	HIST1H2BH
TC0200009189.hg.1	8,98	8,1	9,14	6,95	7,26	GYPC
TC1100009097.hg.1	6,8	7,01	5,48	5,13	5,55	HTR3B
TC1100010418.hg.1	11,35	11,54	11,86	10,07	8,54	KIF18A
TC2000009462.hg.1	11,09	10,43	11,54	8,79	10,51	SALL4
TC1700011364.hg.1	9,14	9,59	9,96	8,28	7,84	BRIP1
TC0100015049.hg.1	6,82	7,06	7,66	6,39	6,09	FRRS1
TC0300012367.hg.1	9,43	9,81	10,14	8,62	6,45	KIAA1257
TC0100006881.hg.1	9,4	9,35	8,98	8,26	8,68	TNFRSF1B; MIR4632; MIR7846
TC0100014910.hg.1	8,49	8,63	8,53	6,45	5,05	TGFBR3
TC1100010792.hg.1	8,16	9,15	10,5	7,98	12,09	FOLH1
TC0200008502.hg.1	11,49	11,6	11,65	9,78	8,22	NCAPH
TC2100007816.hg.1	10,38	10,19	10,71	8,98	8,7	CYYR1
TC0700010604.hg.1	6,13	5,8	6,33	5,38	5,13	CPVL
TC0400012620.hg.1	11,34	11,23	11,56	10,75	9,29	CENPU
TC1300006802.hg.1	9,02	9,38	10,1	8,25	7,7	BRCA2
TC0100017733.hg.1	7,06	6,92	7,08	6,94	5,15	TSNAX
TC0600011818.hg.1	10,22	10,1	10,13	9,8	8,41	C6orf132
TC1800007014.hg.1	7,58	7,46	8,12	6,26	6,31	DSG2
TC0800010234.hg.1	9,35	10,1	10,95	8,48	8,88	SFRP1
TC0X00010837.hg.1	8,47	8,91	9,05	8,18	7,65	MBNL3
TC0100016254.hg.1	5,93	6,77	5,43	5,21	4,77	RXRG
TC1100007727.hg.1	10,26	10,36	11,42	9,29	8,09	FAM111B
TC0400008237.hg.1	11,47	11,5	12,26	8,76	7,87	MTTP
TC0100014202.hg.1	9,55	9,77	10,13	8,37	7,41	ORC1
TC0600007293.hg.1	8,34	8,34	10,15	7,95	5,9	HIST1H2BI
TC1200008041.hg.1	8,07	8,02	8,57	7,56	6,5	HMGA2
TC1100007453.hg.1	13,04	13,17	13,87	10,97	11,24	MDK
TC1500009505.hg.1	13,9	13,69	14,39	10,71	12,78	PRTG
TC0400011548.hg.1	10,72	10,73	10,4	9,61	9,67	LEF1
TC1700008511.hg.1	6,48	7,62	9,07	6,52	5,95	TBX2
TC0800012388.hg.1	6,47	7,02	7,67	5,29	5,27	DLC1
TC1600007965.hg.1	10,92	11,6	11,36	9,38	8,38	MT1F
TC0400007371.hg.1	9,32	9,84	9,94	9,44	6,91	SHISA3
TC0200008793.hg.1	8,25	9,25	9,62	6,45	6,43	SLC5A7
TC0300011956.hg.1	9,02	9,09	9,39	8,23	6,3	DPPA4
TC0100007457.hg.1	8,79	8,41	10,2	7,85	7,77	LIN28A
TC0500010651.hg.1	9,57	10,19	10,57	8,1	7,17	FGF10
TC0500007349.hg.1	6,8	8,5	7,94	5,94	6,03	ISL1
TC0700010719.hg.1	9,92	10,98	11,97	7,58	7,82	TBX20

Table 6.10: To highest fold change normalized fold changes (log2) for top 100 downregulated genes during the process of neuronal differentiation at ND7.

ID	Eto ND7 Avg (log2)	ctr ND7 Avg (log2)	GCNF ND7 Avg (log2)	GCNFVP16 ND7 Avg (log2)	NGN2 ND7 Avg (log2)	Gene Symbol
TC0700008263.hg.1	-0,06	-0,01	0,00	-0,21	-0,16	DBF4
TC1500009795.hg.1	-0,05	-0,06	0,00	-0,24	-0,03	IGDCC3
TC2100007821.hg.1	-0,01	-0,05	0,00	-0,28	-0,35	ADAMTS1
TC0200006677.hg.1	-0,05	0,00	-0,03	-0,24	-0,40	RRM2
TC1000007885.hg.1	-0,07	-0,15	-0,08	0,00	-0,17	SRGN
TC1200009913.hg.1	0,00	-0,02	-0,02	-0,22	-0,49	YBX3
TC1800007298.hg.1	0,00	0,00	-0,06	-0,49	-0,43	LIPG
TC0300009524.hg.1	-0,05	-0,02	0,00	-0,22	-0,33	ECT2
TC0300012164.hg.1	0,00	-0,04	-0,01	-0,22	-0,27	POLQ
TC0300006968.hg.1	-0,13	-0,15	-0,02	-0,42	0,00	CMTM7
TC1000006880.hg.1	0,00	-0,09	-0,01	-0,15	-0,15	PTER
TC0200013912.hg.1	-0,05	-0,04	0,00	-0,19	-0,47	CKAP2L
TC0300009119.hg.1	-0,02	0,00	-0,14	-0,35	-0,37	AGTR1
TC0100007243.hg.1	-0,16	-0,08	0,00	-0,17	-0,13	ALPL
TC0X00007936.hg.1	-0,16	-0,13	0,00	-0,22	-0,34	CENPI
TC0X00010851.hg.1	-0,05	-0,01	0,00	-0,23	-0,01	GPC3
TC0400011920.hg.1	-0,10	-0,03	0,00	-0,39	-0,34	SLC7A11
TC0100012328.hg.1	-0,11	-0,11	0,00	-0,06	-0,30	TRIM58
TC0800006869.hg.1	0,00	-0,01	-0,08	-0,13	-0,31	SLC7A2
TC1200006604.hg.1	-0,73	-0,82	-0,71	0,00	-0,80	CD9
TC0100012172.hg.1	-0,09	-0,14	0,00	-0,24	-0,39	EXO1
TC1300006919.hg.1	-0,04	-0,01	0,00	-0,04	-0,25	FREM2
TC1000012477.hg.1	-0,07	-0,08	0,00	-0,21	-0,31	HELLS
TC0X00007537.hg.1	-0,14	-0,14	0,00	-0,39	-0,65	KIF4A
TC0700007345.hg.1	-0,04	-0,03	0,00	-0,16	-0,08	STK17A
TC1000010758.hg.1	-0,02	-0,05	0,00	-0,15	-0,27	RTKN2
TC2100007198.hg.1	-0,28	-0,23	0,00	-0,27	-0,54	BACE2
TC1200012597.hg.1	-0,12	-0,24	0,00	-0,31	-0,42	MGST1
TC0500007415.hg.1	-0,16	-0,20	0,00	-0,55	-0,50	GPX8
TC0700008875.hg.1	-0,23	0,00	-0,06	-0,54	-0,52	MET
TC1500009756.hg.1	-0,09	-0,11	0,00	-0,40	-0,47	RBPMS2
TC0600007282.hg.1	-0,05	-0,09	0,00	-0,08	-0,42	HIST1H2BF
TC0400008134.hg.1	-0,09	-0,21	0,00	-0,53	-0,60	MMRN1
TC1000012011.hg.1	-0,26	-0,35	-0,15	-0,58	0,00	RGS10
TC1800007316.hg.1	-0,03	-0,01	0,00	-0,22	-0,38	SKA1
TC0600008630.hg.1	-0,07	-0,05	0,00	-0,22	-0,42	TTK
TC0600013431.hg.1	-0,09	0,00	-0,03	-0,05	-0,10	PLAGL1; HYMAI
TC1200011470.hg.1	-0,08	-0,04	0,00	-0,05	0,00	DUSP6
TC0600007377.hg.1	-0,09	-0,11	0,00	-0,12	-0,45	HIST1H2BM
TC1600007958.hg.1	-0,02	0,00	-0,04	-0,13	-0,35	MT1L
TC0300010476.hg.1	-0,07	-0,05	0,00	-0,23	-0,42	SGOL1
TC1600011399.hg.1	-0,05	0,00	-0,02	-0,20	-0,24	MT1X
TC1200009397.hg.1	-0,02	-0,16	0,00	0,00	-0,17	FZD10
TC0600007700.hg.1	0,00	-0,05	-0,01	-0,23	-0,42	KIFC1
TC1500009738.hg.1	-0,08	-0,04	0,00	-0,24	-0,46	KIAA0101; CSNK1G1
TC1100012229.hg.1	-0,12	-0,10	0,00	-0,23	-0,64	KDELC2
TC1600011405.hg.1	-0,08	-0,14	0,00	-0,19	-0,39	GINS3
TC0600011635.hg.1	-0,08	-0,07	0,00	-0,38	-0,19	FKBP5
TC1800009268.hg.1	-0,10	-0,06	-0,03	-0,45	0,00	DSC2
TC1800006484.hg.1	-0,01	-0,01	0,00	-0,21	-0,41	NDC80
TC1200010493.hg.1	-0,05	-0,11	0,00	-0,40	-0,11	DBX2
TC1400010715.hg.1	-0,06	-0,11	0,00	-0,57	-0,80	AJUBA
TC1200006946.hg.1	0,00	-0,09	-0,02	-0,04	-0,45	H2AFJ
TC0X00010512.hg.1	-0,08	-0,05	-0,03	-0,21	0,00	CHRDL1
TC0700007596.hg.1	-0,16	-0,15	0,00	-0,40	0,00	EGFR
TC1100006525.hg.1	-0,02	0,00	-0,10	-0,01	-0,24	KRTAP5-5
TC0500007368.hg.1	0,00	-0,08	-0,05	-0,26	-0,45	ITGA2
TC0100008807.hg.1	-0,07	-0,09	0,00	-0,42	-0,34	NEXN
TC0400012903.hg.1	-0,05	-0,11	0,00	-0,29	-0,34	PROM1
TC0600011130.hg.1	-0,13	-0,08	0,00	-0,08	-0,61	HIST1H4C
TC0600007290.hg.1	-0,06	-0,08	0,00	-0,09	-0,29	HIST1H2BH
TC0200009189.hg.1	-0,03	-0,17	0,00	-0,40	-0,33	GYPC
TC1100009097.hg.1	-0,04	0,00	-0,36	-0,45	-0,34	HTR3B
TC1100010418.hg.1	-0,06	-0,04	0,00	-0,24	-0,47	KIF18A
TC2000009462.hg.1	-0,06	-0,15	0,00	-0,39	-0,13	SALL4
TC1700011364.hg.1	-0,12	-0,05	0,00	-0,27	-0,35	BRIP1
TC0100015049.hg.1	-0,17	-0,12	0,00	-0,26	-0,33	FRRS1
TC0300012367.hg.1	-0,10	-0,05	0,00	-0,23	-0,65	KIAA1257
TC0100006881.hg.1	0,00	-0,01	-0,07	-0,19	-0,11	TNFRSF1B; MIR4632; MIR7846
TC0100014910.hg.1	-0,02	0,00	-0,02	-0,42	-0,77	TGFBR3
TC1100010792.hg.1	-0,57	-0,40	-0,20	-0,60	0,00	FOLH1
TC0200008502.hg.1	-0,02	-0,01	0,00	-0,25	-0,50	NCAPH
TC2100007816.hg.1	-0,05	-0,07	0,00	-0,25	-0,30	CYYR1
TC0700010604.hg.1	-0,05	-0,13	0,00	-0,23	-0,30	CPVL
TC0400012620.hg.1	-0,03	-0,04	0,00	-0,10	-0,32	CENPU
TC1300006802.hg.1	-0,16	-0,11	0,00	-0,29	-0,39	BRCA2
TC0100017733.hg.1	0,00	-0,03	0,00	-0,03	-0,46	TSNAX
TC0600011818.hg.1	0,00	-0,02	-0,01	-0,06	-0,28	C6orf132
TC1800007014.hg.1	-0,10	-0,12	0,00	-0,38	-0,36	DSG2
TC0800010234.hg.1	-0,23	-0,12	0,00	-0,37	-0,30	SFRP1
TC0X00010837.hg.1	-0,10	-0,02	0,00	-0,15	-0,24	MBNL3
TC0100016254.hg.1	-0,19	0,00	-0,32	-0,38	-0,51	RXRG
TC1100007727.hg.1	-0,15	-0,14	0,00	-0,30	-0,50	FAM111B
TC0400008237.hg.1	-0,10	-0,09	0,00	-0,48	-0,64	MTTP
TC0100014202.hg.1	-0,09	-0,05	0,00	-0,28	-0,45	ORC1
TC0600007293.hg.1	-0,28	-0,28	0,00	-0,35	-0,78	HIST1H2BI
TC1200008041.hg.1	-0,09	-0,10	0,00	-0,18	-0,40	HMGA2
TC1100007453.hg.1	-0,09	-0,07	0,00	-0,34	-0,30	MDK
TC1500009505.hg.1	-0,05	-0,07	0,00	-0,43	-0,17	PRTG
TC0400011548.hg.1	0,00	0,00	-0,05	-0,16	-0,15	LEF1
TC1700008511.hg.1	-0,49	-0,25	0,00	-0,48	-0,61	TBX2
TC0800012388.hg.1	-0,25	-0,13	0,00	-0,54	-0,54	DLC1
TC1600007965.hg.1	-0,09	0,00	-0,03	-0,31	-0,47	MT1F
TC0400007371.hg.1	-0,09	-0,01	0,00	-0,07	-0,52	SHISA3
TC0200008793.hg.1	-0,22	-0,06	0,00	-0,58	-0,58	SLC5A7
TC0300011956.hg.1	-0,06	-0,05	0,00	-0,19	-0,58	DPPA4
TC0100007457.hg.1	-0,21	-0,28	0,00	-0,38	-0,39	LIN28A
TC0500010651.hg.1	-0,14	-0,05	0,00	-0,38	-0,56	FGF10
TC0500007349.hg.1	-0,32	0,00	-0,10	-0,52	-0,50	ISL1
TC0700010719.hg.1	-0,27	-0,12	0,00	-0,66	-0,61	TBX20

Table 6.11: Fold Change (log2) for top 100 downregulated genes during the process of neuronal differentiation at ND14.

ID	Eto ND15 Avg (log2)	ctr ND15 Avg (log2)	GCNF ND15 Avg (log2)	GCNFVP16 ND15 Avg (log2)	NGN2 ND15 Avg (log2)	Gene Symbol
TC0700008263.hg.1	9,44	9,64	10,25	8,97	9,81	DBF4
TC1500009795.hg.1	13,59	13,09	14,4	11,2	13,29	IGDCC3
TC2100007821.hg.1	4,99	4,81	5,62	4,63	5,22	ADAMTS1
TC0200006677.hg.1	9,48	10,04	10,44	8,91	7,76	RRM2
TC1000007885.hg.1	6,79	7,13	6,66	7,86	6,8	SRGN
TC1200009913.hg.1	9,77	9,63	9,78	8,28	7,77	YBX3
TC1800007298.hg.1	7,68	7,37	8,23	6,99	6,82	LIPG
TC0300009524.hg.1	8,78	9,05	9,94	8,26	8,28	ECT2
TC0300012164.hg.1	7,11	7,45	7,94	6,53	5,51	POLQ
TC0300006968.hg.1	7,1	6,74	7,94	5,71	7,75	CMTM7
TC1000006880.hg.1	4,86	4,7	4,25	4,14	4,55	PTER
TC0200013912.hg.1	8,09	8,83	9,25	7,9	7,3	CKAP2L
TC0300009119.hg.1	4,66	4,17	5,2	4,18	4,66	AGTR1
TC0100007243.hg.1	4,99	4,59	5,67	4,73	4,93	ALPL
TC0X00007936.hg.1	7,61	7,9	8,02	6,88	7,09	CENPI
TC0X00010851.hg.1	6,99	7,66	7,31	6,87	9,16	GPC3
TC0400011920.hg.1	7,13	7,92	7,89	6,29	6,71	SLC7A11
TC0100012328.hg.1	5,63	5,63	5,66	5,67	6	TRIM58
TC0800006869.hg.1	5	4,91	5,59	4,59	4,53	SLC7A2
TC1200006604.hg.1	4,36	4,51	4,81	7,2	4,28	CD9
TC0100012172.hg.1	7,91	8,12	8,35	6,9	6,28	EXO1
TC1300006919.hg.1	4,16	4,44	4,5	4,28	4,21	FREM2
TC1000012477.hg.1	10,26	10,56	10,84	9,67	8,92	HELLS
TC0X00007537.hg.1	7,98	8,37	9,04	7,04	6,26	KIF4A
TC0700007345.hg.1	7,45	7,81	8,47	7,53	7,76	STK17A
TC1000010758.hg.1	9,81	10,37	10,73	10,18	8,85	RTKN2
TC2100007198.hg.1	5,01	4,99	5,58	4,48	4,21	BACE2
TC1200012597.hg.1	11,19	9,89	11	9,6	9,25	MGST1
TC0500007415.hg.1	6,38	6,65	7,85	5,65	5,22	GPX8
TC0700008875.hg.1	7,03	6,39	6,84	5,39	6	MET
TC1500009756.hg.1	6,96	6,23	7,82	4,99	5,67	RBPMS2
TC0600007282.hg.1	9,36	9,74	9,62	9,31	9,65	HIST1H2BF
TC0400008134.hg.1	7,71	7,25	7,58	6,1	5,39	MMRN1
TC1000012011.hg.1	4,44	5,02	5,43	4,11	6,03	RGS10
TC1800007316.hg.1	5,98	5,95	6,52	5,48	5,4	SKA1
TC0600008630.hg.1	9,7	9,92	11	9,04	8,61	TTK
TC0600013431.hg.1	7,09	7,65	7,31	7,76	7,51	PLAGL1; HYMAI
TC1200011470.hg.1	7,27	7,87	7,99	8,12	8,45	DUSP6
TC0600007377.hg.1	12,84	12,6	13,6	11,7	10,15	HIST1H2BM
TC1600007958.hg.1	10,03	10,33	10,58	10,35	9,73	MT1L
TC0300010476.hg.1	8,6	8,56	9,39	7,85	6,86	SGOL1
TC1600011399.hg.1	11,41	11,96	12,5	10,47	10,33	MT1X
TC1200009397.hg.1	6,89	6,39	7,01	6,29	5,34	FZD10
TC0600007700.hg.1	8,57	9,15	9,94	7,75	6,98	KIFC1
TC1500009738.hg.1	7,81	8,38	9,01	6,75	6,52	KIAA0101; CSNK1G1
TC1100012229.hg.1	6,61	6,62	7,85	6,38	5,72	KDELC2
TC1600011405.hg.1	7,03	7,71	7,34	6,8	6,74	GINS3
TC0600011635.hg.1	8,62	8,95	9,5	7,53	8,36	FKBP5
TC1800009268.hg.1	6,36	5,89	7,71	4,86	7,45	DSC2
TC1800006484.hg.1	8,13	8,92	9,47	7,68	7,2	NDC80
TC1200010493.hg.1	8,57	8,94	10,12	8,2	8,71	DBX2
TC1400010715.hg.1	8,38	8,08	8,38	6,56	5,81	AJUBA
TC1200006946.hg.1	6,56	6,63	6,91	6,28	6,29	H2AFJ
TC0X00010512.hg.1	6,78	6,61	7,3	7,22	8,38	CHRDL1
TC0700007596.hg.1	6,39	6,01	7,18	6,58	6,8	EGFR
TC1100006525.hg.1	5,51	5,55	5,28	5,83	5,83	KRTAP5-5
TC0500007368.hg.1	4,59	4,53	4,15	4,27	3,91	ITGA2
TC0100008807.hg.1	6,53	6,12	6,41	6,13	5,38	NEXN
TC0400012903.hg.1	11,2	11,07	11,66	9,89	9,08	PROM1
TC0600011130.hg.1	6,94	6,99	7,12	6,17	6,62	HIST1H4C
TC0600007290.hg.1	11,69	11,71	12,01	10,97	10,33	HIST1H2BH
TC0200009189.hg.1	7,06	7,08	7,64	6,08	7,15	GYPC
TC1100009097.hg.1	5,26	5,41	5,07	5,03	5,48	HTR3B
TC1100010418.hg.1	9,07	9,33	9,86	8,5	7,73	KIF18A
TC2000009462.hg.1	9,87	9,36	10,58	9,14	9,55	SALL4
TC1700011364.hg.1	7,82	8,43	8,83	7,54	7,37	BRIP1
TC0100015049.hg.1	5,81	5,7	5,66	5,19	4,61	FRRS1
TC0300012367.hg.1	8,32	7,83	8,6	7,47	6,48	KIAA1257
TC0100006881.hg.1	7,56	7,21	8,28	7,21	7,79	TNFRSF1B; MIR4632; MIR7846
TC0100014910.hg.1	6,72	6,56	6,96	5,47	5,53	TGFBR3
TC1100010792.hg.1	6,27	6,37	8,39	5,59	10,07	FOLH1
TC0200008502.hg.1	8,76	9,05	9,78	7,82	7,33	NCAPH
TC2100007816.hg.1	8,59	8,37	9,09	7,35	7,52	CYYR1
TC0700010604.hg.1	5,05	4,74	4,73	4,91	4,72	CPVL
TC0400012620.hg.1	9,25	9,82	10,16	9,26	8,11	CENPU
TC1300006802.hg.1	7,92	8,36	9,23	7,4	6,79	BRCA2
TC0100017733.hg.1	4,46	4,25	4,44	4,77	5,06	TSNAX
TC0600011818.hg.1	7,43	7,62	7,53	7,35	7,4	C6orf132
TC1800007014.hg.1	5,79	6,32	6,74	5,08	5,64	DSG2
TC0800010234.hg.1	7,52	7,81	10,11	7,74	8,74	SFRP1
TC0X00010837.hg.1	6,76	7,62	7,4	6,65	6,94	MBNL3
TC0100016254.hg.1	4,18	4,52	4,55	3,98	5,58	RXRG
TC1100007727.hg.1	8,59	8,7	9,5	7,37	6,69	FAM111B
TC0400008237.hg.1	8,89	9,42	10,56	8,92	7,46	MTTP
TC0100014202.hg.1	7,39	7,75	8,42	6,78	6,64	ORC1
TC0600007293.hg.1	7,08	6,98	7,85	5,98	5,57	HIST1H2BI
TC1200008041.hg.1	6,33	6,16	6,29	5,99	5,8	HMGA2
TC1100007453.hg.1	11,06	11,24	12,38	10,13	10,45	MDK
TC1500009505.hg.1	11,69	11,79	12,76	9,73	11,68	PRTG
TC0400011548.hg.1	8,69	8,78	8,79	8,56	8,52	LEF1
TC1700008511.hg.1	4,76	5,2	6,08	4,83	5,08	TBX2
TC0800012388.hg.1	4,41	4,42	4,54	4,76	5,41	DLC1
TC1600007965.hg.1	6,81	7,9	7,87	7,4	6,97	MT1F
TC0400007371.hg.1	6,44	6,38	7,11	6,86	6,68	SHISA3
TC0200008793.hg.1	5,95	6,21	6,92	5,11	6,49	SLC5A7
TC0300011956.hg.1	6,04	5,93	7,2	6,09	5,89	DPPA4
TC0100007457.hg.1	6,19	5,93	6,27	5,94	6,44	LIN28A
TC0500010651.hg.1	6,38	6,78	7,34	6,03	6,27	FGF10
TC0500007349.hg.1	4,63	4,5	4,97	4,53	5,57	ISL1
TC0700010719.hg.1	6,32	6,6	7,4	6,05	6,75	TBX20

Table 6.12: To highest fold change normalized fold changes (log2) for top 100 downregulated genes during the process of neuronal differentiation at ND14.

ID	Eto ND15 Avg (log2)	ctr ND15 Avg (log2)	GCNF ND15 Avg (log2)	GCNFVP16 ND15 Avg (log2)	NGN2 ND15 Avg (log2)	Gene Symbol
TC0700008263.hg.1	-0,12	-0,09	0,00	-0,19	-0,06	DBF4
TC1500009795.hg.1	-0,08	-0,14	0,00	-0,36	-0,12	IGDCC3
TC2100007821.hg.1	-0,17	-0,22	0,00	-0,28	-0,11	ADAMTS1
TC0200006677.hg.1	-0,14	-0,06	0,00	-0,23	-0,43	RRM2
TC1000007885.hg.1	-0,21	-0,14	-0,24	0,00	-0,21	SRGN
TC1200009913.hg.1	0,00	-0,02	0,00	-0,24	-0,33	YBX3
TC1800007298.hg.1	-0,10	-0,16	0,00	-0,24	-0,27	LIPG
TC0300009524.hg.1	-0,18	-0,14	0,00	-0,27	-0,26	ECT2
TC0300012164.hg.1	-0,16	-0,09	0,00	-0,28	-0,53	POLQ
TC0300006968.hg.1	-0,16	-0,24	0,00	-0,48	-0,03	CMTM7
TC1000006880.hg.1	0,00	-0,05	-0,19	-0,23	-0,10	PTER
TC0200013912.hg.1	-0,19	-0,07	0,00	-0,23	-0,34	CKAP2L
TC0300009119.hg.1	-0,16	-0,32	0,00	-0,32	-0,16	AGTR1
TC0100007243.hg.1	-0,18	-0,30	0,00	-0,26	-0,20	ALPL
TC0X00007936.hg.1	-0,08	-0,02	0,00	-0,22	-0,18	CENPI
TC0X00010851.hg.1	-0,39	-0,26	-0,33	-0,42	0,00	GPC3
TC0400011920.hg.1	-0,15	0,00	-0,01	-0,33	-0,24	SLC7A11
TC0100012328.hg.1	-0,09	-0,09	-0,08	-0,08	0,00	TRIM58
TC0800006869.hg.1	-0,16	-0,19	0,00	-0,28	-0,30	SLC7A2
TC1200006604.hg.1	-0,72	-0,67	-0,58	0,00	-0,75	CD9
TC0100012172.hg.1	-0,08	-0,04	0,00	-0,28	-0,41	EXO1
TC1300006919.hg.1	-0,11	-0,02	0,00	-0,07	-0,10	FREM2
TC1000012477.hg.1	-0,08	-0,04	0,00	-0,16	-0,28	HELLS
TC0X00007537.hg.1	-0,18	-0,11	0,00	-0,36	-0,53	KIF4A
TC0700007345.hg.1	-0,19	-0,12	0,00	-0,17	-0,13	STK17A
TC1000010758.hg.1	-0,13	-0,05	0,00	-0,08	-0,28	RTKN2
TC2100007198.hg.1	-0,16	-0,16	0,00	-0,32	-0,41	BACE2
TC1200012597.hg.1	0,00	-0,18	-0,02	-0,22	-0,27	MGST1
TC0500007415.hg.1	-0,30	-0,24	0,00	-0,47	-0,59	GPX8
TC0700008875.hg.1	0,00	-0,14	-0,04	-0,38	-0,23	MET
TC1500009756.hg.1	-0,17	-0,33	0,00	-0,65	-0,46	RBPMS2
TC0600007282.hg.1	-0,06	0,00	-0,02	-0,07	-0,01	HIST1H2BF
TC0400008134.hg.1	0,00	-0,09	-0,02	-0,34	-0,52	MMRN1
TC1000012011.hg.1	-0,44	-0,26	-0,15	-0,55	0,00	RGS10
TC1800007316.hg.1	-0,12	-0,13	0,00	-0,25	-0,27	SKA1
TC0600008630.hg.1	-0,18	-0,15	0,00	-0,28	-0,35	TTK
TC0600013431.hg.1	-0,13	-0,02	-0,09	0,00	-0,05	PLAGL1; HYMAI
TC1200011470.hg.1	-0,22	-0,10	-0,08	-0,06	0,00	DUSP6
TC0600007377.hg.1	-0,08	-0,11	0,00	-0,22	-0,42	HIST1H2BM
TC1600007958.hg.1	-0,08	-0,03	0,00	-0,03	-0,12	MT1L
TC0300010476.hg.1	-0,13	-0,13	0,00	-0,26	-0,45	SGOL1
TC1600011399.hg.1	-0,13	-0,06	0,00	-0,26	-0,28	MT1X
TC1200009397.hg.1	-0,02	-0,13	0,00	-0,16	-0,39	FZD10
TC0600007700.hg.1	-0,21	-0,12	0,00	-0,36	-0,51	KIFC1
TC1500009738.hg.1	-0,21	-0,10	0,00	-0,42	-0,47	KIAA0101; CSNK1G1
TC1100012229.hg.1	-0,25	-0,25	0,00	-0,30	-0,46	KDELC2
TC1600011405.hg.1	-0,13	0,00	-0,07	-0,18	-0,19	GINS3
TC0600011635.hg.1	-0,14	-0,09	0,00	-0,34	-0,18	FKBP5
TC1800009268.hg.1	-0,28	-0,39	0,00	-0,67	-0,05	DSC2
TC1800006484.hg.1	-0,22	-0,09	0,00	-0,30	-0,40	NDC80
TC1200010493.hg.1	-0,24	-0,18	0,00	-0,30	-0,22	DBX2
TC1400010715.hg.1	0,00	-0,05	0,00	-0,35	-0,53	AJUBA
TC1200006946.hg.1	-0,07	-0,06	0,00	-0,14	-0,14	H2AFJ
TC0X00010512.hg.1	-0,31	-0,34	-0,20	-0,21	0,00	CHRDL1
TC0700007596.hg.1	-0,17	-0,26	0,00	-0,13	-0,08	EGFR
TC1100006525.hg.1	-0,08	-0,07	-0,14	0,00	0,00	KRTAP5-5
TC0500007368.hg.1	0,00	-0,02	-0,15	-0,10	-0,23	ITGA2
TC0100008807.hg.1	0,00	-0,09	-0,03	-0,09	-0,28	NEXN
TC0400012903.hg.1	-0,06	-0,07	0,00	-0,24	-0,36	PROM1
TC0600011130.hg.1	-0,04	-0,03	0,00	-0,21	-0,11	HIST1H4C
TC0600007290.hg.1	-0,04	-0,04	0,00	-0,13	-0,22	HIST1H2BH
TC0200009189.hg.1	-0,11	-0,11	0,00	-0,33	-0,10	GYPC
TC1100009097.hg.1	-0,06	-0,02	-0,11	-0,12	0,00	HTR3B
TC1100010418.hg.1	-0,12	-0,08	0,00	-0,21	-0,35	KIF18A
TC2000009462.hg.1	-0,10	-0,18	0,00	-0,21	-0,15	SALL4
TC1700011364.hg.1	-0,18	-0,07	0,00	-0,23	-0,26	BRIP1
TC0100015049.hg.1	0,00	-0,03	-0,04	-0,16	-0,33	FRRS1
TC0300012367.hg.1	-0,05	-0,14	0,00	-0,20	-0,41	KIAA1257
TC0100006881.hg.1	-0,13	-0,20	0,00	-0,20	-0,09	TNFRSF1B; MIR4632; MIR7846
TC0100014910.hg.1	-0,05	-0,09	0,00	-0,35	-0,33	TGFBR3
TC1100010792.hg.1	-0,68	-0,66	-0,26	-0,85	0,00	FOLH1
TC0200008502.hg.1	-0,16	-0,11	0,00	-0,32	-0,42	NCAPH
TC2100007816.hg.1	-0,08	-0,12	0,00	-0,31	-0,27	CYYR1
TC0700010604.hg.1	0,00	-0,09	-0,09	-0,04	-0,10	CPVL
TC0400012620.hg.1	-0,14	-0,05	0,00	-0,13	-0,33	CENPU
TC1300006802.hg.1	-0,22	-0,14	0,00	-0,32	-0,44	BRCA2
TC0100017733.hg.1	-0,18	-0,25	-0,19	-0,09	0,00	TSNAX
TC0600011818.hg.1	-0,04	0,00	-0,02	-0,05	-0,04	C6orf132
TC1800007014.hg.1	-0,22	-0,09	0,00	-0,41	-0,26	DSG2
TC0800010234.hg.1	-0,43	-0,37	0,00	-0,39	-0,21	SFRP1
TC0X00010837.hg.1	-0,17	0,00	-0,04	-0,20	-0,13	MBNL3
TC0100016254.hg.1	-0,42	-0,30	-0,29	-0,49	0,00	RXRG
TC1100007727.hg.1	-0,15	-0,13	0,00	-0,37	-0,51	FAM111B
TC0400008237.hg.1	-0,25	-0,16	0,00	-0,24	-0,50	MTTP
TC0100014202.hg.1	-0,19	-0,12	0,00	-0,31	-0,34	ORC1
TC0600007293.hg.1	-0,15	-0,17	0,00	-0,39	-0,50	HIST1H2BI
TC1200008041.hg.1	0,00	-0,04	-0,01	-0,08	-0,13	HMGA2
TC1100007453.hg.1	-0,16	-0,14	0,00	-0,29	-0,24	MDK
TC1500009505.hg.1	-0,13	-0,11	0,00	-0,39	-0,13	PRTG
TC0400011548.hg.1	-0,02	0,00	0,00	-0,04	-0,05	LEF1
TC1700008511.hg.1	-0,35	-0,23	0,00	-0,33	-0,26	TBX2
TC0800012388.hg.1	-0,29	-0,29	-0,25	-0,18	0,00	DLC1
TC1600007965.hg.1	-0,21	0,00	-0,01	-0,09	-0,18	MT1F
TC0400007371.hg.1	-0,14	-0,16	0,00	-0,05	-0,09	SHISA3
TC0200008793.hg.1	-0,22	-0,16	0,00	-0,44	-0,09	SLC5A7
TC0300011956.hg.1	-0,25	-0,28	0,00	-0,24	-0,29	DPPA4
TC0100007457.hg.1	-0,06	-0,12	-0,04	-0,12	0,00	LIN28A
TC0500010651.hg.1	-0,20	-0,11	0,00	-0,28	-0,23	FGF10
TC0500007349.hg.1	-0,27	-0,31	-0,16	-0,30	0,00	ISL1
TC0700010719.hg.1	-0,23	-0,17	0,00	-0,29	-0,13	TBX20

6.4 Abbreviations

Abbreviation	Full name	Abbreviation	Full name
%	Percent	dCTP	Deoxycytosine triphosphate
°C	Degrees Celsius	DCX	Doublecortin
18s rRNA	18s ribosomal RNA	ddH2O	Double distilled water
2D	Two dimensional	DEG	Differential expressed genes
3D	Three dimensional	Δ	Delta
4CPL	4µM CHIR, Purmorphamine, L-Ascorbic accid	DEPC	Diethyl pyrocarbonate
A/T/C/G	Adenine/Thymine/Cytosine/Guanine	dGTP	Deoxyguanine triphosphate
Acc	Accutase	Diff	Differentiation
AF	Activator function	DIG-AP-Fab	Anti-Digoxigenin AP, FAB fragment
AM	Active Motif	DLX2	Distal-Less Homeobox 2
Amp	Ampicillin	DMEM	Dulbecco's Modified Eagle's Medium
AP	Alkaline phosphatase	DMEM-F12	Dulbecco's Modified Eagle's Medium/Ham's Nutrient Mixture F12
AP2a	Activating enhancer binding protein 2 alpha	DMSO	Dimethyl sulfoxide
APC	Allophycocyanin	DNA	Deoxyribonucleic acid
ApE	A plasmid editor	dNTPs	Nucleoside triphosphate
APS	Ammonium persulfate	DOC	Deoxycholic acid sodium salt
ASCL1	Achaete-scute homolog 1	DOX	Doxycycline
BCA	bicinchoninic acid	DPBS	Dulbecco's phosphate-buffered saline
BCL11A	B-cell lymphoma/leukemia 11A	DR0	Direct repeat with zero spacer
BD	Becton Dickinson	dTTP	Deoxythymine triphosphate
BDNF	Brain-derived neurotrophic factor	E	Embryonic day
bHLH	basic helix–loop–helix	E. coli	Escherichia coli
BMP	Bone morphogenetic proteins	e.g.	exempli gratia
Bp	Base pair	EDTA	Ethylenediaminetetraacetic acid
Brn2	POU class 3 homeobox 2	EdU	5-Ethinyl-2'-Desoxyuridin
BSA	Bovine serum albumin	EF1a	Elongation factor-1 alpha
c-Myc	Cellular myelocytomatosis oncogene	EGF	Epidermal growth factor
Ca^{2+}	Calcium	EMSA	Electrophoretic Mobility Shift Assay
Cas9	CRISPR associated protein 9	EN1/2	Homeobox protein engrailed-1
CD	Cluster of Differentiation	ESC	Embryonic stem cells
cDNA	complementary DNA	EtOH	Ethanol
ChIP	Chromatin Immunoprecipitation	FBS	Fetal bovine serum
cm	Centimeter	FGF	Fibroblast growth factors
CMV promoter	Cytomegalovirus promoter	FITC	Fluorescein isothiocyanate
CNS	Central nervous system	FLC	Flowcytometry
CO_2	Carbon dioxide	FoxA	Forkhead-Box-Protein
CREB	cAMP response element-binding protein	FRZB/SFRP3	Secreted Frizzled-Related *Protein*
CRIPTO-1	teratocarcinoma-derived growth factor-1	FSC-A	Forward scatter area
CRISPR	Clustered regularly interspaced short palindromic repeats	g	Gram
CT	Cycle threshold	GABA	gamma-Aminobutyric acid
CTE	C-terminal extension	GAPDH	Glycerinaldehyd-3-phosphat-Dehydrogenase
ctrl/ctr	Control	GCNF	Germ cell nuclear factor
CuSO4	Copper sulphate	GOI	Gene of interest
CYP26	Cytochrome P450 26A1	gp	Guinea pig
DACH1	Dachshund Family Transcription Factor 1	GPI-anchor	Glycosylphosphatidylinositol
DAPI	4',6-Diamidino-2-phenylindol	gRNA	Guide RNA
dATP	Deoxyadenosine triphosphate	GT	Geltrex
DBD	DNA binding domain		

Abbreviation	Full name	Abbreviation	Full name
h	Hour	NaCl	Sodium chloride
h	Human	NaOH	Sodium hydroxide
HBSS	Hanks' Balanced Salt Solution	NCBI	National Center for Biotechnology Information
HCl	Hydrochloric acid,	NCoR	Nuclear receptor co-repressor 1
HEK-293FT	Human embryonic kidney 293 FT	ND	Neuronal differentiation day
HES	Hairy and enhancer of split-1)	NEB	New England Biolabs
HEY	Hairy/enhancer-of-split related with YRPW motif protein	Neg	Negative
hiPSCs	Human induced pluripotent stem cells	NESTIN	Neuroepithelial stem cell protein
hNSCs	Human neural stem cells	NFIB	Nuclear factor 1 B-type
HRP	Horseradish peroxidase	NGN2	Neurogenin 2
HSV	Herpes Simplex virus	NGS	Normal goat serum
ICC	Immunocytochemistry	NIAID	National Institute of Allergy and Infectious Diseases
Igepal	Octylphenoxypolyethoxyethanol	NIH	National Institutes of Health
IgG	Immunoglobulin G	NPC	Neural progenitor cells
IP	Immunoprecipitation	NR	Nuclear receptor
iPSCs	Induced pluripotent stem cell	NSC	Neural stem cell
IR	Infrared	NTD	N-terminal domain
ISH	In situ hybridization	NTMT	NaCl, Tris-cl, MgCl2, Tween-20
IVT	In vitro transcription	NuRD	Nucleosome Remodeling and Deacetylase
KCl	Potassium chloride	OCT4	Octamer-binding transcription factor 4
KLF4	Kruppel-like factor 4	OTX2	Orthodenticle Homeobox 2
KSR	Knockout Serum Replacement	p	p-value
LB medium	lysogeny *broth* medium	PAULA	Personal AUtomated Lab Assistant
LBD	Ligand binding domain	PAX6	Paired Box 6
LRH-1	Liver receptor homolog-1	PBS	Phosphate-buffered saline
lt-NES	Long-term self-renewing neuroepithelial stem cells	PBS-PP	Phosphate-buffered saline plus detergent
M	Molar	PCA	Principal component analysis
M	Mouse	PCR	Polymerase chain reaction
MAP2	Microtubule-associated protein 2	PCYT1B	Choline-phosphate cytidylyltransferase B
MEM-NEAA	MEM Eagle Non-essential Amino Acid Solution	PEG6000	Polyethylenglycol
MeOH	Methanol	Pen/Strep	Penicillin-Streptomycin
mg	Milligram	PFA	Perfluoroalkoxy alkanes
$MgCl_2$	Magnesium chloride	pH	Power of hydrogen
$MgSO_4$	Magnesium sulfate	PCM	Phase contrast microscopy
min	Minutes	PI	Protease Inhibitor
miR	microRNA	PMSF	Phenylmethylsulfonyl fluoride
mL	Milli Liter	Pol II	Polymerase II
MLC1	Megalencephalic Leukoencephalopathy with Subcortical Cysts Protein-1	Pos	Positive
mm	Millimeter	PSCs	Pluripotent stem cells
mM	Millimolar	PSD95	Postsynaptic density protein 95
mRNA	Messenger RNA	Puro	Puromycin
ms	Mouse	PVDF	Polyvinylidene fluoride
mut	Mutated	QC	Quality control
MyoD	Myoblast determination protein 1	qRT-PCR	Quantitative real time PCR
Myt1l	myelin transcription factor 1 like	R-NSC	Rosette stage NSCs
n	Number of experiments	RA	Retinoic acid
Na	Sodium	rb	Rabbit
$Na_3P_2O_7$	Tetrasodium pyrophosphate		

Abbreviation	Full name	Abbreviation	Full name
RE1	RE1 binding site	xg	Times gravitational-force
REST	RE1-silencing transcription factor	ZF	Zinc finger
RI	Rho kinase inhibitor	ZO1	Zonula occludens-1
RIPA	Radioimmunoprecipitation assay	µg	Micro gram
RNA	Ribonucleic acid	µL	Microliter
rpm	Revolutions per minute	µm	Micrometer
rRNA	Ribosomal RNA	µM	Micromolar
RT	Room temperature		
s	Second		
SD	Standard deviation		
SDS	Sodium dodecyl sulfate		
SEM	Standard error of mean		
SEMA3C	Semaphorin 3C		
SF1	Splicing factor 1		
SHD	SH2 domain-containing adapter protein D		
SHH	Sonic hedgehog		
shRNA	Short hairpin RNA		
smNPCs	Small molecule neural precursor cells		
SMRT	Silencing mediator for retinoid or thyroid-hormone receptors		
SNP	Single nucleotide polymorphism		
SOC	Super Optimal Broth		
SOX2	Sex determining region Y		
SR	Serum replacement		
ss-cDNA	Singe stranded cDNA		
SSC	High stringency wash solution		
SSC-A	Sideward scatter area		
ßIII-TUB	βIII-tubulin		
Str8	Rhodanese-like domain-containing protein 8		
SV40	Simian-Virus 40		
SWI/SNF	SWItch/Sucrose Non-Fermentable		
SYBR	N',N'-dimethyl-N-[4-[(E)-(3-methyl-1,3-benzothiazol-2-ylidene)methyl]-1-phenylquinolin-1-ium-2-yl]-N-propylpropane-1,3-diamine		
TAD	Transactivator domain		
TBS-T	Tris-buffered saline with Tween-20		
TC	Tissue culture		
TE	Trypsin-EDTA		
TEA	TRIS-Acetat-EDTA		
TEMED	N,N,N′,N′-Tetramethylethylendiamin		
TGFb	Transforming growth factor β		
TRE	Tetracycline response element		
TRIF	Transiently retinoid-inducer factor		
tRNA	Transfer RNA		
UTR	Untranslated region		
V	Volt		
VP16	Virus protein 16		
vRG	Ventricular radial glial cells		
WB	Western Blot		
WNT	Wingless-related integration site		
X	Times		

6.5 Acknowledgements

First of all, I would like to thank Prof. Dr. Oliver Brüstle for the opportunity to perform my PhD thesis in the Institute of Reconstructive Neurobiology. I would like to thank you for your support and guidance throughout the years of my PhD thesis.

I am also very thankful to the other three members of my thesis committee: Prof. Dr. Waldemar Kolanus, PD. Dr. Gerhild van Echten-Deckert and Prof. Dr. Evi Kostenis. Thank you for taking time to be part of my thesis committee and for your interest in my work.

Furthermore, I would to express my gratitude to my former supervisor and working group leader Dr. Laura Stappert. Thank you for giving me the chance to continue working on the GCNF project and your guidance and support for the first half of my PhD thesis and beyond after you left the Institute.

I would also like to thank Dr. Andreas Till for his support during the final stage of my thesis. Thank you also for your advice, your kindness and all the warm words.

I would like to thank Dr. Michael Peitz for supporting me and the GCNF project.

Moreover, I would like to thank all former members of the AG Stappert: Mohamad Hajo – I think, we did a really good job, when it was just the two of us left, thank you for dealing with me and supporting me –, Monika Veltel – Thank you for your amazing technical and emotional support. I loved working with you –, Silvia Brocchetti – Even though you only joined us for the time of your Master's thesis, you filled my days with fun and friendship –, Nils Christian Braun – Nils, there are no words to describe how much I enjoyed working and discussing with you about science or society issues. Thank you for being my partner in crime –, Sarah Schütte – Thank you for your reliable, technical support and friendly kind – and Kayeon Jung – You were a great student and did a really good job. Thank you for helping me to explore the functionality of GCNF-VP16 as tool for accelerated neuronal differentiation.

Furthermore, I would like to thank Prof. Sandra Blaess and her former work group members Erick Martinez Chavez and Marianna Tolve for teaching me how to perform RNA *in situ* hybridization assays and the provision of embryonic mouse brain tissue. I would like to thank Julia Ladewig and Ammar Jabali for providing me with cryosections of cortical organoids to conduct the RNA ISH experiments.

Thank you, Tamara Bechler for the technical support and Cornelia Thiele not only for the technical support, but also for all the little extra things you did to make my life a bit easier.

I would also like to thank the members of the Cellomics platform, Vanessa Frickel, Dr. Mona Mathews and Michaela Segschneider, for "adopting" me and supporting me.

Additionally, I would like to express my gratitude to Alexandra Rabe and Bärbel Wagner for helping me with all bureaucratical or organizational issues in the last years and to Claudia Schmidt, who answered all my panic-driven questions in the last weeks with patience and friendliness.

I would like to thank the internal research funding program of the medical faculty (Rheinische Friedrich-Wilhelms-Universität Bonn) BONFOR for financially supporting this research project and my position (O-172.0040).

A special thanks to my former colleagues, who created a great, supportive and fun atmosphere in the lab. I am happy to call you my friends: Dr. Lea Berg, Natalia Garcia Perez, Luzia Heidrich, Fabio Marsoner, Dr. Pascal Röderer, Dr. Marinna Tolve, Dr. Kevin Weynans and Dr. Jannis Wißfeld.

Moreover, I am grateful for all my friends outside of the Institute. The last years were the hardest in my life and I am so happy that you stuck with me, even though I went radio silent for so many times. Thank

you to my oldest friends Katharina Brinker, Sina-Marie Haake, Saskia Mendes, Dr. Selena Röthemeier and Julia Siemon, thank you to Vanessa Dusend, Dr. Isabelle Erenburg, Dr. Laura Grundewald, Juan Luis Guzman, Dr. Kathrine Lundø Jørgensen and Catharina Wiese.
I would like to thank Andreas Becker and his immediate family. You are wonderful. Thank you, Andreas for supporting me, calming me down, introducing me to “Friends” and teaching me about things like “Löffel, Messer, Gäbel”.
In addition, I would like to thank my grandparents Hans Klaus and Irene Becker for their support and love and for being flatteringly proud of me. Thank you to my amazing parents, Jürgen and Petra Klaus, who supported me in every decision I ever took and thank you for always having my best in mind. Thank you for never putting pressure on me. Thank you, Annika Klaus, for being the best, little sister I could have ever wished for, thank you for caring for me and understanding me without words. Thank you for being there, whenever I needed you. And last, but not least, I would like to thank Yannik Breitkreuz for feeding me, looking out for me and dealing with all my quirks and tics. I cherish your presence in my life. I could not have done it without you <3.